University of Messina

Department of Engineering

PhD Course in Engineering and Chemistry of Materials
and Buildings
XXX cycle

Thermal energy storage systems for low-grade heat applications

Design and experimental testing of lab-scale prototypes

Valeria Palomba

Supervisors: Angelo Freni
Antonio Galvagno

October 2017

Abstract

The main objective of this thesis is the development of prototypes of thermal energy storages suitable for coupling with low-grade waste heat (e.g. non-concentrating solar, industrial process heat) and their experimental testing.

Benefits of thermal energy storages are several, but the experience in non-sensible heat storage is still limited, especially in the design of prototypes. High temperature heat storage (T >150°C) has been the subject of a quite extensive research, but low-grade heat sources are still not fully exploited, due to the competition with water, that is available at a risible cost.

In the present thesis, two different technologies were investigated, latent heat and adsorption heat, by design and experimental testing of lab-scale storages. In particular, data from experimental testing on Phase Change Materials carried out at CNR-ITAE were used for the development of thermal energy storages using latent heat technology (with phase change materials). Since only limited data on PCM-based devices in the investigated temperature range were available, two approaches were followed: a custom fin-and-tube heat exchanger and a commercial plate heat exchanger were tested with the same PCM (a paraffin) and the results used for a design analysis. In order to complete the analysis, a simplified numerical model was developed through the commercial software COMSOL Multiphysics and validated against experimental results. The model was able to describe the behaviour of the fin-and-tube system with low computational effort, showing good possibility for a future design optimization and easy adaptability to different configurations.

Measurement on adsorption equilibrium curves available for adsorbent materials, instead, were used as the input for the development of a thermal energy storage making use of adsorption technology. While the storage was designed to use the same heat sources as the latent thermal ones, different operating conditions on the user-side were considered, taking into account both cold or hot storage possibilities.

The experimental measurements on both the technologies highlighted the good potential of the investigated systems and therefore that further research in the specific temperature range analysed is feasible and will allow overcoming the limitations that still exist. However, the intense research activity that is on-going in the field of thermal energy storage cannot preclude from a standardization, both in the definition of relevant indicators and the assessment of

the systems. To this aim, an attempt has been made at comparing the developed storages (2 latent heat storages and 1 adsorption storage), by defining common performance indicators and evaluating whether they can be applied to such different cases, in terms of characteristics, sizes and application.

Results obtained have shown that both technologies allow reaching a higher energy storage density than water, under all the examined conditions (i.e. charging temperature of 75°C to 90°C), with values up to 900 kJ/kg in the case of the adsorption heat storage. The operating parameters affecting storage operation were analysed as well: indeed, it was found that the performance of the storages is strongly dependent not only on the heat sources and external ambient conditions, but also on the control of the system (i.e. the flow rate imposed, the part load operation) and the construction features, such as the material used for the shells or the insulation.

Finally, the methodology suggested for the evaluation of the storage could be successfully applied to all the systems, allowing a qualitative and quantitative comparison.

The main outcomes of the work here reported can then lead the path towards the optimization of the heat storage systems, from lab-scale to pre-commercial ones, thus increasing the technology readiness level and making a step forward towards practical application.

Table of contents

List of figures

List of tables

Chapter 1

Introduction

1.1 Background

Energy production is the fulcrum of economical, scientific and social development worldwide. However, economic crisis, instability in the price of oil and gas, a difficult geo-political situation and a growing environmental conscience have favoured a massive introduction and development of renewable energy sources, clean, worldwide available and inexhaustible [1]. Moreover, energy efficiency has become an important target since energy savings and high-efficiency systems represent a fundamental part in the development towards a more sustainable and cleaner world [2]. Global energy policies reflect such a situation, both in the Western and Eastern countries. Indeed, production of energy from renewable sources represents a consistent share in the energy mix of most countries, including some emergent countries and, surprisingly, the majority of South American and African countries, as shown in Figure 1.1. Trend is towards an increase of installed capacity of systems employing renewable energy sources, as shown in Figure 1.2 for the solar thermal case.

Such a situation is also boosted by support policies promoted by governments for both privates and industries, in order to sustain the production, R&D and commercial diffusion of such systems. In fact, as to 2014, 144 countries have defined renewable energy targets and developed energy policies aimed at efficiency [3]. European Union has indicated the notorious 2020 targets as [4]:

- 20% reduction of greenhouse gaseous emissions;
- 20% of renewables share;
- 20% increasing of energy efficiency.

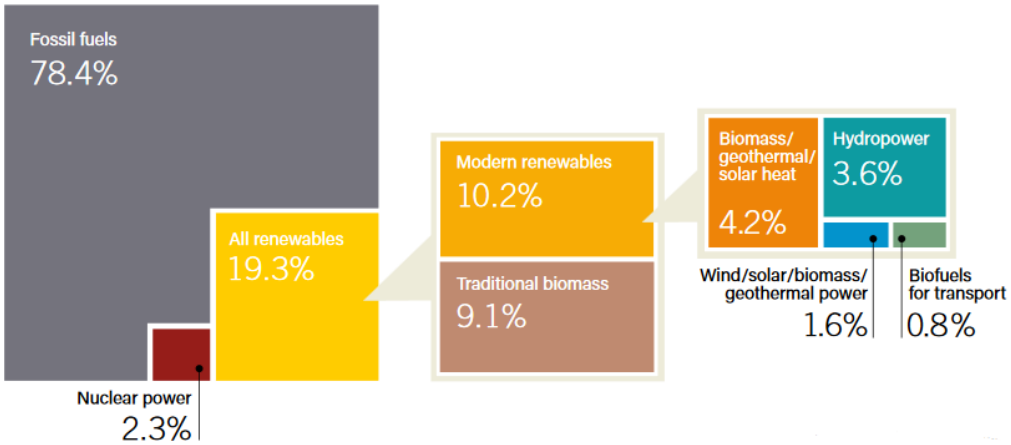

Fig. 1.1 Share of renewables worldwide. SOurce:IEA

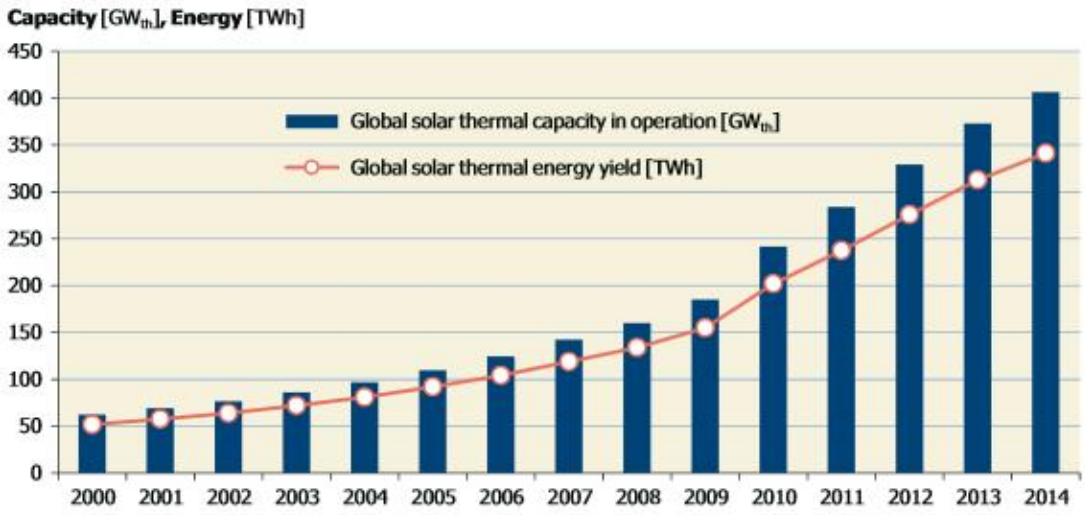

Fig. 1.2 Global solar thermal capacity installed in the last years.

Energy efficiency and reduction in CO_2 emissions, however are linked not only to renewable energies, but also to waste heat recovery. Considering as an example the transportation sector, a total of about 450 ktons of CO_2 per year emissions can be estimated, half of which could be reduced by reducing the fuel needed for propulsion, mainly thanks to waste heat recovery [3, 5]. In such a context is hence clear that, in the next future, there would be an increasing and urgent need for architectures built for energy efficiency, in the residential, industrial and mobility fields. Key component for a system created for efficiency enhancement is a thermal storage, to cover for the gap between heat generation and heat demand and to effectively distribute it through the various users.

1.2 Benefits of using a thermal storage

The utilization of thermal energy storage in various fields has long been established [6, 7] , not only in residential applications, but also in district heating [8] and in commercial and industrial ones [9, 7]. The main advantages deriving from the application of a thermal storage system can be summarised as follows:

- decoupling of the time between availability of a thermal source and its request;
- better exploitation of energy, due to the possibility of producing and storing energy when the cost is lower;
- reduction of peak demand, allowing energy providers to reduce the costs related to energy production and to increase the efficiency of generation;
- reduction of CO_2 emissions;
- possibility to size energy generation and distribution equipment for a lower power, with significant cost benefits.

1.3 Objective of the thesis

The present thesis deals with thermal storage technologies, with special focus on heat storage from solar radiation and waste heat recovery (e.g. from industrial processes and internal combustion engines). The main objective of the thesis are the development and experimental testing of thermal energy storage systems suitable for low-grade waste heat applications (T <100°C). The design of the systems will be described and the experimental measurements presented. Through the experimental benchmarking of the realised systems,

some considerations and optimization regarding the actual application of them under real boundaries will be discussed. Finally, a quantitative comparison between the technologies will be proposed, serving also a starting point for the definition of future standards.

1.4 Outline of the thesis

The thesis will be composed as follows:

- Chapter 2 will discuss the available technologies for thermal energy storage, starting from the theoretical basis and discussing the actual state-of-art with respect to material, component and prototype applications. In particular, thermal energy storage through the use of PCMs and sorption material will be investigated, by presenting the available materials with their advantages and disadvantages, the possible enhancement in their properties and the design issues related to the application in a full-scale system.

- Chapter 3 will present the development of two thermal energy storage prototypes using latent heat technology (with phase change materials) through experimental testing of lab-scale prototypes. numerical modelling and experimental measurements. Experimental results measured through a specifically designed testing rig will be analysed to discuss the behaviour of the components under the tested boundary conditions. Moreover, a numerical model, realised through the commercial software COMSOL Multiphysics and suitable for the simulation of latent heat storages, will be presented. Results from the experiments were used to validate the model.

- Chapter 4 will present the development of a thermal energy storage making use of adsorption technology. Thermodynamic and dynamic considerations used in the design phase will be presented. Experimental results measured in a dedicated testing rig will also be analysed and discussed.

- Chapter 5 will be dedicated to the discussion of the experimental methodology used for the assessment of the performance of the two systems. Some parameters will be identified for the description and comparison of thermal energy storage systems, according to the work currently ongoing within ECES Annex 30. Indeed, the parameters defined will be applied to the case studies presented in the previous Chapters and the open issues will be further discussed.

Chapter 2

Thermal energy storage: basics, materials and technologies

2.1 Basics

Thermal Energy Storage (TES) is the whole assembly of technologies allowing for heat or cold energy to be used at a different time from generation. The basic flow diagram for a thermal energy storage process is shown in Figure 2.1: when excess hot or cold energy is available, this is used to charge the storage. When a demand for such energy exists, the storage is discharged. The storage period in between can vary from a few hours to months.

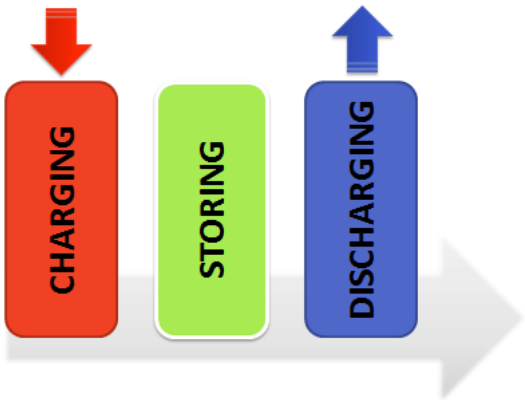

Fig. 2.1 Flow diagram of a thermal energy storage process.

A general classification of the methods for thermal energy storage which will be further analysed in the following sections, is given in Figure 2.2 [10].

A qualitative comparison between the various storage technologies, based on the different energy density levels achievable with the above-mentioned technologies is shown in

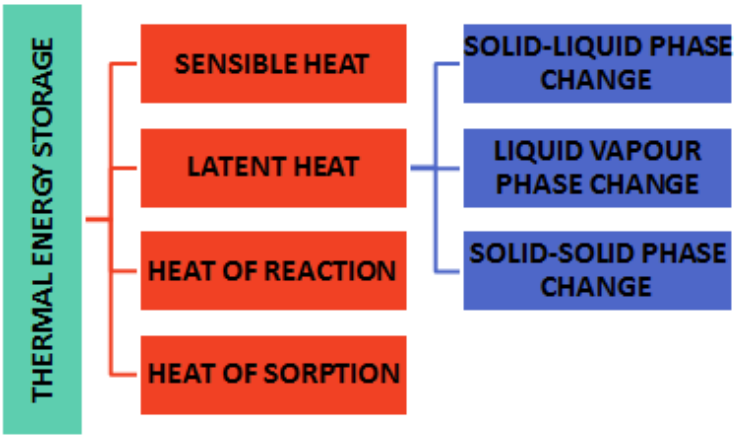

Fig. 2.2 Classification of thermal storage methods.

Figure 2.3 [10]. It clearly shows that, starting from traditional sensible heat storage to the most efficient methods employing physical or chemical processes, the density enhancement can reach a ratio up to 8. The same concept is depicted in Figure 2.4, where volume needed to store 1850 kWh (with consideration of 25 % heat losses, based on a 70°C temperature increase for water) is shown [11].

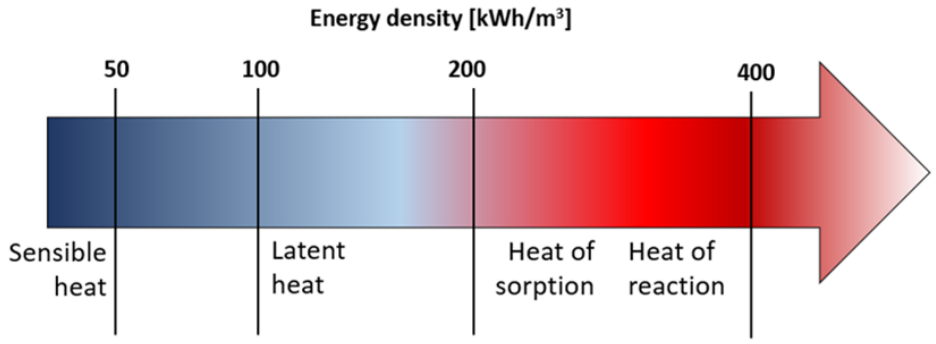

Fig. 2.3 Energy density level for the different thermal storage technologies.

2.1.1 Storage with sensible heat

Sensible heat is the traditional methods used for storing energy. It is based on the increment in temperature of a storage medium when this is heated. The energy stored is linked to the temperature by a direct proportionality, as shown in Figure 2.5. The amount of energy stored

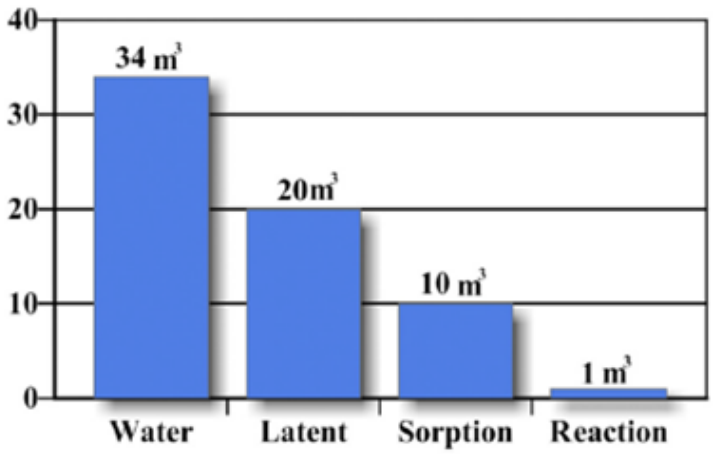

Fig. 2.4 Volume needed to store 1850 kWh, comparison among technologies.

can be expressed through an equation of the type:

$$\Delta Q = mc_p \Delta T \tag{2.1}$$

With m the mass of the storage medium and c_p its specific heat. Different heat storage

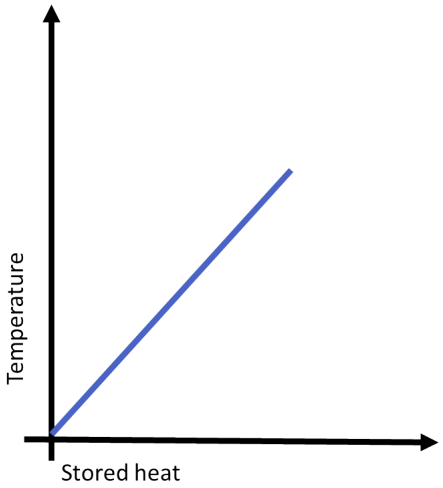

Fig. 2.5 Energy as a function of temperature,sensible heat.

materials can be applied for this type of storage, both in solid and liquid form, as summarised in Table 2.1 [12]. The temperature range covered by such materials is very high, from 0°C to 400°C. The advantage of liquid materials over solid ones is that active storage can be applied (without the need of an heat exchanger) and in general they require a simpler and cheaper storage design, because of the higher heat transfer efficiency. On the contrary, solid materials

do not have problems related to vapour pressure and the formation of possibly corrosive or explosives compounds and are in general very cheap. Since some of them are traditional construction materials, their implementation for the thermoregulation of buildings is easy. Their low thermal conductivity requires high contact area with the heat transfer fluid (HTF).

2.1.2 Storage with latent heat

Latent heat systems allow to accumulate energy by means of a phase change —mainly the solid-liquid one— as shown in Figure 2.6. Indeed, phase changes are associated to absorption or cession of energy at constant temperature. In this case, stored energy can be defined as:

$$\Delta Q = \Delta H \tag{2.2}$$

Where the ΔH is the enthalpy associated to the phase change. In case of the solid-liquid phase change:

$$\Delta H = \lambda_m \tag{2.3}$$

With λ_m being the latent heat of fusion/solidification. If phase change is completed, further energy is stored in the form of sensible heat and therefore, for a material starting in solid form at an initial temperature T_0 and heated to a final temperature T_{fin}, superior than melting temperature, the total amount of heat storable is given by [13]:

$$Q_{total} = Q_{sensible,solid} + Q_{latent} + Q_{sensible,liquid} = \int_{T_0}^{Tm} mc_{p_s} dT + \lambda_m + \int_{T_m}^{T_{fin}} mc_{p_l} dT \tag{2.4}$$

Materials usually employed for TES with latent heat are called phase change materials or PCMs. The main advantages deriving from the utilization of latent heat, if compared to other technologies, are:

- higher energy density than sensible heat media;
- dependence of thermal behaviour from phase change temperature, a feature allowing to tailor the material according to the specific application to be realised. [13, 14].

2.1.3 Storage with chemical reactions

Chemical reactions can be used for heat storage/release, since between the reactants and the products of a chemical reaction there is a different enthalpy content, which is the so-called heat of reaction. When there is an exothermic reaction, heat will be released to the

Table 2.1 Materials for sensible heat storage and their properties.

Class	Material	Density	Melting point	Specific heat	Heat of fusion	Thermal conductivity
-	-	kg/m^3	°C	kJ/(kgK)	kJ/kg	W/(mK)
Water	Water	1000	0	4.184	333.55	0.58
Mineral oils	Therminol VP-1	1068	12	1.546	-	0.137
Nitrate salts	$NaNO_3$	2261	306	1.655	172	0.514
Nitrate salts	KNO_3	2109	335	0.953	266	0.514
Hydroxide salts	NaOH	2100	318	0.92	165	
Hyroxide salts	KOH	2040	380	1.34	150	0.5
Chloride salts	$ZnCl_2$	2907	280		75	0.5
Salt composites	Solar salt $NaNO_3$-KNO_3 (50-50)	1920	220		100.7	0.56
Solid materials	Rocks	2560		0.960		0.48
Solid materials	Concrete	2200		0.85		1.5
Solid materials	Sand	1602		0.83		
Solid materials	Magnesia fire bricks	3000		1.15		5
Solid materials	Cast steel	7800		0.6		40

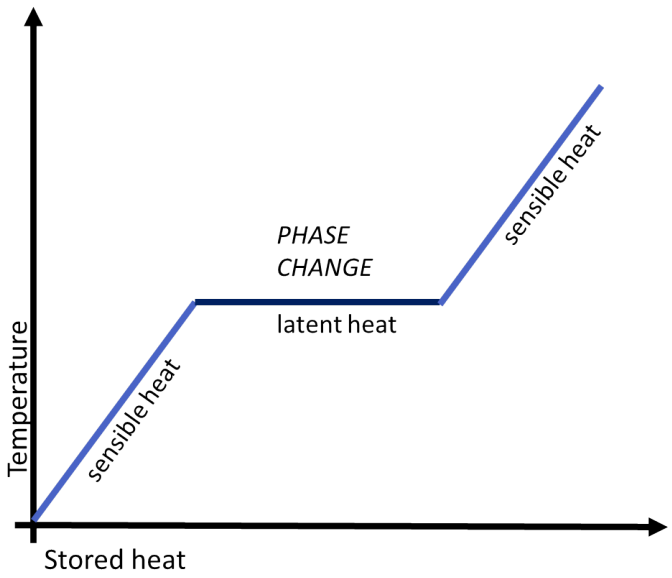

Fig. 2.6 Energy as a function of temperature,latent heat.

environment, while an endothermic reaction will allow storing heat, as shown in Figure 2.7. Some conditions must be respected in order for a reaction to be useful for heat storage [10]:

- heat of reaction should be relatively high, which does not usually happens when all of the components in the reaction are liquid or solid;
- the products of the reaction must be storable;
- the reaction must be reversible.

As for latent heat storage, the heat stored with chemical reactions, can be expressed in the form:

$$\Delta Q = \Delta H_r \tag{2.5}$$

Where ΔH_r is the heat of reaction associated to the particular chemical system.

Drawbacks in the use of chemical reaction for energy storage are linked to the fact that they involve chemical bonding, which are strong, and accordingly require a huge amount of energy to be modified. Direct consequence is that chemical reaction are generally useful only for high temperature energy storage. Some examples of chemical reactions and their correspondent temperature levels are given in Table 2.2.

It is possible to notice that several chemical reactions exist, with the potential to store heat at a temperature level variable from 100°C to 1500°C and high energy density. However, as previously stated, the difficulties in handling the products of the reaction and the control of the reaction itself have limited the practical application of such systems up to now.

Table 2.2 Example of reactions usable for heat storage

Class of material	Reaction	Tr	ΔH_r	ΔH_r
-	-	°C	kJ/mol	kWh/m^3
Hydroxides	$Mg(OH)_2 \Leftrightarrow MgO + H_2O$	268	78	442
Hydroxides	$Ca(OH)_2 \Leftrightarrow CaO + H_2O$	521	100	410
Ammonium salt	$NH_4HSO_4 \Leftrightarrow NH_3 + H_2 + SO_3$	467	337	727
Salt hydrates	$MgSO_4 \cdot 7H_2O \Leftrightarrow MgSO_4 + 7H_2O$	122	411	389
Salt hydrates	$CaCl_2 \cdot 2H_2O \Leftrightarrow CaCl_2 \cdot H_2O + H_2O$	174	48	84
Salt hydrates	$CuSO_4 \cdot 5H_2O \Leftrightarrow CuSO_4 \cdot H_2O + 4H_2O$	104	226	287
Salt hydrates	$CuSO \cdot 4H_2O \Leftrightarrow CuSO + 4H_2O$	205	73	163
Peroxide salts	$BaO_2 \Leftrightarrow BaO + \frac{1}{2}O_2$	782	75	305
Peroxide salts	$KO_2 \Leftrightarrow \frac{1}{2}K_2O + \frac{3}{4}O_2$	668	101	423
Carbonates	$CaCO_3 \Leftrightarrow CaO + CO_2$	896	167	626
Carbonates	$BaCO_3 \Leftrightarrow BaO + CO_2$	1497	212	661
Metal hydrides	$MgH_2 \Leftrightarrow Mg + H_2$	293	79	605
Metal hydrides	$Mg_2NiH_4 \Leftrightarrow Mg_2Ni + 2H_2$	253	128	-
Catalytic reactions	$NH_3 \Leftrightarrow frac12N_2 + \frac{3}{2}H_2O$	195	49	546
Catalytic reactions	$SO_3 \Leftrightarrow SO_2 + \frac{1}{2}O_2$	767	98	678
Reforming	$CH_4 + H_2O \Leftrightarrow CO + 3H_2$	687	205	-
Reforming	$CH_4 + CO_2 \Leftrightarrow 2CO + 2H_2$	687	247	-

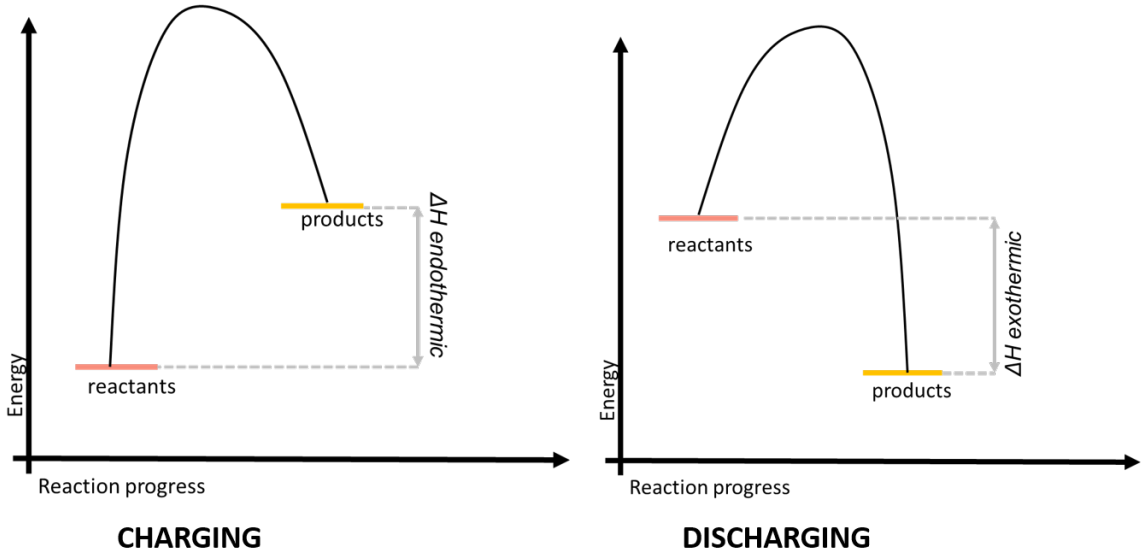

Fig. 2.7 Heat storage process with chemical reaction

2.1.4 Storage with heat of adsorption

Adsorption is the phenomenon involving bonding of a vapour or gaseous substance on the surface of a solid material, as schematically shown in Figure 2.8. During adsorption the gas molecules are concentrated on the surface of the solid, while during the reverse process, called desorption, molecules leave it.

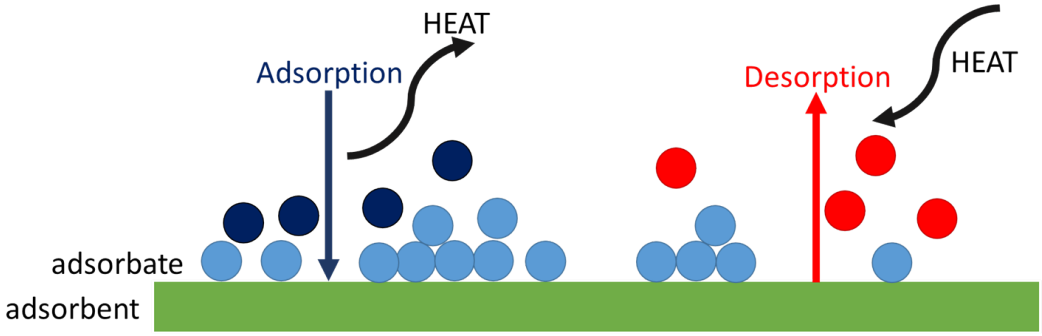

Fig. 2.8 Heat storage process through adsorption.

The material capable of adsorbing other components is called adsorbent, while the material being adsorbed is called adsorbate [15]. A general distinction is made between:

- physical adsorption, or physisorption, involving Van Der Waals forces and hydrogen bonding;
- chemical adsorption, or chemisorption, involving chemical valency bonding.

As shown in the picture, desorption process requires heat, which is released when adsorption occurs. Such amount of heat, called heat of adsorption, could be stored if a proper system architecture is built. Therefore, for a thermochemical system employing adsorption process, stored heat can be expressed as:

$$\Delta Q = \Delta H_{ads} \tag{2.6}$$

Where ΔH_{ads} is the adsorption heat linked to the process.
Chemisorption, involving stronger forces, is associated with a higher heat of adsorption than physical bonding, but the latter is almost unanimously preferred, since it does not require elevated activation energies for the reaction to occur [15].

2.1.5 Comparison of thermal energy storage technologies

Table 2.3 presents a comparison between the available thermal energy storage technologies, focusing especially on the technical aspects and their level of readiness. In general, it is possible to assert that sensible storage is commercially available, also in bigger sizes and presents the easiest construction. On the other hand, its applicability is limited to short term storage and the energy density achievable is low. Latent heat storage presents a higher energy density. The application of PCMs is often limited by their degradation over cycling and the low thermal conductivity. Thermochemical storages present the highest energy density and have a storage period that is theoretically unlimited, without the need for bulky insulation and, when referring to sorption storage, with limited corrosion issues. On the contrary, the system layout is complex and requires several components, which have caused its application to be restricted mostly to laboratory scale up to now. Instead, in Figure 2.9, the most suitable technology for each of the common applications requiring a thermal storage is shown. Such an indication is based on either intrinsic limitations of the technology (e.g. the use of latent heat storage for district heating and cooling networks is limited by the relevant effect of heat losses) or design consideration: the use of thermochemical storage for building applications is not advisable due to the bulky dimensions of such systems, which make them more suitable for industrial applications. In the case of mobile applications, where high energy density and no limitations on heat storage period are key constraints, only thermochemical systems were listed as suitable. Instead, in the case of cold storage, systems with high efficiency and compact enough for real applications belong to the category of latent TESS, since sensible heat storage presents time limitations and thermochemical systems have an intrinsic efficiency that is quite low (their theoretical COP never exceeds 0.67).

Table 2.3 Comparison of thermal energy storage technologies

	Sensible TES	**Latent TES**	**Thermochemical TES**
Temperature range (°C)	0÷1200	-100÷1000	150÷1500
Storage density (kWh/t)	10÷50	50÷100	150÷250
Storage density (kWh/m^3)	50	100	500
Power (kW)	1÷10000	1÷100	10÷1000
Efficiency(%)	50÷90	50÷90	50÷100
Storage period	hours to days	hours to days	hours to months
Lifetime	long	limited due to degradation of materials over cycling	theoretically unlimited
TRL	9	4÷7	4÷6
Environmental impact	negligible	negligible	negligible
Safety issues	no	depends on materials used, but usually limited	limited for sorption TES, higher concern for chemical TES
Corrosion issues	mild	medium to high	low for sorption TES, high for chemical TES
Impact of insulation	high	high	low
Technical complexity of the system	low	medium	high
Flexibility (regulation, partial charge/discharge etc)	high	medium	low

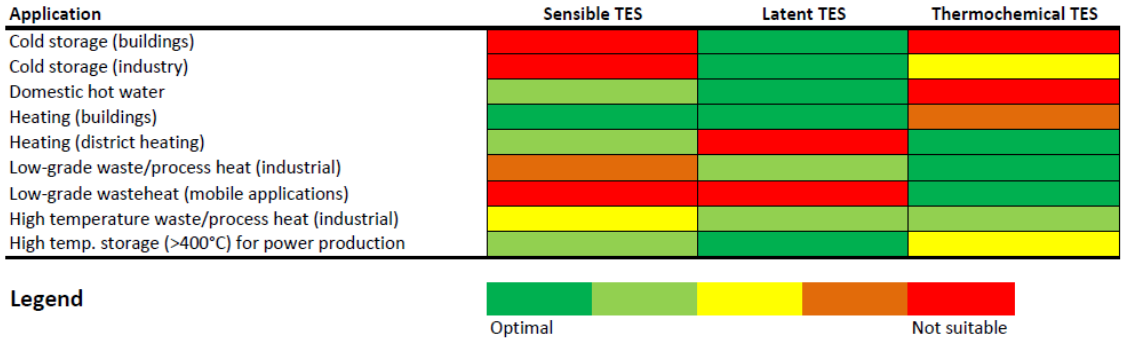

Fig. 2.9 Comparison of heat storage technologies on the basis of their application.

2.2 Latent heat thermal energy storage: materials and technology

As previously stated, the definition of PCM materials includes all the materials undergoing a phase change and adoptable for thermal energy storage. However, since solid-liquid phase change is definitely the most common studied and employed in practical systems, only the classes of PCMs used for this phase change will be considered in the following description.

A lot of effort has been recently put in the search for optimal PCMs for the most different applications, ranging from solar energy storage to ice storage, from thermoregulation of buildings to food storage systems [16]. The properties required for an ideal PCM are several, and often contrasting one another: it is consequently impossible for a material to possess all of them, even when manipulation with external compounds is realised. Indeed, the following features are required: [14, 17, 13]:

THERMAL PROPERTIES

- Phase change temperature compatible with the characteristic temperature level of the desired application;
- High latent heat per volume unit, as to allow storing high amount of heat in a compact volume;
- High specific heat, in order to store a significant amount of energy also during heating phase;
- High thermal conductivity both in solid and liquid status to minimise the temperature difference needed for phase change.

PHYSICAL PROPERTIES

- Low volume expansion due to the temperature variation, in order to reduce the volume needed to compensate for thermal expansion;
- Low vapour pressure, to facilitate the eventual encapsulation;
- High density, to reduce storage volume.

CHEMICAL PROPERTIES

- Long-term stability, to avoid or reduce material degradation due to cycling during operation;
- Compatibility with materials of the storage, to reduce problems related to corrosion or chemical reaction with the containers;
- No toxicity, no flammability and no explosion hazard, to guarantee for a reliable and safe employment in all the environments, especially in residential application.

KINETIC PROPERTIES

- Absence of or limited subcooling, to avoid thermal heat transfer to happen at temperatures different from design conditions;
- High nucleation and growth rate, to ensure phase change is completed in short times.

ECONOMIC PROPERTIES

- Abundance;
- Easy provisioning;
- Low cost.

2.2.1 Classification of Phase Change Materials

The most general classification of PCMs is the one based on the phase transition for which they are used, i.e. solid-solid, solid-liquid and liquid vapour. Even though transitions from solid or liquid to vapour state are the ones associated with the highest enthalpies [16], for practical reasons solid-liquid transitions are the ones widely employed in the various applications. There is no unique classification of PCMs belonging to this class and several models can be found in literature, but one of the most complete, which will be taken as

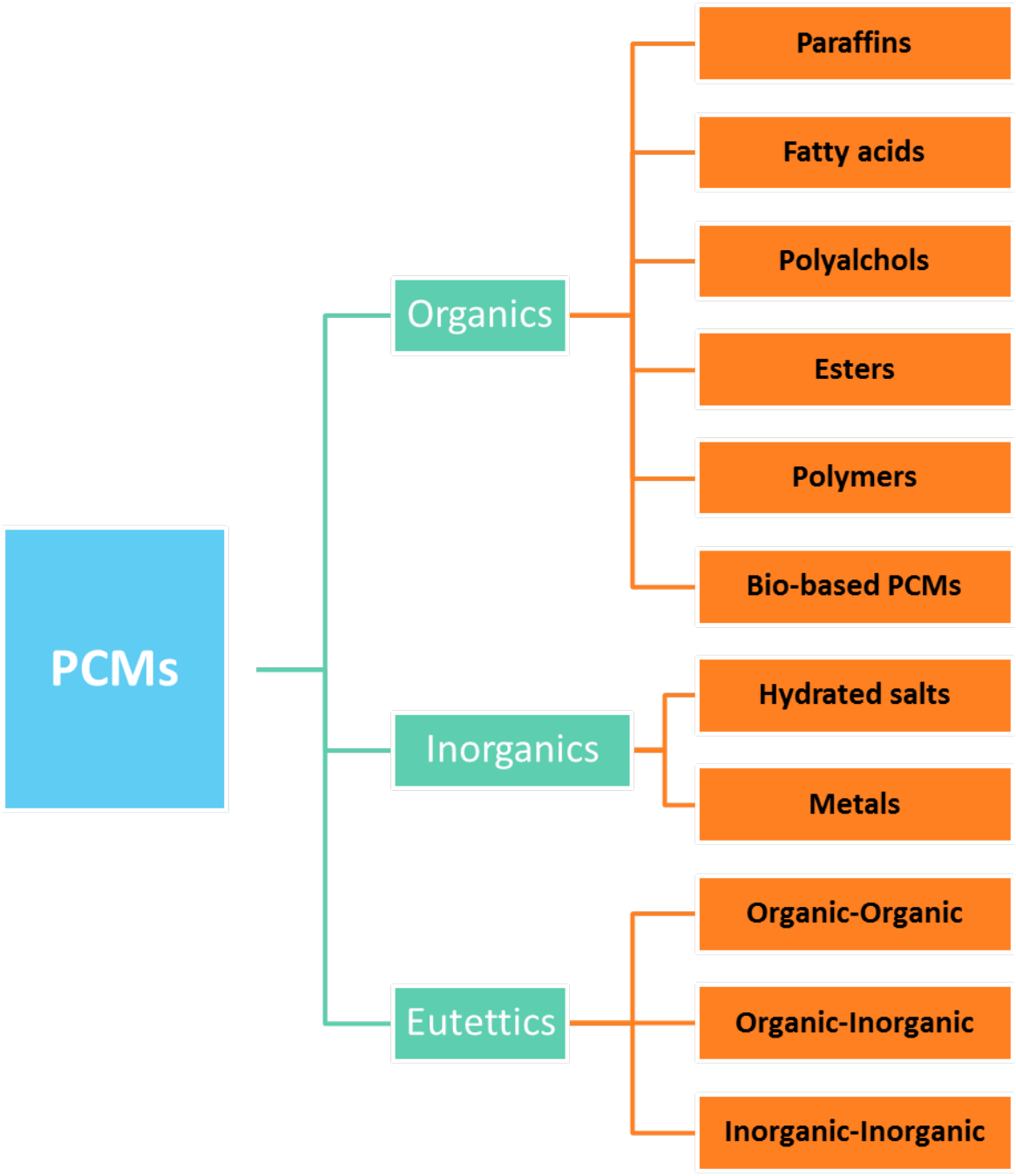

Fig. 2.10 Classification of PCMs

reference, is the one reported in [18] and schematically represented in Figure 2.10. In the following sections, general information about each class of materials, with special focus on the recent advancement of the research will be given, while at the end a comparison between the various classes of materials will be presented.

2.2.2 Organic PCM

Organic PCMs are in general stable both physically and chemically, thus avoiding the need for stabilisers or additives. One common feature of organic PCMs is the congruent phase change, meaning no segregation or latent heat decrement arises after multiple melting/solidification cycles, which occurs also with high nucleation rates. Other peculiarities are the low corrosion rates with metal and recycling possibilities. However, disadvantages in the application of this class of PCMs include the low thermal conductivity, the high volume expansion during phase transition, low density, flammability and the elevated cost [16, 14].

Paraffins

Among organic PCMs, an important class for solar and low-grade waste heat storage is those of paraffins, a mixture of mostly straight chain n-alkanes C_nH_{2n+2}, with n ranging between 20 and 40. Among the advantages determining a wide research associated with paraffins, there are their non-toxicity, low segregation, high stability, no corrosion problems on metals and a low cost. As stated in the previous section, like most organic PCMs, paraffins are characterised by low density, low conductivity and flammability. Melting temperature (the operating temperature for a PCM), density and latent heat can be increased by increasing chain lengths or creating mixtures of different hydrocarbons [18].

Fatty acids

Fatty acids are organic compound with chemical formula $CH_3(CH_2)_{2n}COOH$, derived from animal or vegetable sources, which makes them biodegradable and non-toxic. Compared to paraffins, they present high latent heat and good stability to cycles, with no subcooling effect, but they present a higher cost (twice or three times that of paraffins) and can determine metal corrosion [19]. Flammability is more marked than in paraffins, and therefore exposition to high temperature, flames or oxidising agents should be avoided [12]. Melting temperature range of fatty acids is generally below 70°C and are then employed mainly for buildings or low-grade heat storage [20, 21, 17].

Polyalcohols

Sugar alcohols (also known as polyalcohols) have been proposed as storage materials at medium temperatures (90–200 °C) for a long time, for their high melting enthalpies, low cost and non-toxicity [14]. On the other hand, different tests made on polyalcohols have reported a high grade of subcooling, which can severely compromise their effective application and which should be addressed in the hypothesis of a massive development. One feature of polyalcohols is the numerous crystalline forms that can be observed, each one with specific characteristics, as a function of additives and the preparation technique employed [22–24].

Esters

Esters are derived from acids in which one hydroxyl (–OH) group is replaced by one alkyl (–O) group [14]. Among the features of fatty acid esters are the narrow melting range and the limited degree of subcoolings. Their melting point is usually lower than 60°C. They are widely available and show excellent stability [22].

Polymeric materials

Importance of polymers among PCMs is continuously growing, thanks to the easiness with which modifications to their structure can be achieved in order to tailor properties for a specific application [14]. Among polymers, two of the most common used are HDPE and polyethilenglycole [16, 14, 24].

Bio-based PCM

Bio-based PCMs are a class of materials obtained from industrial residues, as soy oil, coconut oil, palm tree oil and animal fat and having melting point between 23°C and 78°C. With respect to other classes of PCMs they possess high latent heat, higher chemical stability, low flammability and no oxidation even after several cycles [25, 26]. Like other organic materials, though, their thermal conductivity is low, but some materials with increased thermal conductivity have been prepared by adding particles of graphite, carbon or metals.

2.2.3 Inorganic PCMs

The class of inorganic phase change materials mainly includes three categories of PCMs: salts and salt hydrates, metals and eutectic mixtures. In general, inorganic materials, if compared to organic ones, have a higher enthalpy (almost double), but a tendency to degradation after cycles, thus reducing their performances, considering also the presence of undesirable

phenomena such as segregation and subcooling . Thermal conductivity is higher and flammability low, but corrosion can arise as a consequence of their contact with metal surfaces [18, 27].

Hydrated salts

Hydrated salts are those salts that, during crystallisation, absorb one or more water molecules, the ratio depending on the specific material. Water included in such structures is generally called crystallisation or hydration water. Generic chemical formula for a hydrated salt is $A_xB_y{\cdot}n(H_2O)$ where n represents number of water molecules and A_xB_y represents metal carbonate, sulfite, phosphate, nitrite, acetate, or chloride. For this class of materials, there is no actual liquid-solid transition, their change is rather linked to hydration or dehydration of the salt, according to the following reactions:
$A_xB_y \cdot n(H_2O) \Leftrightarrow A_xB_y \cdot m(H_2O + (n-m)(H_2O)$
$A_xB_y \cdot n(H_2O) \Leftrightarrow A_xB_y + (n(H_2O)$

Hydrated salts are particularly interesting for their application as PCMs for their latent heat, high thermal conductivity, low thermal expansion, low corrosion rate on metals and compatibility also with plastics, low toxicity and affordable cost [16, 27]. The behaviour of the salts during phase transition is quite complex and is influenced by a wide variety of factors, such as the presence of additives or the velocity with which temperature variation occurs. According to these, melting can be:

- congruent, if dehydrated salt is completely soluble in crystallisation water at phase change temperature;
- incongruent, if the salt is not completely soluble in crystallisation water at phase change temperature;
- semi-congruent, if solid and liquid have different composition because of conversion of the hydrate into a lower-hydrated material through the loss of water [18].

Incongruent behaviour is the main limitation to their usage: since n moles of water of hydration are not sufficient to dissolve one mole of salt, the resulting solution is supersaturated and the solid salt, due to its higher density, settles down at the bottom of the container and is unavailable for recombination with water. This results in a constant decrement of latent heat available [18]. Numerous techniques have been studied to try to solve the complications linked to the incongruent melting, such as the addition of external water at regular times to reduce precipitation of solid: this is known as the “extra water principle”, which gives good results in terms of material stability but, at the same time, increases the temperature range

for melting and, more importantly, reduces latent heat of melting and requires complicated storage tanks. Another proposed solution is the addition of thickening agents to hold the solid in suspension (at the expense of kinetic of heat transfer) or encapsulation to reduce separation [22].

Metals

Metals and metal alloys could be considered optimum PCMs, especially for high temperature applications, because of their high latent heat per volume unit, high thermal conductivity, low vapour pressure, good stability and repeatability of the phase change, However, not much literature exists on their application [28].

Eutectics

An eutectic is a minimum-weight composition of two or more components which melt and freeze congruently, in order to form a mixture of the component crystals. The main advantage of eutectic compounds is that segregation is not likely to occur, considering also that melting happens at a specified temperature instead of a range. Eutectics used in thermal energy storage applications are mainly binary and ternary mixtures of inorganic salts: nitrate, chloride and sulphate salts of alkali and alkaline metals, such as magnesium, potassium, lithium and calcium are used as the main compounds to produce medium temperature eutectic mixtures [20], mainly for applications in concentrated solar plants.

2.2.4 Comparison of PCMs

In Table 2.4 the main thermophysical properties of the various classes of PCMs are reported, while in Table 2.5 a more comprehensive comparison between the materials is presented, highlighting the advantages and issues related to the application of each class of materials. All data have been taken from [28, 16, 18, 14, 25, 29, 27, 12, 30, 31, 22, 32]. Organic PCMs present low to medium melting points (-10 to 90 °C) and are widely available at a low cost (even though fatty acids are comparatively much more expensive than paraffins and esters). They have excellent thermal and chemical stability and a good latent heat per unit of weight, even though their density is generally lower than other class of materials, which penalises the latent heat on volume basis. Moreover, the exhibit little or no subcooling. On the other hand, they have extremely low thermal conductivity, high volume expansion and are flammable. Inorganic PCMs are characterised by higher latent heat per unit of weight and volume and the thermal conductivities are higher than organic materials, especially in the case of metal. Salt hydrates and eutectics are also widely available at cheap or reasonable prices and are not

flammable. On the other hand, they require nucleating and thickening agents to minimize the subcooling and they are highly reactive to metal materials. Their melting points (80 to 700°C) make them promising candidates for medium to high temperature applications. Finally, in Table 2.6, the applications that have been investigated, both in literature and at a commercial stage, are schematically represented: organic PCMs are the most extensively used, both in buildings and for coupling with solar systems of various types (production of domestic hot water, concentrated and non-concentrated solar for heat production), as well as in the textile industry, mainly for military textiles. Sugar alcohols, despite their poor thermal stability, have been considered for solar and waste heat storage, the same applications that fit the class of polymers. Hydrated salts have been extensively studied as well, especially since they are cheap, mainly for medium temperature applications. Up to now, the sector where PCMs have been extensively studied and applied is the thermoregulation of buildings, either with passive or active methods (i.e. inclusion of PCMs in gypsum and wallboards or coupling with heat pumps and air conditioning systems), but other fields of application are growing, such as the transportation industry, for the thermal buffer of vehicles, and the cooling of electronic devices. Further R&D is instead needed for medium to high temperature storage, both in industry and solar-related cases.

	Paraffins	Fatty acids	Sugar alcohols	Esters	Polymers	Bio-based	Hydrated salts	Metals	Eutectics
Melting range (°C)	-10÷80	10÷80	20÷200	10÷60	20÷200	-10÷80	30÷130	300÷1000	25÷250
Latent heat (kJ/kg)	140÷250	140÷220	250÷350	100÷200	150÷250	50÷150	150÷300	180÷500	100÷350
Specific heat (kJ/(kgK)	1.8÷3	2.0÷2.5	1.3÷1.7	2.0÷2.5	1.8÷2.6	2.0÷2.5	1.5÷3.3	2.0÷4.0	1.0÷1.7
Thermal conductivity (W/mK) (solid state)	0.1	0.15	0.2÷0.7	0.2	0.2÷0.5	0.1÷0.3	0.4÷1.6	8÷50	0.5÷1.3
Density (kg/m^3) (solid state)	700÷900	700÷900	1200÷1800	800÷1200	900÷1600	800÷1200	1500÷2200	1800÷7000	1500÷2200

Table 2.4 Thermophysical properties of the various classes of PCMs

	Paraffins	Fatty acids	Sugar alcohols	Esters	Polymers	Bio-based	Hydrated salts	Metals	Eutectics
Melting range (°C)	+	++	+++	++	+++	+	++	++++	+++
Latent heat	++	++	+++	+	++	+	+++	++++	+++
Thermal conductivity	+	+	++	++	+	+	++	++++	+++
Density	++	++	+++	++	+	+	+++	++++	+++
Thermal stability	++++	+++	+	+++	+++	++	++	+++	+++
Subcooling	+	+	++++	+	++	+	+++	++	+
Segregation	-	-	-	-	-	-	++++	++	-
Corrosivity	+	+	++	++ *	+++ *	+	++++	+++	++
Flammability/Explosivity	++++	+	+	+++	+++	++	+	+	+
Toxicity	++	+	+	+	++	+	+++	+++	++
Cost	+	++	++++	++	++	+	+	++++	+++
Availability	++++	++++	++	++++	++++	++++	++++		

+ low ++++ high

* corrosivity towards plastics, for the other materials the corrosivity is indicated towards metals

Table 2.5 Comparison of the various classes of PCMs

	Paraffins	Fatty acids	Sugar alcohols	Esters	Polymers	Bio-based	Hydrated salts	Metals	Eutectics
Heating/cooling of buildings	X	X		X	X	X			X
Cooling of electronic devices	X	X							X
Solar water heating	X	X							
Solar energy storage	X		X		X		X		X
Solar dryer	X								
Solar cooker		X	X						
Industrial waste heat (low temperature)	X						X		
Industrial waste heat (medium to high temperature)			X		X		X	X	X
Mobile applications (transportation)	X		X						
Textiles	X	X		X	X				

Table 2.6 Comparison of the various classes of PCMs according to their application.

2.2.5 Design issues: heat transfer enhancement of PCMs

One of the main drawbacks limiting the actual performance of latent heat storage systems is the low thermal conductivity of most PCMs, which negatively affects the heat transfer in the final system and reduces the practical applicability of such a technology. Figure 2.11 presents an overview of the methods proposed and studied for increasing the heat transfer when dealing with PCMs embedded in a storage system [27, 33, 30]. Great research efforts have been dedicated to the development of the material and the enhancement of its intrinsic characteristics. One of them is the addition of highly conductive porous materials to the base PCM. Such a choice brings a double benefit: the overall thermal conductivity of the material is increased, and extended heat exchange area is available, thus further increasing heat transfer. In [33], various experimental and numerical studies are reported. Porous materials used as matrix include metal foams (aluminium and copper) and graphite (either expanded or as a foam) , while in the majority of cases paraffin is used as the base PCM. It has been found that aluminium foam and expanded graphite are the most widely used thermal conductivity enhancers and allow reaching thermal conductivities up to 8 times higher than the one of the base material. It is, however, worth noticing that the low mass/volume fraction of the porous media decreases the volumetric heat storage density of the system. The use of highly conductive materials dispersed in the base PCM has also been investigated recently. Among such filler, there are nanopowders (such as Al, CuO, Cu, SiC), nanowires (NW) and carbon fillers (nanotubes). Outcome of the various studies has been that such material can increase the thermal conductivity of the PCM up to an order of magnitude. Among the low density materials that can, instead, be dispersed, carbon fibres, especially in combination with paraffins, have been studied. Such a method, even if not as effective as the previous ones, can overcome the problem of reducing the volumetric heat storage density of the system due to the high fraction of void of the matrix.

When considering the design of the storage system, heat transfer enhancement can also be achieved by using external devices, such as fins and heat pipes. Fins are metal surfaces that allow increasing the heat transfer area in contact with the PCM and can be realised in various shapes. Anular, elicoidal, longitudinal and transversal fins have been studied, mainly on shell and tube heat exchangers [33], and in all cases (i.e. disregarding the geometry and materials of the fins) the addition of fins has proved to increase the storage power, as well as the efficiency of the system during both charge and discharge. Common materials used for finned configurations include aluminium, copper and graphite. One important aspect to take into account is that fins do not affect the flow of the HTF, thus they do not increase the pressure drop of the storage. Another outcome of all the studies reported in literature is that

CFD simulation is often needed to proper design an optimized layout, in terms of geometry and number of the fins employed.

Another technique suitable to increase the thermal performance of a latent thermal energy storage (LTES) is the use of heat pipes, that make use of the condensation/evaporation of a fluid for the transfer of heat to the PCM. The advantage in the use of heat pipes is that they are able to transfer a high amount of heat in a narrow temperature difference, which is the case of application of the vast majority of latent heat storages. Up to now, however, the technical implementation of such devices is still under exploitation and further work is necessary.

Finally, a method proposed for heat transfer enhancement is the combination of PCMs with different melting temperatures, so that the heat flow inside the system is kept constant [33], especially when shell-and-tube configurations are used. However, most of the existing studies are numerical, while the practical and engineering aspects need to be developed. One of the most promising field of research is the application of "combined heat transfer enhancement": increasing the heat transfer area and enhancing the thermal conductivity of PCM simultaneously, which could lead to a massive application of latent heat storage technology in future years and a commercialization of more systems based on this technology.

2.3 Adsorption heat thermal energy storage: materials and technology

Differently from latent heat storage, storage involving the adsorption process requires a basic understanding of the working principles behind the phenomena on which it is based, that will be briefly described in the following section, while a general overview on materials for adsorption storage will be presented consecutively.

2.3.1 Operating principle of adsorption TES

Adsorption TES is based on the chemical potential deriving from the breaking of bonds between the sorbent material and the working fluid. It is mainly distinguished in:

- open adsorption storages; in which the system is not isolated from external environment and heat exchanges are made between air streams and the adsorbent bed;
- closed adsorption storages, in which the system is “air-free” and isolated from the environment, as in adsorption heat pumps.

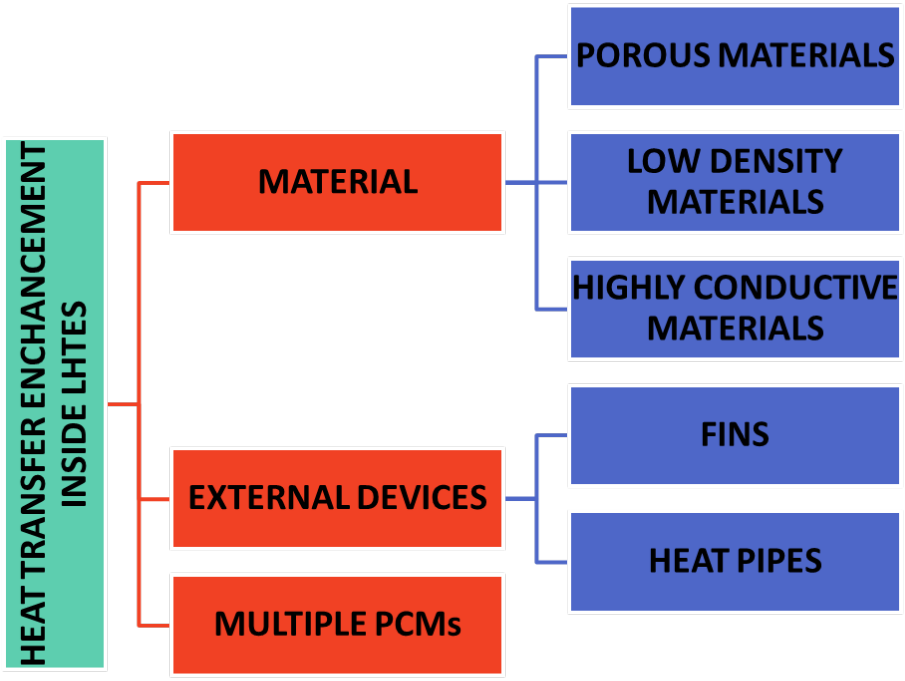

Fig. 2.11 Heat transfer enhancement methods for latent heat storage systems.

The working principle of open and closed adsorption storage is represented in Figure 2.12 and Figure 2.13, respectively.

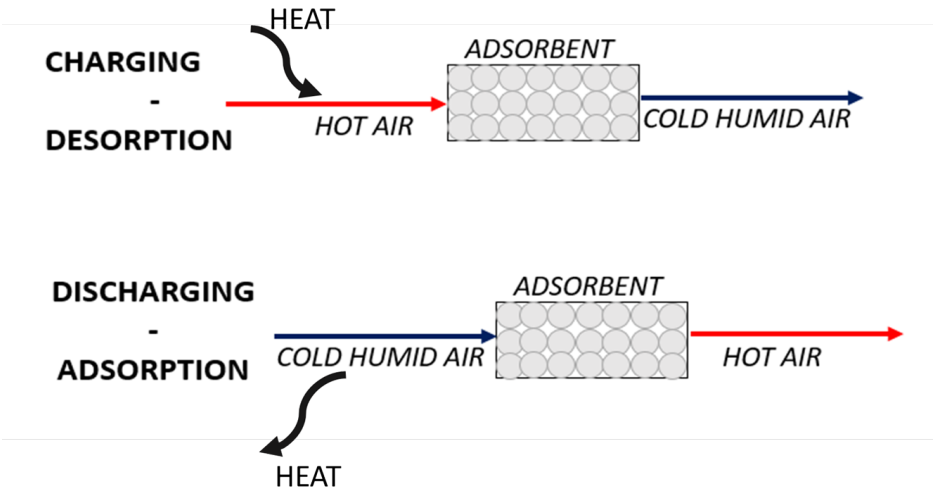

Fig. 2.12 Working principle of heat storage with open adsorption systems.

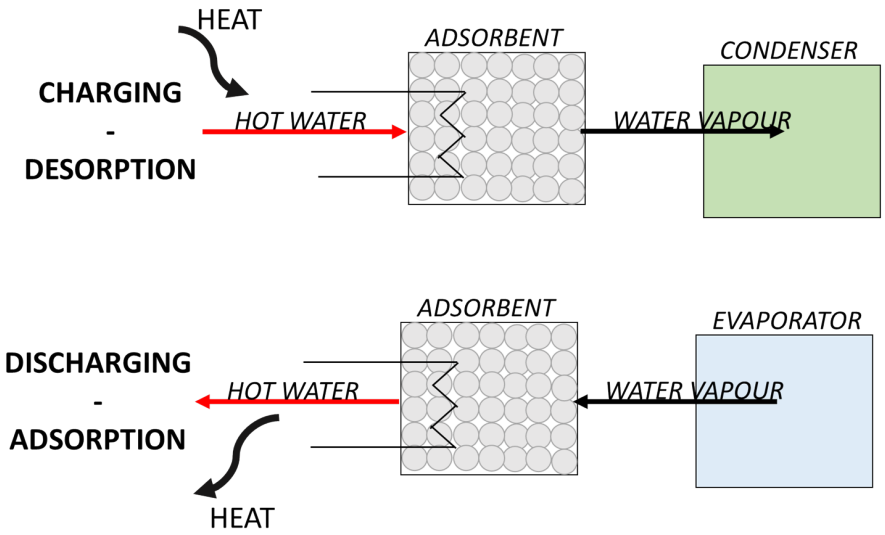

Fig. 2.13 Working principle of heat storage with closed adsorption systems.

In an open system, heated dry air, exiting for example from a solar panel, passes through a heat exchanger containing the adsorbent, generally in pellet or grains, thus releasing water contained in it, and exits the bed cool and saturated [34]. During discharge, humid air enters the adsorbent, which adsorbs its water content, leaving the air stream warmer and drier. It has to be noted that, for the discharging process to occur at acceptable rates, humidity content of

entering air through the adsorbent bed must be high [35]: when this condition is not fulfilled a humidifier is used to wet the air [34]. From the system design point of view, advantages in open systems are linked to their low investment cost and easiness in realisation, since only one component is needed.

In closed systems, the storage tank is composed of two vessels, connected by a duct for vapour to pass among the chambers. During charging, hot water is supplied to the reactor, which is a vessel containing a heat exchanger filled with the adsorbent, as to realise the desorption process. Adsorbate vapour flows through the connection into the other vessel, which is a condenser/evaporator. During charging, vapour passes into liquid form and condensation heat is released to a heat sink. Discharging process makes use of an external heat source to drive the evaporation process in the second vessel, working in this case as evaporator and then the adsorbate vapour flows through the other vessel, where adsorption occurs. Depending on the practical requirement, a cooling effect can be produced by the evaporator or a heating effect can be created by the reactor [35]. This feature makes the sorption thermal storage processes able to offer "cold storage" function in summer and "heat storage" function in winter. If external temperature is too low to drive evaporation process during discharging, another source, such as ground boreholes, is needed. Compared to open systems, closed ones involve a more complex configuration, leading to higher investment costs, together with maintenance necessities since the whole system works under vacuum conditions that should be periodically checked. However, flexible operation and a wider choice of working pairs make them promising and interesting for application in TES.

2.3.2 Basic cycle of closed adsorption TES

Figure 2.14 reports the working cycle for a closed adsorption TES on the Clapeyron diagram, where the main heat fluxes associated with each phase are represented. Indeed, the following sections will be mostly devoted to closed adsorption systems, but Figure 2.15 and Figure 2.16 schematically represent the typical adsorption TES architecture both for open and closed systems, where the heat contributions to each phase of the storage process are highlighted. In a closed adsorption TES, during charge (i.e. desorption), the the adsorbent material, which is at the maximum content of adsorbate, is regenerated by supplying the amount of heat:

$$Q_{ch} = Q_{ish} + Q_{des} \tag{2.7}$$

Q_{ish}, is the isosteric heat, which represents the amount of sensible thermal energy spent to heat up the adsorbent material and the adsorbate under isosteric conditions, in order to increase the pressure of the adsorber up to the condenser pressure p_{cond}. Q_{des} instead is

the energy spent to desorb the adsorbate, plus a small amount of specific heat to increase the adsorbent material temperature up to the final temperature, T_{des}. During this phase, the desorbed vapour is condensed in the condenser, where the heat of condensation, Q_{cond}, is released. Once the charging process is completed, the connection between condenser and adsorber is closed. If the adsorbent and adsorbate are kept separated, the energy can be stored for a theoretically infinite period. During discharging phase (i.e. adsorption), the adsorbent material is enriched in adsorbate content, releasing the amount of heat:

$$Q_{disch} = Q_{isc} + Q_{ads} \tag{2.8}$$

Q_{isc}, is the isosteric heat delivered during the cooling process, during which the pressure of the adsorber is lowered to the evaporator pressure p_{ev}. Q_{ads} instead is the enthalpy of adsorption, plus a small amount of specific heat associated to the cooling of the adsorbent to the final adsorption temperature, T_{ads} During this phase, the adsorbate is evaporated in the evaporator adsorbing heat from the ambient, Q_{ev} [36].

According to the operation of the storage, a different useful effect can be obtained:

- if short term heat storage is needed, the useful energy extracted from the storage is the energy of condensation and the energy of adsorption;
- if long term heat storage is required, the useful energy extracted from the storage is the energy of adsorption;
- if the storage is needed to provide cold energy, energy of evaporation represents the useful effect of the process.

2.3.3 Thermodynamics of closed adsorption TES

The heat provided during the charging process is defined as [34]:

$$Q_{ch} = \int_{T_{des}}^{T_{ads}} \int_{w_{min}}^{w_{max}} mc_{p_{adsorbent}}(T)dw + \int_{w_{min}}^{w_{max}} \Delta H_{ads} dw \tag{2.9}$$

The specific heat of the adsorbent material is calculated according to the rule of linear addition [36]:

$$c_p(w) = (1-w)c_{p_{dry}} + wc_{p_{ref}} \tag{2.10}$$

where: $c_{p_{dry}}$ is the specific heat of the dry adsorbent material, w_{ave} is the average amount of refrigerant processed and $c_{p_{ref}}$ is the specific heat of the refrigerant. The heat provided

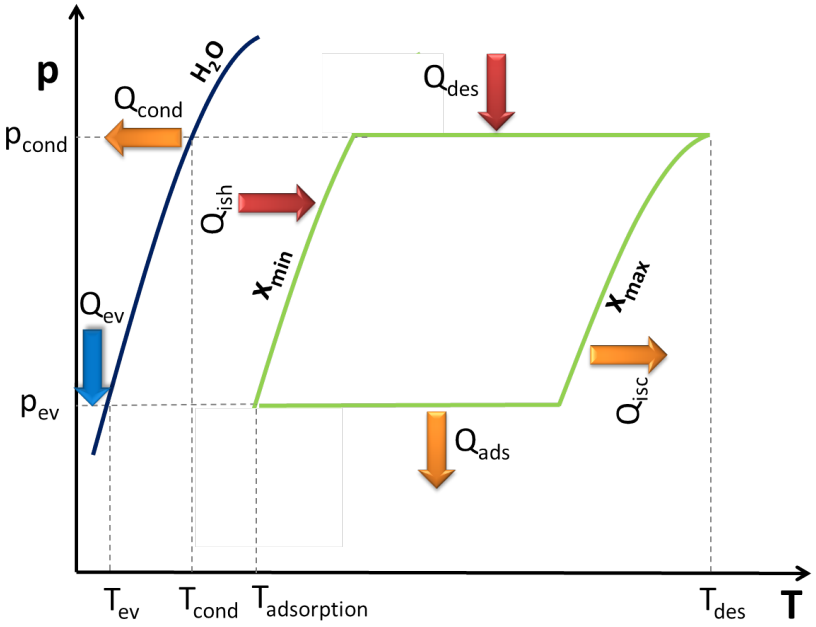

Fig. 2.14 Clapeyron diagram for a closed adsorption TES.

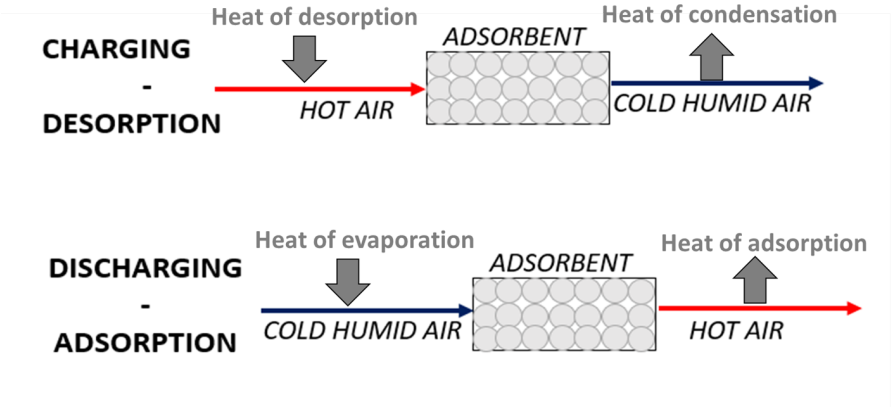

Fig. 2.15 [Heat fluxes in an open adsorption TES.

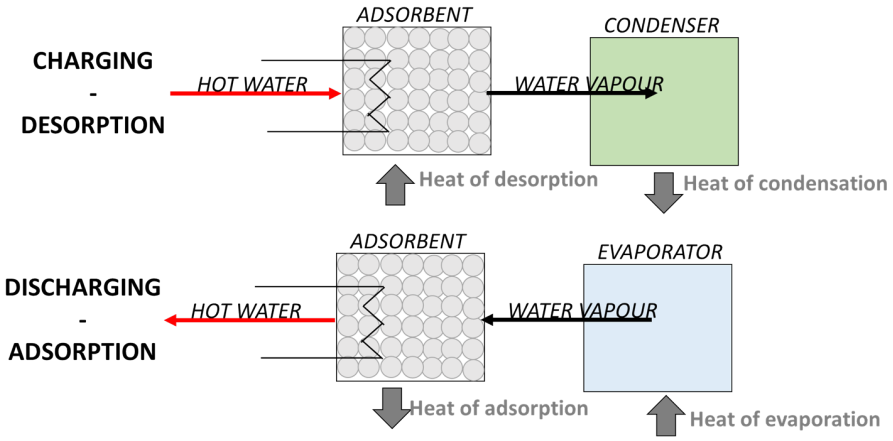

Fig. 2.16 Heat fluxes in a closed adsorption TES.

during the discharging process is similarly defined as:

$$Q_{disch} = \int_{T_{des}}^{T_{ads}} \int_{w_{min}}^{w_{max}} mc_{p_{adsorbent}} dw + \int_{w_{min}}^{w_{max}} \Delta H_{ads} dw \tag{2.11}$$

The heat released at the condenser is given by:

$$Q_{cond} = \lambda_{cond_{ref}}(T_{cond})(w_{max} - w_{min}) \tag{2.12}$$

where $\lambda_{cond_{ref}}$ is the heat of condensation of the refrigerant, calculated at the condensation temperature. The heat at the evaporator is given by:

$$Q_{ev} = \lambda_{ev_{ref}}(T_{ev})(w_{max} - w_{min}) \tag{2.13}$$

where $\lambda_{ev_{ref}}$ is the heat of evaporation of the refrigerant, calculated at the evaporation temperature.

Usually, when speaking of adsorption TES, the energy density of the material is calculated considering the adsorption enthalpy [35]:

$$E_{m_{ads,TES}} = \frac{\Delta H_{ads} \Delta w}{m_{adsorbent}} \tag{2.14}$$

or

$$E_{V_{ads,TES}} = \frac{\Delta H_{ads} \Delta w}{V_{adsorbent}} \tag{2.15}$$

2.3.4 Adsorbent materials

The main features for an adsorbent to be suitable for thermal storage are [34, 35, 37]:

- high energy storage density, which means high heat of adsorption;
- low charging temperature;
- high differential uptake of adsorbate;
- high heat and mass transfer properties to ensure designed output power;
- thermal stability;
- low cost.

Indeed, as for PCMs, no material among the currently synthesized ones possesses all these features, and therefore a choice must be made based on specific application. A general outline of materials available for solid sorption systems is given in Figure 2.17.

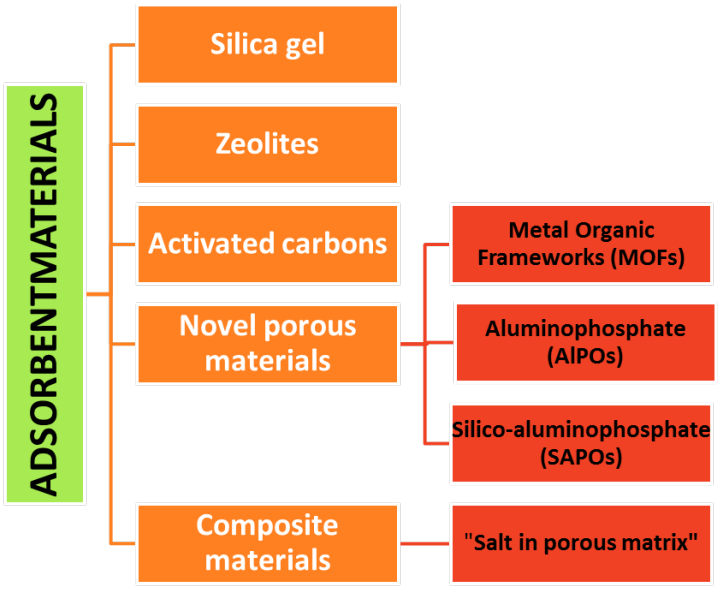

Fig. 2.17 Classification of adsorbent materials.

Silica gels

Silica gels are the most common among sorbents used in heat pumps applications, for their low cost and reliability and for the desorption temperatures lower than 90°C. However, their calculated storage density is lower than water (50 kWh/m^3 against 70 kWh/m^3 of water for

at ΔT of 60°C) and therefore they might possess some attraction only for seasonal energy storage [35].

Zeolites

Zeolites are crystalline aluminosilicates of alkali or alkali earth elements, such as sodium, potassium, and calcium [38], with a tetrahedral structure, with each tetrahedron centred on an Al or Si atom and the oxygen atoms on the vertexes. Both natural and synthesised zeolites are available, the most common being types 4A, 5A, 10X, 13X and Y Several studies have been conducted on the use of natural zeolites for thermal storage [35], for their low cost and wide accessibility. The main drawbacks linked to the use of such materials is the high heat temperature needed to drive the desorption, which occurs at 150-200°C. Among the studies on zeolites, Shigeishi et al. [39] compared activated alumina and silica gel with synthetic zeolite 4A, 5A, and 13X and determined zeolite 13X was the best adsorbent, with an energy density of 148 Wh/kg. Janchen et al. [38] studied in a lab-scale storage prototype different modified zeolites of the type NaX, NaY and NaA as well as mesoporous materials impregnated with hygroscopic salts. Their results showed that for Mg and Li-exchanged zeolite an energy density of 149 Wh/kg to 225 Wh/kg can be obtained.

Novel Porous Materials

Nowadays, (silico)aluminophosphates (SAPOs,AlPOs) and metallic organic framework (MOFs) can be considered the most promising classes of sorbents in terms of high water adsorption capacity and low regeneration temperature [40]. A number of studies were carried out on different types of (silico)aluminophosphates (ALPO5, ALPO18, SAPO34, etc.) [41, 42], confirming the interesting properties of such materials for adsorption cycles. Regarding their application for thermal energy storage, Janchen et al. [38] have measured the density energy of SAPO-34 and obtained a value of 290 Wh/kg.

In addition, evaluation of super-molecular Metal-Organic Frameworks (MOFs) for application in sorption systems is a major trend of the research in this field. These materials are made of metal ions or clusters connected to organic molecules. MOFs attracted attention due to the open crystalline structure and very high surface area. Some studies revealed a large capacity of water adsorption under realistic operating conditions [41, 42]. Possible obstacles for practical use are a significant ad/desorption hysteresis and insufficient stability.

Composite materials

Composites “salt in porous matrix”, are two-components materials invented by BIC-RAS (Novosibirsk, Russia) based on a porous host matrix with a salt inside its pores [43]. A proper choice of the matrix and pore filling solution allows a wide variation of the sorbent properties to fit the requirements of various applications. Possible issues that must be further investigated for practical utilization are the risk of leakage of the corrosive salt and the long-term hydrothermal stability. Among composite materials [44, 45], composites with $CaCl_2$ have showed superior heat storage density, with values up to 264 Wh/kg. Yu et al. [46] have developed new consolidated sorbents with activated carbon (AC) and LiCl, which have a theoretical storage density up to 500 Wh/kg, as well as a silica gel/LiCl [47] impregnated sorbent, which has been found to have a storage density of 150 Wh/kg at 90°C.

2.3.5 Comparison of adsorbents

Differently from the case of PCMs, a comparison of adsorbent materials requires the definition of the boundary conditions under which the material will be employed. In Table 2.7, the main thermophysical properties of the various adsorbents are presented. Instead, in Table 2.8, a comparison table of the various material is presented, highlighting the main drawbacks and benefits associated to each class. All the data used in Table 2.7 and Table 2.8 are taken from [36, 42, 48–53]. It is worth remarking that the "+" and "++++" values in Table 2.8 do not indicate a negative or positive value, respectively, but rather a low or high value from a quantitative point of view. Newly-developed materials (composites, MOFs, novel aluminophosphates) can be effectively regenerated at lower temperatures, significantly below 100°C and, especially in the case of the MOFs and the composite materials, have a higher uptake under the typical boundary conditions of their application. In particular this applies to the adsorption of alcohols on "modified salt in matrix" silica gels, MOFs and some classes of activated carbons. On the other hand, such classes of materials are still expensive or not commercially available. Silica gels and most classes of zeolites (13X, 4A) are cheap and easily available, but present the worst performances. It is also worth noticing that the thermal conductivity of the materials is generally low, and therefore modifications have been proposed to enhance it (for example, by adding carbonaceous structures). One important remark is that, despite the low toxicity and corrosivity of the adsorbent materials, the toxicity, flammability and compatibility with the construction materials of the refrigerants must be carefully checked.

Finally, in Table 2.9, the various classes of adsorbents are compared according to their possible applications. By comparing Table 2.9 with Table 2.6, it is possible to notice that some

application of PCMs and adsorbents overlap (e.g. solar water heating, mobile applications). One of the advantages of using adsorption technology is the possibility to realise a cold storage charged with waste heat, as in solar ice-makers and systems for food preservation [54].

	Silica gels	Zeolites	AlPOs/ SAPOs	Composites	MOFs	Activated carbons
Adsorption heat (kJ\kg)	160÷180*	50÷300*	250÷300*	50÷250*	20÷200**	45÷900***
Typical desorption temperatures [°C]	50÷80	70÷350	60÷90	60÷90	60÷150	80÷200
Density (kg/m^3)	650÷700	650÷900	800÷900	300÷600	1000÷1200	700÷750
Specific heat (kJ/kgK)	0.8÷0.9	0.85÷0.95	0.85÷0.95	0.95÷1.05	0.8÷1.2	0.8÷1.5
Thermal conductivity (W/mK)	0.15÷0.20	0.15÷0.25	0.15÷0.25	0.15÷0.30	0.10÷015	0.15÷0.75
Possible refrigerants	water	water	water	water,methanol, ethanol	water,methanol, ethanol	methanol,ethanol, ammonia
Amount of uptake exchanged in a typical cycle [g/g]	0.03÷0.10	up to 0.2	up to 0.25	up to 0.8	0.16÷0.40	015÷0.60

* the heat of adsorption is calculated for a cycle with T_{des}=100°C, T_{cond}=30°C, T_{ads}=50°C, T_{ev}=10°C, with water as sorbate

**the heat of adsorption is calculated from isotherms at 298 K, 303 K and 333 K, with water as sorbate

***the range for the heat of adsorption is calculated with methanol and ammonia as sorbates

Table 2.7 Thermophysical properties of the various adsorbents.

	Silica gels	Zeolites	AlPOs/ SAPOs	Composites	MOFs	Activated carbons
Adorption heat	+	++	+++	+++	+++	++++
Density	++	++	+++	++	++++	+
Thermal conductivity	+	+	+	++	++	+++
Desorption temperature	+	+++	++	++	+++	++
Uptake exchange in a typical cycle	+	++	++	++++	+++	++++
Thermal stability	++++	++++	++++	+++	++	++++
Dynamic properties	++	+++	+++	++	+++	++
Toxicity	-	-	-	-	-	++
Cost	+	++	+++	+++	++++	+
Availability	++++	+++	++	+	++	++++
		+ low	++++ high			

Table 2.8 Comparison of adsorbent materials.

	Silica gels	Zeolites	AlPOs/SAPOs	Composites	MOFs	Activated carbons
Heating/cooling of buildings	X		X			
Solar water heating			X			
Solar energy storage		X				
Solar dryer	X	X				
Industrial waste heat (low temperature)		X		X	X	
Industrial waste heat (medium to high temperature)		X			X	
Mobile applications (transportation)		X				
Cold storage for food/medical preservation		X	X		X	X

Table 2.9 Comparison of adsorbent materials according to their application.

2.4 Thermal energy storage for low-grade heat

The development and analysis of the thermal storage systems described in the present thesis, is limited to a specific — and still underexploited — field: low-grade heat storage, i.e. at temperatures below 120°C. Indeed, while high-grade waste heat has been widely studied and exploited [55], heat at lower temperatures is often wasted, despite its great potential. As an example, in Figure 2.18 and Figure 2.19 taken from [55], waste heat availability in iron, steel and copper works industry is represented for various processes, together with the corresponding temperature level: what is clear is that the amount of heat under 90°C is huge and heterogeneous.

However, the processing industry is not the only field where the application of a thermal energy storage for low-grade heat could be beneficial: the possible areas of applications identified for such systems are reported in Figure 2.20 and will be briefly discussed in the following sections, in order to highlight the current situation and the possible benefits arising in the addition of a storage system, or the replacement with a more efficient one.

Buildings

The energy consumption of the building sector (including both residential and commercial) amounts to about 40% of the overall demand in Europe [56]. It follows that the application of methods to increase the energy efficiency and reduce the need for heating and cooling systems in building is a key topic. In this context, multiple applications of TES have been investigated and tested [56, 57]:

- active thermoregulation, by integrating the storage in the constructive elements of the building (façade, walls, HVAC ducts or air handling units, ceiling and floor), which is usually accomplished with low-temperature PCM (i.e. with melting temperature lower than 40°C).

- Warm storage (45-70°C) for the production of DHW or direct feeding of the heating system. Usually, solar plants installed in residential houses include a sensible heat storage using water to fulfil such a need.

- Heat storage in the range 80°C-120°C, coupled to solar thermal heating and cooling plants. In the vast majority of installed plants, water storage tanks are included to serve as a thermal buffer of the solar section of the system. However, several studies have highlighted the great improvement achievable by replacing sensible heat storages with latent or sorption ones [57–59].

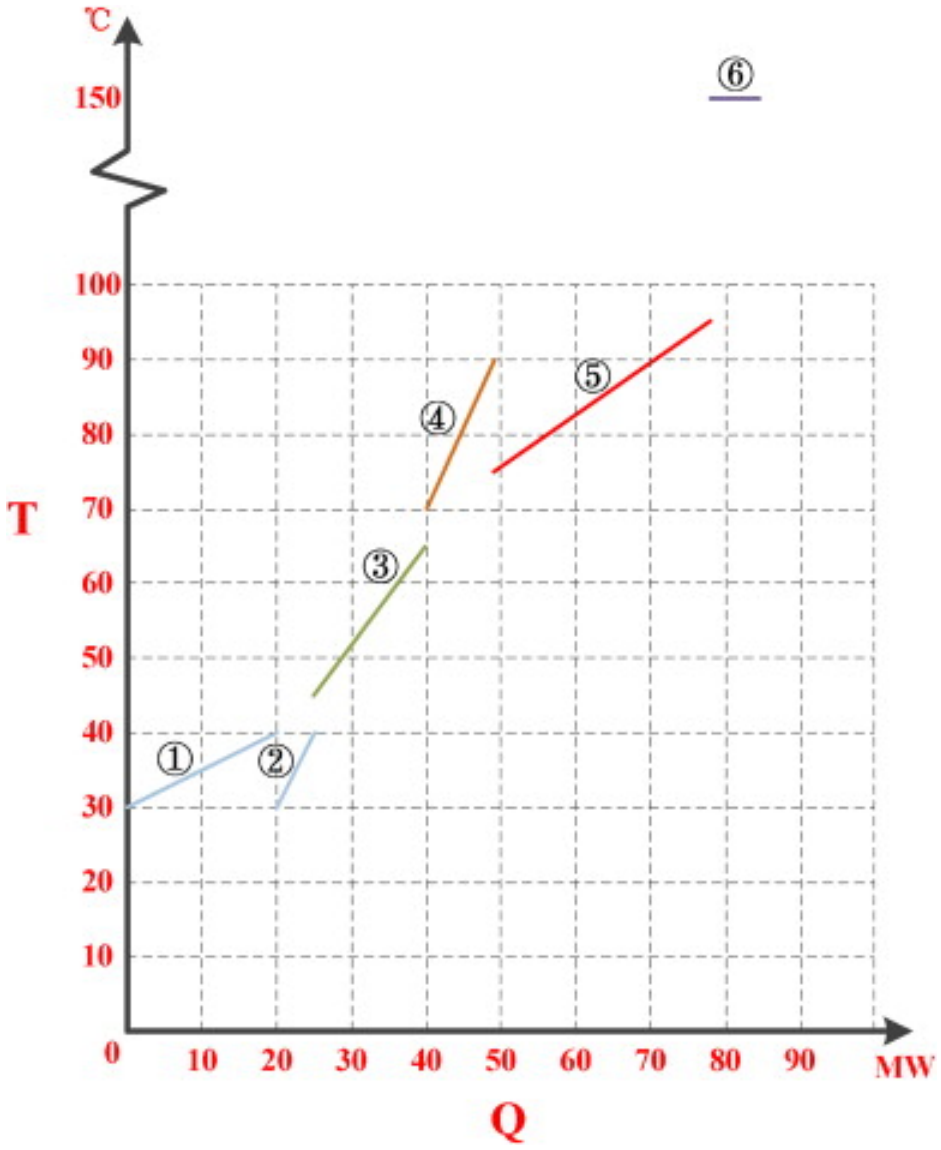

Fig. 2.18 Waste heat distribution in a typical copper smelter, in terms of temperature level and amount of heat available. Each number represents a different process.

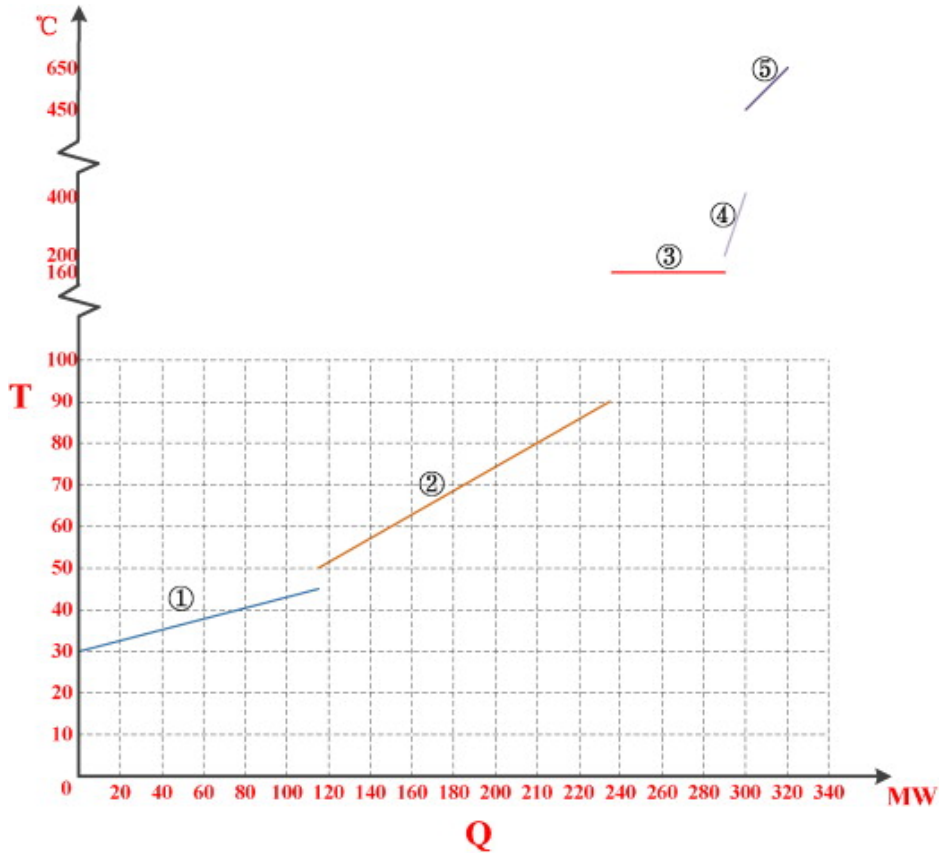

Fig. 2.19 Waste heat distribution in a typical iron and steel works, in terms of temperature level and amount of heat available. Each number represents a different process.

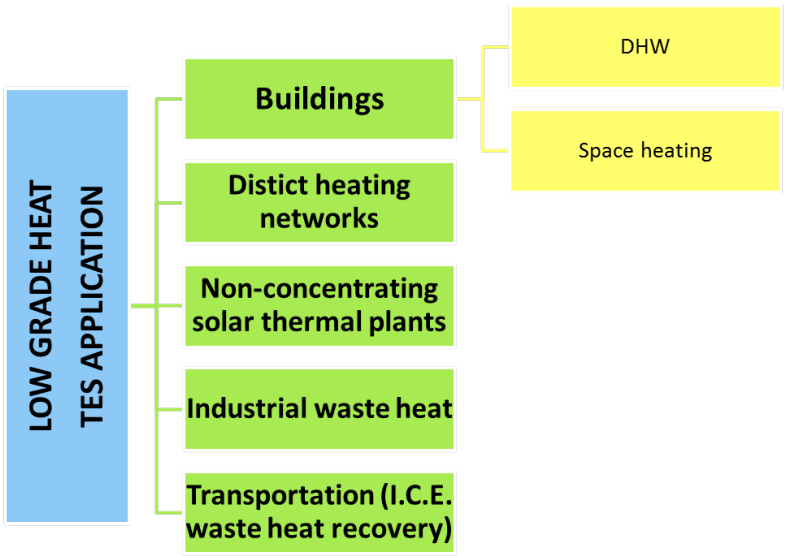

Fig. 2.20 Fields of application for low-grade heat TES.

District heating networks

The European Commission, with its report, Energy Roadmap 2050, has defined the scenarios under which 80% reduction in annual greenhouse gas emissions in 2050 compared to 1990 levels can be achieved. One of the strategies that show a great potential towards this target is the upgrade from single generators to district heating networks [60]. The simulation of such a scenario indicates that, not only is possible to achieve the target proposed, but also at a cost for heating/cooling 15% lower than current alternatives. Moreover, as reported in [61], the new generation district heating networks should be designed for high efficiency at low temperatures and peak shaving, objectives that can be fully satisfied only with the integration of thermal storage systems for DHW and the heating substations. At the moment, the facilities including a thermal storage make use of sensible systems (with water or pressurised water), aquifer storages or soil storages [62].

Non-concentrating solar plants

Most of non-concentrating solar plants, using flat plate or evacuated tube collectors, are those installed in residential or office buildings [57, 35], where a storage tank is almost always present. Indeed, the application of water for sensible heat storage is basically the only option available, especially for the extremely low cost of the solution.

Industrial waste heat

Industrial process heat is a great resource, which is often wasted, as stated before. Moreover, a great number of different applications exist and could be profitable. A systematic analysis based on cases from different sectors is presented in [63]: what clearly emerges is that heat at different temperature levels is available, and in the order of some MWh. In accordance with what reported in [64], the industrial sectors where the main share of heat at a temperature lower than 100°C is available are mainly the chemical industries, the paper and pulp processing and the food and beverages sector. According to the estimation made in [64], more than 40 TWh/y are needed for the secondary sector in Germany within this temperature range. The benefits of using a TES in such an industrial context has been highlighted also in the analysis on a medium-sized brewery performed in [65, 66]. According to the analysis in [63, 65], the current situation either comprises the usage of sensible materials or no storage are included in the process layout at all.

Transportation

Increasing the energy efficiency in vehicles is one of the key issues that have lead to a broad investigations of waste heat recovery on-board. Several possibilities exist for the utilization of a thermal energy storage on passenger, commercial and military vehicles, as summarised in [67]:

- passenger cooling or heating, by replacing the electrical air conditioner with a thermally-driven one making use of waste heat as driving source. In this case, the studies are focused on the application of sorption systems, either directly coupled to the engine or using a latent heat storage.

- Thermal protection of the electronic equipment on board of military vehicles, since they can reach temperatures up to 85°C. This is usually accomplished with a cooling loop similar to that of the main engine, but some studies have revealed the great potential of PCMs.

- Thermal buffering of the battery pack of electric vehicles, since during charging and operation they undergo heating, which, in turns causes a drop of the power output from the rated one. The commercially available vehicles use the cabin air conditioner to prevent such a phenomenon.

- Thermal buffering of the coolant loop, which is usually oversized to fulfil peak power: using a suitable storage system, the size of the components in the loop could be reduced.

Chapter 3

Development of a latent thermal energy storage system

3.1 Definition of the problem and methodology

In this chapter, the whole process of development of a lab-scale storage using a phase change material as the storage medium will be reported. The approach followed in the description of the activity is focused at highlighting the progress with respect to the state-of-art. Accordingly, after a short description of the main features of the system, the recent developments regarding the specific application will be drawn. After the overall presentation of the activity carried out, the main outcomes will be summarised.
The main boundaries of the project and the target characteristics required to the storage are:

- temperature of the heat source in the range 80°C-100°C;
- temperature of the heat to be supplied to the user in the range 65-70°C;
- energy density higher than 100 MJ/m^3.

This is consistent with charging through non-concentrating solar collectors and discharging in a temperature range suitable for Domestic Hot Water (DHW) production or driving of thermal chillers/heat pumps. The methodology followed in the development of the system is summarised in Figure 3.1. In particular, the choice of the storage material was realised starting from an experimental campaign carried out at CNR-ITAE (and not described in detail in the present work). Once the best performing material was identified, a first design of the system was proposed, following the criteria reported in [68]. Since not much data is available in literature on prototypal systems based on latent heat storage in the temperature range identified, it was decided to follow a double approach: on the one hand, a custom-made

system based on fin-and-tubes configuration was realised; on the other hand, an asymmetric plate heat exchanger chosen among commercial ones was tested and compared to the former configuration. Both systems were experimentally characterised using a testing rig at CNR-ITAE, that was specifically adapted for the testing of hybrid and latent heat storages with charging temperatures up to 100°C. The results of the experimental benchmarking were used for a critical review of the design of the system and propose an optimization. In order to accomplish such a goal, a simplified model was developed in COMSOL Multiphysics 5.2a, suitable for the definition of an improved design of the system, and validated with the experimental measurements.

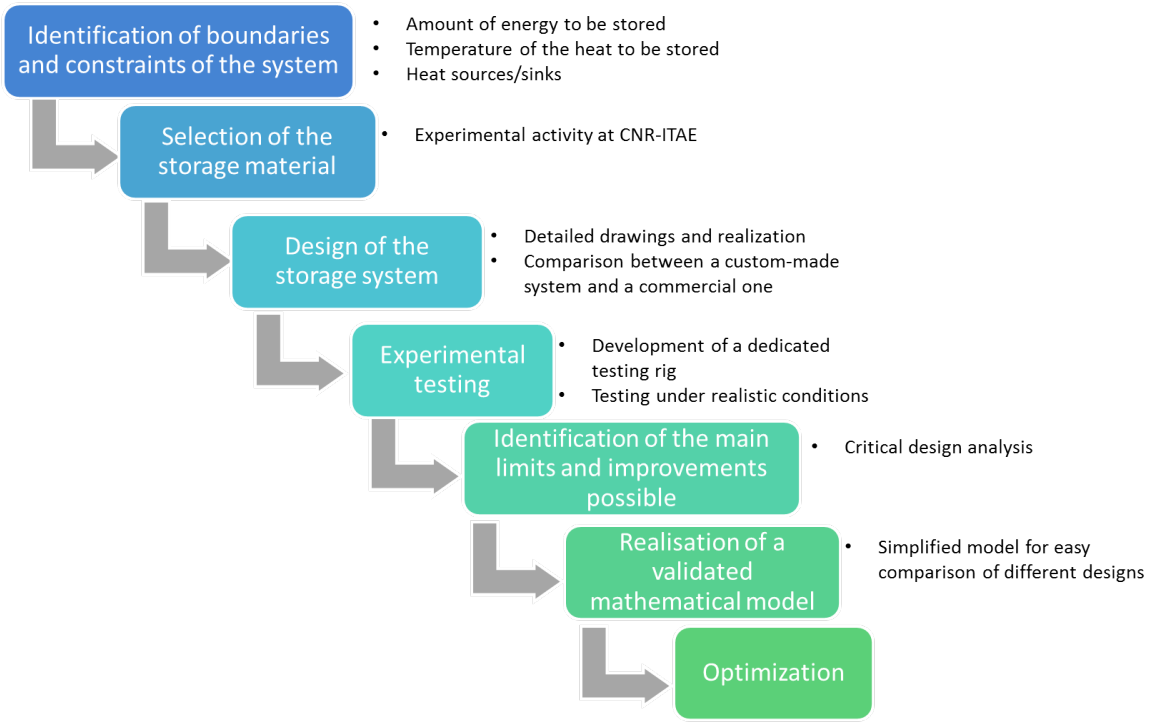

Fig. 3.1 Methodology followed in the development of a latent heat storage system.

3.2 Recent developments: LTES for low-grade waste or solar heat

Design of the system

The issues related to the design of a latent heat storage system are summarised in [68] and are schematically reported in Figure 3.2. It is possible to distinguish three different levels before the final realisation and application of a latent thermal energy storage (LTES): a first screening has to be made regarding the materials available and their practical application, that can be limited by problems such as the cycling stability, degradation, subcooling and so on. In addition, as already discussed, heat transfer inside a PCM is often a critical issue and therefore both the design of the material and the component should take that into account. At the component level, the decisions on the layout of the system and its thermal insulation should be made. However, as for the case of the material and component level, an overlapping with the system level can be identified, mainly regarding the operation of the system (e.g. the possibility of simultaneous charge/discharge that influences the construction of the heat exchanger that is included in the storage). One aspect that is not commonly addressed is the analysis of the whole life cycle of the system, that should be instead regarded in the future, in order to be actually able to compare the operation of this type of storages with traditional sensible heat ones.

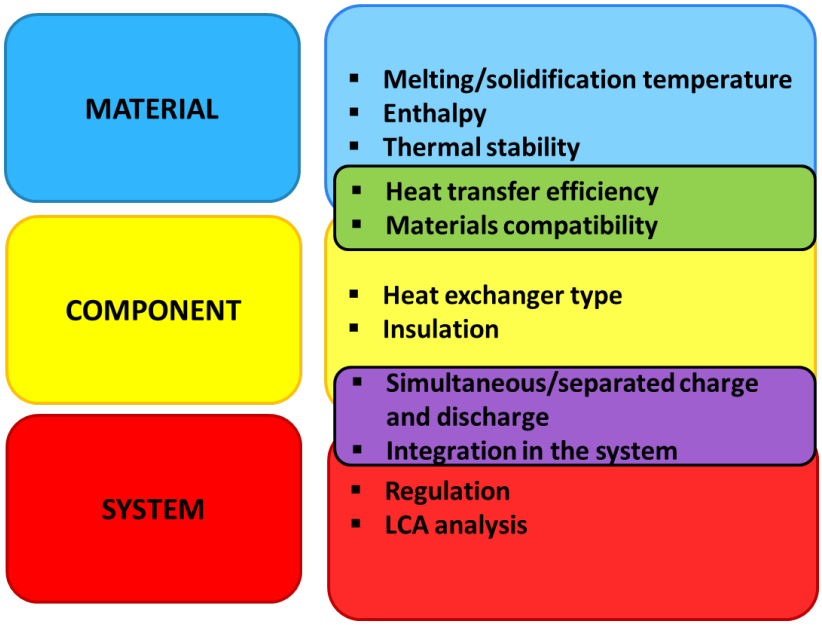

Fig. 3.2 Design of a latent heat storage system.

Prototypes of LTES for low-grade heat applications

The studies in literature regarding the application of phase change materials in systems with heat at 60°C-100°C mainly comprise the coupling with solar systems, either for domestic or industrial use [20, 69]. Within this field, different applications have been investigated:

- systems for DHW production, with the storage embedded either in the solar collector [70, 71] or as a stand-alone component [72, 73];
- systems based on air solar collectors and PCM-based thermal storage for building heating applications [74];
- non-concentrating solar thermal [75].

Many of the studies for this specific application focus on numerical modelling or energy analysis. For instance, [75] reports the energetic analysis of a solar cooling plant employing a latent thermal storage on the medium temperature loop to support the heat rejection of the absorption cooling machine to the ambient. [57, 76] focus on energy, exergy and economic analysis in including a latent heat storage into solar cooling plants equipped with absorption chillers. In [77] a comparison is carried out between a standard open wet tower and a PCM storage inserted in the heat rejection loop of a solar cooling plant. The analysis was conducted through system simulation in different zones in Spain and was aimed at proving the feasibility of the technical solution proposed.

Regarding the experimental works carried out on materials and components, the majority of them is focused on high temperature thermal storage for coupling with concentrating solar collectors (e.g. parabolic through, Fresnel collectors) [78–80]. In [81], a prototype is described, made up of a vertical spiral heat exchanger filled with paraffin wax having a melting temperature range around 80°C. Tests have been carried to analyse the solid-liquid transition, and natural convection occurring within the melting PCM was found to be a great parameter of influence on heat transfer dynamic.

Outcome of the presented literature analysis is that, in the investigated temperature range (60-100 °C) further experimental work is needed towards the characterization of latent heat storage systems.

3.3 Research activity on PCMs at ITAE

The identification of promising PCMs to be employed in high temperature thermal storage for solar cooling applications started from the definition of the reference system configuration. The activity was carried out at CNR-ITAE and is described in detail in [82]. Since the activity

is not object of the present thesis, in the following sections only the main results will be presented. After having carried out a literature and market survey, nine different PCMs were identified and acquired for their experimental characterization. The selected PCMs have nominal melting temperature in the range above reported and belong to different classes of materials, both organic and inorganic. Three of them are already on the market and are manufactured by the PCMproducts company. In Table 3.1 the selected PCMs are summarized along with their nominal melting temperature and enthalpy and the specific cost.

	Class		Material and purity	Nominal melting temperature °C	Nominal melting enthalpy kJ/kg	Specific cost €/kg
Non-commercial	Organics	Phenols	α-Naphthol (≥99%)	96	163	900
		Sugar alcohols	Xylitol (≥99%)	94	263	400
		Sugar alcohols	D – Sorbitol (≥98%)	97	185	150
		Amide	Acetamide (~99%)	81	241	200
	Inorganics	Salt hydrates	$KAL(SO_4)\cdot 12H_2O$ (APSD) (≥98%)	91	184	350
		Salt hydrates	$(NH_4)AL(SO4)_2\cdot 12H_2O$(AASD) (≥99%)	95	269	150
Commercial	Organics	Paraffins	Plus-ICE A82	82	155	15
	Inorganics	Salt hydrates	Plus-ICE S83	83	141	8
		Salt hydrates	Plus-ICE S89	89	151	8

Table 3.1 PCMs selected for the experimental characterization at ITAE.

The characterization of the selected PCMs was performed by means of a DSC-1 Mettler Toledo, by performing five consecutive heating and cooling cycles between 30°C and 110°C with heating rate of 5°C/min, with about 10 mg sample of material, in closed crucible configuration with stainless steel crucibles. Results were analysed by calculating the average values, the standard deviation and the percentage difference between the first and the last tests. Moreover, since some of the investigated material either did not re-crystallize after the first melting or were affected by a high degree of subcooling, some cycle tests were performed on the same material employing a larger amount (up to 50 g).

3.3.1 Calorimetric results

α-naphtol

The sample of α-naphtol showed repeated melting and solidification under DSC cycling conditions. The melting enthalpy and temperature obtained for the first cycle were 139 J/g and 95.3°C, respectively. Nevertheless, the material exhibited a high degradation when cycling:

after 5 cycles, more than 15% of the initial melting enthalpy was lost, while a subcooling from 28°C to 58°C was evidenced going from the first to the fifth cycle. Structural characterization, by means of X-ray diffraction, confirmed a degradation of the crystalline structure.

Acetamide

Acetamide showed a very high melting enthalpy (i.e. 215 J/g) and a suitable melting temperature (i.e. 80.4°C) during the first melting. Nevertheless, the subsequent cycles showed a strong reduction of the melting temperature, which was stable at 65.7°C, with a lower melting enthalpy of 175 J/g. This behavior is caused by a polymorphic transformation from the initial rhombohedral structure to the more stable orthorhombic structure [82]. The above reported feature, coupled to the carcinogenic nature of this material, allowed also acetamide to be considered unsuitable for this application.

Sugar alcohols - Xylitol and D-sorbitol

Both selected and characterized sugar alcohols showed a high melting enthalpy (i.e. 226 J/g and 132 J/g for xylitol and D-sorbitol respectively). However, both materials were not able to re-crystallize after the first melting, both for small size samples, tested in the DSC, and in larger samples (i.e. 50 g) tested under cycling conditions in a thermo-cryostat. This behavior has been justified in literature since this class of materials tends to keep a metastable amorphous phase, due to the slow crystallization rate. This feature clearly limits their applicability in real systems.

Hydrated salts - Aluminum Ammonium Sulfate Dodecahydrate (AASD) and Aluminum Potassium Sulfate Dodecahydrate (APSD)

The melting enthalpy measured on the selected hydrated salts resulted the highest among the selected materials (i.e. 217 J/g and 255 J/g for APSD and AASD respectively). Nevertheless, the materials did not re-crystallize after the first melting in the DSC. Accordingly, the same analysis on a larger amount of material (i.e. 50 g) was conducted in a thermo-cryostat. After having performed some cycles, two different behaviours were highlighted for the two materials. APSD showed an incongruent melting, which causes a continuous degradation of the melting enthalpy due to the phase separation between solid and structural water. This degradation was highlighted by testing the cycled material in the DSC, obtaining a melting enthalpy reduction of 50% after 10 cycles coupled to a melting temperature reduction of 12.5%. Differently, AASD showed a congruent melting with a slight enthalpy reduction,

which reached a plateau at 200 J/g after 10 cycles. On the contrary, no appreciable melting temperature variation was obtained.

Commercial inorganic materials - PlusIce S83 and PlusIce S89

The two commercial salts are mainly based on Magnesium Nitrate, hydrated and anhydrous, as highlighted by XRD analysis. The measured melting enthalpy and temperatures of both salts are in agreement with the values reported by the company. The main difference is due to the presence of two separated peaks, the smallest one at about 75°C and the biggest one at the nominal melting temperature. This is probably caused by the coexistence of two phases and the presence of nucleating agents employed to limit the subcooling effect.Indeed, PlusIce S89, during the first three melting phases, shows three peaks, that tend to reduce their intensity and disappear with cycling, thus indicating that the material is evolving towards a single-phase structure. Regarding the subcooling observed, it is almost identical for both materials and is between 22°C and 27°C going from the first to the last performed cycle.

Commercial paraffin - PlusIce A82

The commercial paraffin is perfectly stable under cycling conditions resulting in a melting enthalpy coherent with the one reported by the company. It must be pointed out that, due to the nature of the paraffin mixture, a wide melting temperature range rather than a single temperature characterizes the melting phase of this PCM.

The main results of the study performed on the materials are schematically summarised in Table 3.2: what emerges from the analysis is that the most suitable material for the selected application is the commercial paraffinic one, PlusIce A82.

3.3.2 The selected material

PlusIce A82 consists of a blend of linear and branched hydrocarbons. The calorimetric characterisation evidenced that, apart from the first endothermic peak, the material has a perfectly repeatable behaviour both during melting and solidification. One important feature when considering the application of the material is its wide melting and solidification range, due to its paraffinic nature (i.e. it is made up of polymeric chains having different lengths and therefore different phase change temperature). On the other hand, the measured subcooling is very low, lower than 5°C in the DSC, which could be further reduced in higher scale applications. Its melting enthalpy is around 140 J/g, which is lower than most hydrated salts or xylitol that, however, did not show a satisfactory stability. The organic nature of the material also leads to a lower density (which results in a lower volumetric energy density

Material	Average melting enthalpy [J/g]	Subcooling	Stability
α -naphtolo	-	High	No
Acetamide	175	High	Yes
Xilitolo	237	-	No
D-sorbitolo	132	-	No
AASD	200	High	Solidification: No Melting: Yes
APSD	217	-	No
PlusICE S83	151	High	Solidification: No Melting: Yes
PlusICE S89	130	High	Solidification: No Melting: Yes
PlusICE A82	140	Low	Yes

Table 3.2 Outcomes of the experimental characterization at ITAE.

of a storage) and a low thermal conductivity, that has to be addressed in the design of the component for the thermal storage. The characterization of the material was completed by measuring its specific heat and the thermal conductivity. The latter was measured by means of a C-Therm Mathis TCi instrument, employing the transient plane source method, at two different temperatures (25°C and 50°C). In Figure 3.3 and Figure 3.4 the thermogram and the integral heat curve measured with the DSC are shown. Indeed, the integral heat curve allows taking into account both sensible and latent heat of the material. It is then a useful tool to evaluate achievable heat storage density under different working boundary conditions in practical application. To this aim, the mathematical fitting for the integral heat curve is shown; the error in the approximation of the integral heat curve with a 6^{th} grade polynomial is lower than 0.005%.

Table 3.3 summarises the main features of the material, employed for the subsequent design, analysis and simulation of the system.

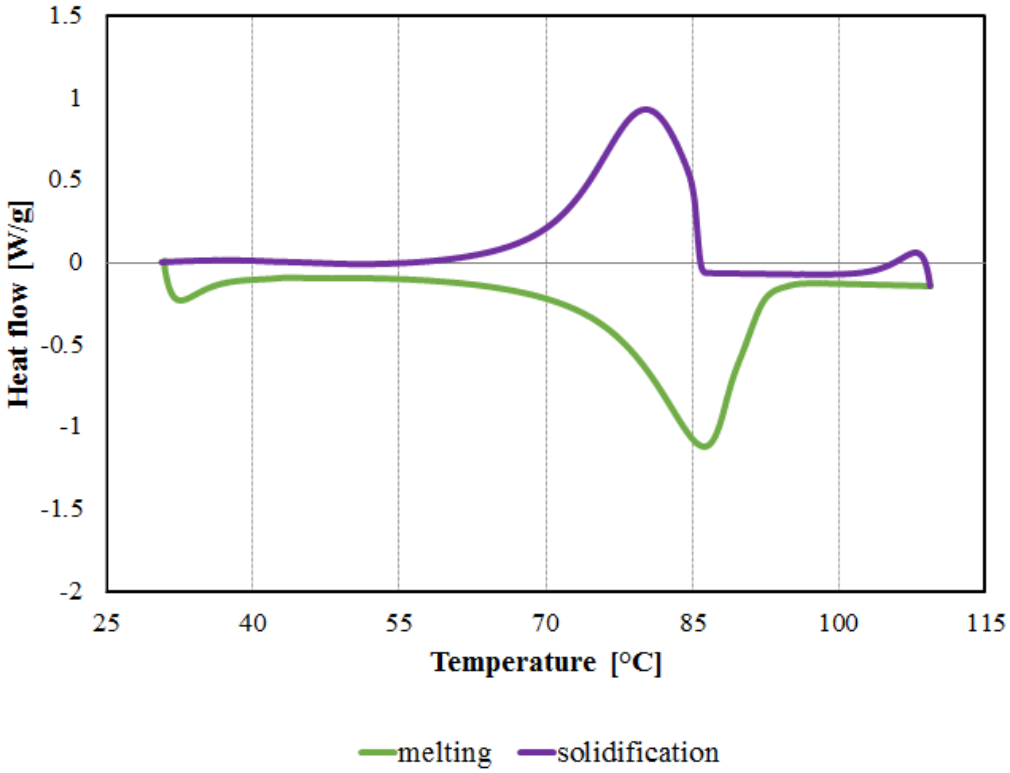

Fig. 3.3 Thermogram of PlusICE A82 measured at ITAE.

Table 3.3 Main features of PlusICE A82.

Property	Unit	Value
Specific heat in solid state (55°C)	kJ/(kgK)	2.75
Specific heat in liquid state (105°C)	kJ/(kgK)	1.92
Thermal conductivity (25°C)	W/(mK)	0.22
Thermal conductivity (50°C)	W/(mK)	0.17
Density, solid state	kg/m^3	900
Density, liquid state	kg/m^3	765
Peak temperature during melting process	°C	85.7
Peak temperature during solidification process	°C	80.7
Onset temperature during melting	°C	74.6
Offset temperature during melting	°C	85.7

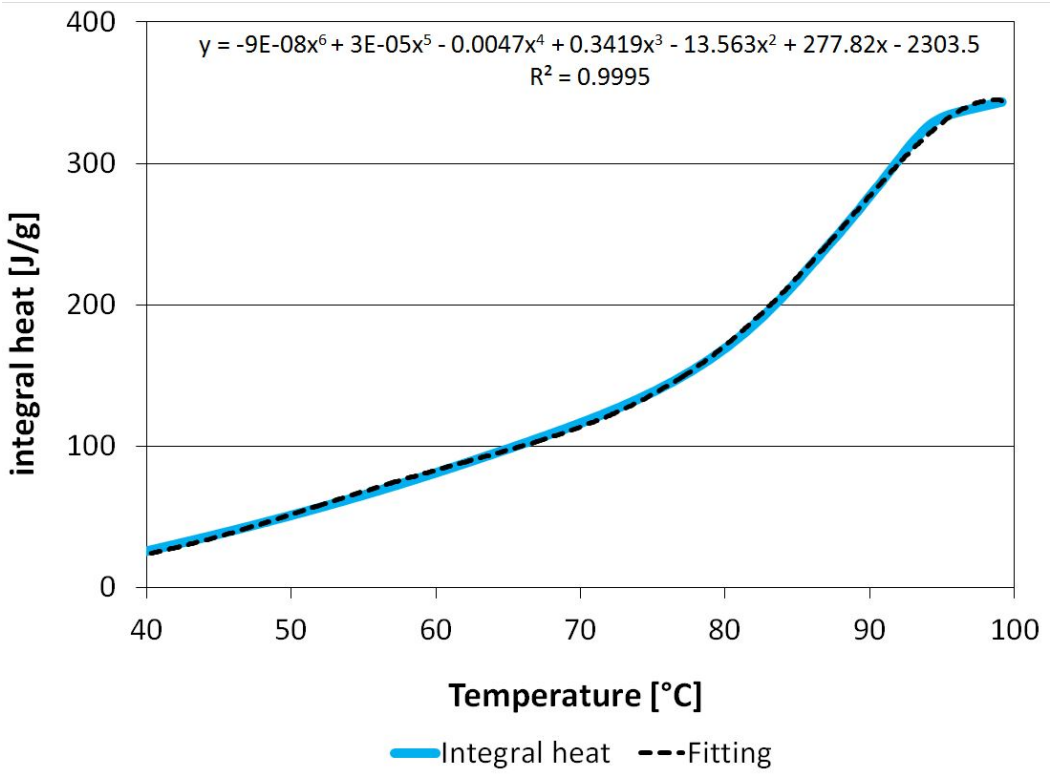

Fig. 3.4 Integral heat curve of PlusICE A82 and its fitting.

3.4 Development of a testing rig for the characterization of TESS

The experimental testing of the prototype was realised on a specific testing rig, suitable for the characterization of thermal heat storages with hybrid or latent heat technology. Main aim of the testing rig is the definition of the heat storage capacity of the system, guaranteeing at the same time the easy interchangeability of the storages to be tested. To this purpose, a testing rig already present at CNR-ITAE and described in [83] was specifically modified. In the design of the testing rig, the following features were regarded:

- flexibility: the testing rig should allow the testing of different systems under the widest range of operating conditions possible;
- automatic operation: the rig should allow for remote control, without the need for an operator to control the charge/discharge;
- real-time acquisition of all the relevant parameters: all the transducers employed should be connected to a suitable datalogging system, to record and control all the main quantities in real time.

Description of the testing rig

The P&ID of the testing rig is shown in Figure 3.5. The main core of the rig is the storage to be tested (called "Storage" in Figure 3.5), that is connected to a second service storage (called "Buffer" in Figure 3.5). The buffer is equipped with an internal heat exchanger and is connected to a 24 kW diathermic oil heater through a plate heat exchanger ("HEX1" in Figure 3.5). In order to allow the operator to set an arbitrary discharge temperature, a second plate heat exchanger ("HEX2" in Figure 3.5) is connected to the return pipe from the buffer and to tap water. A motorised mixing valve is used to control the temperature of the water exiting from HEX2. Such a valve works according to a PID algorithm implemented in LabVIEW. Each component of the testing bench is isolated by using two-way valves, in order to facilitate maintenance and replacement. A picture of the testing rig is shown in Figure 3.6. The main characteristics of the testing rig, that make it suitable for the experimental benchmarking planner are:

- use of water as heat transfer fluid, which is non-toxic, easy to handle and allows employing standard components;
- quick connection of the storage to be tested, that can be easily coupled or disconnected from the testing rig;
- wide range of boundary conditions selectable, including charge and discharge temperature and flow rate of the heat transfer fluid (HTF), in order to reproduce different source or load profiles.

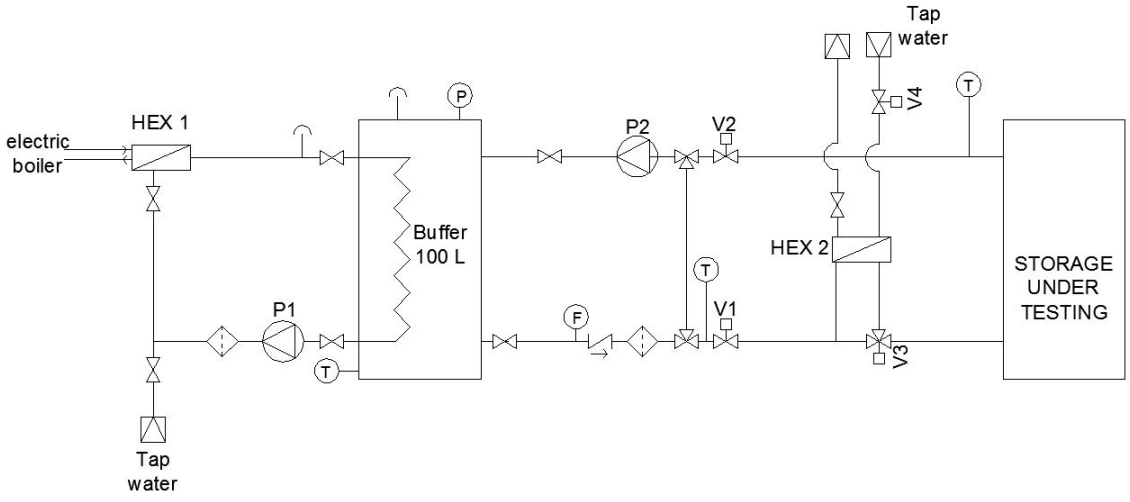

Fig. 3.5 P&ID of the testing rig for TES characterization at CNR-ITAE.

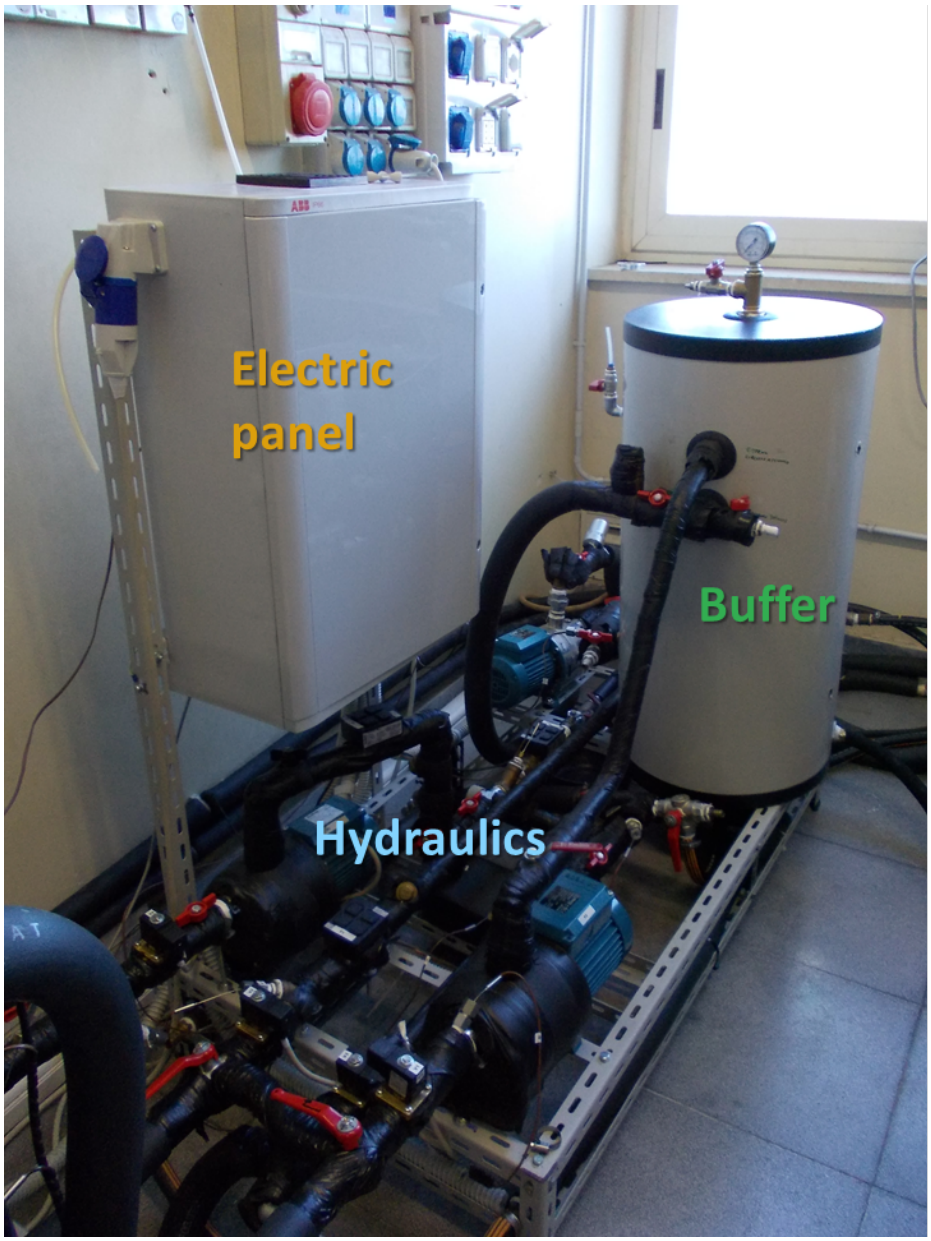

Fig. 3.6 The testing rig for TES characterization at CNR-ITAE.

Operation of the testing rig: charge process

The charge of the storage to be tested is realised in three step:

1. filling of the whole hydraulic pipes and the storages, thanks to the connection to tap water;
2. pre-charge of the buffer storage, that is heated up to the user-selected temperature thanks to the connection with the heater;
3. charge of the latent or hybrid storage, by opening the connection with the buffer storage.

During the last two steps, the hydraulic pump P1 (as called in Figure 3.5) is used to circulate the HTF in the buffer. The final temperature of the buffer can be set on the diathermic heater in the range 50°C-99°C. The pump has a head of 5.5 to 20.5 m and a maximum flow rate of 4.8 m^3/h. The plate heat exchanger HEX1 is a brazed plate heat exchanger, with plates in AISI316L, chosen in order to tolerate the temperature and pressure conditions required during operation. A by-pass pipe, in which the HTF is circulate with the pump P2, has been installed, with the aim of speeding up the pre-charge of the buffer.

During the charge of the storage, the pump P2 is used for the circulation of the fluid between the buffer and the storage under testing. The connection is open or closed thanks to the solenoid valves V1 and V2, that are controlled through the LabVIEW software realised. The pump P2 has a maximum flow rate of 4.8 m^3/h and a maximum head of 42.5 m. Moreover, on both the storages, safety valves have been installed to avoid dangerous pressures. Figure 3.7 shows a detailed view of the installed hydraulics, where the main components described are indicated.

Operation of the testing rig: discharge process

The discharge process is realised in 2 steps:

1. pre-charge of the buffer;
2. discharge of the storage to be tested.

The pre-charge of the buffer is realised as during the charge process, by controlling the connection of the component with the diatermic oil heater. During the discharge, instead, the desired discharge temperature is set on the LabVIEW user interface. At each acquisition step, the set is compared to the inlet temperature to the storage under testing. According to

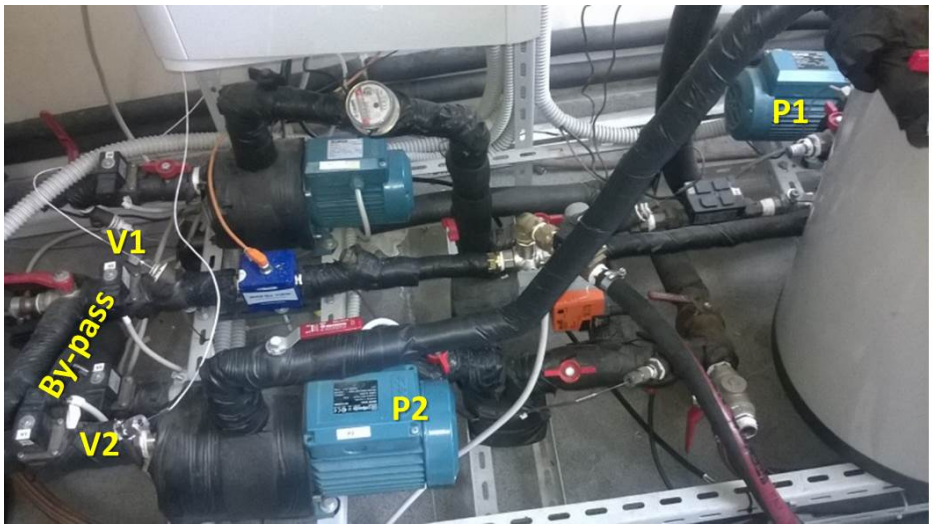

Fig. 3.7 Detail of the hydraulic circuit of the testing rig.

the difference between the two values, a 0-10 V command signal is sent to the mixing valve V3. The mixing valve is connected to the inlet pipe of the storage to be tested and mixes the water coming from the plate heat exchanger HEX2, that is connected to tap water, and the circuit of the buffer storage, that is at high temperature.

The chosen mixing valve is a ball valve, with modulating motor and analogue signal. The maximum differential pressure of the valve is 350 kPa and the leakage class according to DIN EN 1349is 1% of kvs. Figure 3.8 shows a detailed view of the installed hydraulics, where the main components described are indicated.

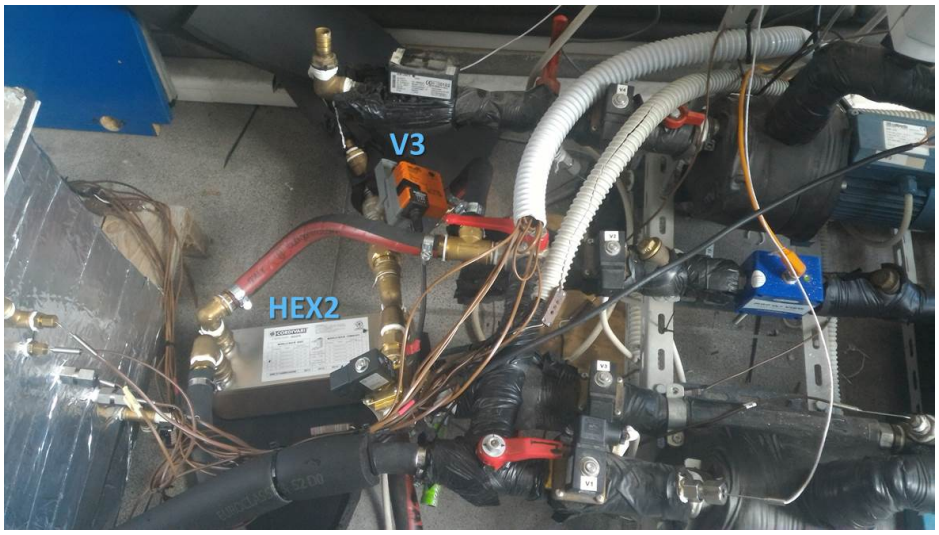

Fig. 3.8 Detail of the hydraulic circuit of the testing rig used for discharge.

Sensors employed and data acquisition

The P&ID of Figure 3.5 shows also the sensors chosen and installed in the testing rig:

- class A T-type thermocouples, used for the measurement of the temperature of the water inside the buffer and of the PCM inside the storage to be tested.
- Pt100 1/10 DIN with 4 wires, used for the measurement of inlet and outlet temperature of the HTF. The high accuracy of these sensors allows a precise evaluation of the energy accumulated by the system. Before the installation, the sensors were calibrated.
- MVM040 magnetic flow meter with 0.25% FS accuracy, used to measure the flow rate ot the HTF.

Moreover, the flow rate of the pump P2 is controlled through a variable speed drive, in order to guarantee flexibility and allow analysing the effect of such a parameter on the storage capacity or power. All the sensors and electric components (pumps and valves) are connected to a National Instruments FieldPoint acquisition system, which is composed of a controller and I/O modules. A detailed picture of the data acquisition system and the electric connections within the testing rig is shown in Figure 3.9. A specifically-developed LabVIEW VI is used to assure the management of the tests (i.e. the opening/closing of the valves, the on/off of the pumps and the control of the mixing valve), the acquisition and the monitoring of all the relevant quantities (Figure 3.10).

3.5 Design of the system: prototype based on a fin-and-tubes HEX

The literature research presented has evidenced that not enough information exists on prototypes of LTES, especially when working in the selected temperature range, and therefore the information for a detailed design are lacking or incomplete. Consequently the approach followed was to orient the design towards the practical aspects and rely on the analysis of experimental data for a successive optimization. The design process can be schematically described as follows:

1. definition of the size of the storage. The selected target was a storage capacity, under nominal conditions, of 7 MJ, which corresponds to a lab-scale size but still representative of a real system.

Fig. 3.9 Electric panel and acquisition system of the testing rig.

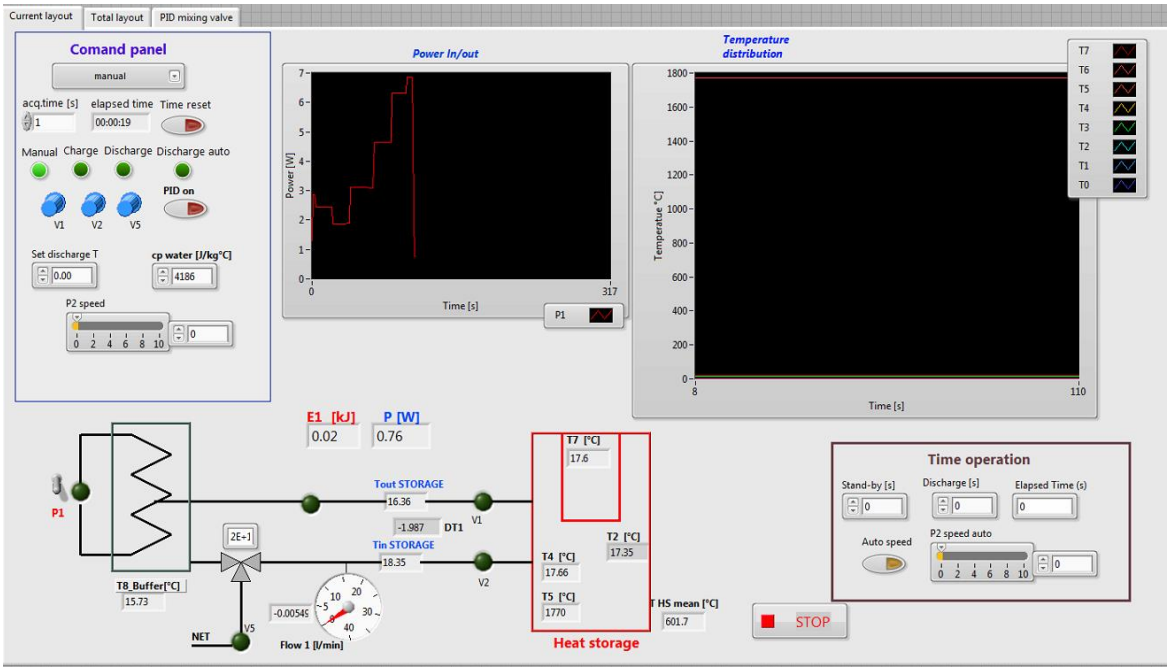

Fig. 3.10 User interface of the VI employed for the control of the testing rig.

2. Definition of the configuration (i.e. the type of heat exchanger to be used). As pointed out in 2.2.5, the low thermal conductivity is the limiting factor often preventing a full exploitation of the potential of the material. In the present case, no heat transfer enhancement has been considered at a material level and therefore the design of the storage should address such an issue. Among the configurations proposed in literature, and compared in [84], a fin-and-tube system was chosen, since it allows increasing the heat transfer area and guaranteeing at the same time a good storage capacity.

3. Definition of the hydraulic configuration when regarding the integration to the system. Separated charge and discharge where considered, so only one circuit is needed.

4. Definition of the geometrical and constructive features of the storage. In particular, the heat exchanger was included into a metal frame. Both components are realised in AISI416 stainless steel. Indeed, paraffins do not exhibit a corrosive behaviour towards metal, but with the aim of a future application of the same storage with hydrated salts or more corrosive materials, stainless steel was selected for the construction. The space between the fins and their thickness —that represent two important parameters in the performance of the storage— were selected as a compromise between the technical limits of the construction technique (welding of the fins onto the tubes) and the possibility of an easy filling of the system.

The heat exchanger

The heat exchanger that represents the main core of the system was realised through welding of the fins onto the tubes, as to guarantee an easy assembly. The fins were realised from 2 mm thickness metal sheets, with a gap of 5 mm. Indeed, commercial systems are usually characterised by a much smaller thickness of the fins; the effect of such a parameter is then an issue to be evaluated. Moreover, when sizing the system, the thermal expansion of the PCM was taken into account, thus allowing for 25% extra volume with respect to the one of the solid material.

In order to have a uniform heat transfer inside the phase change material, the flow was divided into 4 ranks, connected to the inlet and outlet of the external circuit thanks to manifolds. A schematic view of the heat exchanger is shown in Figure 3.11.

Manifolds

The distribution of the fluid inside the heat exchanger is obtained by means of manifolds, each having four 1/2" connections for the tubes in the ranks of the heat exchanger and a 1 1/2" connection for the external circuits.

Frame

The heat exchanger is contained inside a metal frame, realised in AISI416. Such a solution is necessary also to avoid any leakage of the PCM outside the storage. The frame is closed through a lid covering the whole heat exchanger. This has been preferred to the installation of viewports in order to facilitate the filling of the material. Moreover, on the frame, connections for the temperature sensors and the screws of the lid were realised.

Assembled system

A render of the assembled system is shown in Figure 3.12, while Figure 3.13 shows an exploded view highlighting all the components of the storage. Finally, Table 3.4 reports the main characteristics of the system.

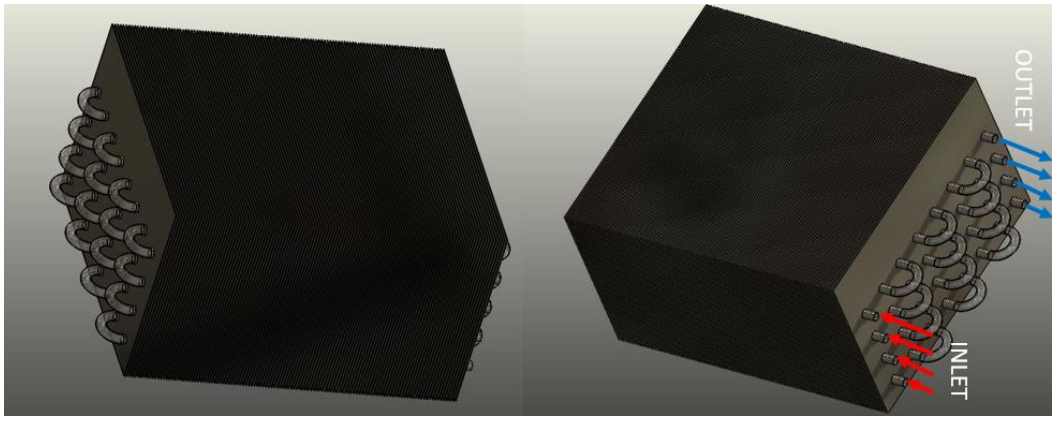

Fig. 3.11 Schematic view of the fin-and-tube heat exchanger embedded in the storage system.

3.6 The realised system: prototype based on a fin-and-tubes HEX

Figure 3.14 shows two view of the realised prototype in the lab of CNR-ITAE. It is possible to notice both the hydraulic circuit and the fins that represent the main part of the heat exchanger.

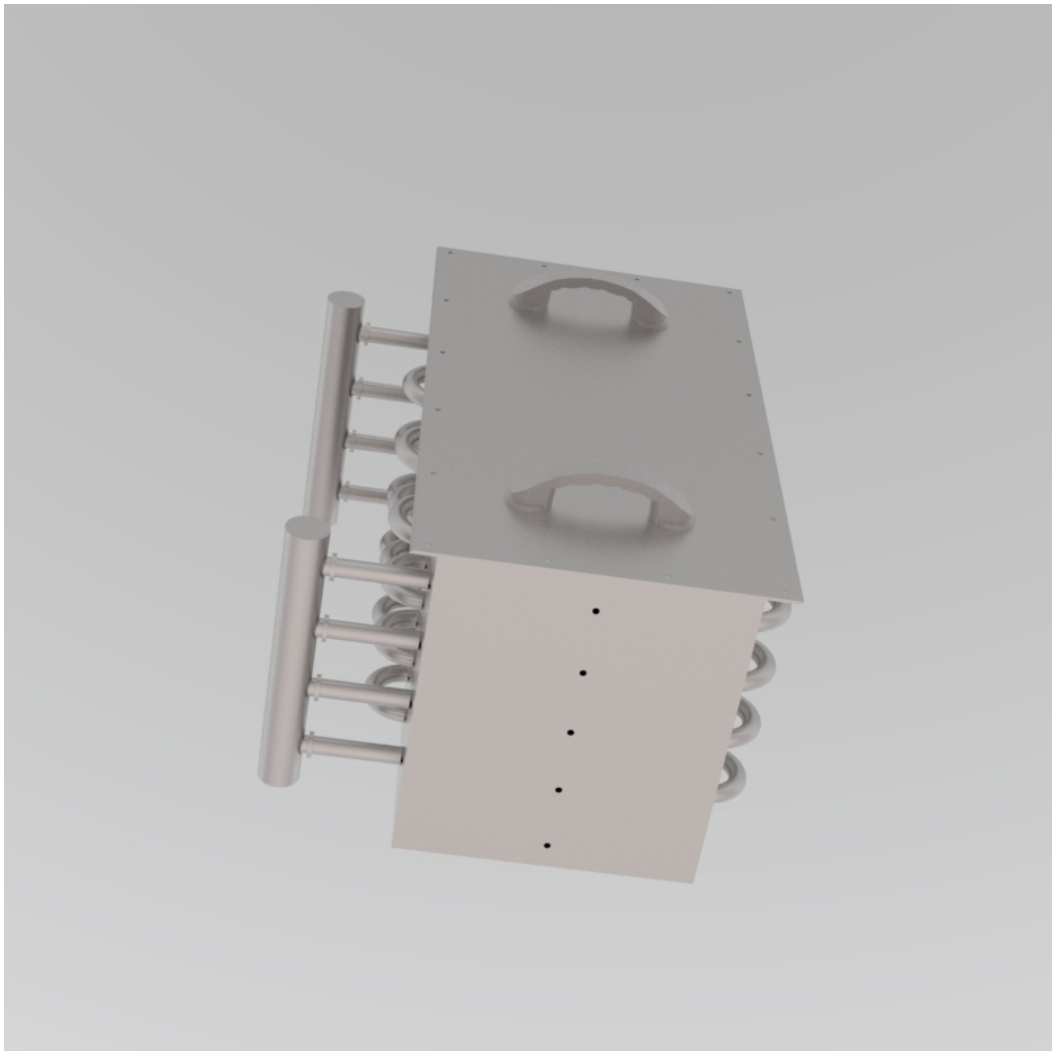

Fig. 3.12 Render of the LTES realised.

Table 3.4 Main features of the realised prototype with fin-and-tube HEX.

Material	AISI 416
Technology	Fin-and-tube heat exchanger with welded fins
Number of pipes	32
Diameter pipes	½ ”
Ranks	4
Number fins	48
Fin dimensions	400 x 650 x 2 mm
Fin space	5 mm
Overall dimensions	400 x 650 x 350 mm
Overall weight	240 kg

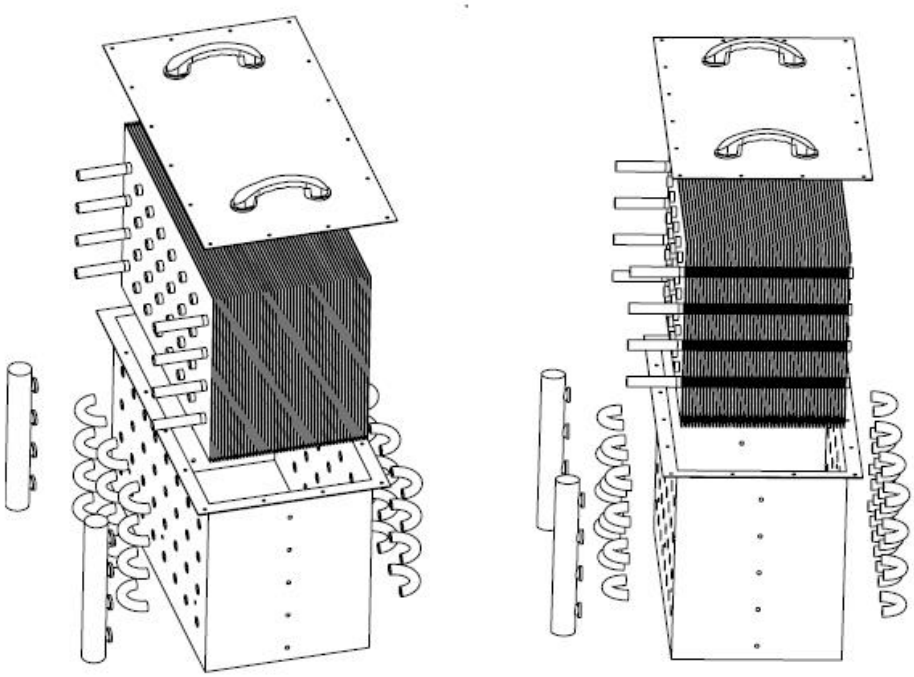

Fig. 3.13 Exploded view of the LTES realised.

Between the main body of the HEX and the lid, a siliconic sealing was realised and placed. The system was then insulated, in order to limit the thermal dispersion in the environment. In particular, a first layer of insulating material consists in an elastomeric foam with thickness of 1.5 cm and thermal conductivity of 0.036 W/mK. Since the external body of the system includes the feedthroughs for the temperature sensors, the elbows of the hydraulic circuit and the manifolds, the insulating material was cut according to specifically-realised guides and then placed on the heat exchanger thanks to a heat-resistant adhesive (Figure 3.15 and Figure 3.16). Subsequently, an aluminium foil was used to cover all the exposed surfaces, in order to reduce also the losses due to radiation. A picture of the system after the application of the reflective foil is shown in Figure 3.17.

The system has then been equipped with the temperature sensors useful for the measurement of the temperature of the PCM in the various points. In particular, the thermocouples were placed as to obtain a 3D-map of the temperatures inside the storage, detecting both longitudinal and transversal temperature gradients. Figure 3.18 shows the location of the thermocouples, while Figure 3.19 shows the prototype connected to the testing rig described in the previous section.

Fig. 3.14 The prototype of fin-and-tube HEX with PCM realised.

Fig. 3.15 The prototype TES after the application of the first layer of insulation.

Fig. 3.16 The prototype of TES after the application of the first layer of insulation.

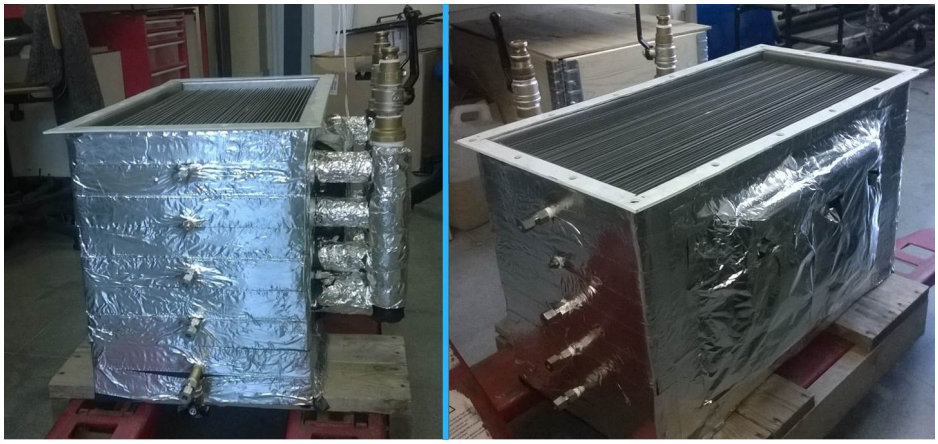

Fig. 3.17 The prototype of TES after the application of the reflective aluminium foil.

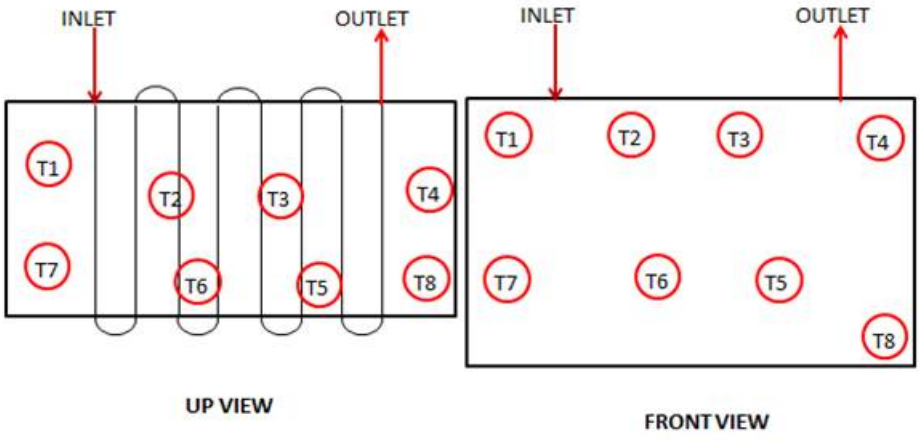

Fig. 3.18 Position of the temperature sensors.

Fig. 3.19 The prototype connected to the testing rig.

3.7 Experimental procedure

The realised storage was charged with 37 kg of PCM and subsequently an experimental campaign aimed at its characterization was carried out.

The experimental procedures followed for the charging and discharging process of the storage are reported in Figure 3.20 and Figure 3.21, respectively. Charge is started when the temperature in the buffer is 5°C above the desired final temperature inside the storage, and it is stopped when the average temperature measured by all sensors approaches such a value. Instead, discharging is realised by setting a desired inlet temperature for the HTF and it is stopped when the measured power is almost zero. Moreover, "dynamic" tests were performed, consisting in a sequence of 3 charging and 3 discharging phases, each lasting for a fixed time. For such tests, complete automatic management through the computer software was employed.

Table 3.5 summarises the different tests and the investigated parameters. During the tests simulating the charge of the storage, the flow rate, the initial temperature of the storage, the final temperature of the storage and the inlet temperature of the HTF were investigated. During discharge, the flow rate, the initial temperature of the storage and the inlet temperature of the HTF were the main parameters investigated. During dynamic tests, instead, the time allowed for each phase and the flow rates of the HTF were varied.

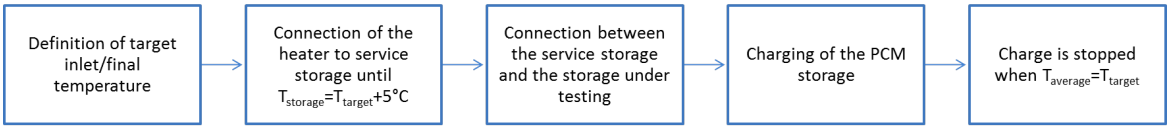

Fig. 3.20 Charge procedure followed in the tests with the LTES.

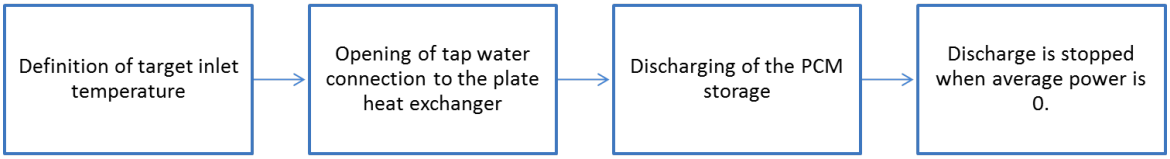

Fig. 3.21 Discharge procedure followed in the tests with the LTES.

Table 3.5 The parameters investigated in the tests of the LTES with fin-and-tube layout.

STATIC TESTS			
CHARGE		**DISCHARGE**	
Parameter	***Value***	***Parameter***	***Value***
Flow rate [kg/min]	5, 10, 15, 20	Flow rate [kg/min]	3, 5, 10, 15, 20
Initial temperature [°C]	20, 25, 30, 45, 50, 55, 65, 75	Initial temperature [°C]	83, 85, 86, 88, 90, 92
Final temperature [°C]	85, 88, 90, 92	Inlet temperature [°C]	65, 70, 75
Inlet temperature [°C]	85, 90, 94	Δ $T_{0\text{-fin}}$[°C]	7, 12, 15, 20
DYNAMIC TESTS			
Parameter	***Value***		
Charge/discharge time [min]	10, 15,20, 30, 45		
Flow rate [kg/s]	10, 20		

3.8 The figures calculated

The following figures were calculated for characterization and comparison purposes:

- Charge/discharge energy, calculated as the integral of the instantaneous power for the whole duration of the charge/discharge process. It is calculated as:

$$E = \int_0^{t_{fin}} \dot{m} c_p \left(T_{in} - T_{out}\right) dt \tag{3.1}$$

  where: Where E is the energy, $\dot{m}$ is the mass flow rate of the heat transfer fluid, cp is its specific heat,T_{in} and T_{out} the inlet and outlet temperatures of the HTF measured in the testing bench, t_{fin} is the final time corresponding to the end of the test.

- Average power, calculated as the average of the instantaneous powers for the whole duration of the process.

$$P_{ave} = \frac{\sum_{i=0}^{t_{fin}} \dot{m}\, c_p \left(T_{in,i} - T_{out,i}\right)}{n_{steps}} \tag{3.2}$$

- Charge efficiency, calculated as the ratio between the theoretical energy given to the system over the total one supplied. The theoretical energy was calculated as the sum

of the integral heat of the material, according to the fitting reported in Figure 3.4, and the sensible energy due to the presence of significant metal masses inside the system.

$$\varepsilon_{ch} = \frac{E_{th}}{E} \tag{3.3}$$

- Discharge efficiency, calculated as the total amount of energy recovered from the system over the theoretical one, calculated from the integral heat for the PCM material and the sensible heat of the metal masses.

$$\varepsilon_{disch} = \frac{E}{E_{th}} \tag{3.4}$$

- Useful energy, calculated as the total energy recovered during discharge process for T_{out}-T_{in}>0.3 °C.

Uncertainty analysis

Uncertainty for the measurements was derived from the theory of extended uncertainty [18] as follows:

$$u_E = u_P = E\sqrt{\frac{u_{\dot{m}}^2}{\dot{m}^2} + \frac{u_{\Delta T}^2}{\Delta T^2}} \tag{3.5}$$

Where u is the uncertainty and the suffix indicates the quantity for which the uncertainty is calculated. The uncertainty from the DSC measurements for the calculation of theoretical energy was considered equal 2%. The range of uncertainties calculated for the uncertainties on energy and efficiency are 6.55% and 8.28%, respectively.

3.9 Prototype with fin-and-tubes HEX: experimental results

3.9.1 Results of charge tests

All the results for the testing of the fin-and-tube system presented in this section and in the following ones are also reported and published in [85].

Results of a typical test

Figure 3.22 and Figure 3.23 show the temperature evolutions during a typical charge test. In both cases, the average inlet temperature of the heat transfer fluid over the test is 93°C

and the average temperature of the PCM inside the storage at the end of the test is 86°C. The main difference between the tests is the initial temperature of the PCM, that is 25°C in one case and 65°C in the other.

What is possible to notice in Figure 3.22 is that all the curves for the different temperature sensors show the same behaviour: the temperature increases quickly during the first minutes of the test. During this time, sensible heating of the PCM (that is still in the solid phase) occurs. Afterwards, the temperature increases slowly, with an almost constant rate until the target temperature is reached and the test is stopped. Such part of the charging tests corresponds to the melting of the PCM. The curves are relative to 5 different temperature sensors: T4 is placed on the side of the heat exchanger, the other sensors are placed in the central part, but, while T2 and T3 are in the first rank from the top, T5 and T6 are in the third rank from the top. Therefore, the difference in the temperature between T2, T3 and T5 ad T6 corresponds to the temperature gradient along the height of the heat exchanger, whereas the temperature difference between T2, T3 and T4 corresponds to the temperature difference of the material along the same plane. What is clear from the results of Figure 3.22 is that the stratification along the vertical direction is not relevant, while a significant temperature gradient along the horizontal plane can be observed, which is mainly due to the poor heat transfer inside the material due to its low thermal conductivity. It is clear that the material in the central part of the exchanger, which is closer to the fins and especially the tubes, exhibits the highest melting rate, whereas the material on the side of the exchanger even after 5 hours has not completed the phase change. At the end of the charge, a temperature gradient of about 12°C along the transversal plane was measured. Similar considerations can be made for the temperature profiles reported in Figure 3.23, which covers only the temperature range of the phase change: the temperature of the material increases constantly from the beginning of the test until the charge is stopped. The gradient is, in this case, smaller but still easily identifiable and a difference of 5°C was measured at the end of the test. It is interesting to notice that, as already reported in [86, 87], the melting range is not easily identifiable even in the test involving only the melting range, since the phase change occurs in a wide range of temperatures.

The poor heat transfer inside the material, that will be further discussed in the next sections, can be visualised by looking at the pictures taken during the melting process and shown in Figure 3.24. For clearness' sake, only half of the heat exchanger is shown. However, it is evident that the phase change starts in the central part of the exchanger, where the tubes are concentrated, and proceeds towards the external part of the exchanger, where there are no tubes. The lack of metal masses causes the material near the side wall of the exchanger not to complete melting. It is worth noticing that such a big temperature difference inside the

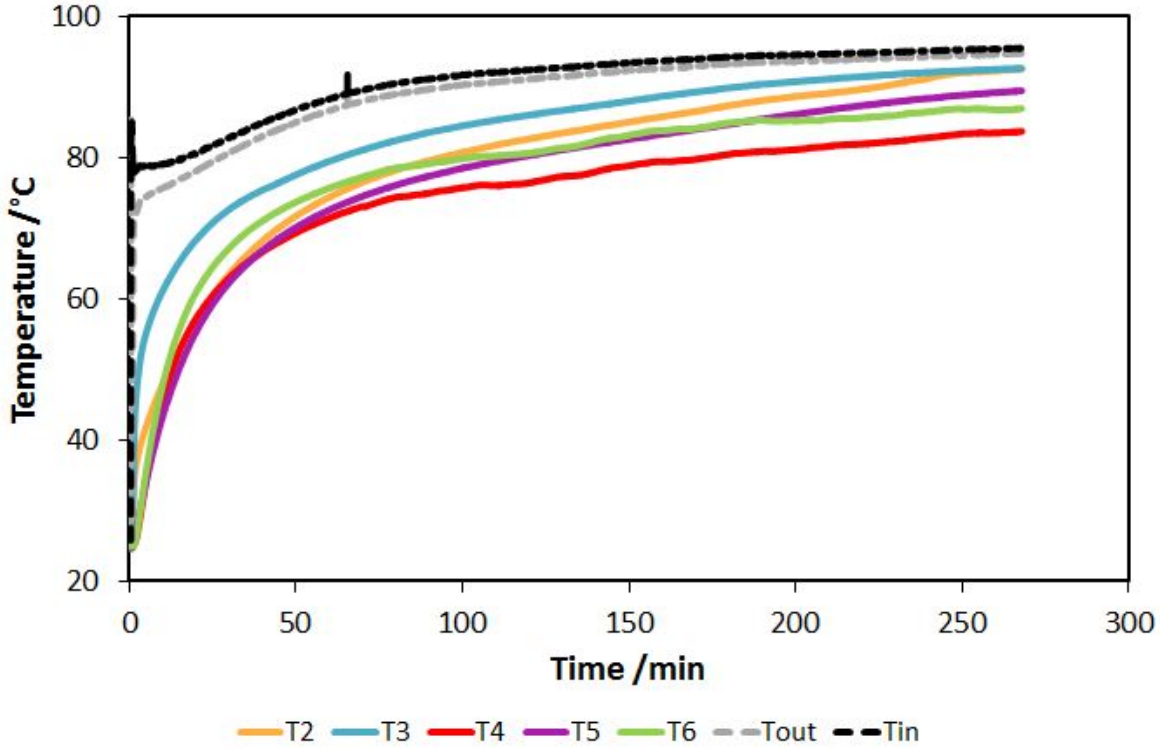

Fig. 3.22 Temperature profiles for a charge test from 25°C to 86°C.

heat exchanger, together with the fact that only part of the material inside the storage actually undergoes the phase change, complicates the interpretation of the results of the tests.

Apart from the temperature profiles, the thermal power — and the correspondent energy — supplied to the storage are recorded for each test. For the charge within 25°C-86°C shown in Figure 3.22, the correspondent instantaneous power and cumulative energy profiles are shown in Figure 3.25. From what previously stated on the temperature profiles inside the storage, it is intuitive to find that the energy has a monotone increasing trend throughout the duration of the test, since the phase change range is not easily identifiable. The poor heat transfer strongly affects the power measured: with the exception of the peak occurring right after the connection with the buffer in the testing bench, the power decreases rapidly and keeps below 2 kW for more than 70% of the duration of the test. The consequence for such a low power actually provided to the system is that the charge requires a long time, about 5 hours.

Effect of the temperature interval

Figure 3.26 shows the efficiency of the charging process, calculated according to Equation 3.3 as a function of the temperature difference between the initial temperature and the final

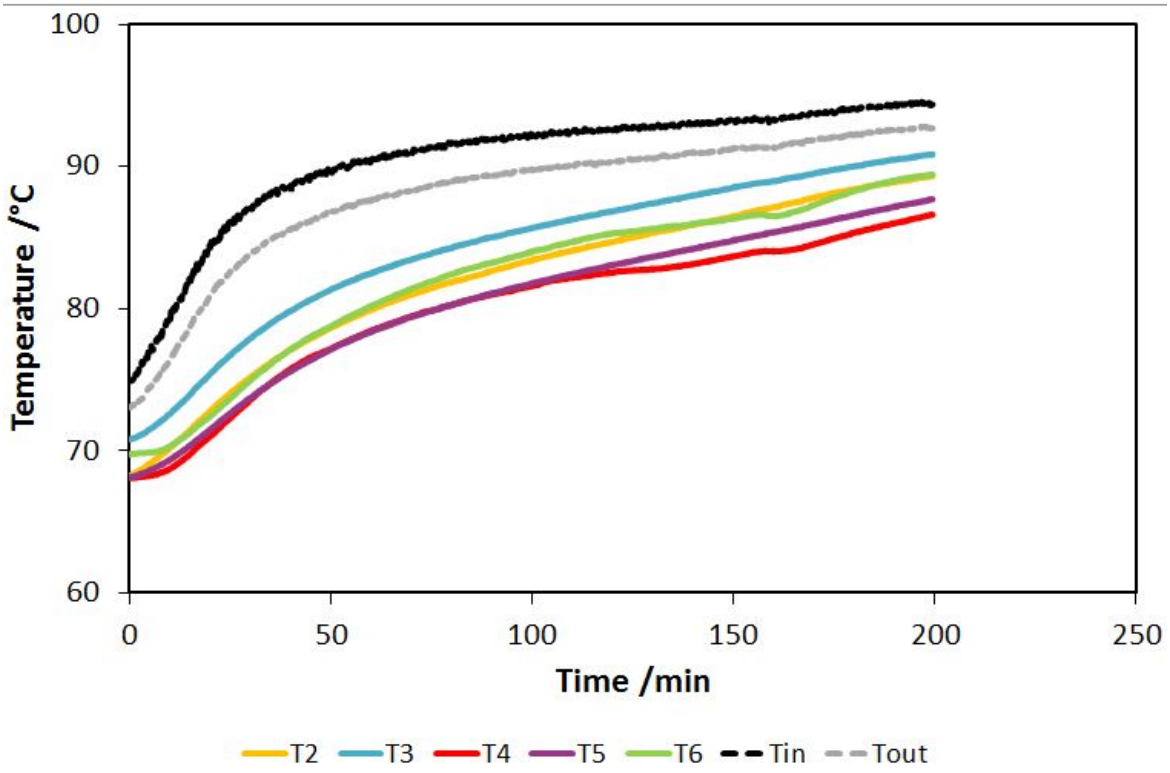

Fig. 3.23 Temperature profiles for a charge test from 65°C to 86°C.

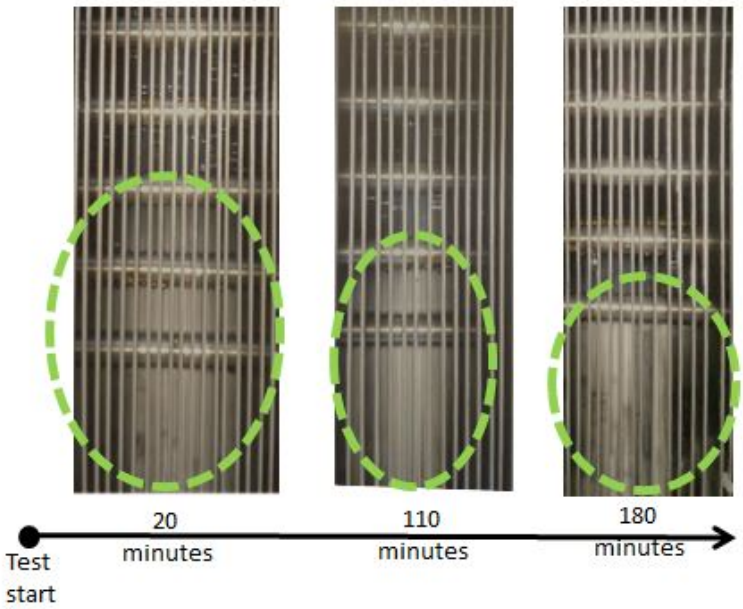

Fig. 3.24 Pictures of the PCM undergoing melting after 20 minutes, 110 minutes and 180 minutes from the beginning of the test.

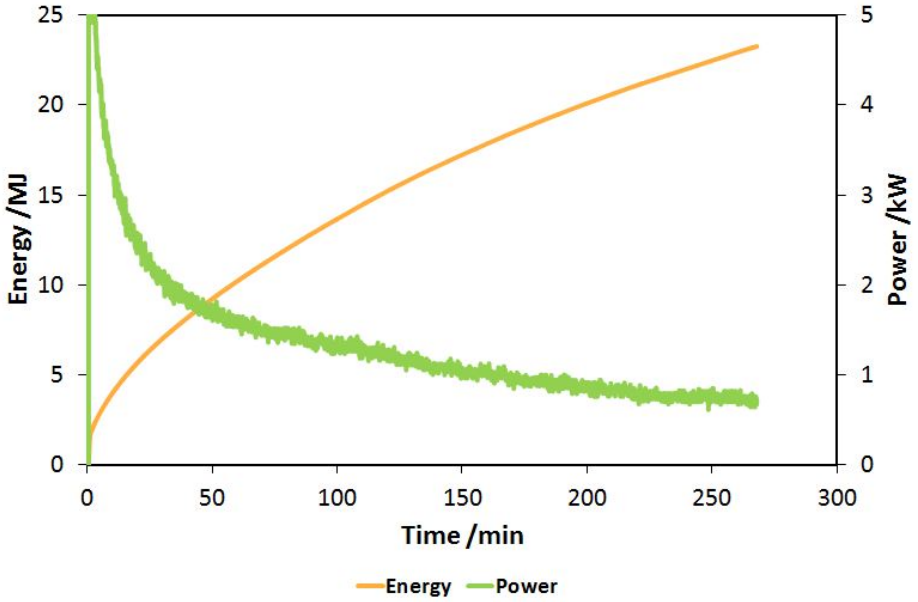

Fig. 3.25 Energy and power profiles for a charging test.

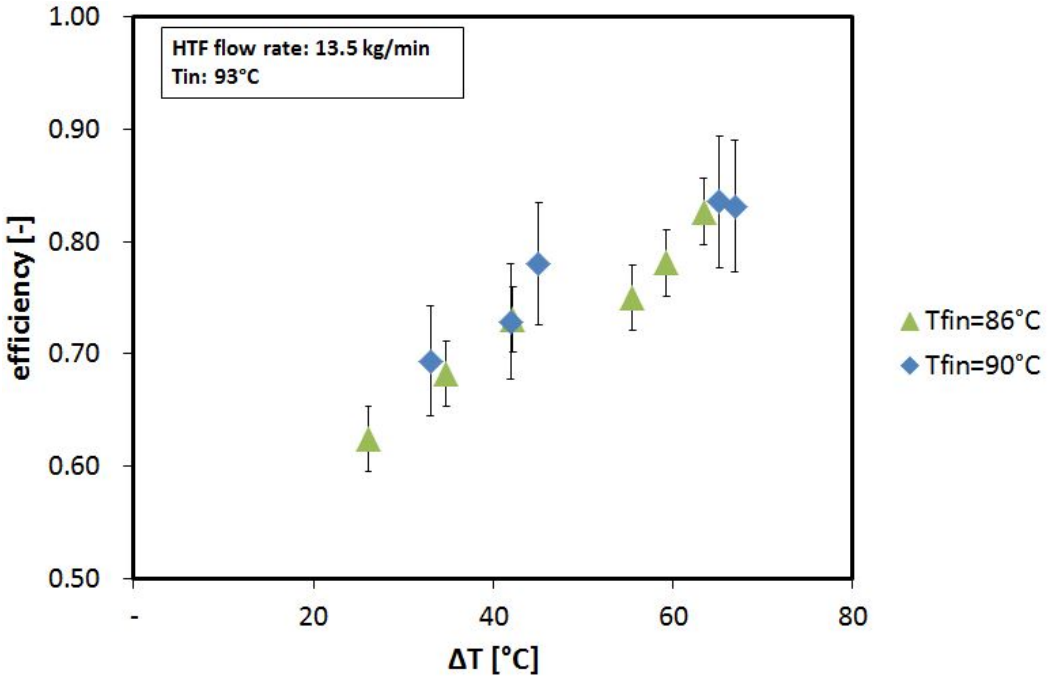

Fig. 3.26 Efficiency as a function of the temperature interval of the charge.

temperature of the storage for two series of tests, differing for the final target temperature. During the tests a wide temperature span has been considered, not only the interval around the phase change: indeed, especially for the daily storage of solar energy, a complete discharge of the system might represent the operating condition and therefore it was decided to investigate also the case of charge from ambient temperature.

What is clear from the picture is that the efficiency increases with the temperature difference considered. Two factors affect the efficiency of the storage: heat losses through the environment and the intrinsic efficiency of the exchanger. Heat losses depend on the temperature difference between the exchanger and the ambient. Instead, the efficiency of the exchanger influences its heat transfer ability, because only a portion of the heat supplied to the HTF is transferred to the heat storage material. Such two factors explain the trend of Figure 3.26. The tests with higher temperature differences —-when both the sensible heating and phase change are involved— are those with an intrinsic slower dynamic, where the effect of heat transfer ability of the exchanger is mitigated.

Effect of flow rate

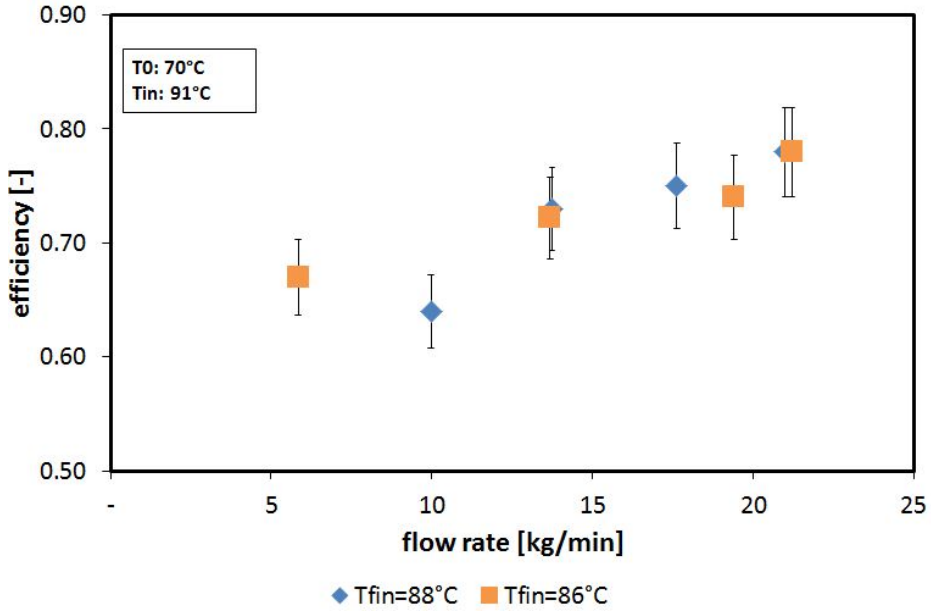

Fig. 3.27 Efficiency as a function of the flow rate of the HTF during charge.

Figure 3.27 shows the effect of flow rate on the efficiency of the storage during charge. Two sets of tests are represented, differing for the final temperature, while initial temperature of the PCM and inlet temperature of the HTF are fixed. It is worth noticing that, for comparison reasons, only the temperature span corresponding to the melting of the PCM is

considered in the calculation of the efficiency. Efficiency shows an increasing trend with flow rate for both cases, however such a variation happens in a small range (0.68-0.76) and the profile is almost flat: this tendency can be explained by the behaviour of the exchanger, that shows no significant improvement in heat transfer at increasing flow rate.

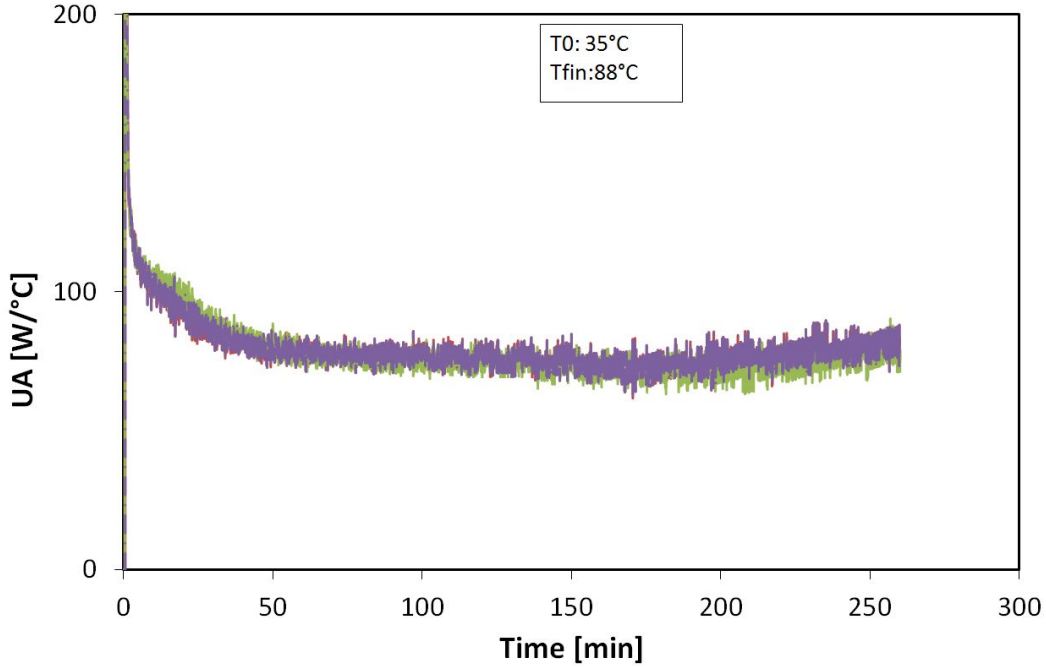

Fig. 3.28 UA for three different charging tests at various flow rates.

This is further highlighted by Figure 3.28, where the parameter UA is represented for tests under the same temperature boundaries but differing for the HTF flow rate. The UA value was calculated, in accordance to what reported in [88], as:

$$UA = \frac{P}{T_{ave} - \frac{T_{in}+T_{out}}{2}} \tag{3.6}$$

As visible in the picture, despite the varying flow rates, the UA value keeps constant. Moreover, the absolute value, around 100 W/°C, is extremely low, thus confirming that there is still a limitation in the heat transfer dynamic and efficiency of the realised thermal storage, due to the low thermal conductivity of the material as well as the limited efficiency of the HEX itself.

Effect of inlet temperature

Finally, Figure 3.29 shows the effect of the average inlet temperature on the charging efficiency and the average power supplied to the storage. Three different conditions are

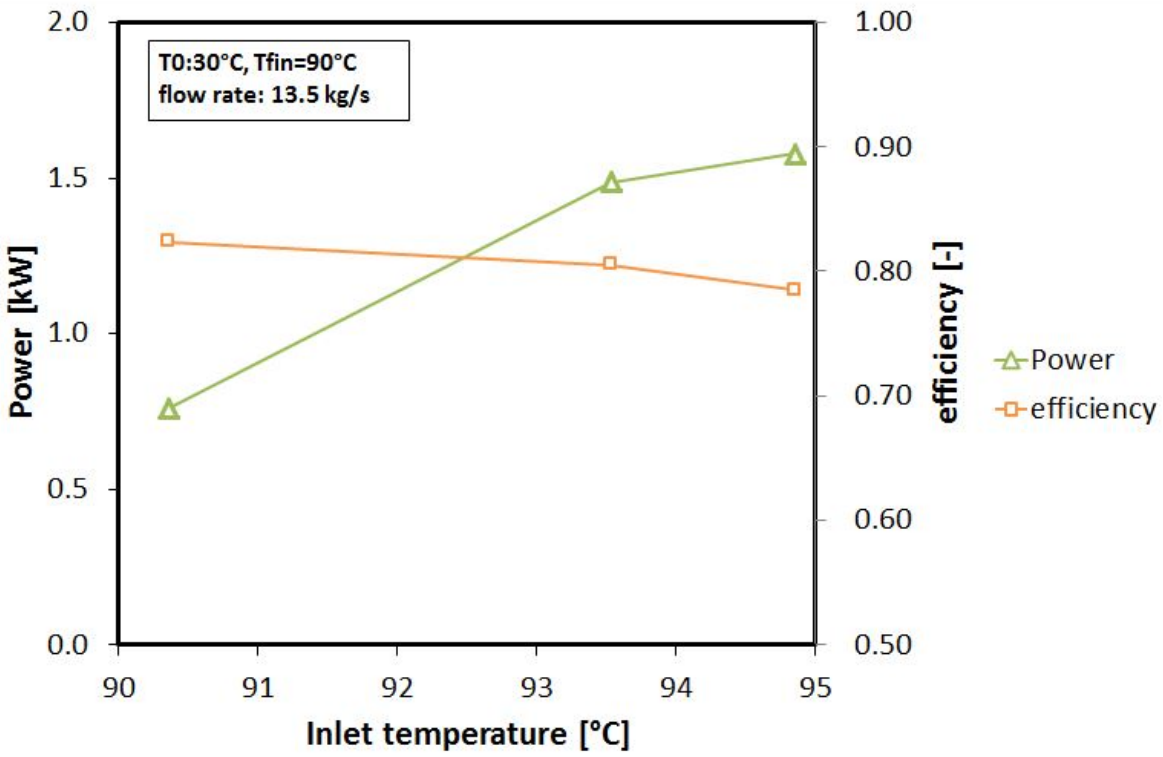

Fig. 3.29 Effect of inlet temperature on the charge of the storage.

compared, with inlet temperature of 90°C, 93°C and 94°C, respectively. The target temperature for the charge is 90°C in all the cases, thus coinciding with average inlet temperature in one condition. As easily suggested, average power increases with the inlet temperature because, especially during the melting process, a higher temperature difference is available to drive the phase change. On the contrary, the efficiency slightly decreases with increasing inlet temperature, since the effect of thermal losses becomes more relevant.

3.9.2 Results of discharge tests

Results of a typical test

Discharging tests on the system under examination were realised considering discharging temperatures of 65°C and 70°C. Figure 3.30 shows the temperature profiles for different thermocouples inside the heat exchanger for a test with 90°C initial temperature, 6 kg/min HTF flow rate and a set temperature for discharge of 70°C. The initial temperatures of the various sensors are quite different because, as previously stated, a significant temperature gradient inside the PCM was measured at the end of the charge. The temperatures indicated as T2 and T3 exhibit a rapid decrease from the initial temperature (that is higher than 90°C)

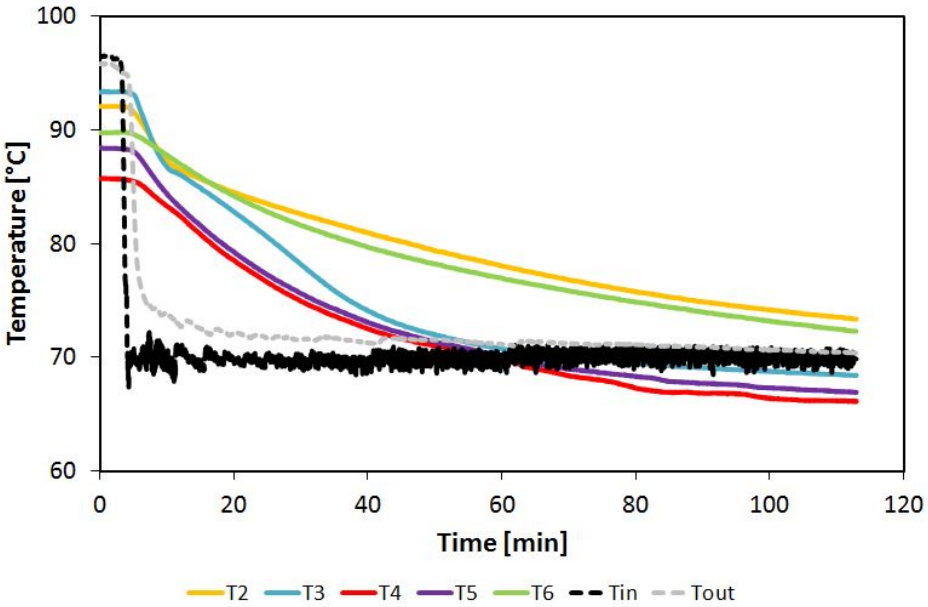

Fig. 3.30 Temperature profiles for a discharge test from 90°C to 70°C with HTF flow rate of 6 kg/min.

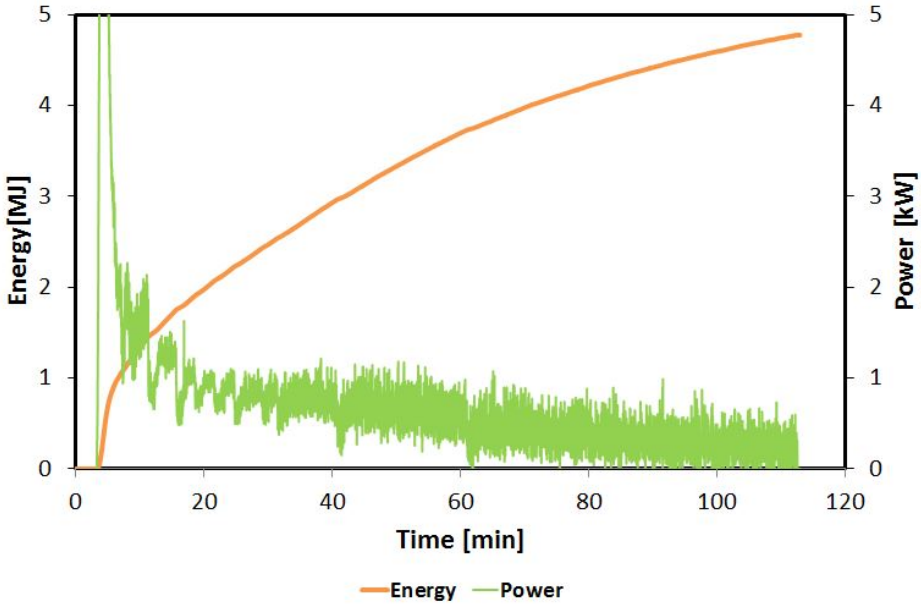

Fig. 3.31 Energy and power profiles for a discharge test from 90°C to 70°C with HTF flow rate of 6 kg/min.

until a temperature of about 85°C-87°C. Such a value corresponds to the onset temperature for the solidification process. Once the solidification starts, the slope of the curve becomes lower, due to the slower dynamic of the phase change process. Instead, the thermocouples indicated as T4 and T5, at the beginning of the examined test are around the onset value for solidification. This means that they exhibit a slow constant reduction in temperature for the whole duration of the test.

As for the case of charging, in Figure 3.31 the instantaneous power and cumulative energy for the test are shown. The same considerations apply: the average power has a peak after the connection to the user is opened and then keeps below 1 kW for the whole duration of the test, thus stressing once again the limitation of the system. The curve for cumulative energy increases constantly up to a value of around 5 MJ.

Effect of initial temperature

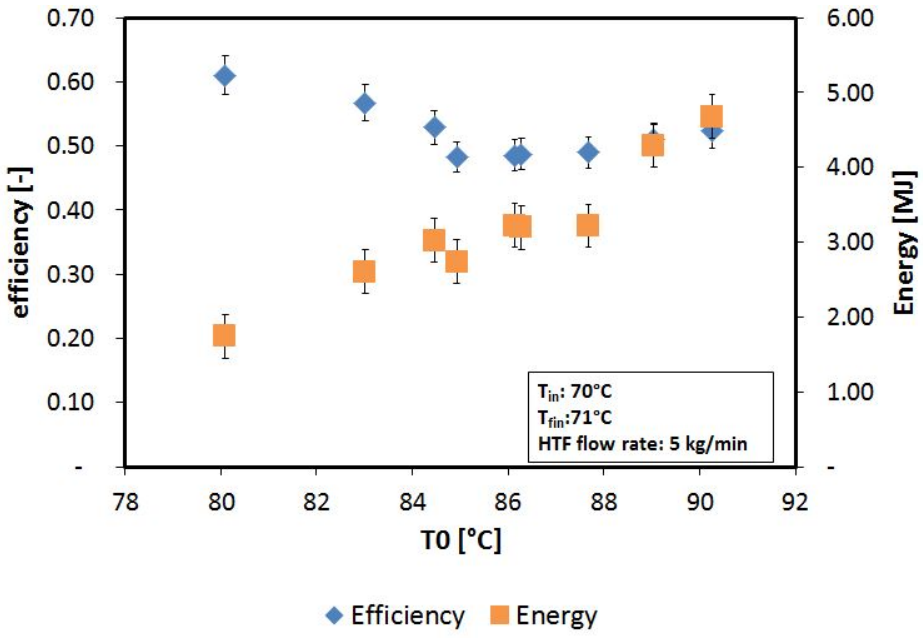

Fig. 3.32 Effect of the initial temperature of the storage on the energy recovered and discharge power.

Figure 3.32 shows the effect of the initial temperature of the storage on its discharge process, by reporting the energy recovered from the storage and its efficiency. As it is intuitive, the energy recovered increases with increasing initial temperature of the storage, because, apart from the latent heat, also part of the sensible heat can be recovered. The values of energy recovered are in the range of 2 to 5 MJ, corresponding to an energy density of

53-133 kJ/kg, while, under the same boundaries, the energy recoverable from water is 38-96 kJ/kg, about 30% lower.

Instead, the efficiency decreases with increasing initial temperature of the storage. To explain such a finding, it is worth reminding that the efficiency for the discharge process has been defined as the ratio between the recovered energy and the total theoretical recoverable energy (Equation 3.4). Then, the higher the efficiency, the higher the quantity of material that is reacting. The higher efficiency obtained for tests at lower temperatures does not mean that a higher amount of energy is recovered, it rather implies that a higher portion of material is cooled down to the final temperature of the test. Instead, when the phase change is involved, the portion of material that is reacting and completely solidifies is lower. This is consistent with what discussed for the case of charging tests.

Effect of flow rate

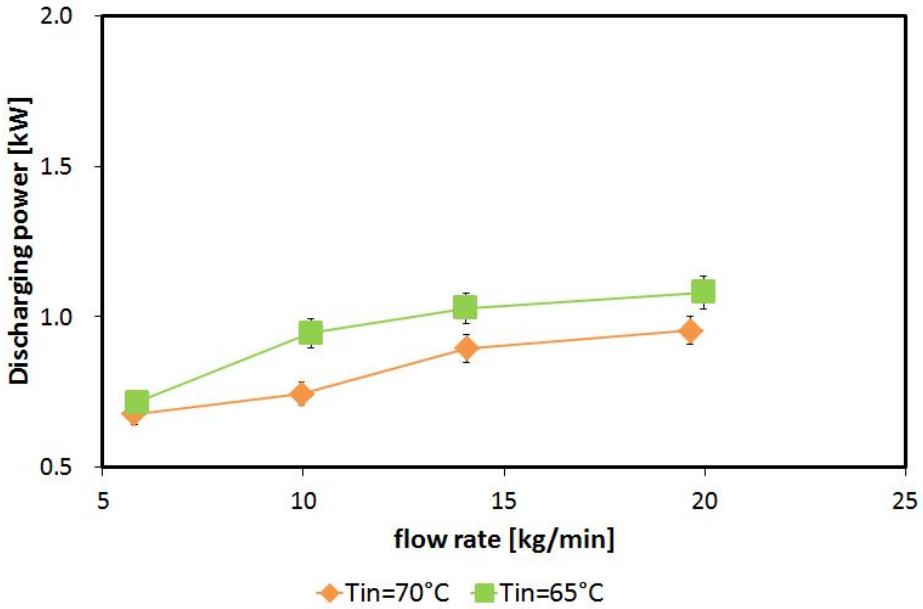

Fig. 3.33 Effect of flow rate on discharge power.

Discharge flow rate is another parameter affecting the performance of the system. Figure 3.33 and Figure 3.34 show its effect on average discharge power and discharge efficiency, respectively : for higher flow rates, the higher average power increases. However, going from 5 to 20 kg/min such an increase is only from 0.5 kW to 1.2 kW, thus indicating that the storage, in the current design, is not able for applications where high instant power is needed. On the contrary, the average time for discharge is 100 minutes, which makes the system suitable for applications where a constant power for a long time is needed. The power

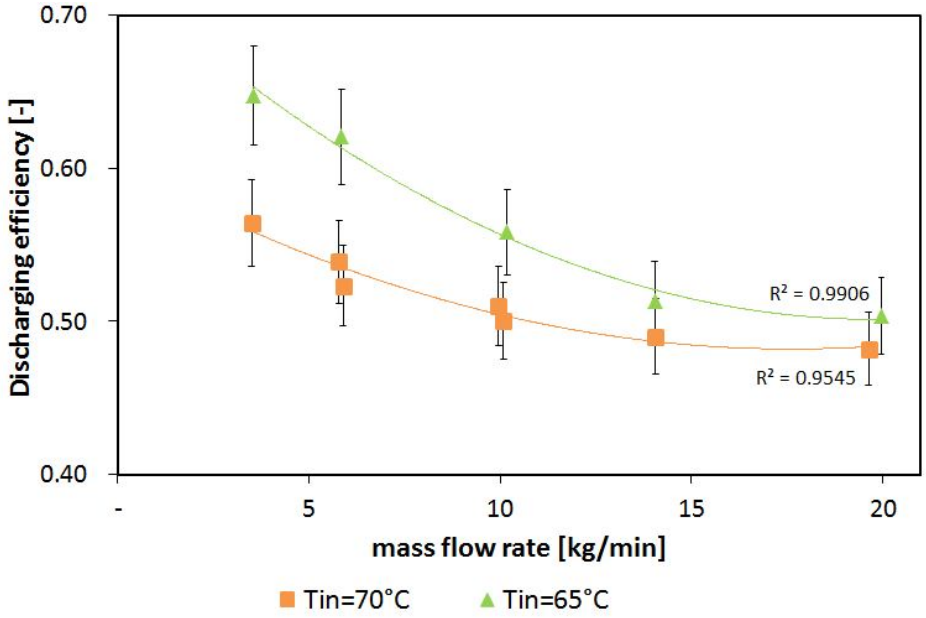

Fig. 3.34 Effect of flow rate on recovered energy.

is higher for the lower inlet temperature since the temperature difference between the PCM and the heat transfer fluid is the driving force for the phase change process.

In Figure 3.33, the effect of flow rate is investigated by plotting the discharging efficiency. The obtained trend matches that widely described in literature [88, 89]: efficiency decreases with increasing flow rate with a quadratic trend. The absolute values of efficiency are higher for the lower supply temperatures, but the overall shape of the two curves is the same.

3.9.3 Dynamic tests

As previously mentioned, a series of “dynamic” tests was made, indicating with such term tests with 3 consecutive discharge/charge cycles with a fixed time for each phase. Aim of these tests was to analyse the behaviour of the system for incomplete charge or discharge. The parameters investigated in this case were the charge/discharge times and the flow rate. The temperature profiles during two typical tests are reported in Figure 3.35 and Figure 3.36. The fixed boundary conditions of the test were: average initial temperature of the storage 87°C, 10 kg/s HTF during discharge, 20 kg/s HTF during charge, inlet temperature during discharge: 70°C, 15 minutes (Figure 3.35) and 30 minutes (Figure 3.36) for charge and discharge. From "static" tests, the long time needed for a proper charge and discharge of the system has been evidenced. Consequently, it is intuitive to find that the tests with a fixed time of 15 minutes, after the first discharge, do not allow a satisfactory charge process. This is particularly clear by looking at the temperatures of the PCM: with the exception of T3 (that

is very close to one of the tubes of the exchanger), the other temperatures have a monotone decreasing trend throughout all the test. This indicates that the energy discharged is not recovered during the partial charge. In the case of the tests with charge and discharge of 30 minutes, an increase in the temperatures of the PCM in the various sections of the heat exchanger can be identified. Moreover, with the exception of the first discharge, that starts from the initial temperature of 87°C, the other 2 are quite similar.

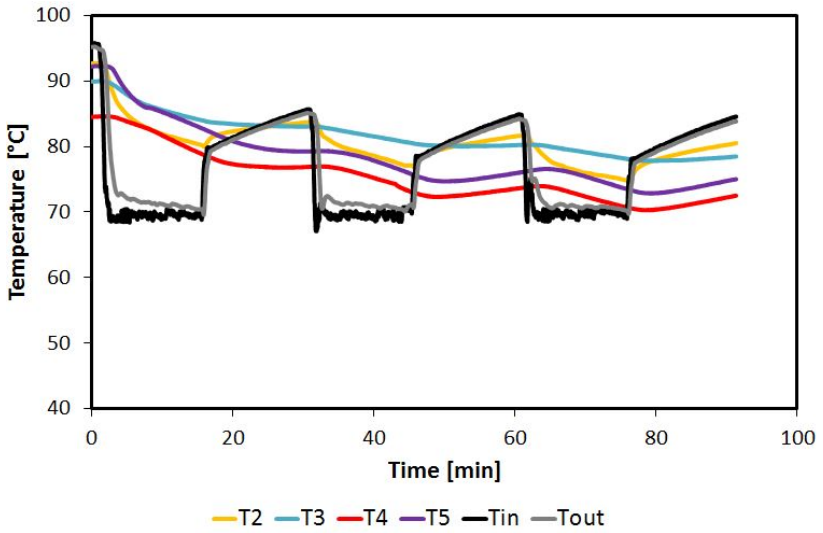

Fig. 3.35 Dynamic test with 15 minutes charge and discharge, temperature profiles.

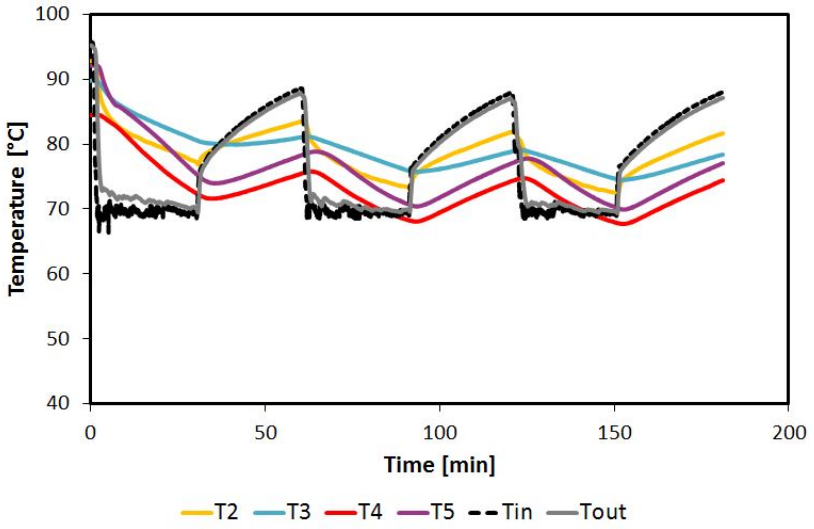

Fig. 3.36 Dynamic test with 30 minutes charge and discharge, temperature profiles.

A quantitative analysis of the results obtained during the dynamic tests is given in Figure 3.37, where the energy associated to each process (energy supplied to the system

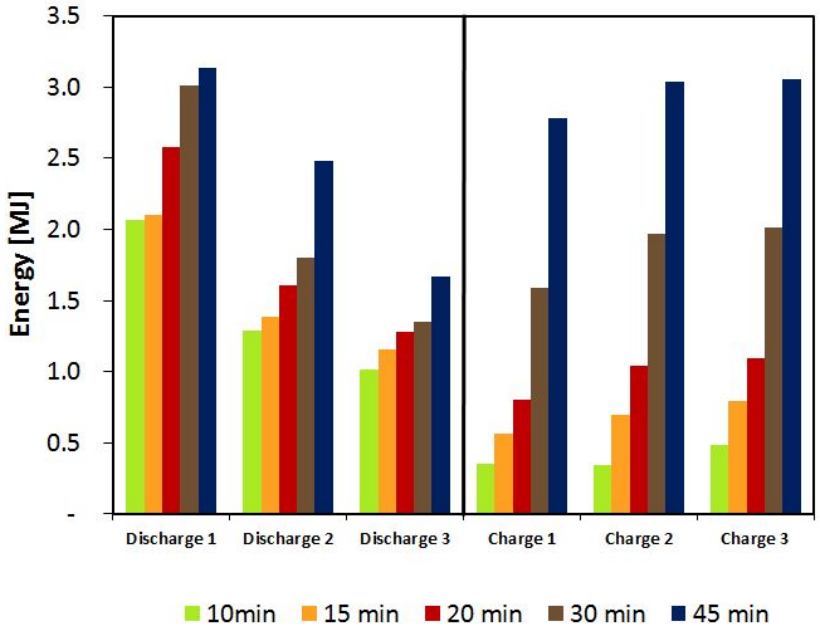

Fig. 3.37 Results, in terms of energy, of dynamic tests with various charge/discharge times.

for charging process and energy recovered during discharging process) is plotted. The tests considered are all under the following boundary conditions: average initial temperature of the storage 87°C, 10 kg/s HTF during discharge, 20 kg/s HTF during charge, inlet temperature during discharge: 70°C, while they differ for the duration of the charge/discharge. As previously stated, looking at the charge tests, under the majority of conditions, the 2nd and 3rd charge are very similar. The difference between the 1st charge and the others is instead explainable by looking at the temperature boundaries of the various charging processes: the first charge covers part of the melting interval of the phase change material, while the others are only associated to the sensible heating of the paraffin. This is the cause of the higher energy supplied during the 1st charge. The same marked difference exists during the 1st discharge and the others: the 1st discharge is realised starting from a high initial temperature (87°C), and most of the latent heat of solidification is exploited, while in the other cases the starting temperature is significantly lower.

3.9.4 Discussion

The main target of the presented testing campaign was to evaluate the effect of the various boundary conditions on a first generation prototype of a heat storage system, suitable for coupling with thermal systems (e.g. sorption chillers, CHP, ecc) where there is the need to store/release heat at a temperature of 75-85°C. To this aim, a custom fin-and-tube heat

exchanger and a commercial paraffinic material were chosen. The analysis of the tests allowed identifying the main heat transfer mechanism in such conditions, i.e. conduction. Charge tests showed that the flow rate used during charging did not hold a significant effect on the performance of the system, in terms of its charging efficiency. This is a counter-intuitive results, especially considering that the heat exchange happened in laminar regime, but it proved to be caused by the poor efficiency of the heat exchanger. Indeed, the design of the exchanger was limited by technical constraints of the manufacturer used and a more complete design should be performed in the future, by properly tailoring the characteristics (surface area, heat transfer coefficient) for the application. Discharge tests performed showed that the amount of material "reacting" (undergoing complete phase change) is only a portion of the total PCM inside the storage. Consequently, the efficiency measured is not high, in the range 45/60%. During discharge, the effect of flow rate, despite being low, was recognisable and a slight decrease in the efficiency of the system for increasing flow rates was detected. The discharge power that the system was able to supply is in the range of 0.70-1.2 kW.

Despite the reported critical issues, the energy stored during all the performed tests is in the range of 75-135 kJ/kg, which is up to 50% more that the energy storable by using the sensible heat of water (the common medium used in such temperature ranges).

Finally, dynamic tests were performed, characterised by 3 continuous discharge/charge periods for a fixed time, that was chosen between 10 minutes and 45 minutes, which is a typical range for practical applications. The results show that the best results are obtained for 30 minutes and 45 minutes tests, but after the first discharge/charge process some of the advantage of using latent heat is lost, since the system is not able to charge fast enough.

Such results indicate that an optimization of the system is necessary. As previously discussed, the heat exchanger employed for the realisation of the storage is not in an optimised configuration. Indeed, for the purpose of a first evaluation of the behaviour of the paraffinic material chosen, a custom-made heat exchanger with welded fins was employed. However, the fins were not perfectly welded to the tubes, thus adding a high heat transfer resistance, which strongly limits the achievable dynamic performance. Instead, commercial fin-and-tube heat exchangers are commonly realised by expanding the fins onto the tubes, which creates a better thermal contact between the elements and reduces the thermal resistance of the component. Moreover, the thickness of the fins of commercial heat exchangers realised by expansion is usually lower than 1 mm, while in the present case the thickness of fins was of 1.5 mm, thus adding a thermal inertia to the system which can be detrimental for its dynamic performance. Another aspect to be considered is that, should the geometry of the system allow for a convective heat transfer (despite than a conduction-dominated one), a faster melting could be achieved. However, for the paraffinic material chosen, that

is characterized by a low thermal conductivity, a careful optimization of the parameter is necessary, because using larger fin spaces (that can allow natural convection inside the material) might determine a slower heat transfer inside the material. In order to realise a performance enhancement, then, starting from the experimental findings here reported, an optimization through a mathematical modelling (validated with the experiment so far realised) can be helpful. The development of this model is reported at the end of the Chapter.

3.10 The realised system: prototype based on a plate HEX

A second approach followed in the development of a prototypal system involved the use of the same PCM, but changing the heat exchanger that represents the core of the heat storage. A commercially available plate HEX was chosen for the purpose. It is an asymmetric plate heat exchanger, with 40 plates, realised in brazed stainless steel, whose main features are reported in Table 3.6. A picture of the system, connected to the testing rig is shown in Figure 3.38. It is possible to notice that, since a brazed system was chosen, the only possible method of insertion of the PCM is through the DN160 port holes in the upper part of the heat exchanger, that were subsequently closed through specifically realised removable lids.

Table 3.6 Main features of the LTES based on the plate HEX.

Material	ASTM316L, copper brazing
Diameter pipes	1 ½" inlet/outlet connections
Number of plates	40
Plate space, fluid side	2.4 mm
Plate space, PCM side	5.2 mm
Overall dimensions	727x320x166 mm
HEX mass	41 kg
PCM mass	16 kg
Heat Transfer Fluid	Water

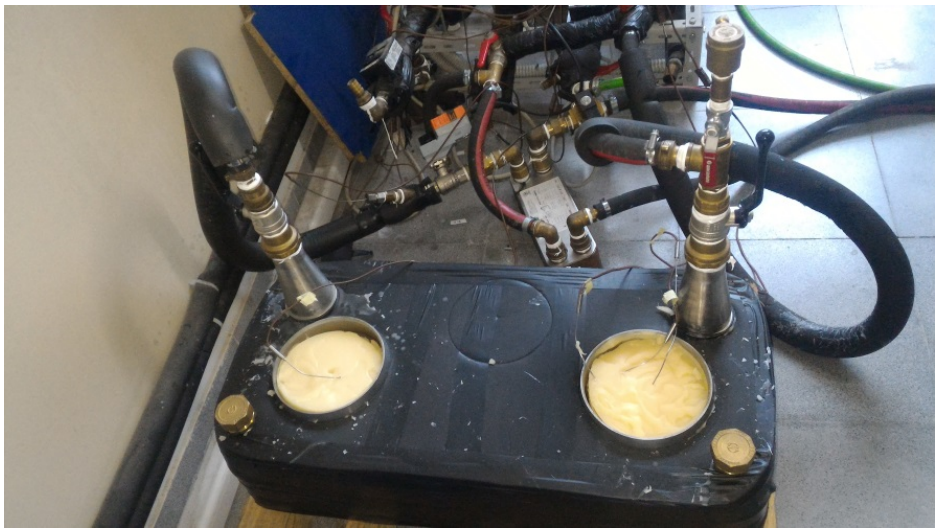

Fig. 3.38 A picture of the LTES based on the plate HEX.

3.11 Prototype with plate HEX:experimental results

For the testing of the TES, the same experimental procedure as for the fin-and-tube system was used, which is described in Section 3.7. The investigated conditions, instead, are reported in Table 3.7.

STATIC TESTS			
CHARGE		DISCHARGE	
Parameter	Value	Parameter	Value
Flow rate [kg/min]	10,15,20,25	Flow rate [kg/min]	5,10,15, 20
Initial temperature [°C]	25, 35, 65, 70	Initial temperature [°C]	85, 88, 90, 92
Final temperature [°C]	85, 90, 93	Inlet temperature [°C]	65, 70, 72
Inlet temperature [°C]	85, 88, 90, 94	$\Delta T_{0\text{-}fin}$[°C]	15, 18, 20, 25, 30

Table 3.7 The parameters investigated in the tests of the LTES with plate HEX.

3.11.1 Results of charge tests

Results of a typical test

Figure 3.39 shows the temperature evolutions during a typical charge test, covering not only the melting range of the material, but also part of the sensible heating in solid and liquid states. The flow rate of the HTF during the test is 15 kg/min. The temperature trends are analogous to those of the prototype with the fin-and-tube HEX: temperature increases rapidly during the sensible heating in the solid phase and subsequently increases monotonously but

more slowly. The three thermocouples measuring the temperature of the PCM, indicated as T1, T2 and T3 are located in the middle of the gap between the second and third plates (T1 and T2) at different distances from the ports and at the bottom of the exchanger, near one of the ports (T3). It is possible to notice that the temperature of the material is strongly influenced by the distance from the channels of the HTF: T3 is significantly lower than the other temperatures, that, instead, follow the trend of the inlet temperature of the HTF. This is due to the fact that the material that is in the cavity of the port holes does not melt, due to the low thermal conductivity and the absence of contact with the active surfaces of the exchanger. Therefore, T3 is strongly influenced by such a mass of material that is only subjected to sensible heating.

Instead, Figure 3.40 shows the power supplied to the storage during charge and the correspondent cumulative energy measured throughout the test. The initial peak in the power is around 12 kW, and it is followed by a gradual decrease, until an average power of 2 kW is reached. The time needed to complete the process is around 85 minutes, under the boundaries considered. The energy supplied increases constantly, reaching a maximum value of 6 MJ, which corresponds to 375 kJ/kg$_{PCM}$.

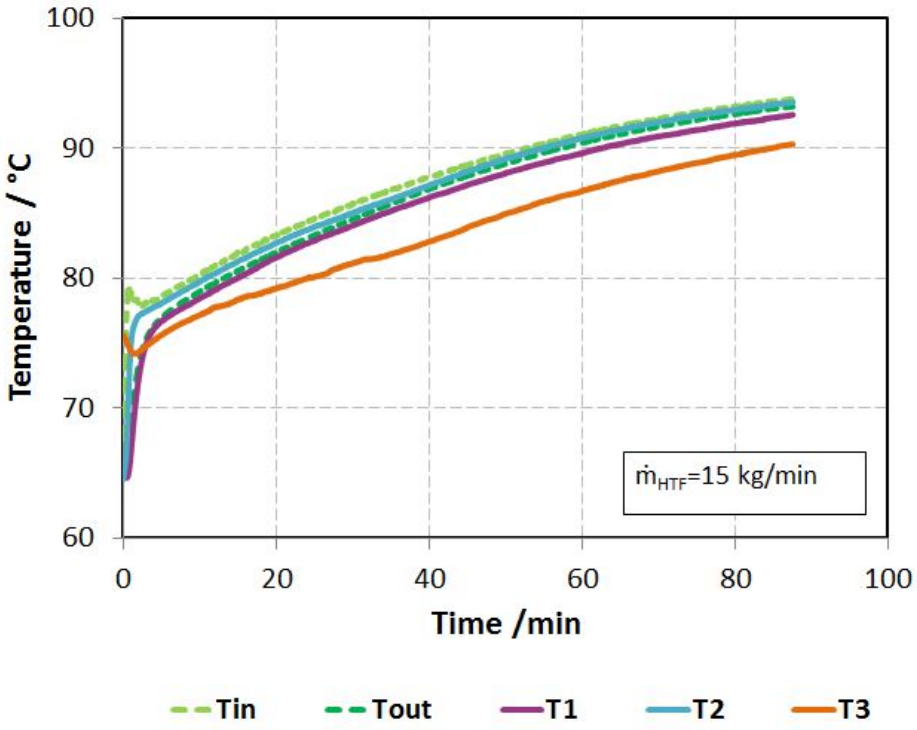

Fig. 3.39 Temperatures during a charge with $\dot{m}$=15 kg/min, T_0=65°C, T_{fin}=93°C.

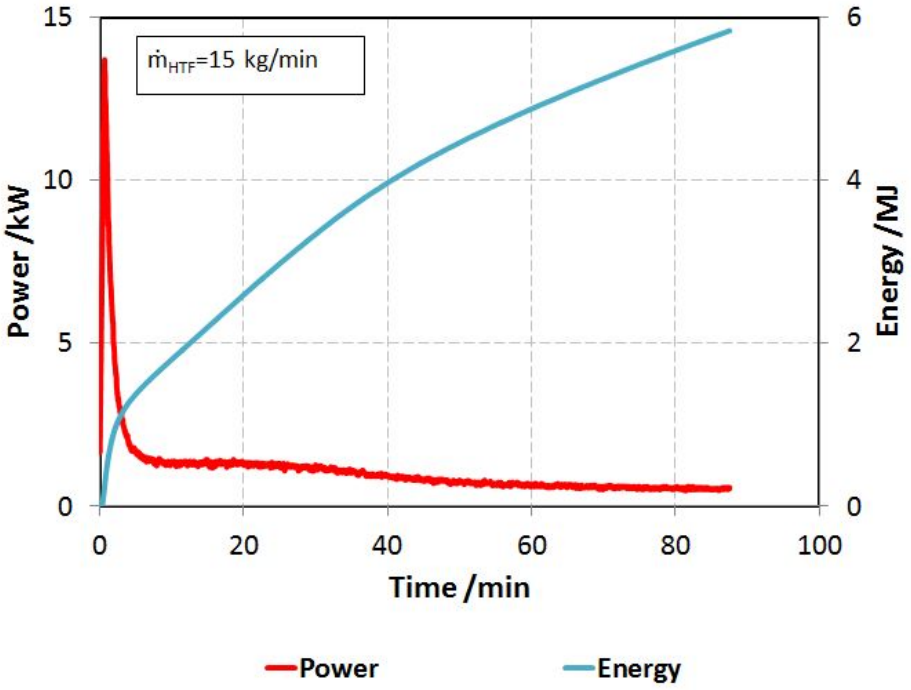

Fig. 3.40 Power supplied and cumulative energy during a charge with $\dot{m}$=15 kg/min, T_0=65°C, T_{fin}=93°C.

Effect of flow rate

The effect of the flow rate on the energy needed to charge the system and the correspondent efficiency is shown in Figure 3.41 and Figure 3.42, respectively. Three sets of tests are presented, differing for the final target temperature, and having in common the initial temperature of the storage, which is equal to 70°C. It is possible to notice that increasing the flow rate reduces the energy to be supplied to the system, thus increasing the efficiency. This is due to the fact that increasing the flow rate of the system improves heat transfer and therefore the dynamics of melting. A faster melting, in turn, allows reducing the charging time and the heat losses during the process. In particular, passing from 10 to 25 kg/min, the efficiency increases of about 10%, corresponding to up to 1 MJ of energy less to be supplied. It is also worth remarking that the efficiency of the system at the lower flow rates is in the range 82 – 92 %, with the lower values corresponding to the case of charging in the melting range only (as already noticed in the measurements on the fin-and-tubes HEX). Instead, when increasing the flow rate, the efficiency becomes independent from the operating conditions, reaching a value of 93%. This is because of the minimised differences in the time needed to complete the charge, and therefore on the heat losses, that represent the main cause for the

deviation between the energy supplied and the theoretical one. More considerations on the heat transfer and the time needed to charge the system will be given in Section 3.11.1.

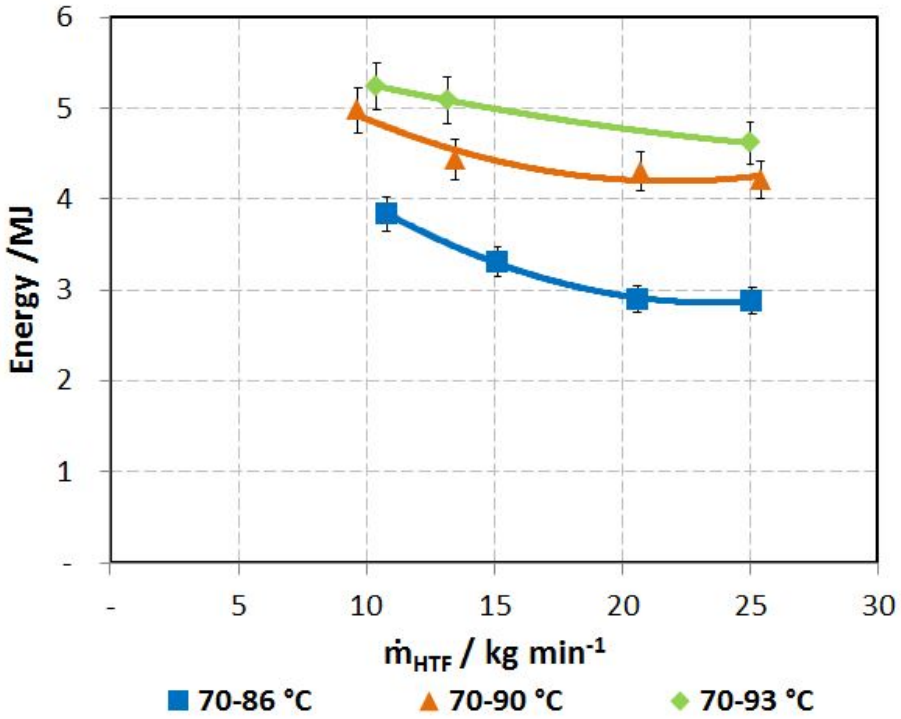

Fig. 3.41 Effect of HTF flow rate on the energy supplied during charging tests starting from 70°C.

Effect of operating temperatures

Figure 3.43 shows the energy supplied and the efficiency of the process for different charging tests, differing for the initial temperature of the storage and HTF flow rate. Charging the storage from 25°C to 93°C requires about 9 MJ, corresponding to 562 kJ/kg, while starting from the onset temperature of melting (70°C) the energy to be supplied is around half. It is then important, when designing the storage, to define whether the operation involves a complete cooling down of the system, up to ambient temperature, since this can have a strong influence on the real performance of the system over the rated one. One example where the temperature of the storage can fall significantly below the onset temperature of solidification is in solar-assisted systems for DHW or heating purposes, after the night (especially in colder climates). In these cases, the contribution of sensible heat in solid phase has to be regarded in the calculation of the peformance and features typical of the charge of the system. The efficiency of the system increases with increasing initial temperature of the storage, since

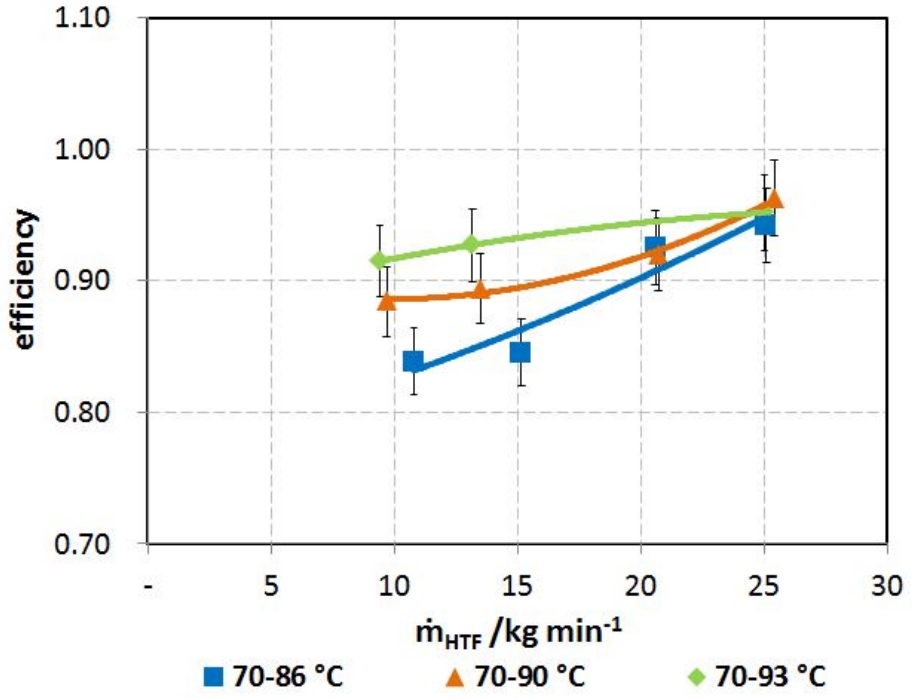

Fig. 3.42 Effect of HTF flow rate on the efficiency during charging tests starting from 70°C.

the contribution of heat losses becomes less relevant. Finally, as already stated before, the efficiency of the system is higher for higher flow rates. For the charges at 15 kg/min, passing from an initial temperature of 25°C to an initial temperature of 70°C, the efficiency increases of about 5%. This indicates that the main parameter to be considered, when analysing different charges, is the initial temperature, followed by the flow rate of the HTF, rather than the efficiency. Table 3.8 reports, in addition to the energy and the efficiency for selected tests, also the average power during the test. It is possible to notice that the values are quite low (1.1 to 1.7 kW). It is interesting to notice that the average power decreases with increasing initial temperature of the storage. Indeed, a higher temperature difference between the HTF and the PCM means that a higher driving force for the melting temperature is available. Instead, with a reduced temperature difference the process becomes slower and a lower power is measured.

Discussion

In some applications (e.g. coupling to solar energy), charge and discharge time are key constraints to be satisfied. Moreover, it is sometimes the case that a complete charge cannot be achieved (e.g. for the lack of solar radiation). It is then interesting to assess the behaviour of the system as a function of the time of charging process. To this aim, two cases are

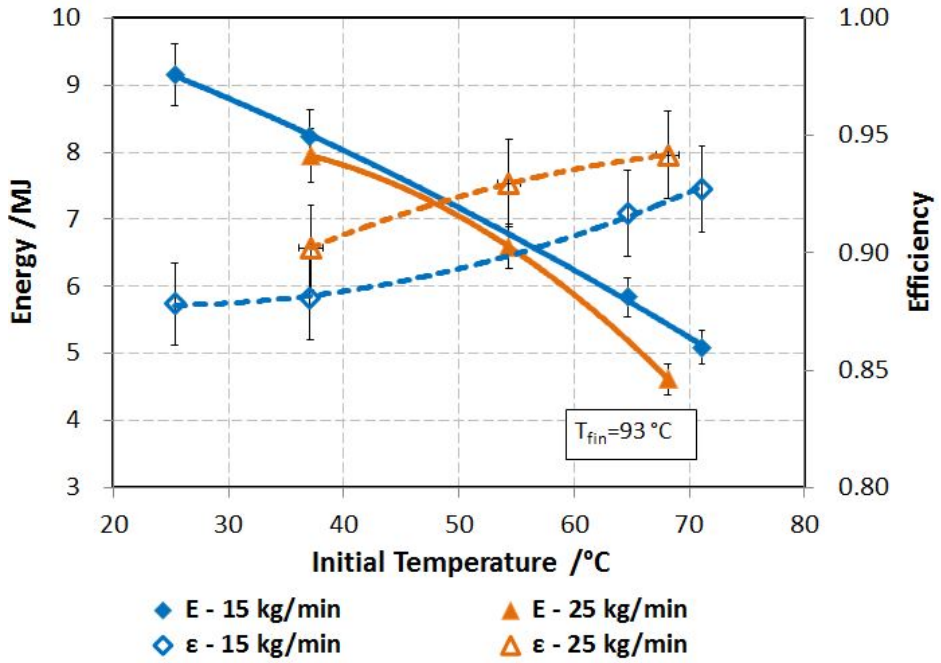

Fig. 3.43 Energy and efficiency for various charging tests at different initial temperatures.

Table 3.8 Energy supplied, efficiency and average power during selected charging tests.

Test	$\mathbf{T_{fin}}$	$\mathbf{T0}$	$\mathbf{\Delta T_{0\text{-}fin}}$	$\dot{m}_{\mathbf{HTF}}$	**E**	ε	$\mathbf{P_{ave}}$
	°C	°C	°C	kg/min	MJ	-	kW
1	93	25	67	14	9.2	0.88	1.7
2	93	37	56	16	8.2	0.88	1.6
3	93	65	28	14	5.8	0.92	1.1
4	93	71	22	14	5.1	0.93	1.1
5	93	37	56	24	7.9	0.90	1.6
6	93	54	29	25	6.6	0.93	1.4
7	93	68	25	25	4.6	0.94	1.2

compared, corresponding to 70°C initial temperature of the storage but different target temperatures, namely 86°C and 93°C. The tests covering the temperature span of 70-86°C correspond to the phase change range only, whereas the tests under 70-93 °C conditions involve the use of sensible heat of the PCM in liquid phase. Figure 3.44 shows the time needed to reach the target temperature for the two temperature ranges and different flow rates of the HTF. The trend is perfectly described by a 2nd grade polynomial expression, thus indicating that, by regulating the HTF flow rate, it is possible to predict or adjust the time for charging of the system according to the process constraints.

Figure 3.45 shows the time needed to transfer to the system a certain amount of the final energy needed to complete the charge. In particular, the time needed to complete 20%, 50%, 70%, 80%, 90% and 95% of the charge were considered. Figure 3.46 presents the same results, but in this case the time needed to complete a fixed part of the charge was normalised over the total time needed for the charge. It is interesting to notice that the time needed to reach a fixed "level" of charge does not depend on the flow rate, but rather on the temperature boundaries of the system. Moreover, in the case of 70-93°C tests, where the last part of the test involves supplying sensible heat to the liquid PCM, the charge is almost completed in 60% of the time, while the remaining time is due only to the sensible heat. Moreover, the points follow a quadratic trend, with the exception of the last part, further highlighting the different phenomena involved.

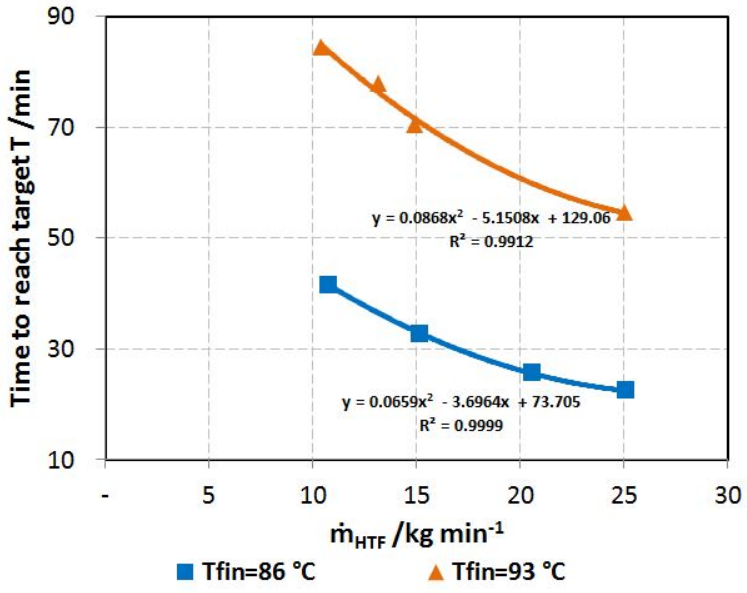

Fig. 3.44 Time needed to reach target temperature as a function of the flow rate of HTF.

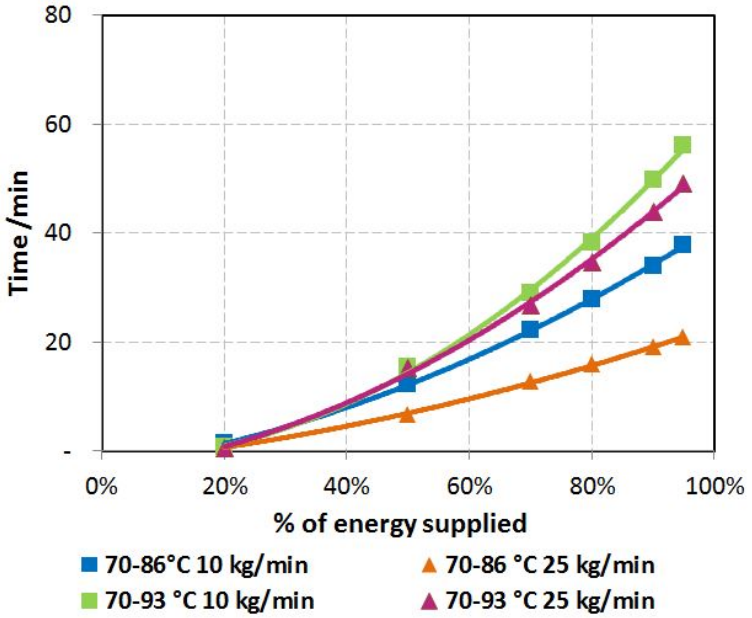

Fig. 3.45 Time needed to transfer 20%, 50%, 70%, 80%, 90% and 95% of the total charging energy.

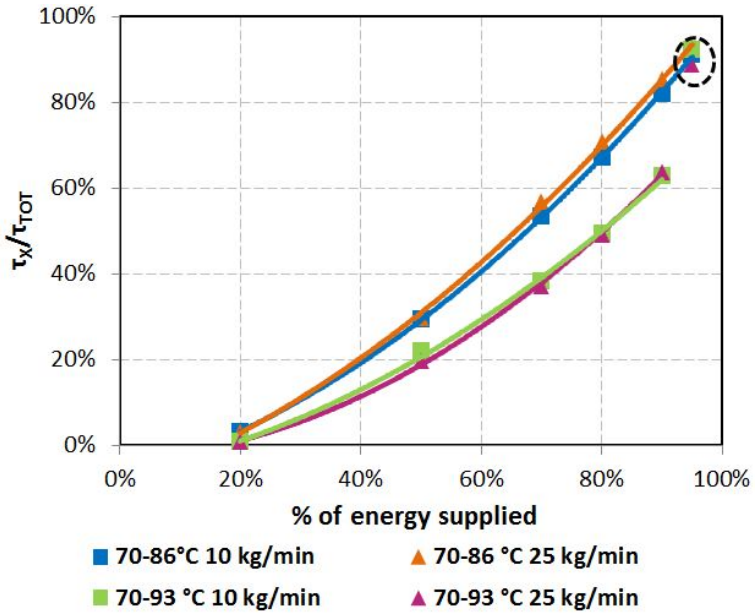

Fig. 3.46 Time needed to transfer 20%, 50%, 70%, 80%, 90% and 95% of the total charging energy normalised over the total charging time.

3.11.2 Results of discharge tests

Results of a typical test

Figure 3.47 shows the temperature evolutions during a typical discharge test, covering not only the solidification range of the material, but also part of the sensible cooling in solid and liquid states. The flow rate of the HTF during the test is 15 kg/min. The temperature of the material decreases rapidly and the solidification is almost completed within 5 minutes from the beginning of the test. The temperature of thermocouple T3, close to the material that does not undergo the phase change, changes much more slowly than the other ones (T1 and T2). This behaviour is similar to that already observed and reported for charges.

Instead, Figure 3.48 shows the power recovered from the storage during discharge and the correspondent cumulative energy measured throughout the test. The power shows the traditional shape for PCM storages: an initial peak is measured, equal to 23 kW, followed by a constant decrease. Differently from what measured in the case of the fin-and-tube system, only in the very last part of the storage the power falls below 1 kW, maintaining a value above 5 kW for more than 60% of the whole duration of the test. The energy supplied increases constantly until minute 8 (which corresponds to an almost zero power and therefore the practical end of the test), reaching a maximum value of 4 MJ, which corresponds to 250 kJ/kg_{PCM}.

Effect of flow rate

The effect of flow rate on the operational characteristics of the system during discharge is highlighted by Figure 3.49, where the energy recovered and the efficiency of the storage are represented for three sets of tests, differing for the initial temperature of the storage. As for the case of charging tests, one set of tests covers the solidification range only (86-70°C tests) while the others involve also releasing of part of the sensible heat of the PCM. It is intuitive to comment that, the higher the initial temperature of the storage, the higher the energy recovered. However, an opposite trend was observed for the efficiency: the highest efficiency was measured during the tests involving only the phase change of the material, the highest value being 78% measured for a flow rate of 10 kg/min. Indeed, the decrease of the efficiency with the flow rate and the lower efficiency measured in the tests starting at higher temperature suggest that, under the tested conditions (where no control is applied on the HEX to limit or regulate the power), the faster dynamics are penalised. This is because, at the end of the test the ΔT at the HTF circuit becomes too low to actually produce or record a useful effect and, therefore, the efficiency is lower than in the case of tests involving only the

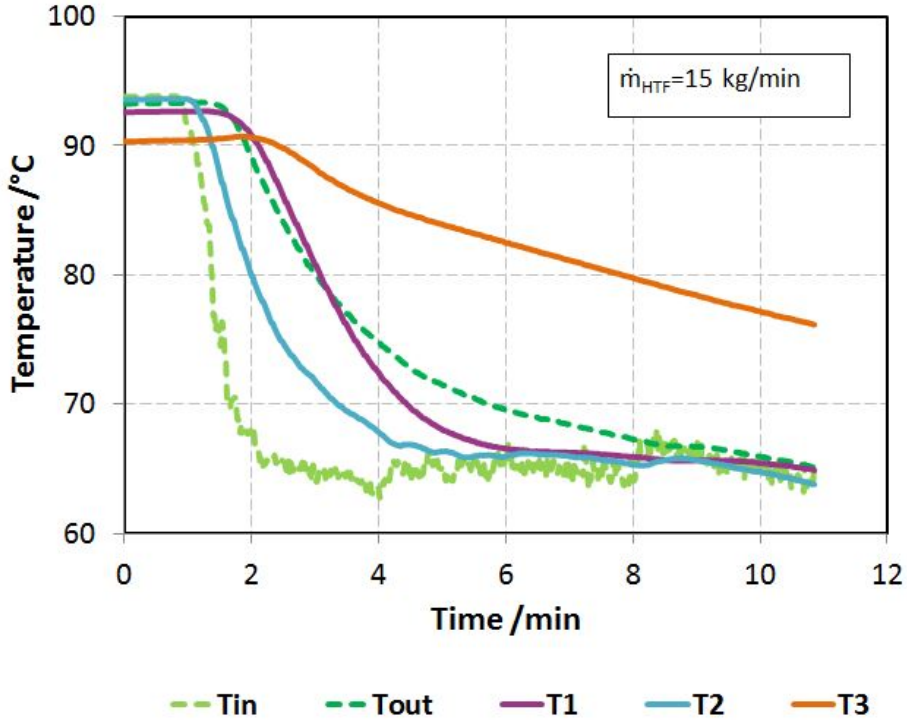

Fig. 3.47 Temperatures during a discharge with $\dot{m}$=15 kg/min, T_0=93°C, T_{in}=65°C

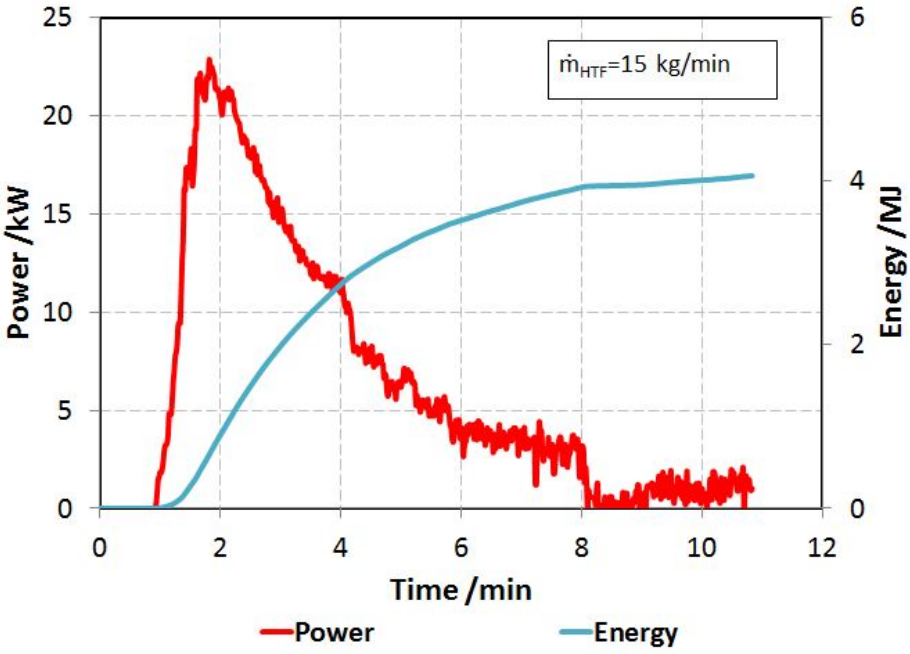

Fig. 3.48 Power recovered and cumulative energy during a discharge with $\dot{m}$=15 kg/min, T_0=93°C, T_{in}=65°C

solidification of the material. The discharging efficiency for all tests is in the range 0.60–0.78, making this system competitive if compared to the other existing technologies.

In Figure 3.50 the average power during the discharging tests is plotted as a function of the flow rate of the heat transfer fluid: the higher the flow rate, the higher the average power during the tests, with values up to 12 kW. The tests where the temperature difference between the HTF and the PCM is higher at the beginning, are those during which higher powers were measured, because a higher driving force for the phase change exists. As visible in the Figure, the lower value measured is around 3 kW, which is still significantly higher (triple) with respect to the values obtained for the fin-and-tube HEX. For flow rates of 15–20 kg/min, the average power is always higher than 6 kW, thus making this system more suitable to cases where a higher output in terms of power is needed.

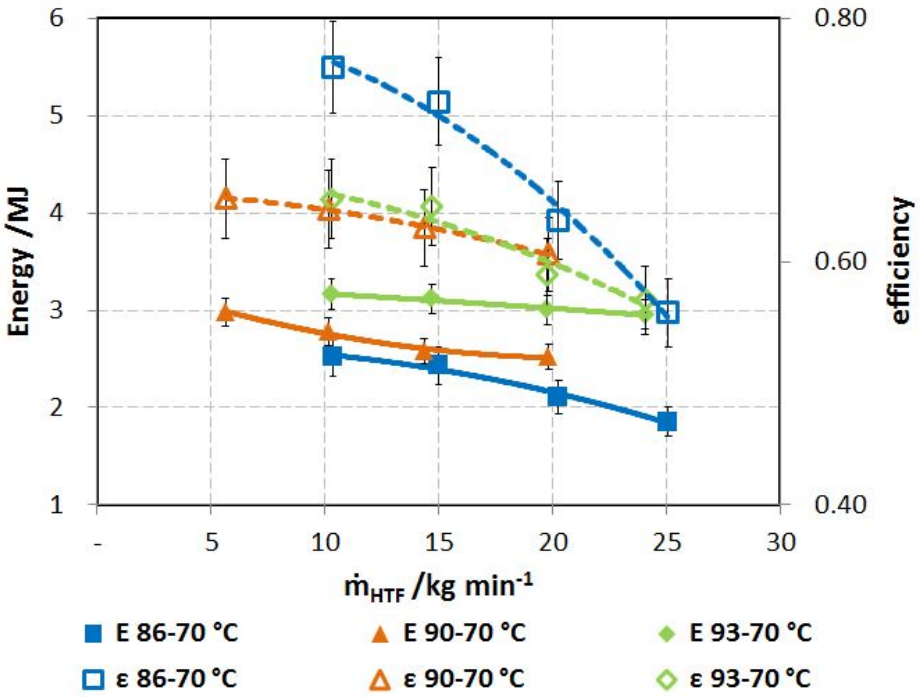

Fig. 3.49 Effect of flow rate on the efficiency and the energy recovered from the storage in different testing conditions.

Effect of operating temperatures

In order to define the effect of boundary temperatures on the operation of the storage, a comparison has been realised considering 2 different inlet temperatures (corresponding also the final temperature of the storage at the end of discharge), 65°C and 70°C, and 3 different initial temperatures 86°C, 90°C and 93°C. The results are compared in terms of energy,

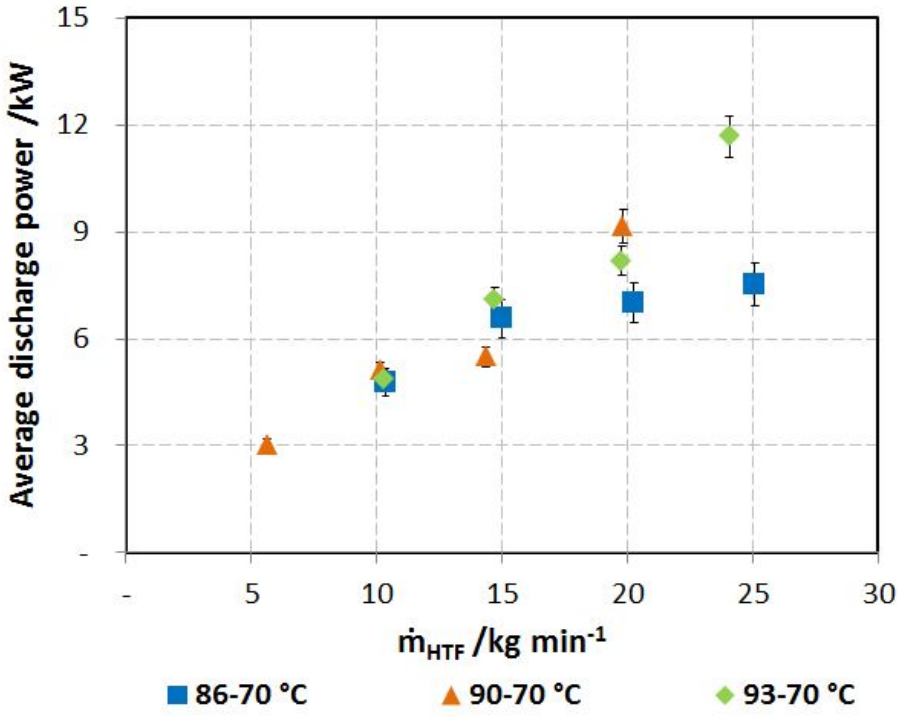

Fig. 3.50 Effect of flow rate on discharge power under different conditions.

efficiency and average discharge power in Figure 3.51. For the energy and efficiency, the difference between the values measured with the two different inlet temperatures for each initial temperature has been indicated. Instead, since average power was scarcely influenced by this parameter, the indication has been omitted.

It is possible to notice that the average difference between the energy recovered during tests at 65°C and 70°C inlet (and thus final temperature of the storage) is always constant and corresponds to around 25%. The difference, when considering the efficiency of the storage, is always around 20%. The range between 65°C and 70°C (which distinguishes the two sets of tests one another) corresponds to the sensible cooling of the material in the solid phase and it is therefore intuitive that the amount of energy recovered or the efficiency of the storage are influenced in the same way disregarding the initial temperature of the system. The power collected by the user is instead quite constant under all conditions. This is in agreement with the results reported in Figure 3.50 where, for flow rates of 10 to 15 kg/min the difference in the power between the different sets of tests considered was low.

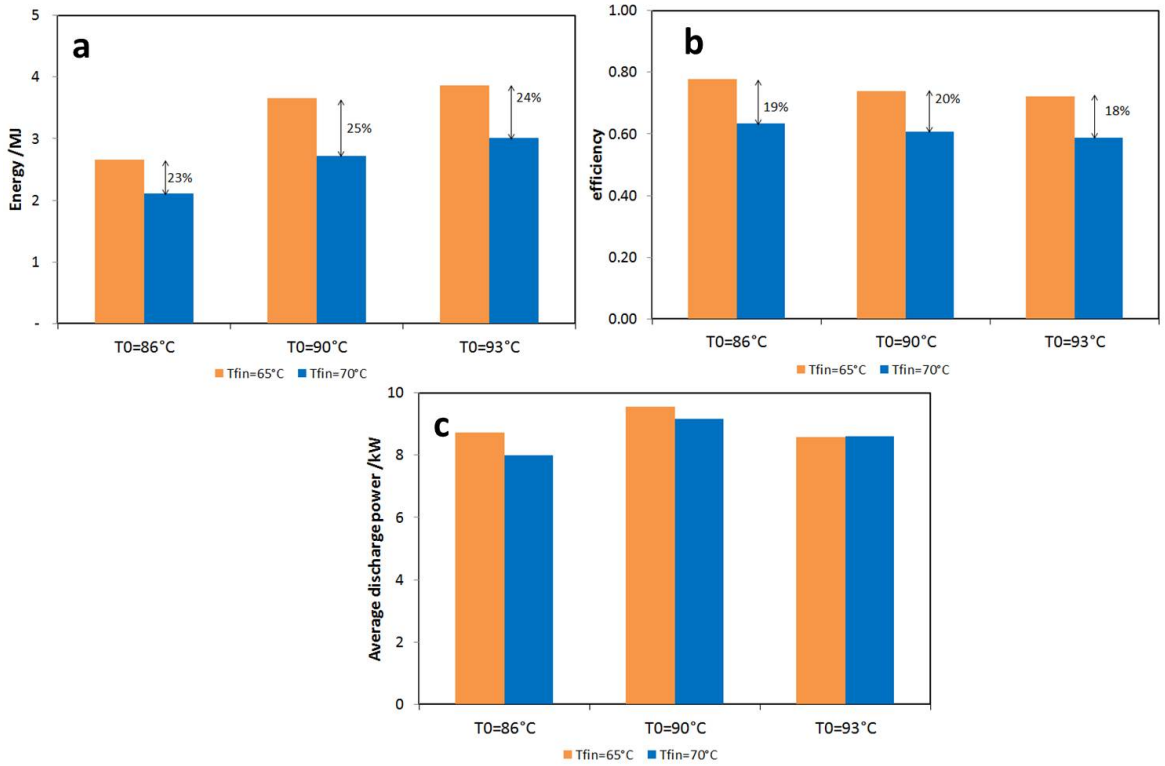

Fig. 3.51 Effect of initial temperature on the discharge of the storage; (a) energy recovered; (b) efficiency; (c) average discharge power. All the tests are carried out with mass flow rate of the heat transfer fluid of 15 kg/min.

Discussion

Figure 3.52 shows the curves of efficiency and average discharge power measured during discharging tests in two different conditions (T_{fin}=70°C and T_0 of 86°C and 90°C). Indeed, as discussed above, efficiency and power have opposite tendency with the flow rate: while higher flow rates lead to higher average discharge power, they also cause efficiency to decrease. Since the experimental trends for both parameters could be described with 2nd grade polynomial expressions, they have been represented on the same chart. For clarity's sake, the results from 70°C-90°C tests shown in Figure 3.49 and Figure 3.50 were omitted. The black point represents the optimum: for higher flow rates, the efficiency will be maximised by penalising discharge power and vice versa. The optimum point is shifted towards higher flow rates for the tests with initial temperature of 86°C, where only latent heat is released, due to the slower intrinsic dynamic of the process.

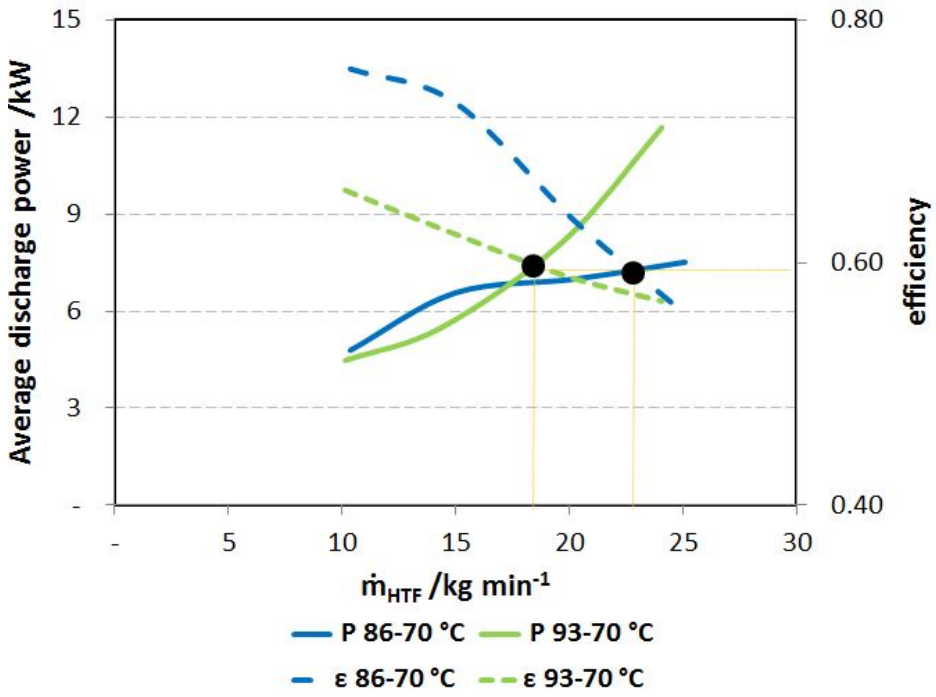

Fig. 3.52 Optimization of power and efficiency during discharge.

In Figure 3.53 the same considerations as Figure 3.46 have been applied: the picture shows the time needed to recover a certain amount of energy from the storage, normalised over the total time needed to complete discharge. Differently from charging tests, however, in this case the flow rate has a non-negligible effect. This is due to the fact that the time needed to complete the discharge is significantly lower than in the case of charge, as shown in Figure 3.54: while the time needed to complete a charge amounted to up to 60 minutes,

discharge is completed in 12 minutes at maximum, with a minimum of 4 minutes for the higher flow rates. Moreover, as shown in Figure 3.55, increasing the flow rate significantly changes the temperature difference between the outlet and inlet of the HTF circuit. This is an intuitive results, but it is worth noticing that such an effect is more evident during discharge than during charge.

From the results of Figure 3.53, it is possible to state that the time needed to release to the user a certain amount of energy increases according to a quadratic trend. It is interesting to notice that the actual time needed to discharge 80% of the overall energy is less than half of the time of the test. According to what reported in Figure 3.55, this is due to the very low ΔT at the end of the discharge tests. Considering that discharge is very fast, this indicates that, in most applications (except, for example production of DHW, where high power and fast response time are required) a way to control the power output from the storage has to be considered and implemented.

One final consideration useful for design is linked to the U value of the heat exchanger, that was calculated according to Equation 3.6 considering that the overall exchange area of the storage is known and equal to 2.16 m^2. U-value is reported in Figure 3.56 for different charging tests. While it is intuitive to comment that the U value of the exchanger depends on the flow rate, it is interesting to find out that it does not depend (or not significantly) on the temperature boundaries of the charging process: this means that, by characterising the heat exchanger, accordingly to what is commonly done for water, it might be possible to size the system without the need for complicated CFD models.

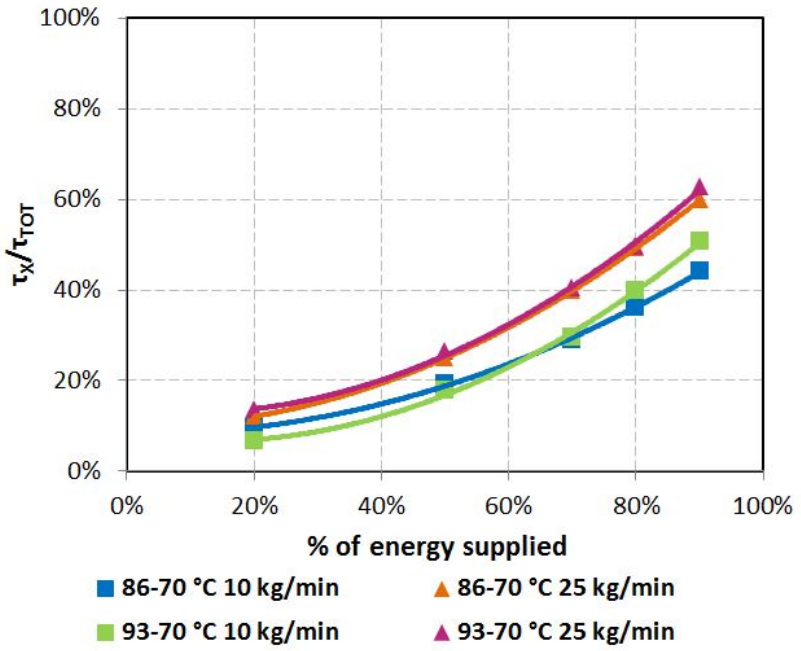

Fig. 3.53 Time needed to recover 20%, 50%, 70%, 80%, 90% and 95% of the total discharging energy normalised over the total charging time.

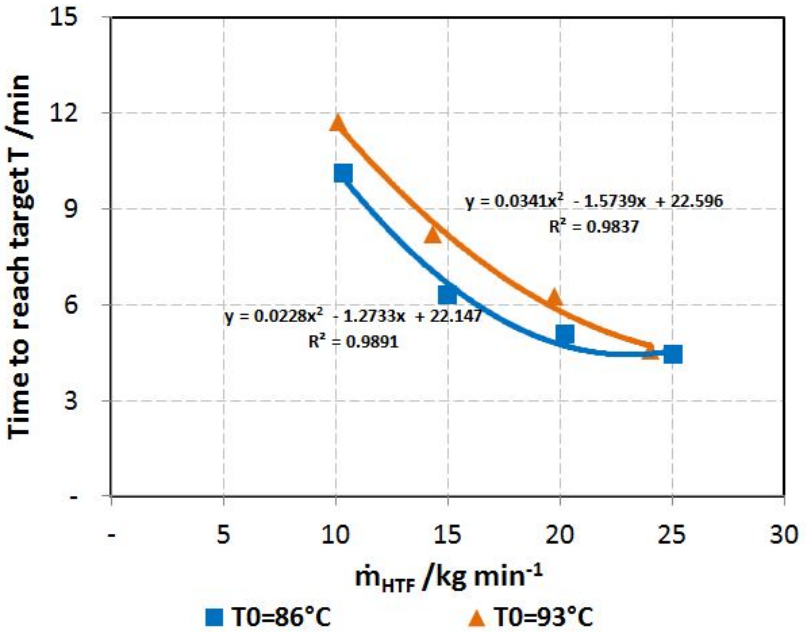

Fig. 3.54 Time needed to complete discharge in different tests with T_{fin}=70°C.

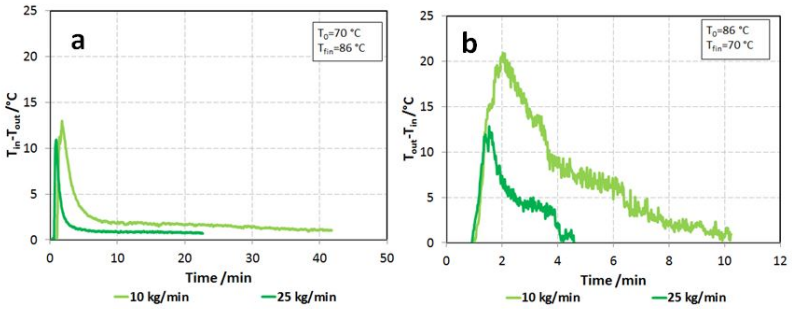

Fig. 3.55 Temperature difference in the HTF circuit during two charges (a) and discharges (b) at different flow rates.The inlet temperature is the temperature indicated as T_0.

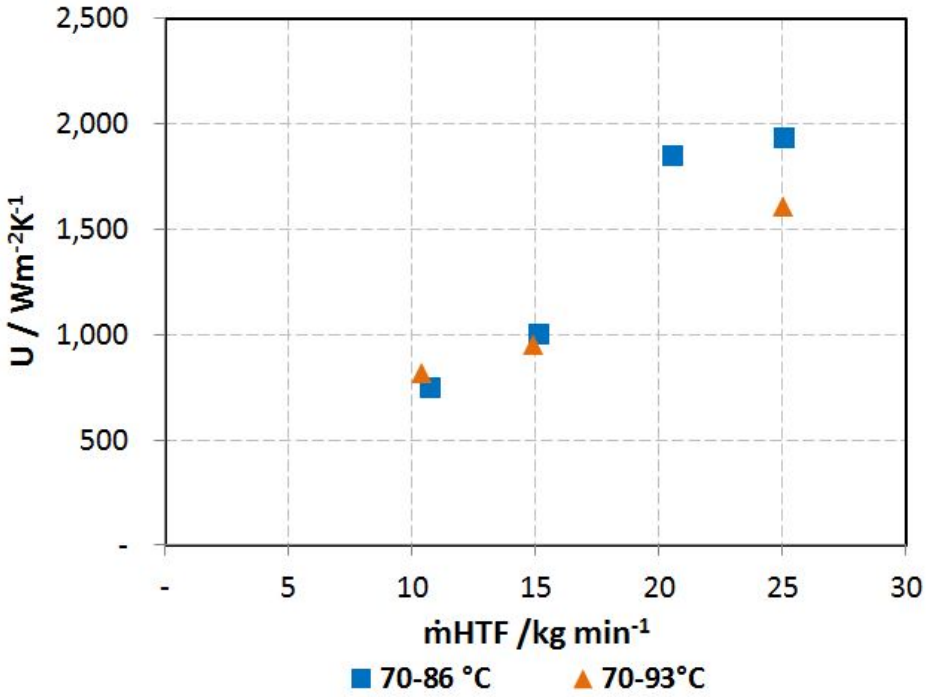

Fig. 3.56 U value for different charges.

3.12 Development of a mathematical model

The proper design of a PCM storage is linked to several complex phenomena, not easily understandable through standard methodologies, as highlighted from the experimental results presented in the previous sections. The utilization of finite elements models represents then a valid help throughout the whole design and optimization process, and is a necessary step for the advancement of PCM storages towards higher TRLs and commercial applications. To this aim, within the framework of the present thesis, a model was realised and implemented in COMSOL Multiphysics. It was applied to the fin-and-tube system previously presented and validated using experimental results.

3.12.1 Numerical models of PCM storages: recent developments

The intrinsic problem in the design of a LTES is that such systems are characterised by a moving boundary between the solid and liquid phases. The behaviour of the moving interface is such that its instantaneous position is unknown *a priori* and must be determined as a part of the solution [90]. Such a problem, traditionally known as the Stefan problem, consists in the determination of a relation between boundary conditions and the variables involved in the phase change (temperature distribution and the thermophysical properties of the material) [91]. An overview of the methods proposed in literature for the solution of such a problem is given in [90–93], while a schematic classification is provided in Figure 3.57.

In order to compare them, it is useful to describe the phase change problem, according to what reported in [93] in a general form of the type:

$$C\frac{\partial \varphi}{\partial t} = \frac{\partial}{\partial x}\left(\Gamma_\varphi \frac{\partial \varphi}{\partial x}\right) + S \tag{3.7}$$

For the three main used methods, the coefficients C, φ and S are presented in Table 3.9

Table 3.9 Coefficients used in the phase change equation for different numerical methods.

Method	**Coefficients**			
	C	φ	Γ_φ	S
Enthalpy	ρ	h	k/c_p	0
Effective heat capacity	$\rho c_{p_{eff}}(T)$	T	k	0
Heat source	$\rho c_{p_{ave}}$	T	k	$-\rho\lambda\left(\frac{\partial f_l}{\partial t}\right)$

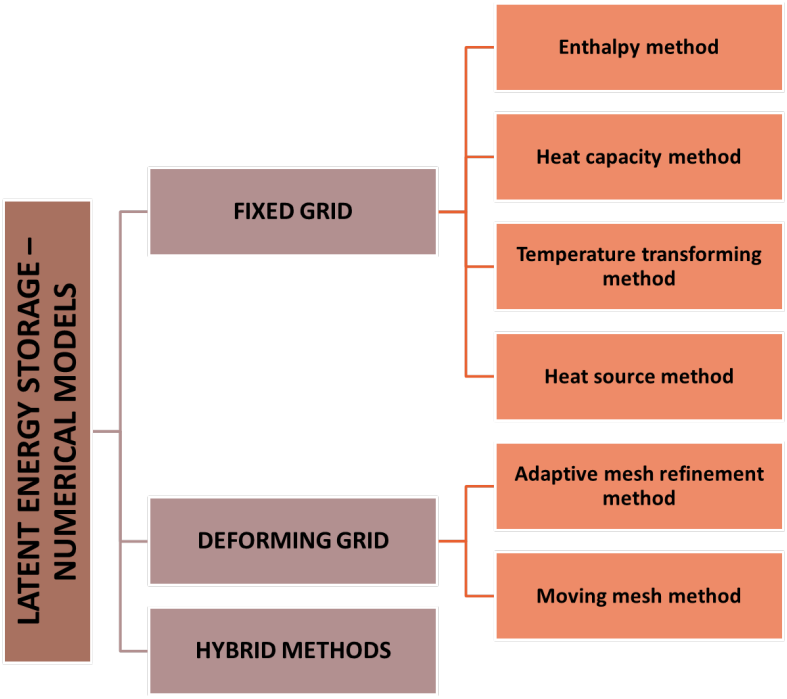

Fig. 3.57 Classification of the numerical methods proposed for the design of PCM-based storage systems.

The effective heat capacity method treats the heat capacity of the material as a function of temperature over the entire range of solidus and liquidus. This can then be defined as sum of a "base" value, the specific heat capacity of the material outside the temperature range of the phase change and an additional specific heat, obtained by Differential Scanning Calorimetry measurements within the PCM melting temperature range:

$$c_{p_{eff}}(T) = \begin{cases} c_{p_s} & T < T_1 \\ \frac{\lambda_m}{\Delta T} + c_{p_s} & T_1 < T < T_2 \\ c_{p_l} & T > T_2 \end{cases} \tag{3.8}$$

where T_1 and T_2 are the temperature of onset and offset of melting, respectively.

This method has the advantage of allowing rewriting the problem in terms of a single variable.

The enthalpy methods makes use of the enthalpy function H to define the energy conservation. Equation 3.7 can be rewritten as:

$$\frac{\partial H}{\partial t} = \nabla[k(\nabla T)] \tag{3.9}$$

Moreover, the interface between the two phases is described by the so-called "mushy region", thus taking into account the existence of a transition range rather than a single phase change temperature. The advantages of such a method are:

- the governing equation are written in terms of a single variable;
- there is no need for explicit boundary conditions at the interface between the phases;
- the implementation is easy.

The heat source method is an alternate method that modifies the source term in the energy equation at the interface and includes latent heat into this term. However, such an approach results in a discontinuity at the interface and therefore convergence problems often arise, thus not representing an ideal choice.

Moving grid methods are based on the idea that the grid density should be higher at the solid-liquid interface and lower elsewhere. By using such an approach, the computational effort should be reduced, when compared to fixed grid methods. The two main variants proposed are the local mesh refinement method and the moving mesh method. In the former, the model starts with an uniform grid and, at each iteration, grid points are added or removed to match the required accuracy. The problem intrinsic to this method is that the number of grid points is changing at each iteration. To avoid that issue, the moving mesh method starts with a uniform mesh and then moves the mesh points, keeping the mesh topology and number of mesh points fixed as the solution evolves. However, the implementation of moving grid methods is usually less intuitive and consequently in most cases fixed grid methods are used [93].

In addition to the heat transfer equation, other phenomena have to be taken into account [90]: among them, the natural convection is the most important, since the buoyancy effect of the melt plays a key role, especially during the melting process. The volumetric expansion of the PCM, the enthalpy hysteresis during melting/solidification and the subcooling phenomenon are other issues that complicate the definition of a detailed model for the phase change problem.

Availability of several simulation and CFD commercial codes and the development of the abovementioned numerical models have increased the research in the simulation of complex LTES configuration. However, as reported in [94], most of the existing numerical models of LTES use a simplified geometry (usaully 1D or 2D semplifications), in order to the reduce the computational effort required. For example, in [95], a shell-and-tube heat exchanger was firstly simulated through a 3D numerical model. Due to the complexity of the heat transfer phenomena inside the PCM and the relative needs of computational resources, a simplified

model reduced to a one-dimensional radial diffusion equation was developed which proved to be sufficiently reliable, especially in predicting performance over long physical time spans.

Nonetheless, accurate simulations and the reproduction of more complex geometries require detailed 3D simulations [96]. In this context, shell-and-tube configuration has been particularly studied: in [94], for example, a LTES using a ternary mixture of salt as PCM and a shell-and-tube heat exchanger was numerically simulated by implementing a 3D model in COMSOL. The simulated results were experimentally validated with good accuracy and used for a parametric study. In [97], a detailed numerical model based on the energy and momentum conservation equations was used to study the effect of the pulsed fluid flow on the heat transfer efficiency of a shell-and-tube heat exchanger. In [98] a numerical 3D model, solved in Fluent, was used to study the optimal geometry of the fins to be used in a shell-and-tube configuration with the aim of improving the heat transfer inside the PCM. In [99], a tube-in-tank HEX with paraffin embedding copper foam as PCM was simulated. The model was implemented in Fluent and validated to analyse the heat transfer mechanisms of the realized storage. [100] reports the model of a cylindrical tank employing a microencapsulated slurry of PCM as thermal storage medium. The model was implemented in Fluent employing the effective heat capacity method and validated against experimental data.

Fin-and-tube configuration has been considerably less studied in numerical applications for latent thermal storage. In [101] the model for a fin-and-tube heat exchanger using high-density polyethylene (HDPE) as PCM is reported. The model represents the whole geometry of the system in 3D and has been implemented in Fluent. Validation with the experimental proved the accuracy of the model, but, at the same time, the computational effort was high.

Main outcome of the reported literature survey is the need to carefully simulate LTES configurations, in order to investigate the most influencing geometrical and physical parameters on the achievable heat transfer efficiency. To do so, 3D model are desirable, but at the same time a model with less computational complexity is needed, in order to reduce the time for simulations.

3.12.2 Goal of the modelling activity

The overview of the methods presented in literature for the simulation of LTES highlighted the advantages of the enthalpy method and the effective heat capacity methods. Starting from such a literature survey, a model was developed for the examined PCM storages, making use of the effective heat capacity approach. The model was realised in COMSOL Multiphysics in collaboration with Fraunhofer ISE in Freiburg im Breisgau (Germany). The model and its validation for two storages (the fin-and-tube here presented and a storage tested at Fraunhofer ISE) were published in [102].

The main features of the models are its simplicity, both in implementation and in terms of computational effort, and the possibility to easily adapt it to different layouts. Indeed, it is worth noticing that the model was applied to the fin-and-tube heat exchanger as a case study, but it could be suitable also for the simulation of the plate heat exchanger, by simply adapting some geometric parameters.

Evaluation of the heat transfer mechanism

Prior to the implementation of the model, a first evaluation was made on the heat transfer mechanism involved, in order to define whether natural convection could be neglected. The effect of natural convection is usually associated with the Rayleigh number, that is linked to the buoyancy-driven flow responsible for natural convection: natural convection does not occur for Ra < 2000 [103]. Rayleigh number in the present case was calculated considering the space among fins as a vertical enclosure, and can then be expressed as [103]:

$$Ra = \frac{g\beta\rho^2 d^3 \left(T_{wall} - T_{PCM}\right) Pr}{\mu^2} \tag{3.10}$$

where the width of the enclosure d has been considered equal to the space between the fins. The Prandtl number for the PCM has been calculated as:

$$Pr = \frac{\mu c_{p_l}}{k_l} \tag{3.11}$$

In Figure 3.58, the results of the calculation as a function of different temperature differences between the material and the fins are shown. It is visible that natural convection can be considered negligible regardless of the temperature difference. Consequently, the simulation of the system will be developed by considering that the only mechanism responsible for heat transfer inside the PCM is conduction.

Assumptions

The basic model consists of two components, modelled separately: the tubes of the heat exchanger are modelled in 1D and the fins-PCM region is modelled in 3D. The following assumptions have been made:

1. The heat transfer in the PCM and the fins is modelled in 3D in order to represent the heat transfer from the fin and the tubes to the PCM as well as in the PCM itself.

2. Convection in liquid state of the PCM is negligible.

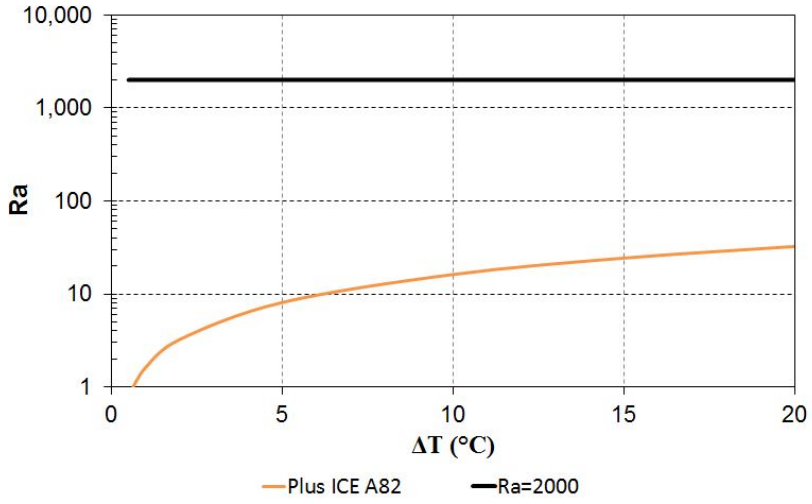

Fig. 3.58 Rayleigh number for different ΔT.

3. In the pipes, the flow is fully developed.
4. The thermal gradient in the heat transfer fluid flow region in radial direction is negligible and therefore heat transfer of the fluid is 1D.
5. The heat transfer between the fluid and the wall is calculated by a Nusselt-correlation under the assumption of constant wall temperature.
6. Volumetric expansion of the PCM during phase change is neglected.
7. The material properties of the PCM differ in solid and liquid phase, but are considered constant in these ranges.
8. The material properties of the heat transfer fluid are considered as temperature dependent.

3.12.3 1D model

The tubes of the heat exchanger have been simulated in 1D as an assembly of 8 sub-domains, each one corresponding to one of the tubes of the heat exchanger in each rank. The 1D model of the tubes employs a user-defined inlet temperature and fluid velocity to calculate the heat flux towards the PCM in each part of the pipe and the outlet temperature of the HTF. A layout of the 1D component, together with the boundary conditions imposed, is shown in Figure 3.59. The equation defining the heat transfer is the monodimensional form of Fourier's law:

$$A_c \rho c_p \frac{\partial T}{\partial t} + A_c \rho c_p u \nabla T + \nabla \left(-A_c k \nabla T\right) = \dot{Q} \tag{3.12}$$

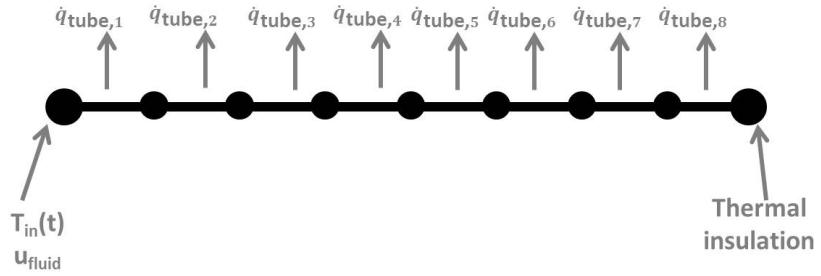

Fig. 3.59 Basic layout of the 1D model for the tube, in which the boundary conditions are indicated in grey.

In each i-th part of the tube, the heat transfer between the fluid and the wall is calculated as:

$$\dot{q}_{tube,i} = h\,(T_{HTF} - Twall, i) \qquad i = 1 \ldots 8 \tag{3.13}$$

The temperature in the i-th part of the wall of the pipe is calculated in the 3D model of the fin and used as input in the 1D model, as will be explained in the next sections. Instead, the heat transfer coefficient h has been calculated according to a Nusselt correlation [104]:

$$h = \frac{Nuk_{HTF}}{d_{inner_{tube}}} \tag{3.14}$$

$$Nu_{laminar} = 3.6568 \qquad Re < 2300 \tag{3.15}$$

$$Nu_{turbulent} = 0.023 Re^{4/5} Pr^{1/3} \qquad Re \geq 10^4 \tag{3.16}$$

$$Nu_{transition} = (1-\gamma) Nu_{laminar} + \gamma Nu_{turbulent} \tag{3.17}$$

with:

$$\gamma = \frac{Re - 2300}{10^4 - 2300} \tag{3.18}$$

As above mentioned, the boundary conditions imposed are:

$$T|_0 = T_{in}(t) \tag{3.19}$$

$$u|_0 = u_{HTF} \tag{3.20}$$

$$Q|_L = 0 \tag{3.21}$$

A tetrahedral mesh with element size in the range 0.013-0.074 m was chosen.

3.12.4 3D model

The PCM and the fins are modelled in 3D. However, to reduce the computational effort needed to solve the model, instead of modelling the whole heat exchanger, half a fin (in the direction of thickness) and half a fin gap filled with PCM is modelled. In order to correlate the results of such a simplified geometry with the experimental ones for the whole heat exchanger a correction factor will be introduced in the next section. The layout of the basic geometry, together with the boundary conditions imposed is shown in Figure 3.60.

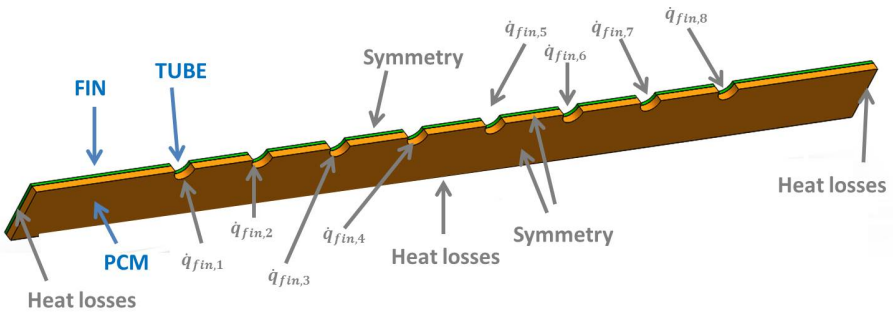

Fig. 3.60 Basic layout of the 3D model for the fin and PCM, in which the boundary conditions are indicated in grey.

The heat transfer is defined by means of the differential form of the Fourier's law:

$$\rho Cp\frac{\partial T}{\partial t}+\rho c_p u\nabla T+\nabla\left(-k\nabla T\right)=\dot{Q} \tag{3.22}$$

The boundary conditions imposed include the symmetry on the fin and the PCM and the heat losses. At the boundary with the tubes, a heat flux has been imposed, due to the exchange with the heat transfer fluid. Such a contribution was calculated by correlating the 3D model to the 1D model of the tube. The mesh chosen is tetrahedral, with an element size in the range 0.00585–0.0325 m, as a mesh study showed that a finer mesh did not lead to better validation results.

Coupling of 3D and 1D models

The 3D and the 1D-model are coupled to each other by means of temperatures and heat fluxes at the inner wall, i.e. each section of the 1D tube is coupled with the inner wall of one tube of the 3D-model:

- The temperature at the boundary of the wall of the pipe, taken from the 3D model, is used for the calculation of the heat flux in the 1D model.

- The heat flux calculated in the 1D model is used as input in the 3D model, for the calculation of the actual temperature of the PCM.

Figure 3.61 shows a sketch of the coupling for the basic 3D model with the 1D model. The heat flux for the 3D model (applied at the boundary with the tube) is the one calculated in the 1D model, but it has to be scaled with the ratio between the corresponding area of the 1D and the 3D model. Thus the actual heat flux applied $\dot{q}_{fin}$ is calculated as:

$$\dot{q}_{fin} = \bar{\dot{q}}_{tube} f = \frac{A_q}{A_{inner_{tube}} n_{fin} N_{sym}} \tag{3.23}$$

$$A_q = \pi \phi_{inner_{tube}} l_{tube} \tag{3.24}$$

where f is the ratio between the corresponding areas in the 3D and the 1D model and N_{sym} is the symmetry ratio taking into account the ratio between the actual heat exchanger and the part simulated in the model.

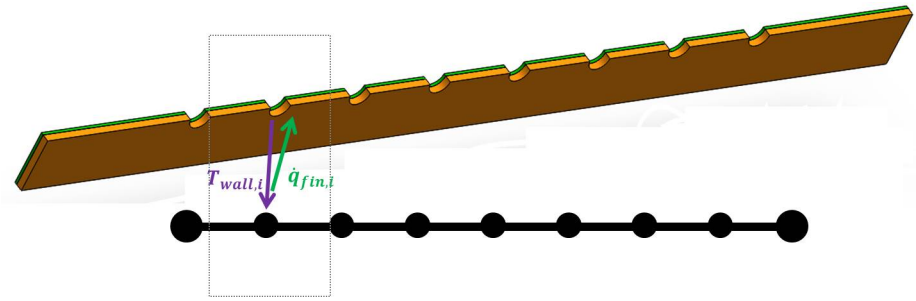

Fig. 3.61 Coupling of the 3D model for the fins and the 1D model for the tubes. Each section of the tube in the 1D model is coupled to one part of the tubes in the 3D model (indicated by the dashed line).

Calculation of heat losses

Thermal losses to the environment represent a relevant contribution in the definition of the energy balance of the system. They can be evaluated considering the convective heat exchange between the TES and the environment, by means of natural convection. The resulting heat flux is defined as:

$$\dot{q}_{losses} = h_{losses} \left(T_{ext,TES} - T_{amb} \right) \tag{3.25}$$

where $T_{ext,TESS}$ is the temperature of the external housing of the storage and T_{amb} is the ambient temperature. For validation purposes, the ambient temperature used is the one

experimentally measured during the tests. Instead the heat transfer coefficient was computed analytically as: :

$$h_{losses} = \left(\frac{1}{h_{air}} + \frac{s_{insulation}}{k_{insulation}} \right) \tag{3.26}$$

where h_{air} is the convective coefficient for natural convection in air, taken from [104], $s_{insulation}$ is the thickness of the insulating material and $k_{insulation}$ the thermal conductivity of the insulating material.

3.12.5 Model validation

The model validation was carried out to define whether the developed model can represent the systems. In particular, the results of simulations and measurements were compared in terms of temperatures and power: the simulated temperatures at the outlet of the heat transfer fluid and at defined points in the PCM were compared to the measured ones, together with the power during charge and discharge. The initial conditions during the simulation were taken from the measurements: the inlet temperature to the storage as a function of time, and the mass flow of the heat transfer fluid as a function of time were supplied to the 1D model for the tube. Moreover, the ambient temperature in the lab was inserted for the calculation of heat losses. In Figure 3.62, the position of the probes used to replicate the temperature sensors of the actual measurements are shown.

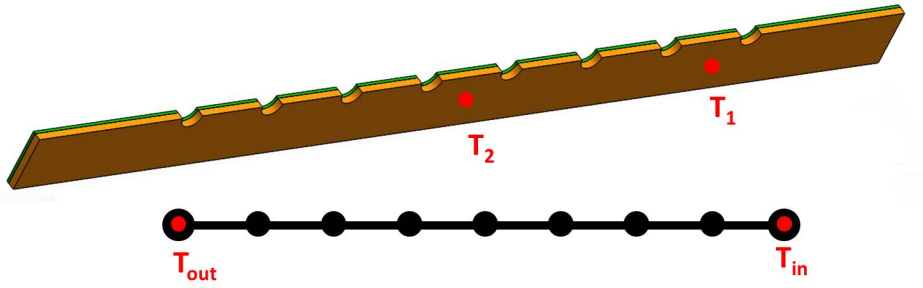

Fig. 3.62 Position of temperature probes in the model.

For the validation of the charging process, a test with a constant mass flow of 10 kg/min and thus a Reynolds number of 1,450 was chosen, while the initial temperature of the storage was 25 °C and the final temperature was 90 °C. Figure 3.63 shows the comparison of the temperatures: there is a good agreement between the simulated and experimental fluid outlet temperature, with a deviation lower than 0.2 K. This indicates that the model is able to adequately predict the behaviour of the heat exchangers and the heat flow associated to the heat transfer fluid. A more noticeable difference is instead visible for the profiles of the temperatures simulated and measured inside the PCM in the storages. It is worth noticing

that, as stated in the description of the experimental measurements, also in the simulation the phase transition is not clearly identifiable from temperature profiles. Instead, an increasing temperature, with a constant slope can be identified, until the set temperature of the heat transfer fluid is reached. However, the maximum deviation between the simulation and the measurement is lower than 4 K, further highlighting the possibility to describe the storage with the realised model. The time needed to complete the simulation was lower than 30 minutes on a Intel(R) Xeon(R) CPU E5-2690 0 @ 2.90GHz with four cores, confirming that the approach followed allows reducing the computational requirements, without losing the accuracy typical of 3D models. In Figure 3.64, the simulated and measured power supplied to the storage during charging is compared, showing, also for this quantity, a good agreement between the measurements and the simulation.

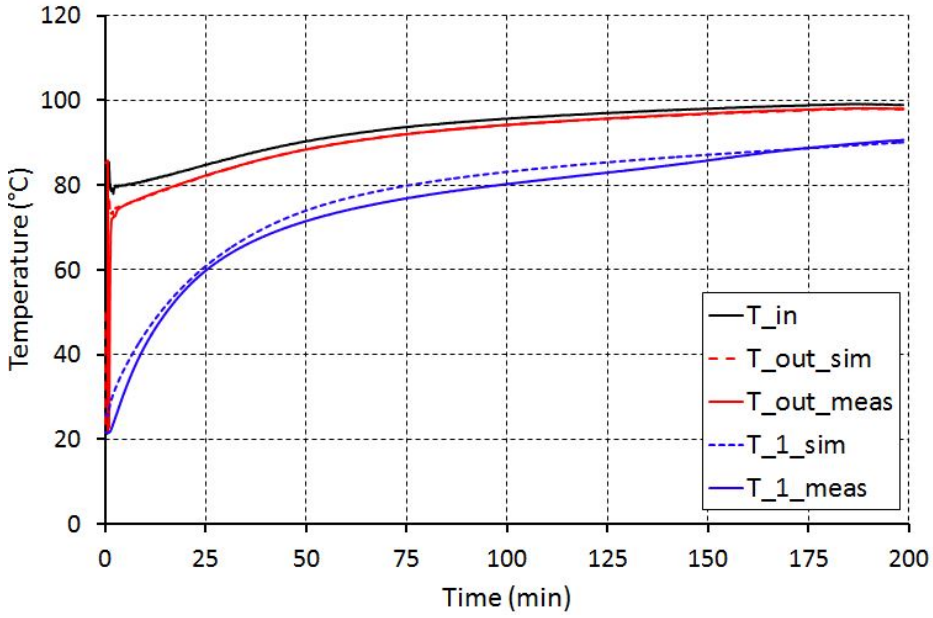

Fig. 3.63 Comparison of simulated and measured temperatures for storage charging.

For the validation of the discharging process a test with a mass flow rate of 5 kg/min and temperatures between 95 °C and 75 °C were used. The comparison of the simulated and measured temperatures is shown in Figure 3.65: the deviations in the inlet and outlet temperatures of the heat transfer fluid are on average around 0.6 K and always lower than 5 K, with some fluctuations visible in the measurement. This is due to the experimental procedure: the temperature of the fluid in the measurement is affected by the operation of the three-way mixing valve used to set the discharge temperature resulting in some peaks. The temperature simulated has a much more stable trend, as expectable. As for the charging process, taking into account the uncertainty of the measurement, the model fits well also for the discharge of

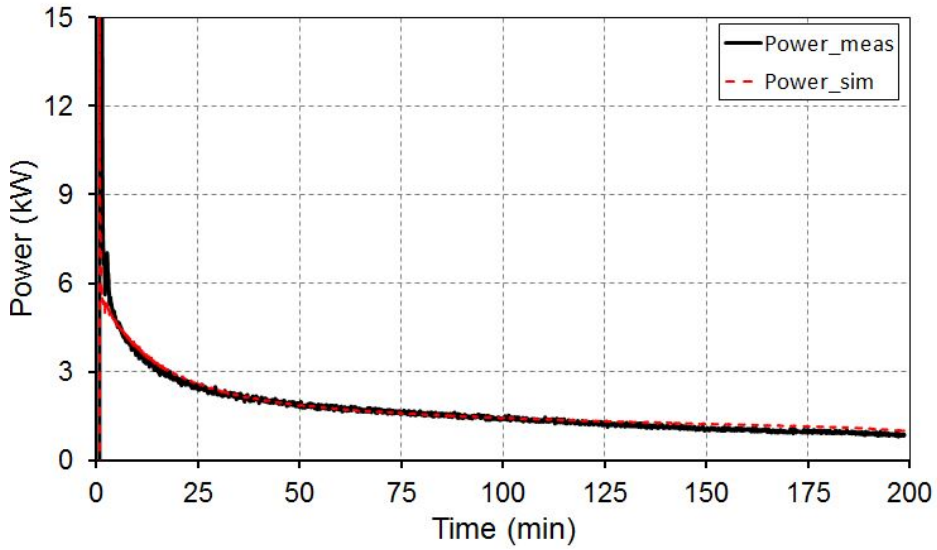

Fig. 3.64 Comparison of simulated and measured power for storage charging.

the storage. The PCM temperature in the simulation showed a deviation always lower than 3 K. Considering as in the charging process the difficulty in reproducing the exact measured position, the validation of the model for the examined case can be considered satisfactory.

Figure 3.66 shows the comparison of measured and simulated power: as stated before, the power shows fluctuation due to the above described reasons of the mixing valve, but the difference between the tests and the simulation is higher than 70 W only after 20 minutes, when the process has been practically completed. It is then possible to confirm that the model can represent the actual heat exchanger with a good degree of accuracy.

Discussion

The model realised fulfils the requested target: describing the behaviour of the fin-and-tube HEX filled with PCM with low computational effort. The validation, presented for just one charge and discharge, has been verified under different conditions, in terms of temperatures and flow rate, with satisfactory results. The possible application of the model for the optimization of the system is then feasible and will represented the next step towards the development of a second generation system with this technology.

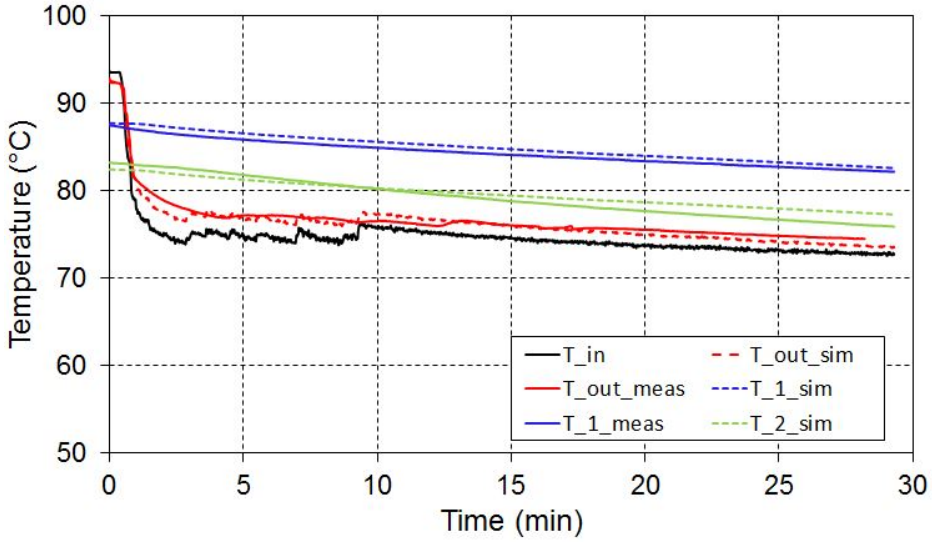

Fig. 3.65 Comparison of simulated and measured temperatures for storage discharging.

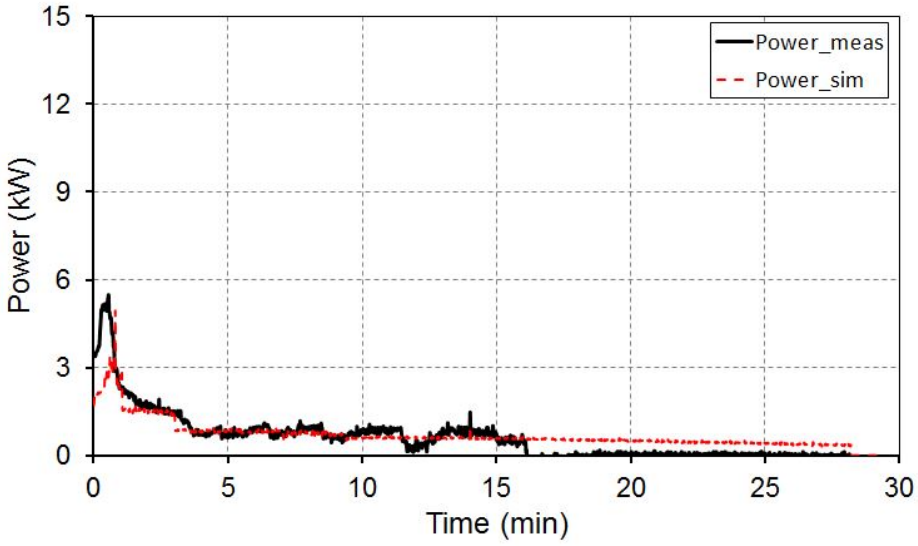

Fig. 3.66 Comparison of simulated and measured power for storage discharging.

3.13 Final remarks and advancement with respect to the state-of-art

The activity proposed in the present chapter can be divided into four main sub-activities:

- development of a testing bench and a testing protocol for latent or hybrid thermal energy storages;
- design and experimental testing of a PCM storage with a customised fin-and-tube HEX;
- experimental testing of a PCM storage employing a commercial plate HEX;
- development and validation of a numerical model for the PCM storages.

The main reasoning of the presented tasks have already been presented, but it is worth remarking that the lack of experimental activities on LTES make the testing benchmarking compelling for the development of these devices towards a higher maturity and commercial possibility.

All the tests were carried out in a specifically modified testing bench, that allowed analysing a wide range of conditions, with uncertainties lower than 8%. The main feature of the testing bench, compared also to other systems already presented in literature, is the possibility to test relatively large systems (up to 50 L) in a temperature range below 100°C, setting the charge and discharge temperatures and flow rate, and thus guaranteeing a good flexibility in reproducing real operating conditions.

Considering also that PCM-based storages in the temperature range 60-100°C have not been the subject of intensive research (mainly due to the direct competition with water) — and consequently not much data exist — two different approaches were adopted in developing a storage: on the one hand, a custom system based on a fin-and-tube HEX was realised and tested and, on the other, a commercial plate HEX was filled with the same PCM and tests in the same conditions were realised. The proposed configurations differ from the shell-and-tube systems that have been mainly proposed ad characterized in literature, thus presenting an element of novelty. Moreover, the experimental testing was performed under a wide range of conditions — not only in the phase change range —, allowing to gather information that can be useful for the design of the system.

With this regard, the experimental results showed the systems exhibit a complicated behaviour. Consequently, a numerical model was developed, in collaboration with Fraunhofer ISE in Freiburg, for the description of PCM storages. Main features of the developed model, that distinguish it from other published work, is the low computational demands and the

coupling of a 1D model for the HTF with a simplified 3D model, that allowed describing the behaviour of the HEX by considering a section of PCM within 2 fins.

In conclusion, the activity has shown that energy storage capacity with up to 50% increase with respect to water can be achieved, but further work is needed for the optimization of the system, through a proper computer-aided design.

Chapter 4

Development of an adsorption thermal energy storage system

4.1 Definition of the problem and methodology

In this chapter, the whole process of development of a lab-scale storage using an adsorption material as the storage medium will be reported. In accordance to the activity related to latent TES, initially a short description of the main features of the system and the recent developments regarding the specific application will be drawn. Following that, the activity carried out will be presented and the main progress with respect to the state-of-art will be highlighted.
The main boundaries of the project and the target characteristics required to the storage are similar to those already described in Section 3.1 and are linked to the application of the system where low-temperature heat is available (e.g. industrial process, non-contentrating solar collectors) for the production of heat at 35°C-45°C, then suitable for space heating or DHW:

- temperature of the heat source in the range 80°C-100°C;
- temperature of the heat to be supplied to the user in the range 35-45°C (which is lower than those required for the LTES);
- energy density higher than 100 MJ/m^3, in accordance to the target already specified for the latent units.

The methodology followed in the development of the system is summarised in Figure 4.1. In particular, the choice of the storage material was done starting from the comparison among the adsorbents in the operating conditions realised through the thermodynamic

model developed in [36], based on the experimental measurement of adsorption isobars and isotherms mainly realised at CNR-ITAE. Once the best performing material was identified, the system was designed and realised. A dedicated set-up was installed in a testing rig already avaialable at CNR-ITAE, that is suitable for the characterization of thermally driven systems. The results of the experimental benchmarking were used for a critical review of the design of the system.

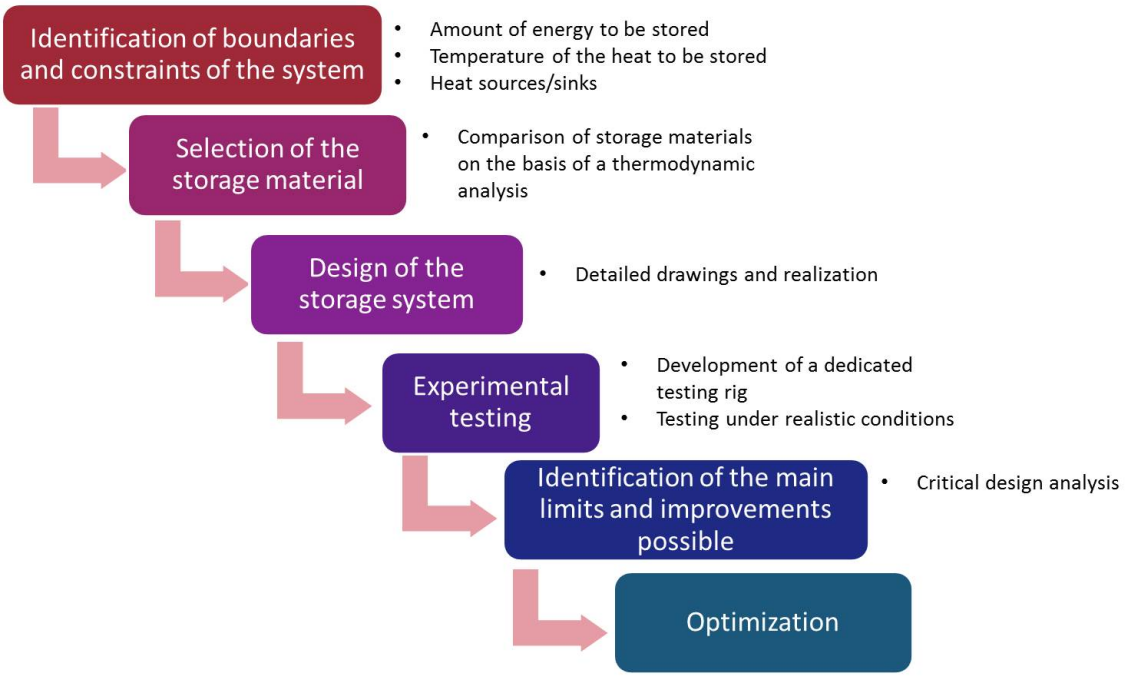

Fig. 4.1 Methodology followed in the development of a thermochemical heat storage system.

4.2 Recent developments: adsorption for low-grade waste heat or solar heat

4.2.1 Design issues

Adsorption systems have been extensively studied, mainly for heat pumping, air conditioning and refrigeration applications. Consequently, a lot of effort has been put in R&D, trying

to address the main issues related to the performance of the system and the increase of volumetric or mass energy and power density [35]. The issues related to the design of a TCS system are are schematically reported in Figure 4.2. As for the case of LTES, it is possible to distinguish three different levels: a first screening has to be made regarding the materials available and their practical application, that can be limited by problems such as the high desorption temperature, the high cost (e.g. in the case of MOFs) and their stability. As for components, the main issues being assessed are heat and mass transfer intensification through the adsorbent-heat exchanger (AdHEX) unit and the design of compact system components, with specific emphasis on the evaporator/condensing unit. Finally, concerning the whole system, activity is aimed at defining the optimal control strategy and thermal management to guarantee high performance and primary energy saving. LCA analysis is also a goal for the future, but it was not applied to the present thesis, dealing with systems still at lab-scale level.

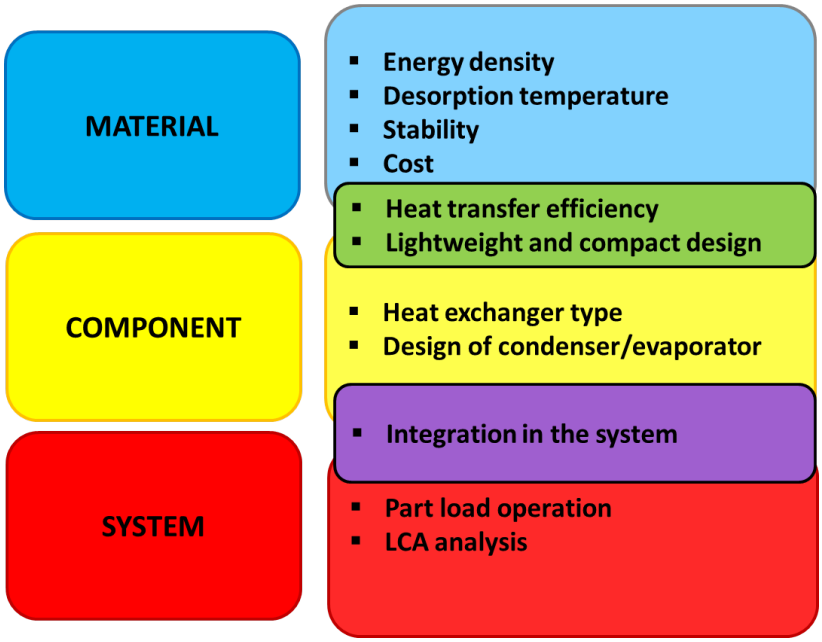

Fig. 4.2 Main issues in the design of a thermochemical heat storage system.

4.2.2 Prototypes of adsorption storages for low-grade heat applications

Regarding thermochemical storage (TCS), many studies are reported in literature giving an overview of the materials available, based on both experimental measurements of adsorption isobars/isotherms or thermodynamic evaluation of promising working pairs. Efforts have also been devoted to the development of modified materials, such as modified zeolites, or the promotion of new adsorbents, such as SWS and MOFs, as extensively reported in

Chapter 2. On the contrary, literature regarding sorption storage lab-scale or real-scale prototypes is even scarcer than those regarding LTES systems, partly because of the recent interest in the topic, but also for the complexity required for the system. An overview of projects available or initiated, but whose results have not been published yet is given in [35]. Among lab-scale prototype with closed systems, Li et al. [105] developed a prototype of a thermochemical battery for sorption storage consisting in a reactor separated by means of an insulator from a storage tank, which operates as condenser, evaporator and tank. Working pair is $SrCl_2/NH_3$, and has been tested both for heat and cold production at temperatures of, respectively, 85°C to 50 °C and -35 °C to -20 °C. Energy densities reached are of 1724 and 674 kJ/kg. Schreiber et al.[66] developed a lab-scale storage prototype containing 20 kg of zeolite 13X for application in a CSP plant serving a brewing process. Results from experiments were used to calibrate a model for large-scale applications. Weber et al. [106] developed a combined water and sorption storage, consisting of a star-shaped container, in which the central part was occupied by a heat exchanger filled with zeolite 13X and connected to solar thermal collectors. Experimental results showed a maximum energy density of 95 kWh/m^3. Hauer [107] reports two demonstrative projects active in Germany: a refrigerated beer keg, consisting of a keg with an external vessel filled with zeolite and an evaporator at the bottom of the keg. Adsorbent is regenerated at 90°C in an oven. The other reported project is a seasonal storage installed in a low emission house near AEE in Austria, consisting of 3 adsorbers filled with silica gel and connected to a solar thermal collectors array. The storage density of the system proved to be below the expectations, with maximum value reached of 150 Wh/m^3. Lu et al. [108] developed a storage for cold distribution in the driver's locomotive of a train in China. The prototype was made of an heat exchanger filled with 85kg of zeolite 13X and was tested during train journeys, reaching a storage density of 600 kJ/kg. As clear from the presented literature survey, still effort and research activity are needed to develop compact and high-performing storages. Moreover, the reported projects are designed for desorption temperatures higher than 90°C, whereas thermal storage from process heat or non-concentrating solar heat requires lower temperatures.

4.3 Selection of the storage material

The storage material has been selected on the basis of the thermodynamic analysis reported in [36]. The achievable theoretical storage energy is given, for a set of boundary conditions (i.e. temperatures of desorption, adsorption, condensation and evaporation) as:

$$E_{storage} = m_{adsorbent} \Delta H_{adsorption} \Delta w \tag{4.1}$$

In order to describe the adsorption potential, either the Dubinin-Astakhov (DA) approach or the Dubinin-Radushkevich (DR) is used. For the DA, the adsorption equilibrium can be described as:

$$w = w_{max} \exp\left(-\left(\frac{A}{E}\right)^n\right) \tag{4.2}$$

where the adsorption potential A is described as:

$$A = RT \ln \frac{p_{sat}}{p} \tag{4.3}$$

Instead, the DR approach is widely used to describes activated carbon/ ammonia working pairs:

$$w = w_0 \exp\left(-k\left(\frac{T_{sat}}{T} - 1\right)^n\right) \tag{4.4}$$

Adsorption enthalpy, in both cases, is calculated as a function of the adsorption potential. For the DA approach:

$$\Delta H_{adsorption}(w) = \Delta H_{ev} + A(w) - T\Delta S(w) \tag{4.5}$$

and, for the DR approach:

$$\Delta H_{adsorption}(w) = RY \frac{T}{T_{sat}} \tag{4.6}$$

where Y represents the slope of the saturated adsorbate line on the Clapeyron diagram, that for ammonia is 2823.4 K. In [36], the fitting of several working pairs is presented, based on data from literature or measurements taken at CNR-ITAE. Results of the analysis are presented in Figure 4.3 and Figure 4.4, where the energy storage density for seasonal storage is plotted against the temperature lift and desorption temperature, respectively. The temperature lift represents the temperature difference between adsorber and evaporator during the adsorption phase and between adsorber and condenser during the desorption phase. The results do not take into account the contribution of condensation energy, hence the characterization for seasonal energy storage (of course, in case of short term energy storage where condensation enthalpy is recovered the energy density can be higher). Both the Figures are taken from [36].

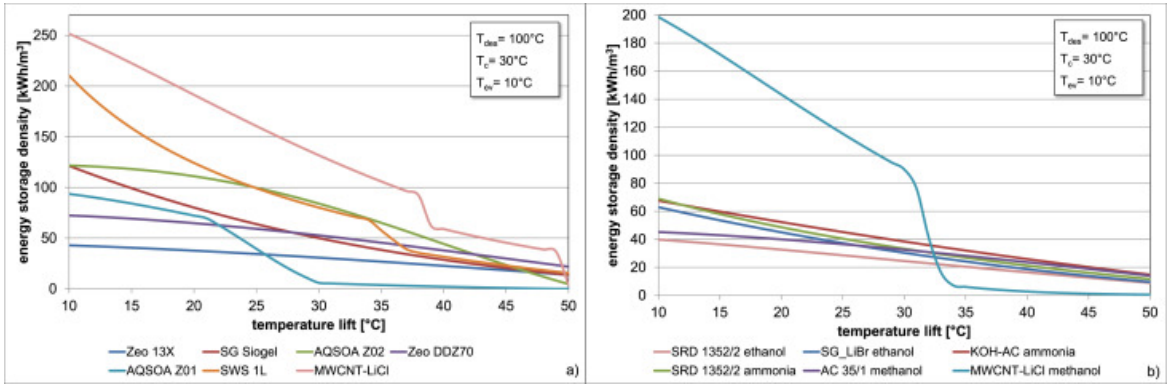

Fig. 4.3 Seasonal energy storage densities of the identified working pairs as a function of the temperature lift: a) water as working fluid; b) other working fluids. Desorption temperature fixed at 100 °C, condensation temperature fixed at 30 °C, evaporation temperature at 10 °C.

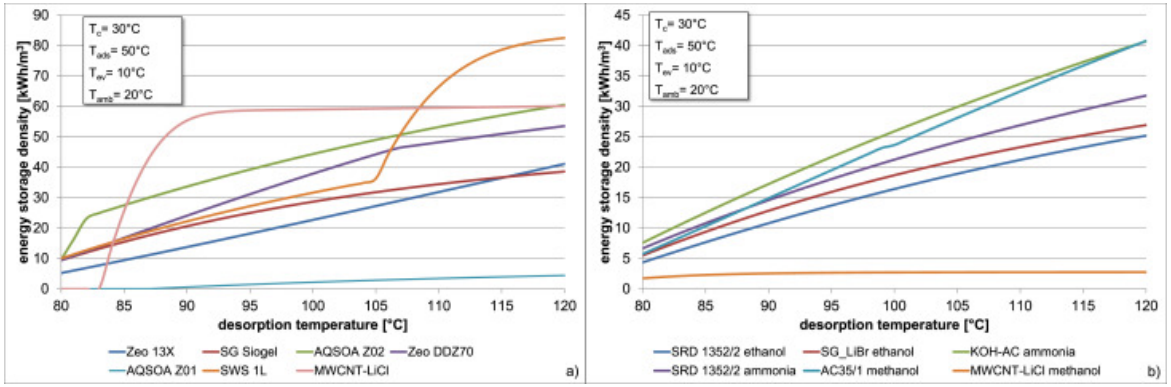

Fig. 4.4 Seasonal energy storage densities of the identified working pairs as a function of the desorption temperature: a) water as working fluid; b) other working fluids. Condensation temperature fixed at 30 °C, adsorption temperature at 50 °C, evaporation temperature at 10 °C.

What emerges from the analysis is that the working pairs employing water usually show higher energy storage density compared to the other working fluids, mainly due to the higher evaporation enthalpy of water. The working pairs that present the higher energy storage density (here represented on a volumetric basis) are SWS 1/water and MWCNT-LiCl operated with methanol. However, both the composite sorbents are not commercial and still present stability issues. Moreover, as visible in Figure 4.3, above about 35 °C for water and 30 °C for methanol, this composites strongly reduce the achievable heat storage density, due to limited interaction between working fluids and salt. In these conditions, instead AQSOA FAM Z02 presents the highest storage density, up to 50 kWh/m^3 for the range of interest of the present application. Moreover, FAM Z02 has been widely studied and several data considering its application are available in literature [35, 48, 109].

4.4 Design of the system

Definition of the amount of zeolite

For the design of the adsorber, the expected boundary conditions for the adsorption cycle were used as input data. Specifically, the used design parameters, that allowed defining the thermodynamic cycle on the Clapeyron diagram are:

- desorption (charge) temperature of 95°C;
- adsorption (discharge) temperature of 35°C;
- condensation temperature of 35°C;
- evaporation temperature of 15°C.

According to the isosteric curves of the material, measured at ITAE and reported in Figure 4.5, the uptake exchange at nominal conditions should be 0.15. Considering the amount of water to be evaporated and the enthalpy of evaporation for water at 15°C, the calculated amount of zeolite required is 5.3 kg.

Design of the adsorber

The design of the system and the experimental results presented in the next sections have been published in [110].

The adsorber was designed considering the utilization of granular zeolite, with grain size in the range 1-2 mm. Indeed, even though from a dynamic point of view the grain size is

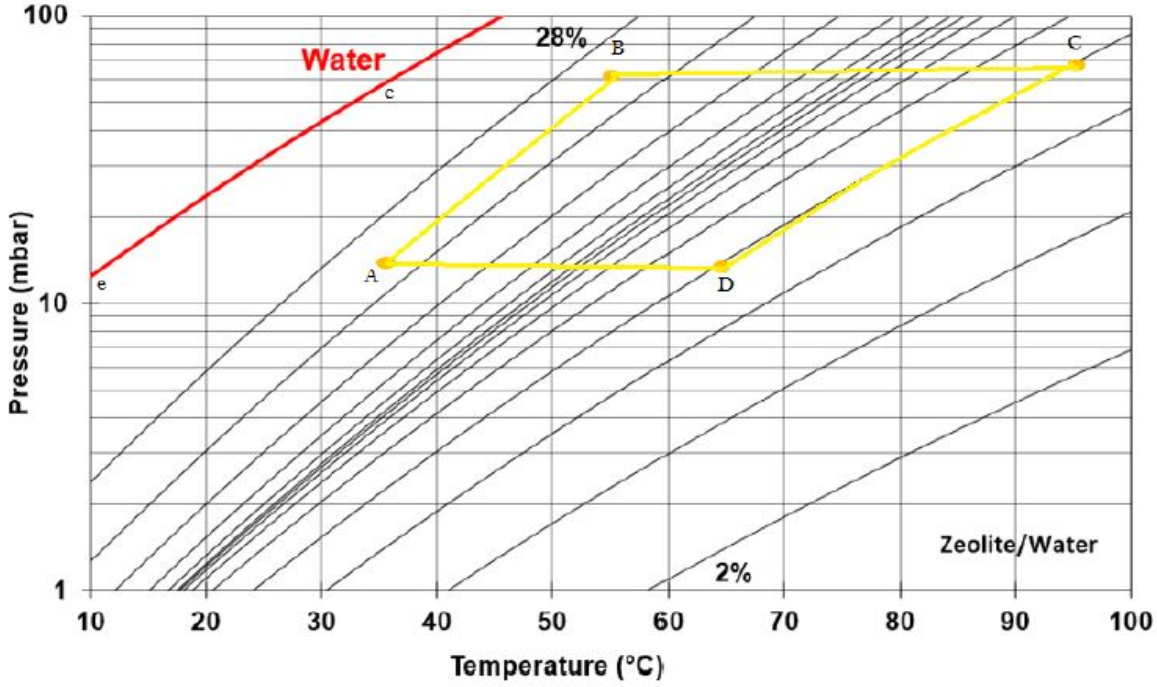

Fig. 4.5 Thermodynamic cycle for the adsorption storage developed.

not the optimal one, for the field of application under investigation, where energy density is more relevant than power delivered, the chosen granulometry was still considered good for a first evaluation purpose. The well-known configuration of a single piece fin-and-tube heat exchanger was used, with the material confined by a metal mesh. The whole system has then been inserted into a vacuum chamber. A picture of the adsorber is shown in Figure 4.6. It is worth noticing that the chosen metal mesh is able, on one hand, to ensure the leakage of the adsorbent material and is easily adaptable to standard production process, since it can be welded, but, on the other hand, it is quite bulky, thus limiting adsorption rate and introducing thermal losses. The overall area of the heat exchanger used for the adsorber is 1.75 m^2. After filling, the amount of zeolite actually inserted into the heat exchanger resulted to be 4.3 kg, about 30% less than the calculated amount. This is due to the overestimation of the internal volume of the heat exchanger and represents a factor to be taken into account for optimization or future prototypal and commercial applications. Starting from the actual amount of zeolite inside the adsorber, a theoretical cooling capacity of 420 Wh was estimated. The chamber for the adsorber has been specifically designed to test different configurations, in terms of storage materials and heat exchangers. It is therefore equipped with a removable lid and flexible manifolds. Some flanges allow the connection to the sensors for the monitoring of the most relevant parameters (pressure, temperature) and the other components of the device.

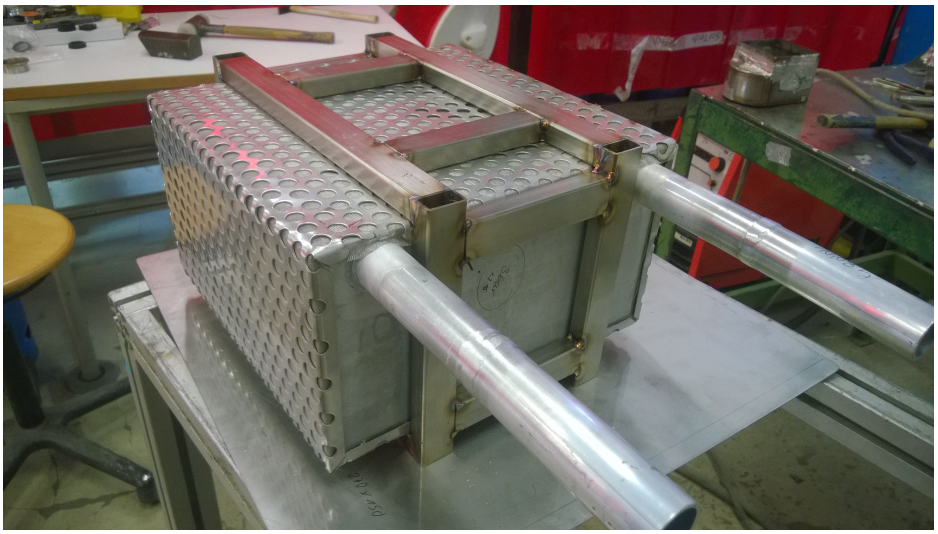

Fig. 4.6 The adsorber filled with zeolite.

Design of evaporator/condenser

Since the prototype will be used for thermal storage with charge and discharge processes separated in time, a single component can been used both as condenser and evaporator. As for the case of the chamber for the adsorber, the phase changer has been oversized, in order to allow the testing of different adsorbers in the future. It consists of 4 commercial fin-and-tube heat exchangers with copper fins and stainless steel tube connected in parallel through an external tubular steel manifold. Each one has an exchange surface of 1.33 m^2. The vacuum chamber is completely welded and equipped with flanges for the connection to the adsorber and the sensors.

The main features of the prototype are reported in Table 4.1, while a picture of the system is reported in Figure 4.7.

Table 4.1 Add caption

Overall dimensions adsorber chamber	250 x 553 x 774 mm
Adsorber heat exchanger	1 aluminium flat-tube heat exchanger
Exchange area adsorber	1.75 m^2
Adsorbent material	4.3 kg AQSOA FAM-Z02
Overall dimensions of the phase changer chamber	304 x 177 x 298 mm
Phase changer heat exchangers	4 x copper/SS tube-and-fin heat exchangers
Exchange area phase changer	5.32 m^2
Refrigerant	water
Amount of refrigerant	4 L

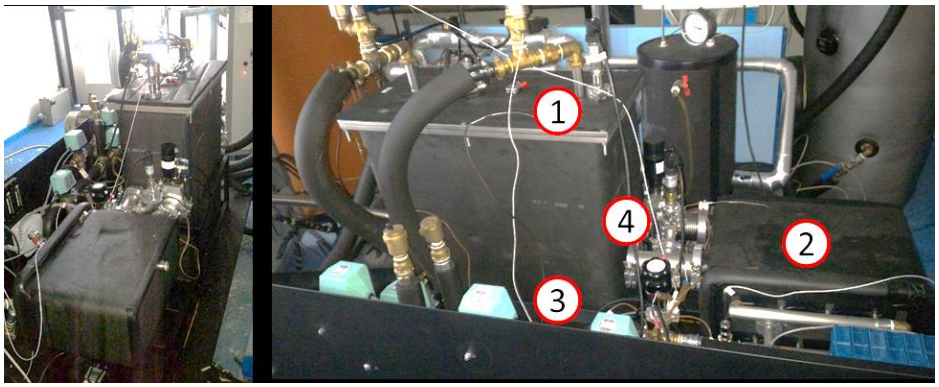

Fig. 4.7 The adsorption storage realised. 1: adsorber, 2: phase changer, 3: hydraulics.4: vacuum valve.

Hydraulic circuit

The prototype is completed by a hydraulic circuit realised with copper Φ12 mm tubes, thermally insulated by a polyurethane foam with thickness of 1.5 cm. The hydraulic circuits includes four 3-way deviating valves electrically operated that allow, for each component, the connection to the external hydraulic circuits of the testing rig already present at C E N T R O P R O V E of ITAE in Messina. They are characterised by fast switch (30 s). A P&ID of the system is shown in Figure 4.8.

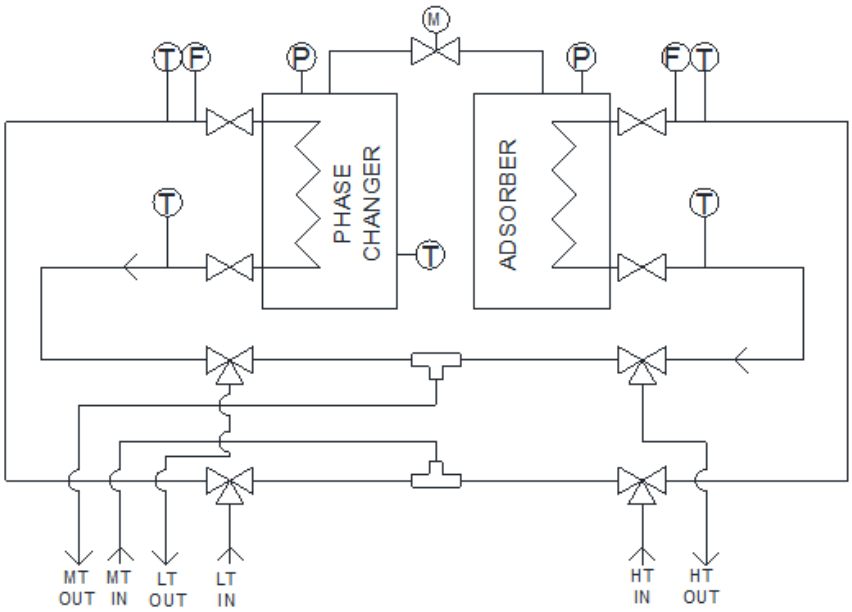

Fig. 4.8 P&ID of the complete prototype, including the hydraulic distribution.

4.5 Testing rig

The experimental testing of the prototype has been carried out on a testing rig already present at CNR-ITAE and suitable for the characterization of thermally driven systems, as described in [111]. The main features of the testing rig are similar to those of the testing rig already described for LTES systems:

- flexibility, in order to be able to test different system under a wide range of operating conditions;
- automatic operation, in order to run tests for several hours or days without the need for an operator;
- real-time monitoring and recording of all the relevant parameters.

Description of the testing rig

The testing rig consists of:

- a skid, equipped with the hydraulic elements (eg. electrovalves) and mechanical elements (eg. pumps and circulators) necessary for the test of the prototype;
- an electric heater with power of 16 kW, to be used as a heat source. It is connected to a 100 L tank in order to obtain a temperature inlet as stable as possible;
- a 63 kW electric chiller connected to a 200 L tank, which works as a heat sink for providing energy at the temperature levels for evaporation and condensation. In particular, the desired level of temperature is obtained, both for condenser and evaporator, by means of a thermoregulator and a mixing valve which mixes the flow in inlet and outlet pipes of the circuit;
- a rack containing the electronics of operation of the elements of the prototypes to be tested, the elements of the control system (National Instruments FieldPoint), a computer and all the sensors specifically used in the monitoring of machines adsorption (sensors temperature, pressure sensors, flow meters).

A P&ID of the testing rig is shown in Figure 4.9, while Figure 4.10 shows a picture of the facility, where all the main components are indicated.

All the components have been thermally insulated to avoid energy losses with 1.5 cm thick polyurethane foam. The correct flow is ensured through the use of 2 circulators and 2 centrifugal pumps. Each pump is equipped with a variable speed drive, in order to be able to

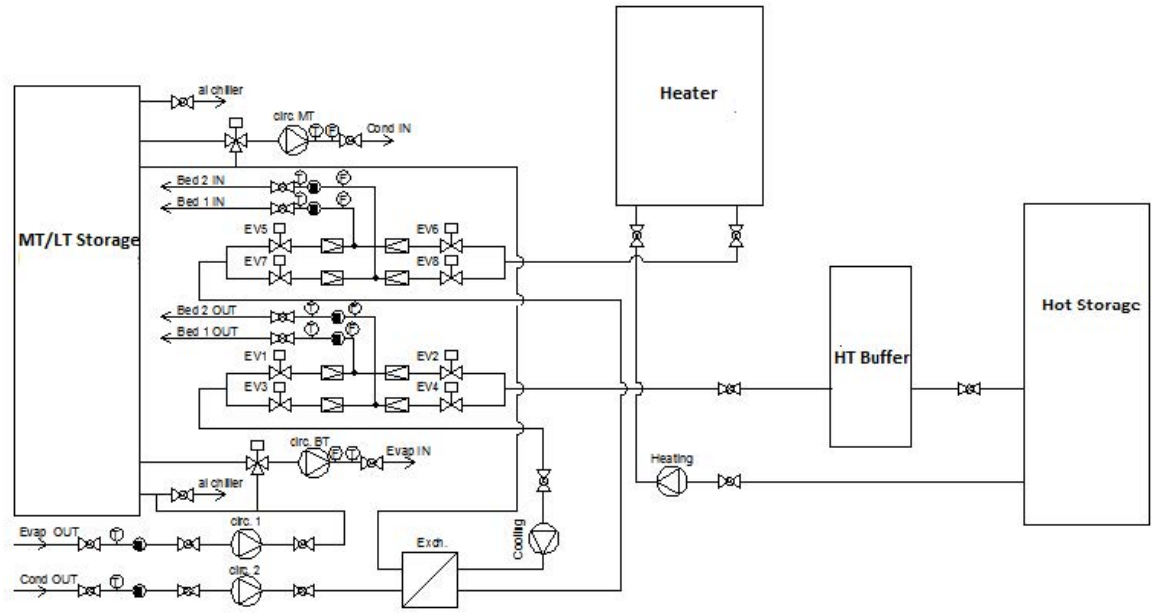

Fig. 4.9 P&ID of the testing rig used for the characterization of the adsorption storage.

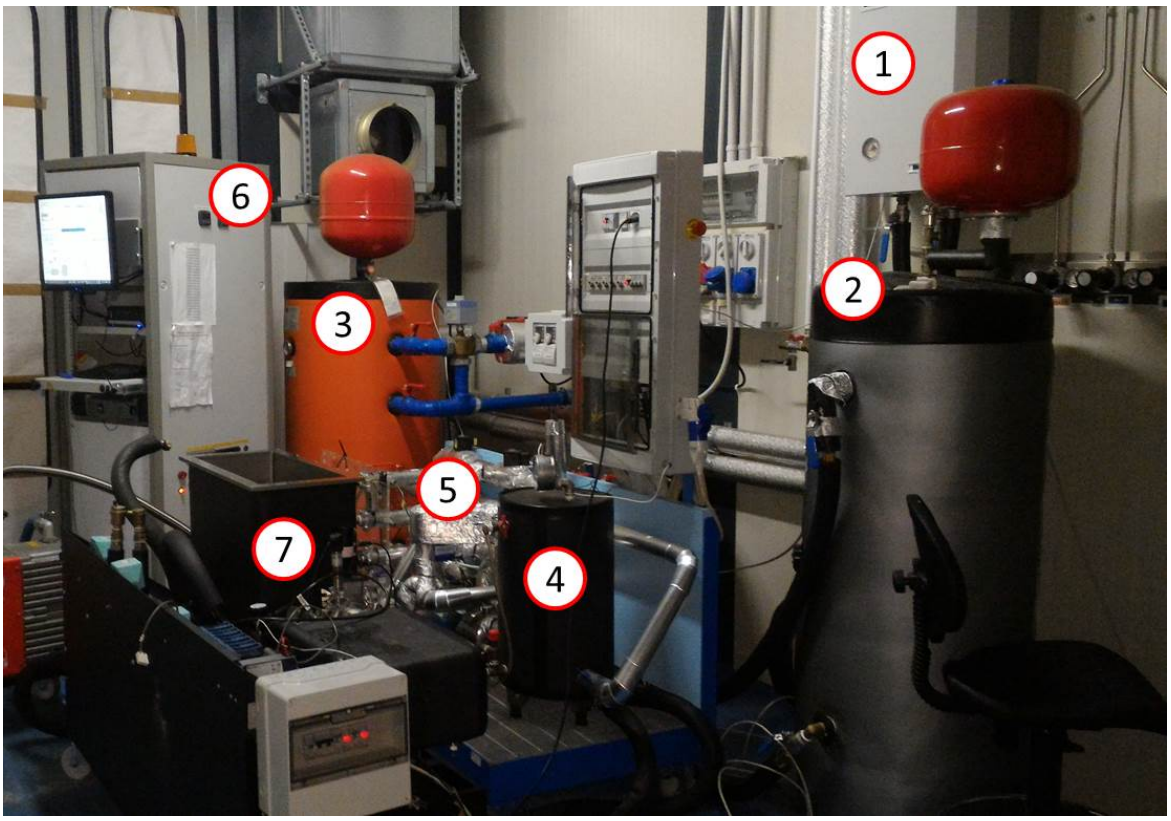

Fig. 4.10 Testing rig at CNR-ITAE lab. 1: heater, 2: hot storage, 3: MT/LT storage, 4:hydraulic connections, 5:plate heat exchanger, 6: management system, 7: Prototype under testing.

change the flow rate of the circuits and therefore test the influence of such a parameter on the operation of the storage.

Sensors employed and data acquisition

The management of both the set-up for thermal storages and the testing bench is realised through a NI FieldPoint acquisition system and a dedicated LABVIEW software. All the components are electrically operated, to fulfil the requirements of real-time acquisition and automatic operation. The following sensors have been installed:

- Pt 100 1/10 DIN with four wires, used for the measurement of inlet and outlet temperatures of the HTF both at the adsorber and the phase changer.
- Class A T-type thermocouple for the measurement of the temperature of the refrigerant inside the phase changer.
- MVM250 magnetic flow meter with 1% FS accuracy to measure the flow rate of the HTF at the adsorber and the phase changer.
- piezoresistive pressure sensors with 0.25% FS accuracy to measure the pressure inside both vacuum chambers.

4.6 Experimental procedure

Regarding the experimental assessment of thermochemical (and hence adsorption) storages, there are not national or international standards describing an assessment procedure to be applied. The same situation is true for latent heat storages, but the more complex operation and higher number of factors influencing the operation of TCSS make it even more compelling to clearly define the procedure used to the characterization. A laboratory characterization should guarantee the following conditions:

- Application of boundary conditions typical of the practical operation of the storage;
- management of steady-state conditions for the whole duration of a test with minimum deviations;
- repeatability of the measurement;
- minimization of external factors that could affect the behaviour of the system;

- adaptability to a wide number of conditions.

For the specific case, a protocol derived from the procedures commonly used for the characterization of thermally-operated chillers, developed within IEA Task 48, which has already proven to be a useful method for the evaluation and comparison of absorption and adsorption systems [112] was used, taking into account the specific features of heat storage operation. It is divided into three operating periods of the testing facilities (pre-conditioning, start-up and operation) and the subsequent data analysis, as described in details in Figure 4.11.

4.7 The figures calculated

The parameters calculated and used for the evaluation of the system are: discharging power, stored energy, energy density and storage efficiency.

- Charge energy (CE), calculated as the overall amount of energy supplied to the storage.
- Discharge Energy (DSE) is defined as the total amount of energy supplied to the user. Such a value has also been normalized for the total amount of adsorbent in the system, to define the specific energy store for unit mass of material.
- Discharge Power (DP), defined as the average power provided by the system during discharging period.
- Discharge efficiency η, calculated as the ratio of the stored energy (which represents the energy actually recovered during one cycle) over the heat input supplied to the system.

Indeed, one of the advantages of adsorption storages is that they can use the heat supplied by the heat source in order to supply heat at a different temperature to the user, but also cold energy. In the evaluation of the results of the tested system, such a peculiarity has been taken into account and the data has been analysed (starting from the same tests) considering three cases:

- short term heat storage (SHS): heat is supplied to the user during both condensation and adsorption;
- long term heat storage (LHS): heat is supplied to the user during adsorption (condensation heat is rejected to the environment);

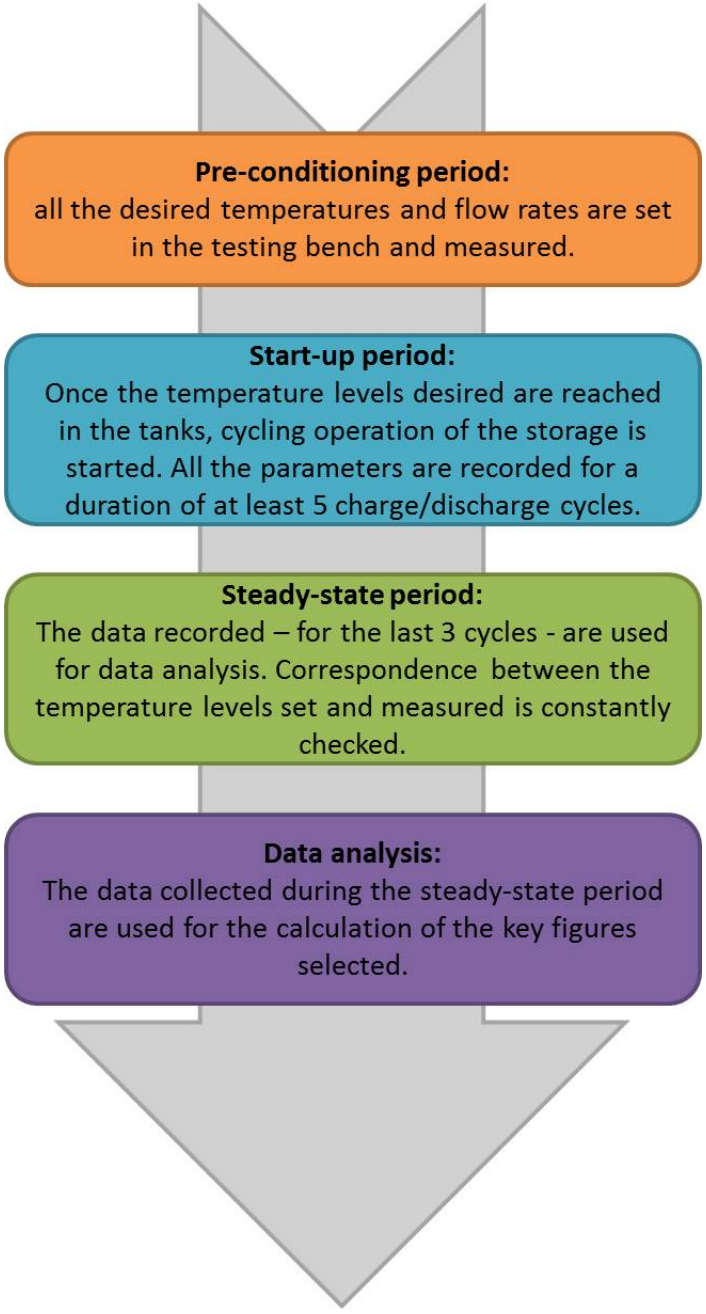

Fig. 4.11 The experimental procedure followed for the characterization of the adsorption storage.

- cold storage (CS): the useful effect is represented by the cold energy produced at the evaporator.

Since three cases have been considered, differing for the useful effect, an overall summary of the equations used in the calculation of the performance figures is given in Table 4.2.

4.8 Results

The investigated conditions for the storage here described are briefly summarised in Table 4.3. All the temperatures listed are the set-point inlet temperatures in the heat exchangers. It is also worth noticing that all tests were realised considering sequential charge and discharge, without any stand-by time. For LHS conditions, this is not representative of the real case operation, where part of the sensible heat will be lost. A dedicated test campaign, aimed at defining the effect of storage time, will be the subject of a future work.

4.8.1 Results of a typical test

In the following, the results obtained during a reference test, with T_{des} = 90°C, T_{ads} = T_{cond} =35°C, T_{ev} =5°C, are presented. Figure 3 shows the temperatures in the adsorber and phase changer; specifically, the sensors measure inlet and outlet temperatures of both the adsorber and the phase changer and the temperature in the liquid phase at the bottom of the phase changer. A fixed time for charge and discharge was selected, equal to 55 minutes.

As indicated by the arrows in the Figure 4.12, 4 phases can be recognised:

- Pre-conditioning: such phases are realised before charging and discharging the storage. During them, the phase changer is heated up or cooled down at the condensation or evaporation temperature. The reason for the insertion of these time steps in the test is to minimise the effect of the metal masses of the system and to ensure that the temperatures in all the components actually match the set-one (which, in turn, correspond to the operating boundaries of the system during charging and discharging phases). The duration of the pre-conditioning was selected by waiting for the temperature inside the phase changer to reach the set value and, at the same time, monitoring the power output from the phase changer and checking that it lied around 0 W, meaning that no more thermal energy is stored in the inert masses of the device.

- Charge: it is realised by heating up the adsorber and opening the connection to the condenser. Condensation occurs at the phase changer and the condensation heat is removed.

Cold storage	
Charge Energy (CE)	$CE=\int_0^{t_{des}} \dot{m}_{ads} c_p (T_{in,ads}-T_{out,ads})\, dt$
Discharge power (DP)	$PD=\frac{\int_0^{t_{ev}} \dot{m}_{pc} c_p (T_{in,pc}-T_{out,pc})\, dt}{t_{ev}}$ [W]
Discharge Energy (DSE)	$SE=\int_0^{t_{ev}} \dot{m}_{pc} c_p (T_{in,pc}-T_{out,pc})\, dt$ [Wh]
Discharge efficiency (η)	$\eta=\frac{\int_0^{t_{ev}} \dot{m}_{pc} c_p (T_{in,pc}-T_{out,pc})\, dt}{\int_0^{t_{des}} \dot{m}_{ads} c_p (T_{in,ads}-T_{out,ads})\, dt}$
Long- term heat storage	
Charge Energy (CE)	$CE=\int_0^{t_{des}} \dot{m}_{ads} c_p (T_{in,ads}-T_{out,ads})\, dt$
Discharge Energy (DSE)	$SE=\int_0^{t_{adsorption}} \dot{m}_{ads} c_p (T_{out,ads}-T_{in,ads})\, dt$ [Wh]
Discharge power (DP)	$PD=\frac{\int_0^{t_{adsorption}} \dot{m}_{ads} c_p (T_{out,ads}-T_{in,ads})\, dt}{t_{adsorption}}$ [W]
Discharge efficiency (η)	$\eta=\frac{\int_0^{t_{adsorption}} \dot{m}_{ads} c_p (T_{out,ads}-T_{in,ads})\, dt}{\int_0^{t_{des}} \dot{m}_{ads} c_p (T_{out,ads}-T_{in,ads})\, dt}$
Short- term heat storage	
Charge Energy (CE)	$CE=\int_0^{t_{des}} \dot{m}_{ads} c_p (T_{in,ads}-T_{out,ads})\, dt$
Discharge Energy (DSE)	$SE=\int_0^{t_{cond}} \dot{m}_{pc} c_p (T_{out,pc}-T_{in,pc})\, dt+\int_0^{t_{adsorption}} \dot{m}_{ads} c_p (T_{out,ads}-T_{in,ads})\, dt$ [Wh]
Discharge power (DP)	$PD=\frac{\int_0^{t_{cond}} \dot{m}_{pc} c_p (T_{out,pc}-T_{in,pc})\, dt+\int_0^{t_{adsorption}} \dot{m}_{ads} c_p (T_{out,ads}-T_{in,ads})\, dt}{t_{cond}+t_{adsorption}}$ [W]
Discharge efficiency (η)	$PD=\frac{1}{2}\left(\frac{\int_0^{t_{cond}} \dot{m}_{pc} c_p (T_{out,pc}-T_{in,pc})\, dt}{t_{cond}}+\frac{\int_0^{t_{adsorption}} \dot{m}_{ads} c_p (T_{out,ads}-T_{in,ads})\, dt}{t_{adsorption}}\right)$

Table 4.2 The figures calculated for the evaluation of the adsorption storage.

Table 4.3 Investigated conditions in the experimental testing of the adsorption storage.

Parameter	SHS	LHS	CS
Charge/discharge time [min]	45, 50, 60	45, 50, 60	45, 50, 60
Desorption temperature [°C]	75, 80, 90	75, 80, 90	85, 90
Condensation temperature [°C]	30,35,40	15,20	25, 30, 33, 35, 40
Adsorption temperature [°C]	30,35,40	35,40	25, 30, 33, 35, 40
Evaporation temperature [°C]	5,10,15	5,10,15	10, 12, 15, 18, 20

- Discharge: it is realised by cooling down the adsorber and opening the connection to the evaporator. Evaporation occurs at the phase changer and the evaporation heat is provided.

What is clear from the picture is that the temperature of the adsorber is almost constant throughout the charge process, while the temperature of the condenser experiences an initial increase of about 5°C, due to the beginning of condensation and then it remains stable at 35°C. During discharge, like for the charging process, after an initial peak, the temperatures keep stable around the set values of 35°C for the adsorber and 5°C for the evaporator.

In Figure 4.13, the power measured in the components during the whole process is shown. In order to distinguish among all contributes, they are plotted on the same chart: a negative power indicates that heat is supplied to a component (desorption heat during charge and evaporation heat during discharge), while a positive power indicates that heat is removed from the component (condensation heat during charge and adsorption heat during discharge). The heat fluxes of the two components during each phase are “symmetrical” and are characterised by an initial peak and a subsequent monotone decreasing. This is due to the fact that a large driving force for the desorption/adsorption process exists at the beginning and therefore the condensation or evaporation rate is higher. Even though fixed duration of charge and discharge were selected, it is possible to identify the end of charging and discharging process as the moment in which the power in the phase changer reaches zero. As expected, the two phases have different actual duration, due to different ad/desorption kinetics [113]: charge ends after 35 minutes, while discharge is completed after 40 minutes.

In Figure 4.14, the cumulative energy measured at the adsorber and phase changer during charge and discharge is shown. As for the case of the power, energy of desorption and evaporation are represented on the negative y-axis, while the energy of condensation and adsorption are in the positive part of the chart. It is clearly visible that, while condensation and evaporation contributes are comparable, a noticeable difference exists between the energy of adsorption and desorption, probably due to the effect of metal masses and heat losses.

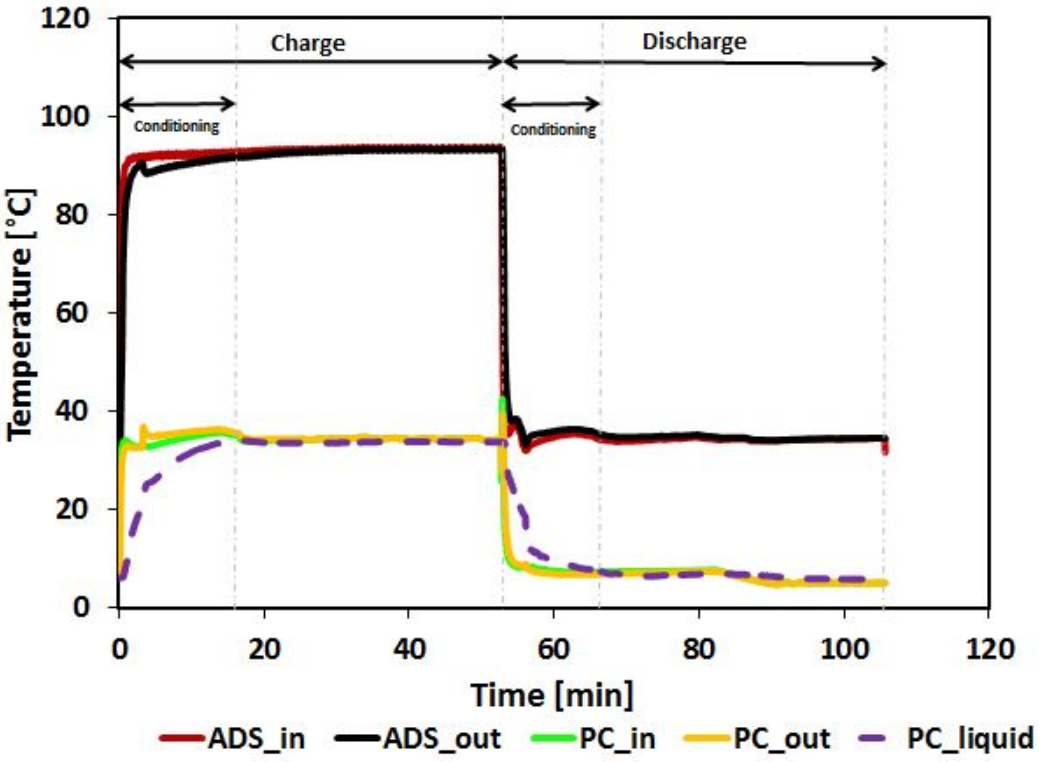

Fig. 4.12 Temperatures during a typical test of the adsorption storage.

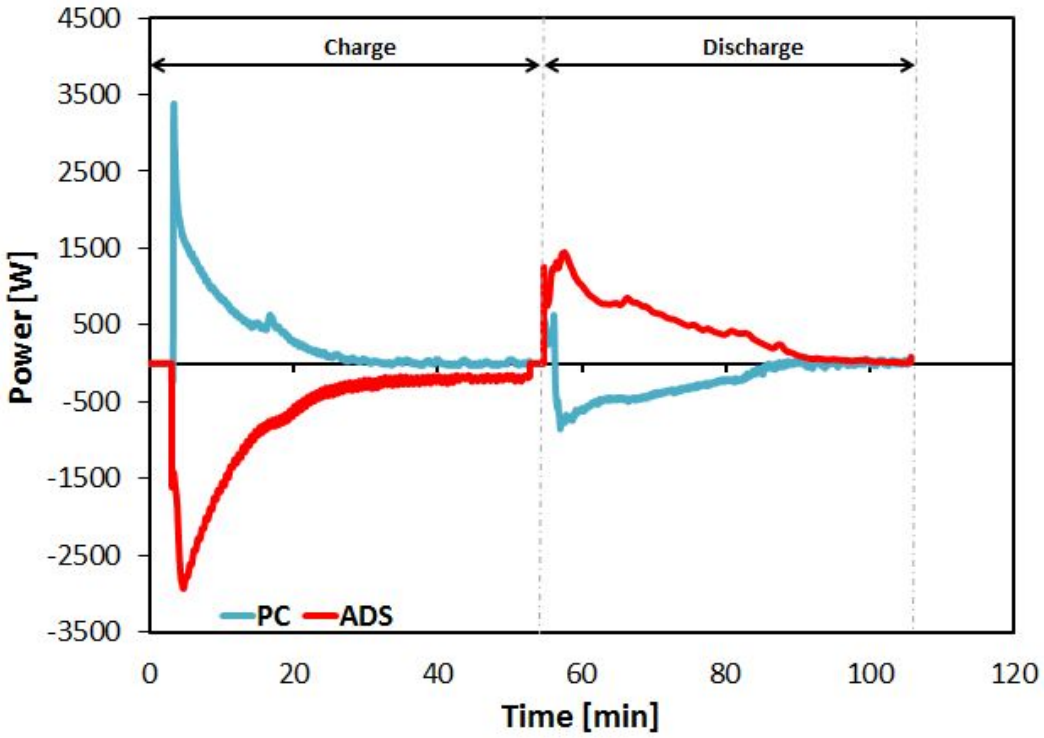

Fig. 4.13 Power at the adsorber and phase changer during a typical test of the adsorption storage.

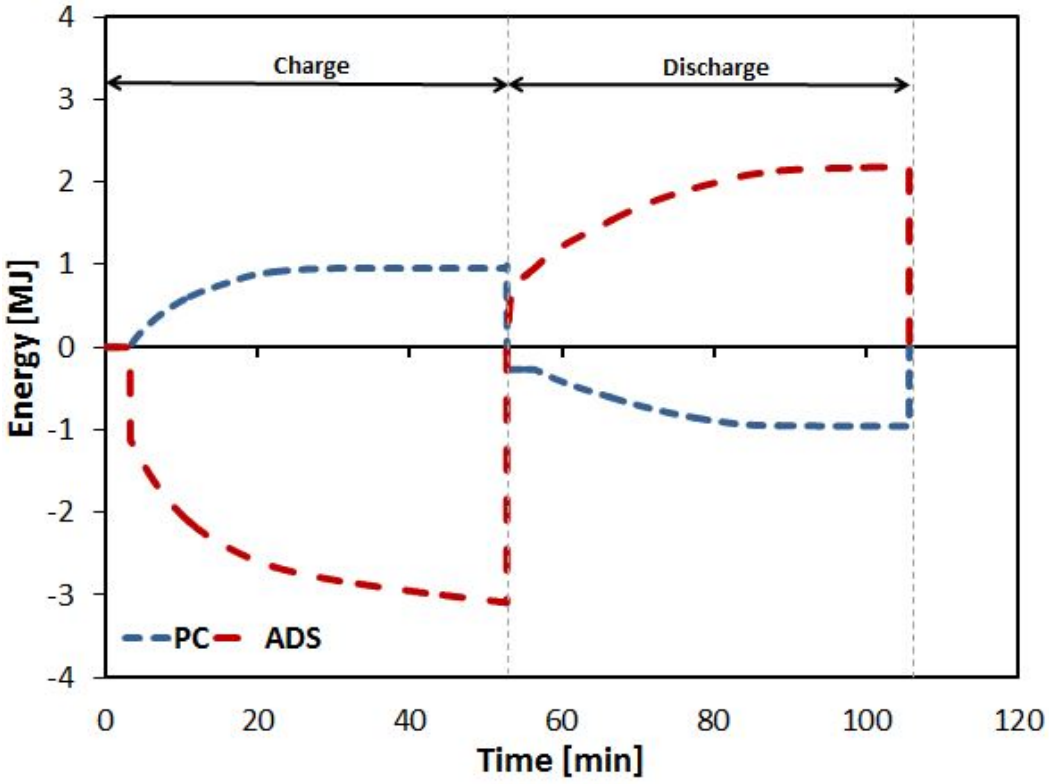

Fig. 4.14 Energy at the adsorber and phase changer during a typical test of the adsorption storage.

4.8.2 Effect of operating temperatures

The operating conditions influencing the performance of an adsorption heat storage are essentially the boundary temperatures and the flow rate in the components. Indeed, by changing the operating temperatures, a different uptake exchange is realised during the cycle. The heat of adsorption, as recalled in Section 4.3 is a function of the uptake variation during the cycle and therefore a higher uptake exchange corresponds to a higher heat of adsorption The heat of condensation or evaporation depends on the amount of refrigerant processed as well, then also this contributions depends on the specific boundaries considered. As a general rule, higher desorption temperatures lead to a better regeneration of the adsorbent (i.e. the amount of refrigerant still inside the pores of the material is lower), while higher condensation temperatures and lower evaporation temperatures lead to a lower uptake exchanged in the charge/discharge process. Such trends were confirmed in the experimental campaign performed.

In Figure 4.15, the energy stored at different desorption temperatures is shown, with fixed evaporation (10°C) and adsorption/condensation temperatures (35°C). What emerges from the charts is that desorption temperature has a significant effect on the energy actually recoverable: in SHS operation, it goes from 2.3 MJ at 75°C to 4 MJ at 91°C. Similarly, for seasonal heat storage, the increase from 75°C to 90°C is of about 40%. This is mainly due to the shape of the isosters of FAM Z02: by regenerating the adsorbent at 90°C, the amount of refrigerant processed is much higher compared to a regeneration temperature of 75°C. On the same chart, the energy density per unit mass of adsorbent is shown on the right axis: the values obtained range from 150 kJ/kg in CS mode, up to 850 kJ/kg for DHS at 90°C. Figure 4.16 shows the effect of evaporation temperature on the energy stored (on the right axis, the results in terms of energy density are shown as well): in this case, the effect is less marked than those of desorption temperature, with the exception of CS operation. Indeed, for CS operation, the energy stored is almost doubled (from 0.7 MJ to 1.4 MJ) increasing the evaporation temperature — that represents the temperature at which the useful effect is delivered to the user — from 5°C to 21°C. The effect on heat storage operation is more evident only in the range 5°C-10°C, while a plateau is reached afterwards. This indicates that these systems have high versatility and can be applied in a wide range of ambient conditions. Finally, Figure 4.17 shows the effect of condensation temperature. For cold storage and seasonal heat storage operation, decreasing condensation temperature corresponds to a higher amount of refrigerant desorbed, which results in about 35% higher amount of energy available during discharge.

According to the application considered, another parameter to be taken into account besides the stored energy is the discharge power. The effect of desorption temperature

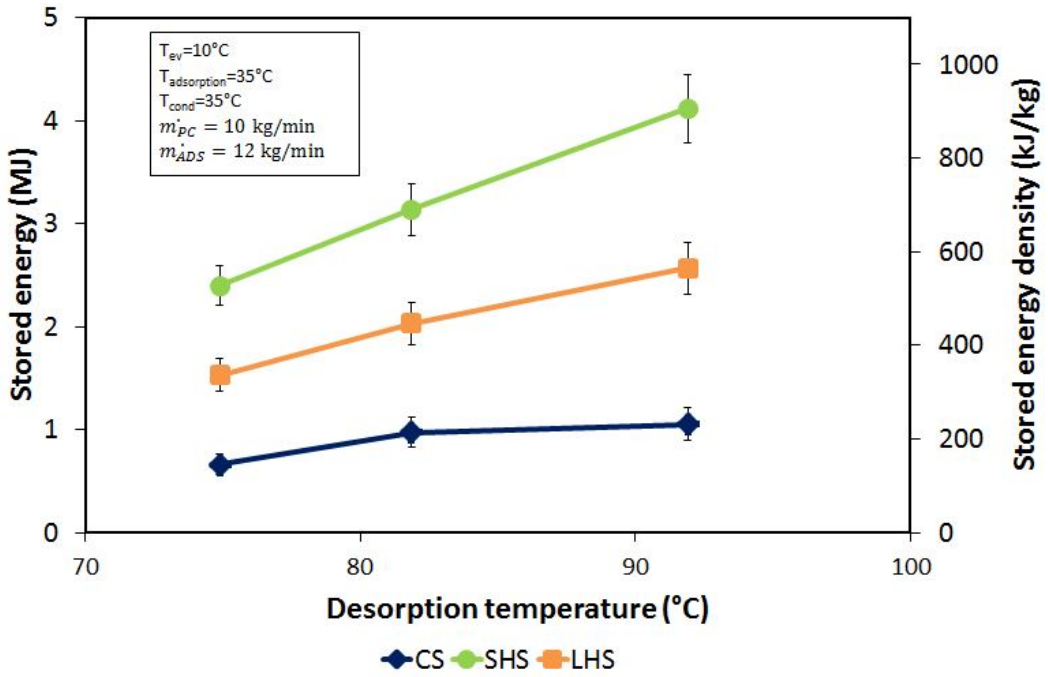

Fig. 4.15 Effect of desorption temperature on the energy stored for the three operating modes examined.

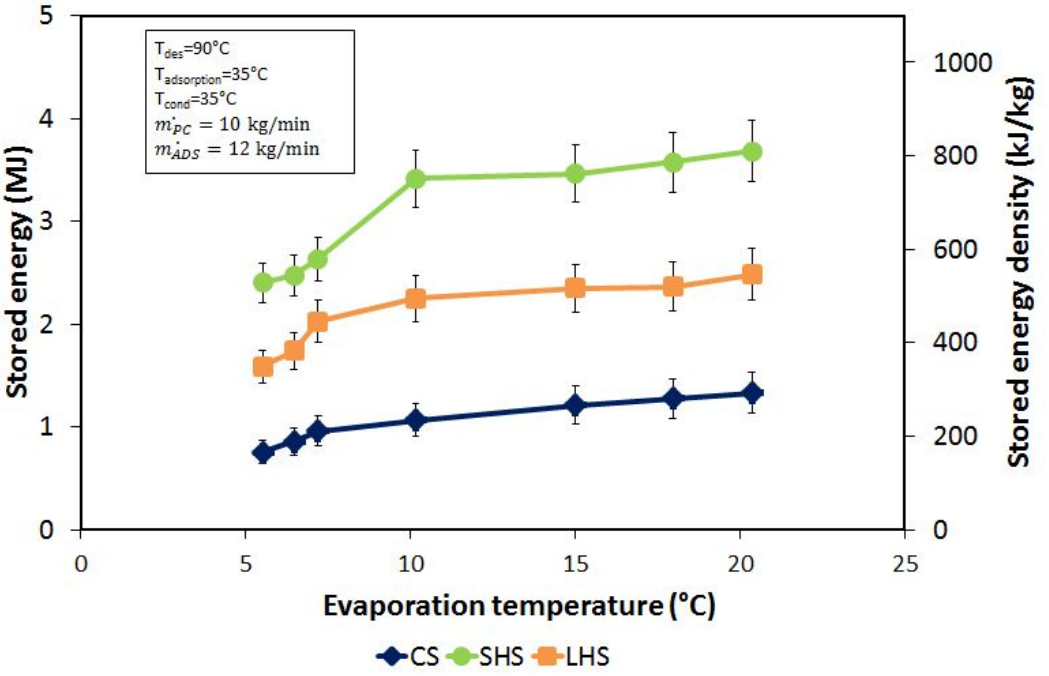

Fig. 4.16 Effect of evaporation temperature on the energy stored for the three operating modes examined.

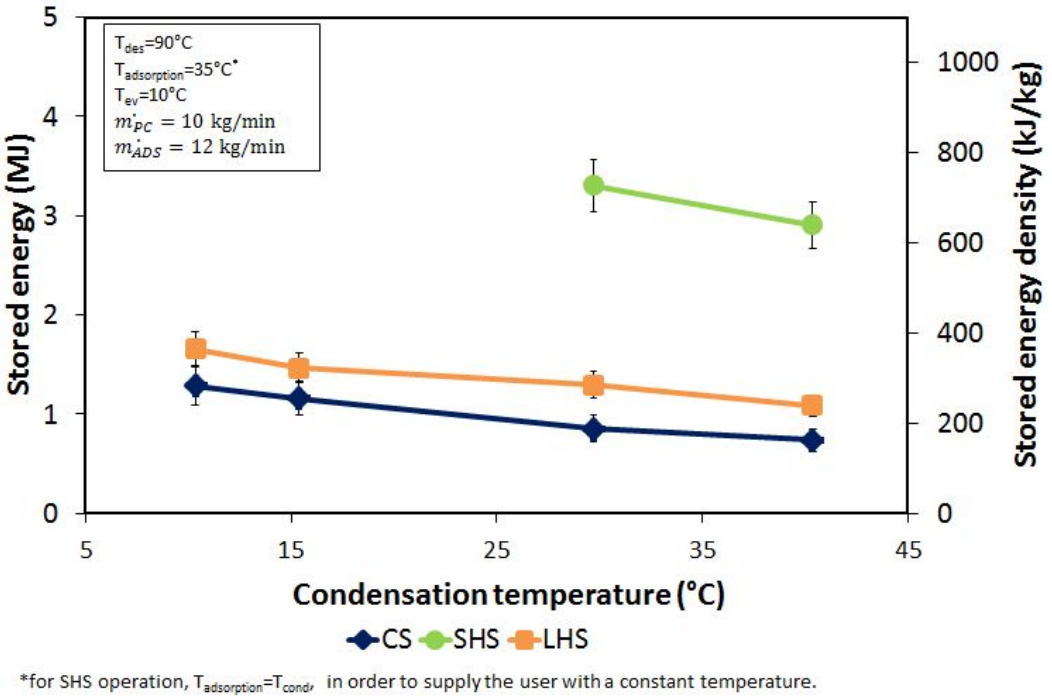

Fig. 4.17 Effect of condensation temperature on the energy stored for the three operating modes examined.

and evaporation temperature on the power available to the user is shown in Figure 4.18 and Figure 4.19, respectively. It is intuitive that discharge power increases with increasing desorption temperature or evaporation temperature, with a more noticeable increase from 75°C to 85°C and from 5°C to 10°C. The average power that the analysed system is able to provide, during its discharging phase, ranges between 200 W and 400 W for cold storage operation, from 300 W to 500 W for SHS and between 500 W and 600 W for daily heat storage.

4.8.3 Effect of flow rate

One crucial aspect for the proper operation of a storage system is the amount of energy that is actually usable. Indeed, if the temperature difference in the circuit connected to the load is too low, it is not possible to effectively recover the energy stored. The operating parameter that mostly influences the temperature difference at the adsorber or phase changer is the flow rate of the heat transfer fluid. During the testing campaign here presented, then, the effect of flow rate on the outlet temperature at the adsorber and phase changer has been evaluated and the results are reported in Figure 4.20. All the tests were carried out with 90 °C desorption temperature, 35 °C adsorption and condensation temperatures and 10 °C

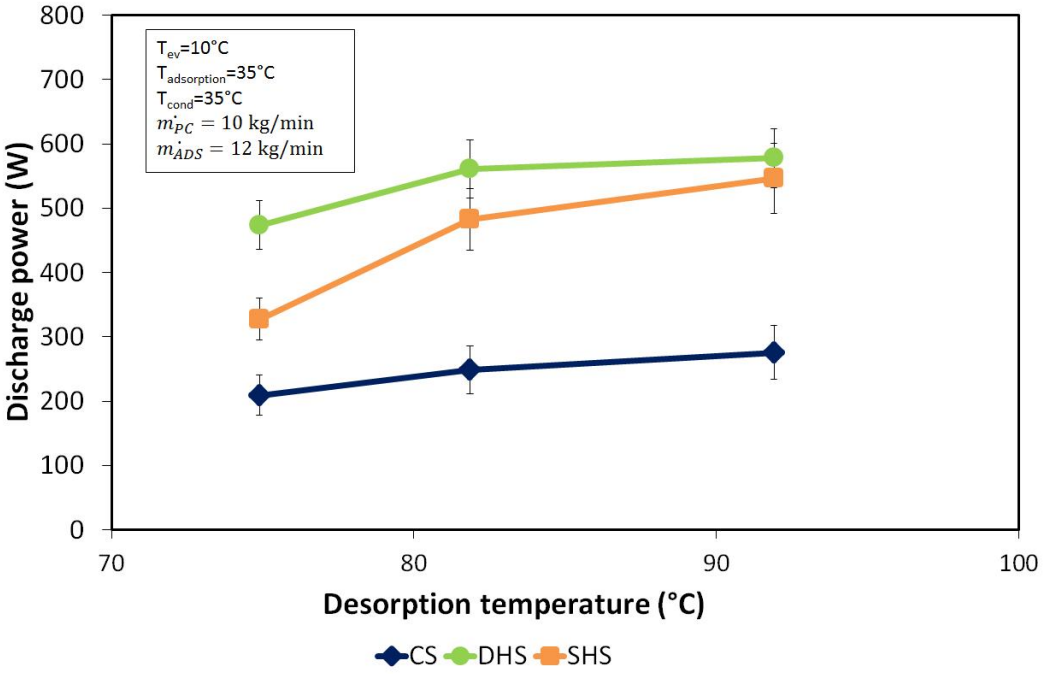

Fig. 4.18 Effect of desorption temperature on the discharge power for the three operating modes examined.

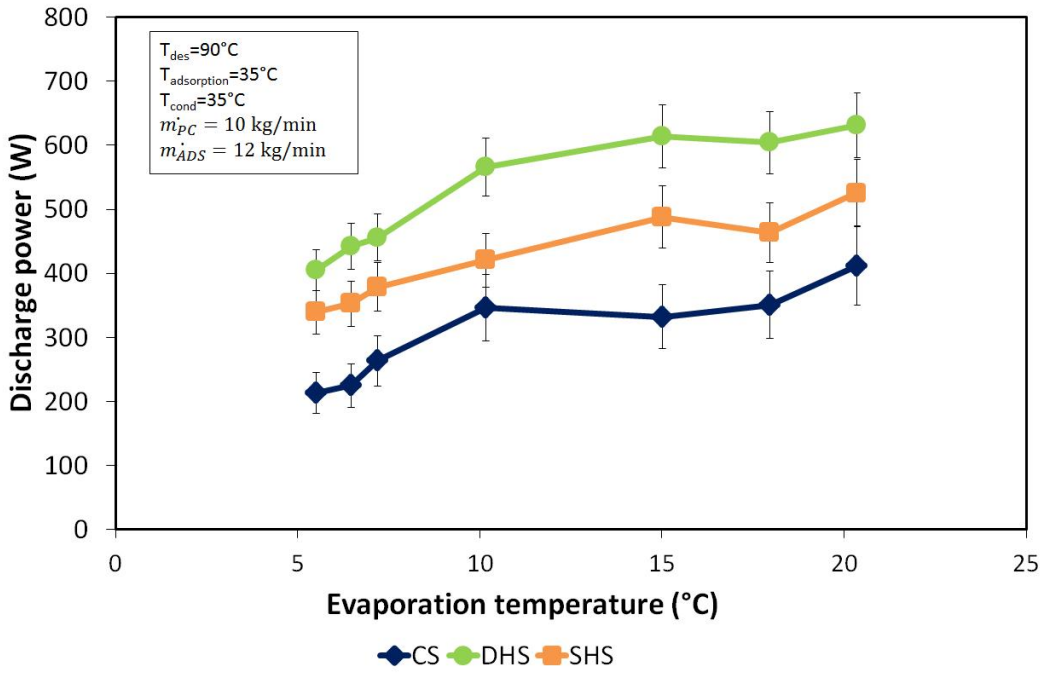

Fig. 4.19 Effect of evaporation temperature on the discharge power for the three operating modes examined.

evaporation temperatures. The range for the flow rate has been chosen according to the typical values for DHW or space heating/cooling systems. By considering 0.4 as the minimum value for an effective utilization of the energy supplied by the storage a maximum flow rate of 15 kg/min should be set. The difference on the energy stored between the tests at 9 kg/min and 15 kg/min is lower than 10% (within the uncertainty of the measurement), thus indicating that lower flow rates are preferable.

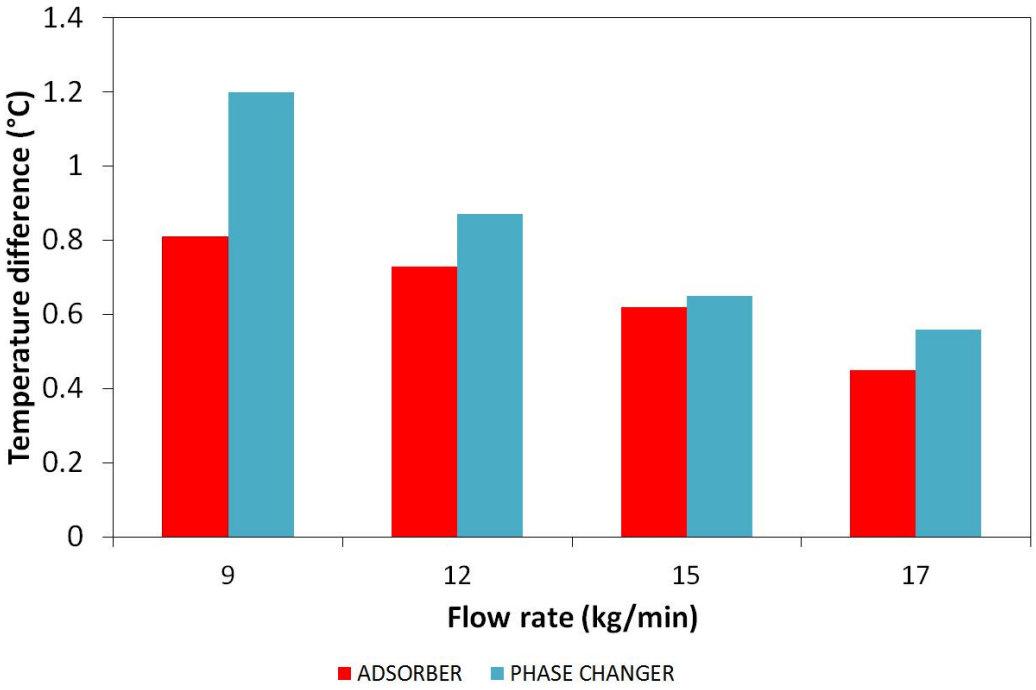

Fig. 4.20 effect of flow rate on the temperature difference in the inlet/outlet circuit of the adsorber and phase changer.

4.9 Discussion

The results obtained during the tests performed, though promising and useful for defining the amount of energy that can be stored in the system under different conditions, have to be analysed considering the theoretical limits, in order to provide useful information towards an improvement of the storage. To this aim, the efficiency of the storage was calculated under different boundaries and the possible causes of discrepancy from the theoretical case were examined.

4.9.1 Storage efficiency

Table 4.4 reports the storage efficiency considering different operating modes. As expected, for short term heat storage (SHS) the system works as an adsorption heat pump, with efficiency higher than 1, and up to 1.5. In the case of cold storage, similarly as for the case of an adsorption chiller, the efficiency is between 0.3 and 0.4, while for seasonal heat storage the efficiency lies in the range 0.4 - 0.5. Hence, a margin for improvement still exists. It is interesting to notice that, even though at a lower desorption temperature the heat losses to the environment are reduced (and therefore a higher efficiency could be expected), the amount of refrigerant processed (due to the particular shape of the FAM Z02 isobars) still penalises the overall performance of the system.

TEST	charge	discharge	T_{des}	$T_{adsorption}$	T_{cond}	T_{ev}	SED_{CS}	SED_{DHS}	SED_{SHS}	η_{CS}	η_{DHS}	η_{SHS}
	min	min	°C	°C	°C	°C	Wh/kg	Wh/kg	Wh/kg	-	-	-
1	50	50	75	35	30	11	43	155	99	0.29	1.05	0.38
2	50	50	81	35	30	11	63	203	131	0.36	1.18	0.41
3	50	50	81	30	15	6	56	226	141	0.30	1.20	0.45
4	50	50	90	35	30	10	68	266	166	0.38	1.48	0.56
5	50	50	91	35	15	10	88	276	196	0.41	1.53	0.56
6	50	50	90	40	40	6	49	155	103	0.33	1.04	0.35
7	50	50	90	40	41	15	78	223	152	0.42	1.21	0.39

Table 4.4 Storage density and efficiency measured in different experimental conditions.

In order to identify the critical aspects to be taken into account during the design, the energy balance on the adsorber during short-term storage operation was realised.

4.9.2 Energy balance on the adsorber

The prototype here presented was realised entirely in stainless steel, the lead principle in the design being the flexibility for testing purposes. Consequently, the adsorber is inside a vacuum chambers with a flanged lid, suitable for the inspection of the adsorbers or the replacement of components. However, this is realised at the expenses of a heavy and bulky system. The effect of such inert masses on the performance of the chiller, especially in terms of COP, can be relevant, since a significant amount of energy is cyclically wasted in heating and cooling the shell and the components. To identify and quantify this effect, an energy balance was performed for a cycle with 90 °C desorption, 35°C condensation and adsorption, 5 °C evaporation and 50 minutes charge/discharge time. In particular, the contributions listed below were considered.

- Sensible heat needed to heat up the material of the chamber, calculated as:

$$Q_{sensible,chamber} = m_{chamber} c_{p_{SS}} \left(T_{chamber,max} - T_{chamber,min}\right) \tag{4.7}$$

Where, $m_{chamber}$ is the total weight of the chambers, c_{pSS} is the specific heat of the stainless steel, $T_{chamber,max}$ and $T_{chamber,min}$ are the maximum and minimum temperatures of the external wall of the chambers during a cycle, experimentally measured through a thermocouple.

- Sensible heat needed to heat up the metal heat exchanger, calculated as:

$$Q_{sensible,HEXs} = \left(m_{HEX} c_{p_{Al}}\right) \left(T_{HEX,max} - T_{HEX,min}\right) \tag{4.8}$$

Where, m_{HEX} is the total weight of the heat exchangers, c_{pAl} is the specific heat of the aluminium of the heat exchangers, $T_{HEX,max}$ and $T_{HEX,min}$ are the maximum and minimum temperatures of the heat exchangers during a cycle. Since the temperature of the HEX was not directly measured, it has been considered equal to the average between the inlet and outlet temperature from the adsorber.

- Sensible heat needed to heat up the adsorbent material, calculated as:

$$Q_{sensible,adsorbent} = m_{adsorbent} c_{p_{zeolite}} \left(T_{adsorbent,max} - T_{adsorbent,min}\right) \tag{4.9}$$

Where $m_{adsorbent}$ is the total mass of zeolite inside the adsorber, and $T_{adsorbent,max}$ and $T_{adsorbent,min}$ are the maximum and minimum temperatures of the adsorbent material during a cycle. Since the temperature of the material was not measured, it has been considered equal to the temperature of the heat exchanger and therefore the average between the inlet and outlet of the adsorber.

- Enthalpy of desorption, calculated starting from the experimental measurement carried out at ITAE [36].

- Heat losses through the environment, calculated as:

$$Q_{losses} = \left(\frac{1}{h_{air}} + \frac{s_{insulation}}{k_{insulation}}\right) A \left(T_{wall} - T_{ambient}\right) \tag{4.10}$$

Where: h_{air} is the convective heat transfer coefficient for natural convection in air, $s_{insulation}$ is the thickness of the insulating material, k_{ins} is the thermal conductivity of the insulating material, A is the area exposed to the environment, T_{wall} is the

temperature measured at the wall of the chamber, and T_{amb} is the ambient temperature during the test.

The results are shown in the graph from Figure 4.21. It is possible to notice that only 62% of the overall heat supplied is needed for the desorption of the material. The thermal losses and the sensible heat of metal, that can be limited by an improved design, account for about 25% of the total. This indicates that at least a 15% improvement in storage efficiency could be obtained by improving thermal insulation or reducing the amount of metal (for example, choosing a cylindrical shape with very thin wall or replacing stainless steel with lightweight non-metallic materials). It is also worth commenting on the sensible heat supplied to the adsorbent material: as already discussed in literature [114], if a time break for stand-by would be considered between charge and discharge, the storage efficiency of the system would be lower than the values reported in Figure 4.4. Indeed, the tests were performed by continuous charge/discharge, allowing only a short time break (20 minutes) for the conditioning of the phase changer. Instead, in practical applications, especially for seasonal storage, charge and discharge could be separated in time, therefore the sensible heat of the adsorbent, amounting to about 17% of the overall heat supplied would be lost.

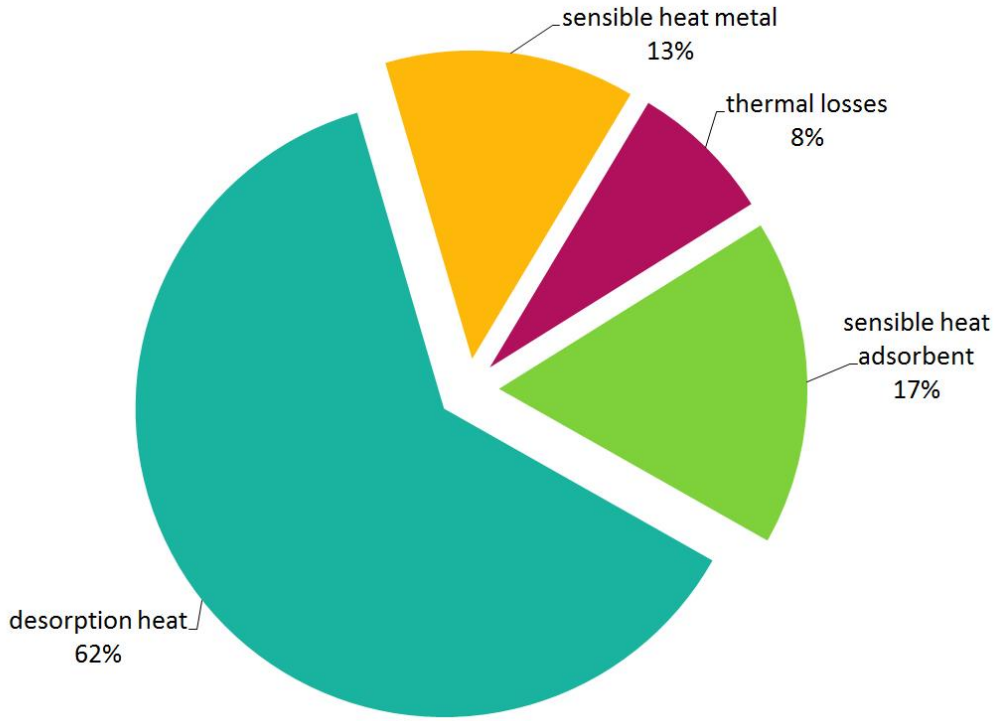

Fig. 4.21 Energy balance of the adsorber for a reference (90-35-5) cycle during desorption.

4.10 Final remarks and advancements with respect to the state-of-art

In the present Chapter, the activity on the development of an adsorption thermal energy storage has been described. Together with the system, a testing set-up was developed, with the aim of guaranteeing flexibility and reproducing real operating conditions with a good accuracy (uncertainty of measurements was always in the range 6-8%).

The experimental activity on closed-cycle thermochemical storage systems is still limited, despite the intense research at materials level, thus allowing to consider the testing campaign carried out as a valuable reference for storages employing adsorption technology in combination with low-grade heat sources. Moreover, while many works focus on hot or cold storage operation only, the possibility of realising both was evaluated.

A design analysis performed showed that further improvement is still possible, in order to reduce volumes and weight of the system, as well as increasing the efficiency and that, design and control logics or regulations should be the topic for further research.

Chapter 5

Comparison of different storages and technologies

5.1 Motivations and methodology

Thermal storage technology is gaining interest, but, while research on materials has been going on for some decades, the maturity of systems alternative to sensible storage is still limited. Commercial applications of PCM storages have been made available only recently and sorption systems for storage purposes are not commercially available, despite an increasing number of prototypes being developed at laboratory scale.

In view of an advancement towards higher TRLs of the various technologies, a standardization is needed on both the assessment procedures and the figure of merits used for the evaluation of the features of the storages. An example of the importance of such a need is clear when considering the work presented in the previous Chapters, where 3 storage systems, differing either for the layout (fin-and-tube or plate HEX with the same PCM) or the technology (latent heat or heat of adsorption storage) have been presented. Without any specific feature for their comparison, the experimental data are of difficult interpretation and useless for design purposes.

In the present Chapter, then, a set of parameters, useful for the description and the comparison of storages, will be suggested and applied to the different cases.

The main features that a Performance Indicator should possess, in order to represent a useful means of evaluation or comparison are:

- unique definition, that cannot generate confusion or misunderstanding;
- applicability to a wide range of cases and processes;

- representativeness of the actual characteristics and specificities of the components;
- scalability, in order to be applied to applications in different sizes.

It is evident that, for each case (i.e. a technology), the specific definition of some parameters might change, and only some of them can be applied for a comparison between the various technologies. Moreover, the selection, among the various parameters, of the "key" ones (the so-called Key Performance Indicators or KPIs) depends on the specific application: for example, the main requirements for a CSP plant or a district heating network are dissimilar and the main constraints are different for the different applications (e.g. in some cases, power is more important than energy density or vice versa).

The approach that will be followed is to propose a set of parameters suitable to be applied for different technologies. Some of them have been defined and are under evaluation within Subtask 2 of ECES Annex 30 "Thermal Energy Storage for Cost-Effective Energy Management and CO_2 Mitigation." A general description of each parameter will be given and, when necessary, a distinct interpretation for the two technologies examined will be given. Subsequently, the case study of latent storage system will be considered for the application of the suggested methodology. Finally, in order to show the potentiality of the proposed approach also for the comparison of systems with different technologies, an overview for the three systems will be reported.

5.2 The Indicators

The indicators defined are reported in Figure 5.1.The comparison was realised for different aspects.

- Construction: a first evaluation involves the construction features of the storage, giving information on the size or weight of the overall system. The two parameters taken into account are:
  - storage-to-material mass: it is the ratio between the overall mass of the storage over the mass of heat storage material inside the system.

$$storage-to-material \quad mass = \frac{m_{storage}}{m_{material}} \tag{5.1}$$

  - storage-to-material volume: it is the ratio between the volume of the storage and the volume of the material contained.

$$storage-to-material \quad volume = \frac{V_{storage}}{V_{material}} \tag{5.2}$$

In the definition of the mass or volume of the storage the boundary (which has to be defined in order to decide which components have to be included or excluded from the calculation) was considered at the "container" level, as shown in Figure 5.2. In the case of the LTES storage, this includes only the heat exchanger and the casing of the material, without any consideration for the insulation or the external piping and manifolds. In the case of the adsorption storage, it is more difficult to define the boundary of the system, since, in order for the storage to work, not only an adsorber but also a phase changer is needed. However, since the technology, structure and location of the phase changer is completely independent from that of the adsorber, the boundary was considered around the adsorber, without any insulation.

- Energy: a second evaluation has to involve the storable energy. Indeed, the deviation between the theoretical and actual energy stored in a system can be due to process or heat transfer limitations and heat losses. The indicators used for the energetic assessment of the storage are:

  – Storage thermal efficiency, calculated as the energy recovered from the storage during discharge over the one supplied during charge. When calculating this contribution, the temperature levels of heat source and load have to be specified, as well as the stand-by period. However, the energy due to auxiliaries (e.g. pumps) was not included.

$$\eta_{storage} = \frac{E_{discharge}}{E_{charge}} \tag{5.3}$$

  – Storage specific energy density, calculated as the energy recovered from the storage during discharge over the total mass of the storage, according to the boundary of Figure 5.2.

$$E_m = \frac{E_{discharge}}{m_{storage}} \tag{5.4}$$

  – Storage volumetric energy density, calculated as the energy recovered from the storage during discharge over the total volume of the storage, according to the boundary of Figure 5.2.

$$E_V = \frac{E_{discharge}}{V_{storage}} \tag{5.5}$$

- Dynamics: a last set of parameters can be used to define the dynamic characteristics in the heat transfer of the storage:

- Maximum, minimum and average power: all the three values are calculated separately for charge and discharge. While their definition is straightforward for the LTES case, in the case of adsorption storage it is worth specifying what these contributions indicate. Indeed, as already specified in Chapter 4, different operating modes were evaluated for the adsorption storage, namely short-term heat storage, long-term heat storage or cold storage. In all cases, the charge power is the power measured at the adsorber during desorption. In the case of short-term heat storage the discharge power figures are calculated referring to both the effect measured at the phase changer during condensation and at the adsorber during adsorption. In case of long-term heat storage, the discharge power refers to the power extracted from the adsorber during adsorption. Finally, in the case of cold storage operation, the discharge power is the power at the phase changer during evaporation.
- UA value: it represents the average of the product between the overall heat transfer coefficient and the heat exchange area of the storage. It was calculated as [88]:

$$UA = \frac{\dot{Q}}{T_{material} - \frac{T_{in}+T_{out}}{2}} \tag{5.6}$$

- Charge/discharge time: it represents the time needed to complete the charge or discharge process. For LTES, this is the time needed to complete the phase change of the material and was calculated as the time until the average temperature in the storage reaches the offset value for melting or solidification. For the adsorption storage, it was calculated as the time until the desorption power or the useful effect during discharge are almost zero. In order to allow comparing different systems, the charge or discharge time has been normalised according to the volume of material inside the storage.
- Response time: it is the time passing between the connection of the storage to the load until nominal power is reached.
- Flexibility: it is a "yes/no" parameter, indicating whether partial charge or discharge is possible.

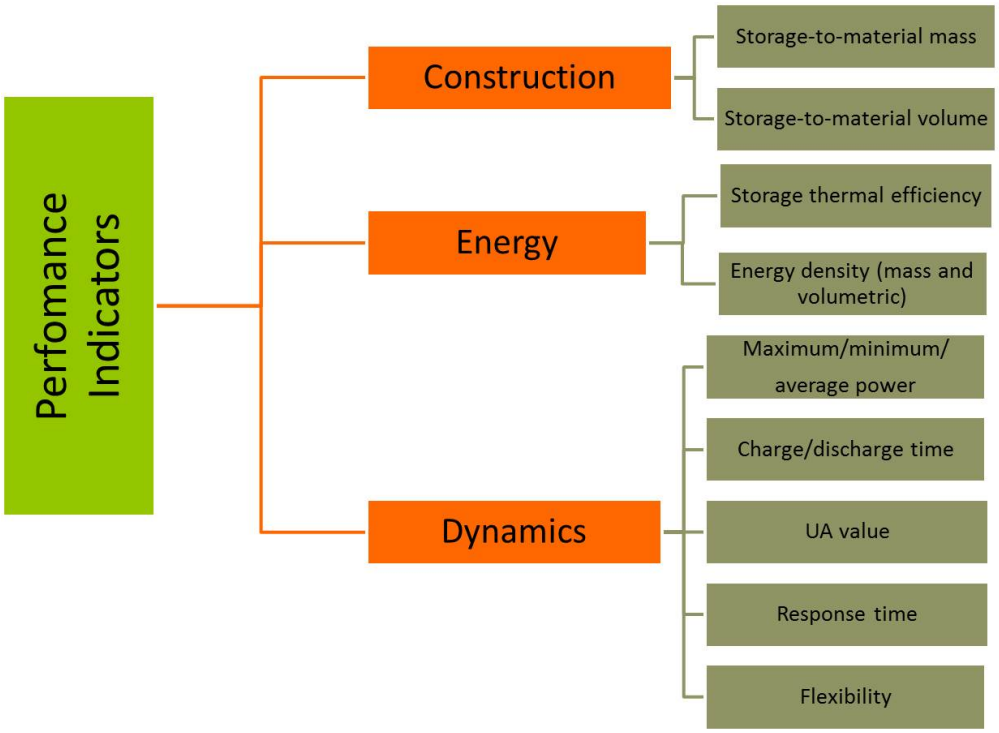

Fig. 5.1 The Performance Indicators defined.

Table 5.1 Construction indicators for the two systems based on latent heat technology.

Storage	Storage-to-Material mass	Storage-to-Material volume
Fin-and-tube storage	5.3	2.1
Plate storage	2.6	2.3

5.3 Calculation of the indicators for LTES systems

5.3.1 Construction

The construction indicators of the two systems are independent from testing conditions and are reported in Table 5.1. It is possible to notice that, when the mass ratio is taken into account, the plate heat exchanger used has a big advantage over the fin-and-tube one. On the contrary (and this is particularly evident with increasing volumes), the volumetric ratio is favourable to the fin-and-tube based system.

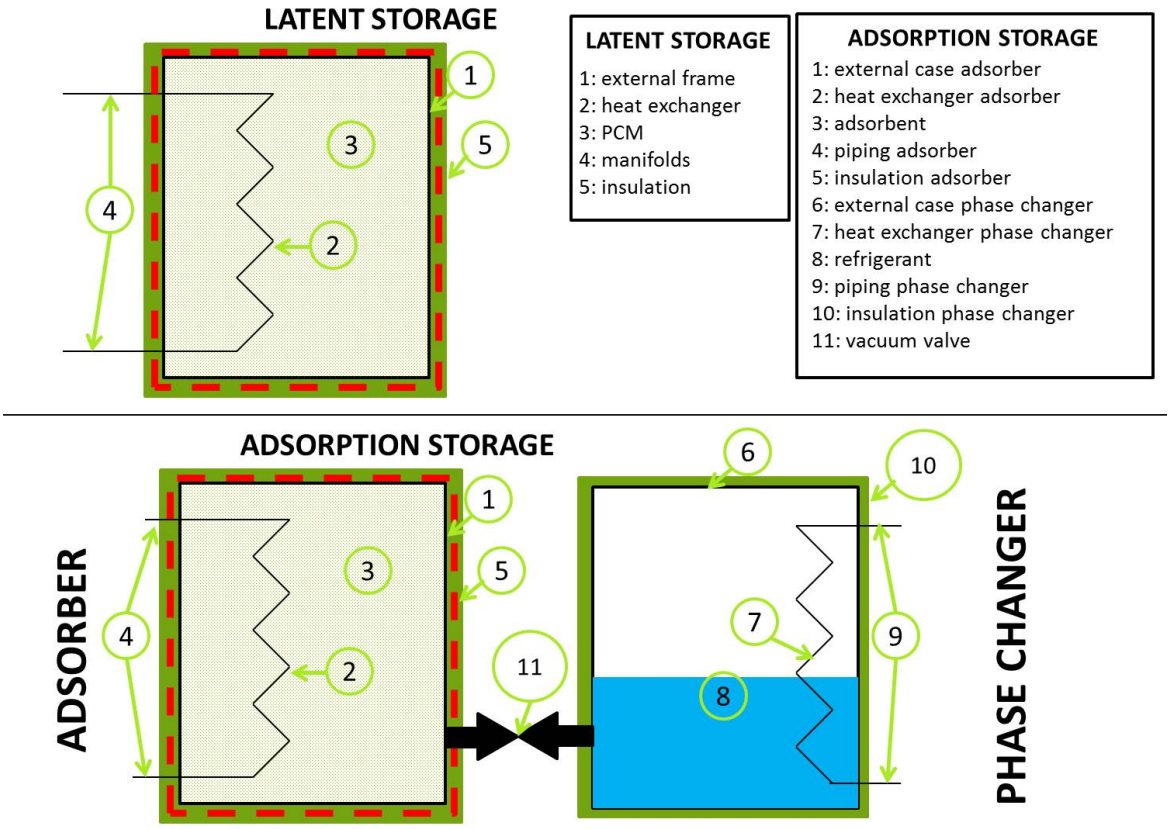

Fig. 5.2 Boundaries used in the calculation of the Performance Indicators. The limit for the calculation is represented by the dashed red line.

5.3.2 Energy

The second group of indicators are those related to the performance of the system from an energetic point of view. They are obviously dependent from the operating parameters of the storage (boundary temperatures, flow rates). In order to make a comparison, some selected tests, performed for both systems under the same boundary conditions, were chosen. The results are reported in Table 5.2. The test selected differ in the temperature span covered by the measurement and the flow rate of the heat transfer fluid. The energetic density (on mass basis)of the whole system is significantly higher in the case of the plate heat exchanger – about 40% higher than the fin-and-tube system. The volumetric energy density is slightly higher in the case of the plate-HEX based system, with values up to 91 MJ/m^3. Indeed, as already pointed out in the calculation of construction indicators, the volumetric material-to-storage ratio is favourable to the fin-and-tube system and, consequently, the high difference existing between the two storages in the energy actually discharged is compensated. It is necessary to specify that, for the specific tests, there is not stand-by period between charge and discharge, since they were realised consecutively.

TESS	CHARGE			DISCHARGE				INDICATORS		
	T_{final}	$T_{initial}$	Flow rate	$T_{initial}$	T_{final}	T_{inlet}	Flow rate	$\eta_{storage}$	E_m	E_V
	°C	°C	kg/min	°C	°C	°C	kg/min	-	kJ/kg	MJ/m^3
FIN-AND-TUBE	87	41	19	87	72	71	10	0.23	55	46
PLATE	89	40	20	87	72	70	10	0.44	139	65
FIN-AND-TUBE	91	25	14	90	74	71	6	0.14	44	43
PLATE	90	26	14	90	73	70	6	0.31	158	76
FIN-AND-TUBE	87	67	14	88	68	65	10	0.49	63	56
PLATE	86	68	14	88	67	65	10	0.79	194	91
FIN-AND-TUBE	86	56	21	86	66	66	21	0.24	84	66
PLATE	86	55	21	86	64	66	21	0.44	137	68

Table 5.2 Energy Indicators for the two developed LTES.

5.3.3 Dynamics

The third group of indicators are those used to describe the dynamics of the system. As for the case of the energy-related ones, they have been calculated for selected tests under defined

boundaries (the same reported in Table 5.2) and are shown in Table 5.4 and Table 5.5. For clarity's sake, the conditions of each test are given in Table 5.3.

Regarding the dynamics of the storages, when compared to the other indicators, the differences between the two systems are quite outstanding: the characteristic charge/discharge time of the plate HEX-based system is almost half of the fin-and-tube system, thus indicating a higher efficiency of the heat exchanger employed. This is also clear from the UA values during charge: for the custom fin-and-tube system, such a value is almost constant in all conditions, around 100 W/K. Instead, in the storage with the plate heat exchanger, UA values up to 3400 W/K were measured, hence an order of magnitude higher. Average power of the plate-HEX system is always higher than the fin-and-tube one: during charge, up to double the power is transferred to the PCM material in the former storage. The difference becomes even more relevant during discharge: discharge of the system is much faster and the average power released can be up to 7 kW, whereas a maximum average power lower than 1.5 kW was measured in the case of the fin-and-tube HEX.

For the discharge, two of the selected indicators were not calculated: UA value and minimum power. Indeed, considering the methodology chosen for the tests, the minimum power achieved during the test is always zero, since this is the condition used to consider the test completed. The definition of the minimum power level that the system is able to supply becomes then ambiguous and of difficult interpretation. Similar considerations apply to the UA value: UA is not a constant value, but rather it ranges between a maximum and a minimum. For the case of charge (especially for the fin-and-tube HEX) the longer time needed to complete the process, the slower dynamics and the lower powers still limit the variation range of the parameter, and therefore allow for the calculation of an average value. On the contrary, the discharge is very fast (especially in the case of the plate HEX) and, as stated above, the methodology adopted requires the power to drop to 0 to stop the process (corresponding, of course, to a zero UA value). The UA then varies in a range of order of magnitudes and it is impossible to calculate a single value. Such considerations should be taken into account when defining the Performance Indicators useful for the evaluation or comparison of the storage.

Two more parameters were defined in the group of Dynamics Indicators: response time and flexibility. Response time, in the case of a lab-scale system tested under controlled boundaries for its characterization cannot be calculated, since a nominal power has not been defined *a priori*. Flexibility instead is related with the potential for part load operation. As shown in Chapter 3, both LTES systems have been tested under incomplete charge or discharge and therefore flexibility can be obtained.

TESS	TEST	CHARGE			DISCHARGE			
		T_{final} °C	$T_{initial}$ °C	Flow rate kg/min	$T_{initial}$ °C	T_{final} °C	T_{inlet} °C	Flow rate kg/min
FIN-AND-TUBE	1	87	41	19	87	72	71	10
PLATE	1	89	40	20	87	72	70	10
FIN-AND-TUBE	2	91	25	14	90	74	71	6
PLATE	2	90	26	14	90	73	70	6
FIN-AND-TUBE	3	87	67	14	88	68	65	10
PLATE	3	86	68	14	88	67	65	10
FIN-AND-TUBE	4	86	56	21	86	66	66	21
PLATE	4	86	55	21	86	64	66	21

Table 5.3 Testing conditions used in the calculation of Dynamics indicators for the two developed LTES.

TESS	Test	CHARGE				
		P_{max} kW	P_{min} kW	P_{ave} kW	UA_{charge} W/K	τ_{charge} min/m^3
FIN-AND-TUBE	1	5.1	0.2	1.1	97	6897
PLATE	1	6.2	0.8	1.9	841	3840
FIN-AND-TUBE	2	5.1	0.2	1.4	91	7175
PLATE	2	5.3	0.7	2.2	2147	3540
FIN-AND-TUBE	3	1.6	0.6	1.0	110	6164
PLATE	3	4.1	0.6	1.4	2754	2280
FIN-AND-TUBE	4	3.3	0.6	1.3	82	7326
PLATE	4	4.3	0.8	1.6	3376	2160

Table 5.4 Energy Indicators for the charge process of the two developed LTES.

TESS	Test	DISCHARGE		
		P_{max} kW	P_{ave} kW	$\tau_{discharge}$ min/m^3
FIN-AND-TUBE	1	2.75	1.01	1491
PLATE	1	15.2	4.79	600
FIN-AND-TUBE	2	1.8	0.8	1768
PLATE	2	9.05	3.03	1020
FIN-AND-TUBE	3	3.15	1.1	1667
PLATE	3	21.49	6.56	696
FIN-AND-TUBE	4	2.63	1.19	1794
PLATE	4	22.64	6.99	402

Table 5.5 Energy Indicators for the discharge process of the two developed LTES.

5.4 Calculation of the indicators for the adsorption system

5.4.1 Construction

The calculation of the construction features of the adsorption storage presented in Chapter 4 according to the boundaries of Figure 5.2 presents a significant issue: the chamber in which the adsorbent material and the heat exchange are inserted is significantly larger than the developed unit (material+HEX), since it is designed for the testing of different systems at different scales. As a consequence, the Construction Indicators would be extremely unfavourable, especially in a comparison with the PCM storages and it was decided to refer the calculation to the volume and weight of the adsorber, meant as the material and the HEX in which it is contained.

According to such an hypothesis, the storage-to-material mass ratio is 4.4 while the storage-to-material volume ratio is 3.18. Compared to the latent storages presented, the system is not optimized, especially in terms of volume, since the storage-to-material volume ratio is about 40% higher than the PCM storages.

5.4.2 Energy

The calculation of Energy Indicators was realised taking into account the possible operating modes that have been previously specified. The results are again presented considering 6 different tests, mainly differing for the boundary conditions in terms of temperature during both charge and discharge. The list of tests and their conditions is presented in Table 5.6.

The results of the various indicators are instead shown in Table 5.7. The operating conditions of the storage are quite different from the ones simulated for the two LTES: while for the PCM storages, discharge at 65-70°C was realised (simulating DHW production or feeding of a thermal chiller), the application field of the adsorption storage was cold production at low temperature (5-18°C) or low-temperature heating (e.g. for coupling with radiant ceiling). It is therefore hard to make a direct comparison between the proposed technologies. It is however possible to notice that the average energy density per mass unit of the adsorption storage is significantly higher than those of PCMs, up to 8 times higher! On the contrary, when considering the volumetric values, the adsorption storage performs worse than the PCM ones. This indicates that still a lot of effort is needed to exploit the huge potential of sorption technology.

TEST	CHARGE				DISCHARGE			
	T_{des}	T_{cond}	Flow adsorber	Flow phase changer	$T_{adsorption}$	$T_{evaporator}$	Flow adsorber	Flow phase changer
	°C	°C	kg/min	kg/min	°C	°C	kg/min	kg/min
1	92	14	11	15	35	9	12	15
2	82	29	13	12	36	11	12	14
3	75	30	12	12	35	11	11	14
4	92	39	12	13	40	6	12	13
5	92	41	12	12	41	15	12	14
6	92	14	11	15	35	9	12	15
7	82	15	13	15	30	6	11	14

Table 5.6 Testing conditions used in the calculation of Energy and Dynamics indicators for the adsorption TES.

5.4.3 Dynamics

Since the aim of the analysis presented in this Chapter is not the definition of performance levels of the storages (which have been analysed in detail in Chapters 3 and 4 for the various technologies), but rather proposing a procedure and figures for the comparison of different storages, some of the parameters that have been presented in Figure 5.1 were not calculated for the adsorption storage. In particular, similarly to the case of the discharging tests of PCM storages, the evolution of the power during a test of the adsorption storage is from an initial peak to a value of 0. Consequently, it is useless to define the minimum power under

TEST	INDICATORS								
	$\varepsilon_{storage}$ CS	$\eta_{storage}$ DHS	$\eta_{storage}$ SHS	E_m CS	E_m DHS	E_m SHS	E_V CS	E_V DHS	E_V SHS
	-	-	-	kJ/kg	kJ/kg	kJ/kg	MJ/m^3	MJ/m^3	MJ/m^3
1	0.38	1.48	0.56	245	957	596	15	57	36
2	0.36	1.18	0.41	225	729	472	13	44	28
3	0.29	1.05	0.38	154	557	356	9	33	21
4	0.33	1.04	0.35	176	559	369	10	33	22
5	0.42	1.21	0.39	282	805	546	17	48	33
6	0.30	1.20	0.45	200	813	507	12	49	30

Table 5.7 Energy Indicators for the developed adsorption TES.

these conditions. For a specific application, where the limit boundaries are known (e.g. the maximum and minimum available temperature of the heat source), the minimum power could be calculated according to the smallest one delivered under the possible operating conditions. For the choice made in the work here presented, where each test is considered separately for the calculation of the Performance Indicators, it is not possible to properly define this parameter.

In addition, due to considerations similar to those for the PCM storages, the UA value was not calculated, neither for charge nor for discharge: the range of variation of UA is too wide and, if it is needed to specify such a parameter, at least a degree of advancement of adsorption/desorption process has to be specified.

The results of the calculations are reported in Table 5.8. If a comparison with PCM technology has to be made, it is interesting to notice that the average time to complete charge/discharge is comparable to the characteristic discharge time of the plate HEX-based LTES. As discussed in Chapter 4, the adsorption storage, especially from a dynamic point of view, is far from optimization and therefore these results highlight the possibility of increasing its promising performance. Another consideration worth making is on average power, which is in the range of 0.5-0.8 kW for all the operating modes during discharge. It is true that this value is far from the average of the plate HEX-based LTES, but the amount of material inside the storage is only 4.4 kg, whereas the fin-and-tube LTES had 37 kg of PCM and the plate LTES 16 kg.

The last two parameters used to define the storage are response time and flexibility. Response time, as for LTES systems, was been calculated. Regarding flexibility, adsorption operation under incomplete charge/discharge is not desirable and therefore the value of this parameter should be "no".

TEST	CHARGE			DISCHARGE				
	P_{max} kW	P_{ave} W	τ_{charge} min/m^3	P_{max} kW	P_{ave} CS W	P_{ave} DHS W	P_{ave} SHS W	$\tau_{discharge}$ min/m^3
1	8.7	887	353	6.8	276	578	546	1037
2	8.4	843	1050	5.2	248	561	482	1105
3	6.2	683	1359	4.3	209	473	327	1643
4	2.5	680	1389	2.0	213	460	340	1383
5	4.6	907	1317	3.5	332	614	488	1500
6	3.5	925	900	2.0	247	612	538	1267

Table 5.8 Dynamics Indicators for the adsorption TES.

5.5 Overview over the three different systems

As already stated in the previous sections, it is not possible to make a direct comparison among the three systems, because they differ for the temperature levels during discharge. However, since the main aim of the activity reported in the present Chapter is to propose a simplified way to compare different storages and technologies, a summary of the calculated indicators in the three cases was realised and is shown in Table 5.9. It is possible to notice, for instance, that the energy density of the adsorption storage, when referred to the mass of material is significantly higher than PCM storages — as expected —, while the volumetric one is not favourable, due to the design that is not optimized. This is just an example remarking that it was possible to define some quantitative parameters that are able to define systems apparently extremely different one another, thus leading the way to the future definition of assessment and evaluation procedures.

5.6 Final remarks

Aim of the present Chapter was the indication of some possible figures to be used in the evaluation of a storage or the comparison of different storages, either employing the same technology or different ones. The parameters calculated were divided into three main categories: construction, energy and dynamics, in order to take into account all the various features that characterise a storage system. The proposed parameters were, firstly, applied to the PCM storages presented in Chapter 3, for which a direct comparison is possible. However, in order to demonstrate the potentiality of the method suggested, they were calculated also for the adsorption storage presented in Chapter 4. The calculation allowed identifying some critical issues, when dealing with the different technologies or processes. In particular, the clear definition of the boundary of the system is of the uttermost importance, since it

	Indicator	PCM fin-and-tube	PCM plate	Adsorption
Construction	Storage-to-material mass	5.3	2.6	4.4
	Storage-to-material volume	2.1	2.3	3.2
Energy	Thermal efficiency	0.3 - 0.4	0.5 - 0.8	0.4 - 1.2
	Energy density [kJ/kg]	45 - 85	130 - 200	180 (cold storage) – 900 (heat storage)
	Energy density [MJ/m^3]	40 - 70	65 - 95	10 (cold storage) – 60 (heat storage)
Dynamics	Maximum power [kW]	1.5 – 3.5	4.0 - 6.0	3 - 7
	Average power [kW]	1.0	1.5 – 3.0	0.2 – 0.6
	Charge/Discharge time [min/m^3]	6000 - 7000	2000 - 4000	1000-1500

Table 5.9 Application of the suggested Indicators to the three storages developed.

significantly affects the final results. Regarding the dynamic features, their application to lab-scale systems and the characterization tests realised in the laboratory is complicated, and for some parameters (e.g. UA or minimum power) it was not possible to provide a satisfactory calculation. Since the definition of parameters for the assessment of storage systems is the objective of Subtask 2 within ECES Annex 30, that has also been the source for some of the calculated figures, the work here presented might represent a basis of discussion for an improvement in such a topic.

Chapter 6

Conclusions

Aim of the present thesis was the research on thermal energy storage for low-grade heat, from solar, industrial processes or internal combustion engines, with focus on experimental activity dealing with the design, realisation and testing of lab-scale prototypes.

In Chapter 2, the state-of-art of thermal energy storage, regarding technologies available was proposed. The literature survey was focused on two technologies: latent heat storage through Phase Change Materials and thermochemical storage through adsorption systems. For both cases, the available storage materials were presented and compared, highlighting also the main design issues. Prototypal or commercial systems under the same boundary of the chosen application (heat source 80-100°C) were discussed, finding out that only a few lab-scale systems exist and therefore only limited information is available.

In Chapter 3, the activity on latent heat storage systems was reported. While the choice of the material was not part of the work of the thesis, the methodology used was presented. Subsequently, two approaches to the design of a LTES were discussed: the realisation of a custom fin-and-tube storage and the usage of a commercial asymmetric plate heat exchanger. Both storages were filled with PlusICE A82, a commercial paraffinic material, characterised by excellent stability and good solidifcation/melting enthalpy but low thermal conductivity. The storages were tested in a testing rig specifically modified at CNR-ITAE and suitable for the characterization of latent or hybrid thermal energy storages coupled with heat sources up to 100°C.

The results of the tests in the fin-and-tube storage highlighted that the main heat transfer mechanism inside the thermal storage is conduction. Charge tests showed that the flow rate used during charging did not hold a significant effect on the performance of the system, in terms of its charging efficiency. Discharge tests performed showed that the amount of material “reacting” (i.e. undergoing complete phase change) is only a portion of the total PCM inside the storage. Indeed, the efficiency measured was in the range 45/60%. Despite

the reported critical issues, the energy stored during all the performed tests, was in the range of 75-135 kJ/kg, which is up to 50% more that the energy storable by using the sensible heat of water (the common medium used in such temperature ranges).

Following the fin-and-tube system, another one was realised, employing a commercial plate heat exchanger filled with the same PCM. The tests performed on such a unit highlighted that, for this system, very fast charge and discharge can be realised (discharge at higher flow rates might take less than 5 minutes). The performance of the system, in terms of efficiency, was good, since efficiencies up to 80% could be reached during discharge and up to 94% during charge. An optimization is still needed since the exchanger is a commercial one and its design does not allow to fully exploit the potential of the material (not all the material reacts, only about 80%).

The experimental results clearly stated that an optimization of the systems is needed and, for such a reason, a mathematical model in COMSOL Multiphysics was realised. The aim of the model was to predict the time-dependent behaviour of the storage in an accurate, but also not too time consuming way. For this purpose, a novel configuration was proposed and applied to the case of the fin-and-tube PCM storage, by simulating the whole system using different components: a 1D model is solved for the tubes of the heat exchanger, and a simplified 3D model for the PCM-fin part. The correlation between the components was defined, as well as the method for the simplification of the fin parts of the heat exchanger, allowing the simulation of only half a fin and half a fin gap filled with PCM. The validation of the model was done with data from experiments, showing that there is a good agreement between the simulated and experimental fluid outlet temperature during charging, with a deviation lower than 0.2 K. Similar accuracy was found for the discharge case, with average difference of 0.6 K.

In Chapter 4, the development of an adsorption storage prototype was reported. The choice of the material was done on the basis of a thermodynamic analysis, showing that the material with the most promising characteristics in the temperature range considered is AQSOA FAM Z02. Subsequently, a storage based on such a material and using a fin-and-tube heat exchanger was designed and realised. It was tested at CNR-ITAE using a dedicated set-up and a testing rig suitable for the characterization of thermally-driven chillers, heat pumps and storages. Different operating modes were tested, namely Cold Storage, Daily Hot Storage and Seasonal Hot Storage, and the effect of boundary conditions (operating temperatures and flow rates) on the performance of the system was evaluated. In daily heat storage conditions, the presented prototype is able to store from 2.3 MJ at 75 °C up to 4 MJ at 91 °C corresponding to a maximum energy storage density of 1000 kJ/kg, while the average power during the discharging phase ranges from 200 W to 650 W. Such results have been

compared to data available in literature, highlighting that the system has a good performance, considering both energy density and efficiency. Indeed, considering a ΔT of 45°C, the system realised is able to store 5 times the energy of water. Eventually, a design analysis was carried out, evidencing that there is still room for improving the system through a more accurate design and the choice of improved materials.

Finally, in Chapter 5, the assessment of the performance of the two systems was discussed. In particular, some parameters were identified for the description and comparison of thermal energy storage systems, according to the work currently ongoing within ECES Annex 30. Three main groups of Performance Indicators were defined: Construction, Energy and Dynamics. They were applied to the case studies presented in the previous Chapters and the open issues were highlighted and analysed.

The main novelties presented in the thesis can be summarised as follows.

- Both for the case of latent heat storage and adsorption heat storage, only a few experimental activities existed, for the selected temperature range. Within the activity here presented, instead, an experimental approach was followed, thus realising 3 different systems, that were tested under operating conditions.

- The results of the experimental measurement highlighted the great potential of the system, that, even under non-optimised conditions, reached an energy density much higher than traditional sensible storages.

- Among the realised prototypes with PCMs, the plate heat exchanger showed superior dynamic capabilities, with very fast response time and short charge/discharge times, thus proving that such systems can be applied also in applications where power is the leading constraint.

- A numerical model for the simulation of latent heat storages was developed and validated. It has two main innovative features: reduced computational demand and possibility to be adapted to different configurations easily.

- Finally, a methodology was suggested for the evaluation of the performance of thermal energy storages, through the definition of a set of parameters, that could be successfully applied to the storages realised, despite their very different operating characteristics and modes.

The outcome of the work presented indicates that the systems realised, if properly optimised, are able to make a step forward from lab-scale to pre-commercial stage, thus marking an important step towards the replacement of traditional sensible heat storage in one

of the field of applications where water is quite competitive. Future work possibilities, in the examined fields, is linked to the optimization of the design of systems: through the use of the mathematical model developed, it is possible to analyse different configurations, in terms of construction materials and geometrical parameters of the system, both in the case of the fin-and-tube and the plate heat exchangers. A similar tool could also be realised for the case of the adsorption storage, useing the same structure (integration of 1D model and 3D model), by adding the proper equations for the description of adsorption phenomena. A geometric optimization and modification of the construction features of the adsorption heat storage could then be realised, in order to further increase the thermal power extracted and the storage capacity of such systems, further increasing their competitiveness.

Nomenclature

Latin letters

$\dot{m}$	Mass flow rate	kg/min
A_c	Area cross-section	m^2
c_p	Specific heat	$kJ/(kgK)$
d	Diameter	m
E	Energy	J
f	Scaling factor	
g	gravity constant	$9.81\ m/s^2$
H	Enthalpy	kJ/kg
h	Convective heat transfer coefficient	$W/(m^2K)$
k	Thermal conductivity	$W/(mK)$
l	Lenght	m
m	Mass	kg
n	Number	
$Nsym$	Symmetry ratio	
Nu	Nusselt number	
P	Power	W
p	Pressure	bar

Pr	Prandtl number	
Q	Heat	J
R	Universal gas constant	$8.3144\ J/(Kmol)$
Ra	Rayleigh number	
Re	Reynolds number	
s	thickness	m
T	Temperature	C
t	Time	s
u	Uncertainty	
V	Volume	m^3
w	Uptake	kg/kg
$\dot{Q}$	Heat flux	W/m^2

Greek letters

β	Expansion coefficient	$1/K$
η	Efficiency	
λ	Heat of phase change	J
μ	Dynamic viscosity	Ns/m^2
ρ	Density	kg/m^2

Subscripts

0	Initial
ads	Adsorption
amb	Ambient
ave	Average
ch	Charge

cond Condensation

des Desorption

disch Discharge

eff Effective

ev Evaporation

fin Final

in Inlet

isc Isosteric cooling

ish Isosteric heating

l Liquid

m Melting

out Outlet

r Reaction

ref Refrigerant

s Solid

sat Saturation

ss Stainless Steel

th Theoretical

Abbreviations

CS Cold Storage

CSP Concentrated Solar Plant

DA Dubinin-Astakhov

DHW Domestic Hot Water

DR Dubinin-Radushkevich

HEX Heat Exchanger

HTF Heat Transfer Fluid

LHS Long term Heat Storage

$LTES$ Latent Thermal Energy Storage

MOF Metal-Organic Framework

PCM Phase Change Material

SHS Short term Heat Storage

TCS Thermochemical Storage

TES Thermal Energy Storage

$TESS$ Thermal Energy Storage System

TRL Technology Readiness Level

Bibliography

[1] T. Kousksou, P. Bruel, A. Jamil, T. El Rhafiki, and Y. Zeraouli. Energy storage: Applications and challenges. *Solar Energy Materials and Solar Cells*, 120:59–80, jan 2014. doi: 10.1016/j.solmat.2013.08.015.

[2] Caroline L. Noblet, Mario F. Teisl, Keith Evans, Mark W. Anderson, Shannon McCoy, and Edmund Cervone. Public preferences for investments in renewable energy production and energy efficiency. *Energy Policy*, 87:177–186, 2015. doi: 10.1016/j.enpol.2015.09.003.

[3] Pallav Purohit and Lena Höglund-Isaksson. Global emissions of fluorinated greenhouse gases 2005–2050 with abatement potentials and costs. *Atmospheric Chemistry and Physics*, 17:2795–2816, 2017. doi: 10.5194/acp-17-2795-2017.

[4] European Commission. Europe 2020 strategy. URL https://ec.europa.eu/info/strategy/european-semester/framework/europe-2020-strategy{_}en.

[5] Gequn Shu, Youcai Liang, Haiqiao Wei, Hua Tian, Jian Zhao, and Lina Liu. A review of waste heat recovery on two-stroke IC engine aboard ships. *Renewable and Sustainable Energy Reviews*, 19:385–401, 2013. doi: 10.1016/j.rser.2012.11.034.

[6] Ibrahim Dincer. On thermal energy storage systems and applications in buildings. *Energy and Buildings*, 34:377–388, 2002.

[7] D Fernandes, F Pitié, G Cáceres, and J Baeyens. Thermal energy storage: " How previous findings determine current research priorities ". *Energy*, 39:246–257, 2012. doi: 10.1016/j.energy.2012.01.024.

[8] Vittorio Verda and Francesco Colella. Primary energy savings through thermal storage in district heating networks. *Energy*, 36:4278–4286, 2011. doi: 10.1016/j.energy.2011.04.015.

[9] L.A. Chidambaram, A.S. Ramana, G. Kamaraj, and R. Velraj. Review of solar cooling methods and thermal storage options. *Renewable and Sustainable Energy Reviews*, 15 (6):3220–3228, 2011. doi: 10.1016/j.rser.2011.04.018.

[10] Harald Mehling and Luisa F. Cabeza. *Heat and cold storage with PCM : an up to date introduction into basics and applications*. Springer, 2008. ISBN 9783540685562.

[11] J.-C Hadorn. Advanced Storage Concepts for Solar Energy, IEA-SHC Task 32 2003-2007. In *Eurosun 2008*, 2008. URL http://www.solarthermalworld.org/sites/gstec/files/Hadorn{_}storage.pdf.

[12] Guruprasad Alva, Lingkun Liu, Xiang Huang, and Guiyin Fang. Thermal energy storage materials and systems for solar energy applications. *Renewable and Sustainable Energy Reviews*, 68:693–706, 2017. doi: 10.1016/j.rser.2016.10.021.

[13] Rainer Tamme, Doerte Laing, Wolf-Dieter Steinmann, and Thomas Bauer. Thermal Energy Storage. In *Encyclopedia of Sustainability Science and Technology*, pages 10551–10577. Springer New York, New York, NY, 2012. doi: 10.1007/978-1-4419-0851-3_684. URL http://link.springer.com/10.1007/978-1-4419-0851-3{_}684.

[14] R.K. Sharma, P. Ganesan, V.V. Tyagi, H.S.C. Metselaar, and S.C Sandaran. Developments in organic solidâ€“liquid phase change materials and their applications in thermal energy storage. *Energy Conversion and Management*, 95:193–228, 2015. doi: 10.1016/j.enconman.2015.01.084.

[15] Ruzhu Wang and Tianshu Ge. *Advances in solar heating and cooling*. Woodhead Publishing Series in Energy: Number 102, 2nd edition edition, 2016. ISBN 9780081003015.

[16] Amy S Fleischer. *Thermal Energy Storage Using Phase Change Materials Fundamentals and Applications*. Springer New York, springerbr edition, 2015. ISBN 978-3-319-20921-0. doi: 10.1007/978-3-319-20922-7.

[17] Xiang Huang, Guruprasad Alva, Yuting Jia, and Guiyin Fang. Morphological characterization and applications of phase change materials in thermal energy storage: A review. *Renewable and Sustainable Energy Reviews*, 72:128–145, 2017. doi: 10.1016/j.rser.2017.01.048.

[18] Atul Sharma, V V Tyagi, C R Chen, and D Buddhi. Review on thermal energy storage with phase change materials and applications. *Rnewable and Sustainable Energy Reviews*, 13:318–345, 2009. doi: 10.1016/j.rser.2007.10.005.

[19] Samer Kahwaji, Michel B Johnson, Ali C Kheirabadi, Dominic Groulx, and Mary Anne White. Fatty acids and related phase change materials for reliable thermal energy storage at moderate temperatures. *Solar Energy Materials and Solar Cells*, 167:109–120, 2017. doi: 10.1016/j.solmat.2017.03.038.

[20] Jose Pereira, Da Cunha, and Philip Eames. Thermal energy storage for low and medium temperature applications using phase change materials:A review. *Applied Energy*, 177:227–238, 2016. doi: 10.1016/j.apenergy.2016.05.097.

[21] A Hasan, S J Mccormack, M J Huang, and B Norton. Characterization of phase change materials for thermal control of photovoltaics using Differential Scanning Calorimetry and Temperature History Method. *Energy Conversion and Management*, 81:322–329, 2014. doi: 10.1016/j.enconman.2014.02.042.

[22] Manish K Rathod and Jyotirmay Banerjee. Thermal stability of phase change materials used in latent heat energy storage systems: A review. *Renewable and Sustainable Energy Reviews*, 18:246–258, 2013. doi: 10.1016/j.rser.2012.10.022.

[23] Aran Solé, Hannah Neumann, Sophia Niedermaier, Ingrid Martorell, Peter Schossig, and Luisa F Cabeza. Stability of sugar alcohols as PCM for thermal energy storage. *Solar Energy Materials and Solar Cells*, 126:125–134, 2014. doi: 10.1016/j.solmat.2014.03.020.

[24] Saman Nimali Gunasekara, Ruijun Pan, Justin Ningwei Chiu, and Viktoria Martin. Polyols as phase change materials for surplus thermal energy storage. *Applied Energy*, 162:1439–1452, 2016. doi: 10.1016/j.apenergy.2015.03.064.

[25] Su-Gwang Jeong, Jeong-Hun Lee, Jungki Seo, and Sumin Kim. Thermal performance evaluation of Bio-based shape stabilized PCM with boron nitride for energy saving. *International Journal of Heat and Mass Transfer*, 71:245–250, 2014. doi: 10.1016/j.ijheatmasstransfer.2013.12.017.

[26] Yujin Kang, Su-Gwang Jeong, Seunghwan Wi, and Sumin Kim. Energy efficient Bio-based PCM with silica fume composites to apply in concrete for energy saving in buildings. *Solar Energy Materials and Solar Cells*, 143:430–434, 2015. doi: 10.1016/j.solmat.2015.07.026.

[27] Shamseldin A. Mohamed, Fahad A. Al-Sulaiman, Nasiru I. Ibrahim, Md. Hasan Zahir, Amir Al-Ahmed, R. Saidur, B.S. Yılbaş, and A.Z. Sahin. A review on current status and challenges of inorganic phase change materials for thermal energy storage

systems. *Renewable and Sustainable Energy Reviews*, 70:1072–1089, 2017. doi: 10.1016/j.rser.2016.12.012.

[28] F. Bruno, M. Belusko, M Liu, and N.H.S. Tay. 9 – Using solid-liquid phase change materials (PCMs) in thermal energy storage systems. In *Advances in Thermal Energy Storage Systems*, pages 201–246. 2015. ISBN 9781782420880. doi: 10.1533/9781782420965.2.201.

[29] Kinga Pielichowska and Krzysztof Pielichowski. Phase change materials for thermal energy storage. *Progress in Materials Science*, 65:67–123, 2014. doi: 10.1016/j.pmatsci.2014.03.005.

[30] Ming Liu, N H Steven Tay, Stuart Bell, Martin Belusko, Rhys Jacob, Geoffrey Will, Wasim Saman, and Frank Bruno. Review on concentrating solar power plants and new developments in high temperature thermal energy storage technologies. *Renewable and Sustainable Energy Reviews*, 53:1411–1432, 2015. doi: 10.1016/j.rser.2015.09.026.

[31] S.M. Shalaby, M.A. Bek, and A.A. El-Sebaii. Solar dryers with PCM as energy storage medium: A review. *Renewable and Sustainable Energy Reviews*, 33:110–116, 2014. doi: 10.1016/j.rser.2014.01.073.

[32] Biwan Xu and Zongjin Li. Paraffin/diatomite composite phase change material incorporated cement-based composite for thermal energy storage. *Applied Energy*, 105:229–237, 2013. doi: 10.1016/j.apenergy.2013.01.005.

[33] Nasiru I. Ibrahim, Fahad A. Al-Sulaiman, Saidur Rahman, Bekir S. Yilbas, and Ahmet Z. Sahin. Heat transfer enhancement of phase change materials for thermal energy storage applications: A critical review. *Renewable and Sustainable Energy Reviews*, 74:26–50, 2017. doi: 10.1016/j.rser.2017.01.169.

[34] Halime Ö Paksoy. *Thermal Energy Storage for Sustainable Energy Consumption*. Springer Netherlands, proceeding edition, 2007. ISBN 9781402052880. doi: 10.1007/978-1-4020-5290-3.

[35] N. Yu, R.Z. Wang, and L.W. Wang. Sorption thermal storage for solar energy. *Progress in Energy and Combustion Science*, 39(5):489–514, 2013. doi: 10.1016/j.pecs.2013.05.004.

[36] Andrea Frazzica and Angelo Freni. Adsorbent working pairs for solar thermal energy storage in buildings. *Renewable Energy*, 110:87–94, 2017. doi: 10.1016/j.renene.2016.09.047.

[37] K. Edem N'Tsoukpoe, Hui Liu, Nolwenn Le Pierr??s, and Lingai Luo. A review on long-term sorption solar energy storage. *Renewable and Sustainable Energy Reviews*, 13(9):2385–2396, 2009. doi: 10.1016/j.rser.2009.05.008.

[38] J. Jänchen, D. Ackermann, H. Stach, and W. Brösicke. Studies of the water adsorption on Zeolites and modified mesoporous materials for seasonal storage of solar heat. *Solar Energy*, 76(1):339–344, 2004. doi: 10.1016/j.solener.2003.07.036.

[39] Ronald A. Shigeishi, Cooper H. Langford, and Bryan R. Hollebone. Solar energy storage using chemical potential changes associated with drying of zeolites. *Solar Energy*, 23(6):489–495, 1979. doi: 10.1016/0038-092X(79)90072-0.

[40] Eng-Poh Ng and Svetlana Mintova. Nanoporous materials with enhanced hydrophilicity and high water sorption capacity. *Microporous and Mesoporous Materials*, 114(1): 1–26, 2008. doi: 10.1016/j.micromeso.2007.12.022.

[41] Stefan K. Henninger, Sebastian-Johannes Ernst, Larisa Gordeeva, Phillip Bendix, Dominik Fröhlich, Alexandra D. Grekova, Lucio Bonaccorsi, Yuri Aristov, and Jochen Jaenchen. New materials for adsorption heat transformation and storage. *Renewable Energy*, 110:59–68, 2017. doi: 10.1016/j.renene.2016.08.041.

[42] Dominique Lefebvre and F. Handan Tezel. A review of energy storage technologies with a focus on adsorption thermal energy storage processes for heating applications. *Renewable and Sustainable Energy Reviews*, 67:116–125, 2017. doi: 10.1016/j.rser.2016.08.019.

[43] Irina A. Simonova, Angelo Freni, Giovanni Restuccia, and Yuri I. Aristov. Water sorption on composite "silica modified by calcium nitrate". *Microporous and Mesoporous Materials*, 122(1):223–228, 2009. doi: 10.1016/j.micromeso.2009.02.034.

[44] Dongsheng Zhu, Huijun Wu, and Shengwei Wang. Experimental study on composite silica gel supported CaCl2 sorbent for low grade heat storage. *International Journal of Thermal Sciences*, 45(8):804–813, 2006. doi: 10.1016/j.ijthermalsci.2005.10.009.

[45] Huijun Wu, Shengwei Wang, and Dongsheng Zhu. Effects of impregnating variables on dynamic sorption characteristics and storage properties of composite sorbent for solar heat storage. *Solar Energy*, 81(7):864–871, 2007. doi: 10.1016/j.solener.2006.11.013.

[46] N. Yu, R.Z. Wang, Z.S. Lu, and L.W. Wang. Development and characterization of silica gel–LiCl composite sorbents for thermal energy storage. *Chemical Engineering Science*, 111:73–84, 2014. ISSN 00092509. doi: 10.1016/j.ces.2014.02.012.

[47] N. Yu, R.Z. Wang, Z.S. Lu, and L.W. Wang. Study on consolidated composite sorbents impregnated with LiCl for thermal energy storage. *International Journal of Heat and Mass Transfer*, 84:660–670, 2015. doi: 10.1016/j.ijheatmasstransfer.2015.01.065.

[48] Yuriy I. Aristov. Adsorptive transformation of heat: Principles of construction of adsorbents database. *Applied Thermal Engineering*, 42:18–24, 2012. doi: 10.1016/j.applthermaleng.2011.02.024.

[49] Yuri I. Aristov. Challenging offers of material science for adsorption heat transformation: A review. *Applied Thermal Engineering*, 50:1610–1618, 2013. doi: 10.1016/j.applthermaleng.2011.09.003.

[50] Belal Dawoud and Yuri Aristov. Experimental study on the kinetics of water vapor sorption on selective water sorbents, silica gel and alumina under typical operating conditions of sorption heat pumps. *International Journal of Heat and Mass Transfer*, 46(2):273–281, 2003. doi: 10.1016/S0017-9310(02)00288-0.

[51] B. Dawoud, M. Imroz Sohel, A. Freni, S. Vasta, and G. Restuccia. On the effective thermal conductivity of wetted zeolite under the working conditions of an adsorption chiller. *Applied Thermal Engineering*, 31(14):2241–2246, 2011. doi: 10.1016/j.applthermaleng.2011.03.016.

[52] Angelo Freni, Gaetano Maggio, Alessio Sapienza, Andrea Frazzica, Giovanni Restuccia, and Salvatore Vasta. Comparative analysis of promising adsorbent/adsorbate pairs for adsorptive heat pumping, air conditioning and refrigeration. *Applied Thermal Engineering*, 104:85–95, 2016. doi: 10.1016/j.applthermaleng.2016.05.036.

[53] Felix Jeremias, Dominik Fröhlich, Christoph Janiak, and Stefan K. Henninger. Advancement of sorption-based heat transformation by a metal coating of highly-stable, hydrophilic aluminium fumarate MOF. *RSC Advances*, 4(46):24073, 2014. doi: 10.1039/c4ra03794d.

[54] Luca Scapino, Herbert A Zondag, Johan Van Bael, Jan Diriken, and Camilo C M Rindt. Sorption heat storage for long-term low-temperature applications: A review on the advancements at material and prototype scale. *Applied Energy*, 190:920–948, 2017. doi: 10.1016/j.apenergy.2016.12.148.

[55] Hao Fang, Jianjun Xia, and Yi Jiang. Key issues and solutions in a district heating system using low-grade industrial waste heat. *Energy*, 86:589–602, 2015. doi: 10.1016/j.energy.2015.04.052.

[56] Lidia Navarro, Alvaro De Gracia, Shane Colclough, Maria Browne, Sarah J Mccormack, Philip Griffiths, and Luisa F Cabeza. Thermal energy storage in building integrated thermal systems: A review. Part 1. active storage systems. *Renewable Energy*, 88:526–547, 2016. doi: 10.1016/j.renene.2015.11.040.

[57] M Noro, R M Lazzarin, and F Busato. Solar cooling and heating plants: An energy and economic analysis of liquid sensible vs phase change material (PCM) heat storage. *International Journal of Refrigeration*, 39:104–116, 2014. doi: 10.1016/j.ijrefrig.2013.07.022.

[58] Arefeh Hesaraki, Sture Holmberg, and Fariborz Haghighat. Seasonal thermal energy storage with heat pumps and low temperatures in building projects—A comparative review. *Renewable and Sustainable Energy Reviews*, 43:1199–1213, 2015. doi: 10.1016/j.rser.2014.12.002.

[59] Kevyn Johannes, Frederic Kuznik, Jean Luc Hubert, Francois Durier, and Christian Obrecht. Design and characterisation of a high powered energy dense zeolite thermal energy storage system for buildings. *Applied Energy*, 159:80–86, 2015. doi: 10.1016/j.apenergy.2015.08.109.

[60] D Connolly, H Lund, B V Mathiesen, S Werner, B Möller, U Persson, T Boermans, D Trier, P A Østergaard, and S Nielsen. Heat Roadmap Europe: Combining district heating with heat savings to decarbonise the EU energy system. *Energy Policy*, 65:475–489, 2014. doi: 10.1016/j.enpol.2013.10.035.

[61] Henrik Lund, Sven Werner, Robin Wiltshire, Svend Svendsen, Jan Eric Thorsen, Frede Hvelplund, and Brian Vad Mathiesen. 4th Generation District Heating (4GDH) Integrating smart thermal grids into future sustainable energy systems. *Energy*, 68:1–11, 2014. doi: 10.1016/j.energy.2014.02.089.

[62] J Xu, R Z Wang, and Y Li. A review of available technologies for seasonal thermal energy storage. *Solar Energy*, 103:610–638, 2014. doi: 10.1016/j.solener.2013.06.006.

[63] Laia Miró, Jaume Gasia, and Luisa F Cabeza. Thermal energy storage (TES) for industrial waste heat (IWH) recovery: A review. *Appied Energy*, 179:284–301, 2016. doi: 10.1016/j.apenergy.2016.06.147.

[64] C. Lauterbach, B. Schmitt, U. Jordan, and K. Vajen. The potential of solar heat for industrial processes in Germany. *Renewable and Sustainable Energy Reviews*, 16(7): 5121–5130, 2012. doi: 10.1016/j.rser.2012.04.032.

[65] Barbara Sturm, Stephan Hugenschmidt, Sharon Joyce, Werner Hofacker, and Anthony P. Roskilly. Opportunities and barriers for efficient energy use in a medium-sized brewery. *Applied Thermal Engineering*, 53(2):397–404, 2013. doi: 10.1016/j.applthermaleng.2012.05.006.

[66] Heike Schreiber, Stefan Graf, Franz Lanzerath, and André Bardow. Adsorption thermal energy storage for cogeneration in industrial batch processes: Experiment, dynamic modeling and system analysis. *Applied Thermal Engineering*, 89:485–493, 2015. doi: 10.1016/j.applthermaleng.2015.06.016.

[67] Nicholas R. Jankowski and F. Patrick McCluskey. A review of phase change materials for vehicle component thermal buffering. *Applied Energy*, 113:1525–1561, 2014. doi: 10.1016/j.apenergy.2013.08.026. URL http://dx.doi.org/10.1016/j.apenergy.2013.08.026.

[68] A. Castell and C. Solé. 11 – Design of latent heat storage systems using phase change materials (PCMs). In *Advances in Thermal Energy Storage Systems*, pages 285–305. 2015. ISBN 9781782420880. doi: 10.1533/9781782420965.2.285.

[69] Soteris Kalogirou. The potential of solar industrial process heat applications. *Applied Energy*, 76(4):337–361, 2003. doi: 10.1016/S0306-2619(02)00176-9.

[70] Monia Chaabane, Hatem Mhiri, and Philippe Bournot. Thermal performance of an integrated collector storage solar water heater (ICSSWH) with phase change materials (PCM). *Energy Conversion and Management*, 78:897–903, 2014. doi: 10.1016/j.enconman.2013.07.089.

[71] P. Feliński and R. Sekret. Experimental study of evacuated tube collector/storage system containing paraffin as a PCM. *Energy*, 114:1063–1072, 2016. doi: 10.1016/j.energy.2016.08.057.

[72] Luisa F. Cabeza, Manuel Ibáñez, Cristian Solé, Joan Roca, and Miquel Nogués. Experimentation with a water tank including a PCM module. *Solar Energy Materials and Solar Cells*, 90(9):1273–1282, 2006. doi: 10.1016/j.solmat.2005.08.002.

[73] Saeid Seddegh, Xiaolin Wang, Alan D. Henderson, and Ziwen Xing. Solar domestic hot water systems using latent heat energy storage medium: A review. *Renewable and Sustainable Energy Reviews*, 49:517–533, 2015. doi: 10.1016/j.rser.2015.04.147.

[74] J F Belmonte, M A Izquierdo-Barrientos, A E Molina, and J A Almendros-Ib Nez. Air-based solar systems for building heating with PCM fluidized bed energy storage. *Energy and Buildings*, 130:150–165, 2016. doi: 10.1016/j.enbuild.2016.08.041.

[75] M. Helm, C. Keil, S. Hiebler, H. Mehling, and C. Schweigler. Solar heating and cooling system with absorption chiller and low temperature latent heat storage: Energetic performance and operational experience. *International Journal of Refrigeration*, 32 (4):596–606, 2009. doi: 10.1016/j.ijrefrig.2009.02.010.

[76] Ali Abbasi Godarzi, Masoud Jalilian, Jalal Samimi, Ali Jokar, and Mohammad Ali Vesaghi. Design of a PCM storage system for a solar absorption chiller based on exergoeconomic analysis and genetic algorithm. *International Journal of Refrigeration*, 36(1):88–101, 2013. doi: 10.1016/j.ijrefrig.2012.08.028.

[77] J.F. Belmonte, M.A. Izquierdo-Barrientos, P. Eguía, A.E. Molina, and J.A. Almendros-Ibáñez. PCM in the heat rejection loops of absorption chillers. A feasibility study for the residential sector in Spain. *Energy and Buildings*, 80:331–351, 2014. doi: 10.1016/j.enbuild.2014.04.057.

[78] Antoni Gil, Eduard Oró, Gerard Peiró, Servando Álvarez, and Luisa F. Cabeza. Material selection and testing for thermal energy storage in solar cooling. *Renewable Energy*, 57:366–371, 2013. doi: 10.1016/j.renene.2013.02.008.

[79] Antoni Gil, Eduard Oró, Laia Miró, Gerard Peiró, Álvaro Ruiz, José Manuel Salmerón, and Luisa F. Cabeza. Experimental analysis of hydroquinone used as phase change material (PCM) to be applied in solar cooling refrigeration. *International Journal of Refrigeration*, 39:95–103, 2014. doi: 10.1016/j.ijrefrig.2013.05.013.

[80] Gerard Peiró, Jaume Gasia, Laia Miró, and Luisa F. Cabeza. Experimental evaluation at pilot plant scale of multiple PCMs (cascaded) vs. single PCM configuration for thermal energy storage. *Renewable Energy*, 83:729–736, 2015. doi: 10.1016/j.renene.2015.05.029.

[81] J Banaszek, R Domañski, M Rebow, and F El-Sagier. Experimental study of solid–liquid phase change in a spiral thermal energy storage unit. *Applied Thermal Engineering*, 19(12):1253–1277, 1999. doi: 10.1016/S1359-4311(98)00120-3.

[82] Vincenza Brancato, Andrea Frazzica, Alessio Sapienza, and Angelo Freni. Identification and characterization of promising phase change materials for solar cooling applications. *Solar Energy Materials and Solar Cells*, 160:225–232, 2017. doi: 10.1016/j.solmat.2016.10.026.

[83] Andrea Frazzica, Marco Manzan, Alessio Sapienza, Angelo Freni, Giuseppe Toniato, and Giovanni Restuccia. Experimental testing of a hybrid sensible-latent heat storage system for domestic hot water applications. *Applied Energy*, 183:1157–1167, 2016. doi: 10.1016/j.apenergy.2016.09.076.

[84] M. Medrano, M.O. Yilmaz, M. Nogués, I. Martorell, Joan Roca, and Luisa F. Cabeza. Experimental evaluation of commercial heat exchangers for use as PCM thermal storage systems. *Applied Energy*, 86(10):2047–2055, 2009. doi: 10.1016/j.apenergy.2009.01.014.

[85] Valeria Palomba, Vincenza Brancato, and Andrea Frazzica. Experimental investigation of a latent heat storage for solar cooling applications. *Applied Energy*, 199:347–358, 2017. ISSN 03062619. doi: 10.1016/j.apenergy.2017.05.037. URL http://www.sciencedirect.com/science/article/pii/S0306261917305470.

[86] Keumnam Cho and S.H. Choi. Thermal characteristics of paraffin in a spherical capsule during freezing and melting processes. *International Journal of Heat and Mass Transfer*, 43(17):3183–3196, 2000. doi: 10.1016/S0017-9310(99)00329-4.

[87] B. Torregrosa-Jaime, A. López-Navarro, J.M. Corberán, J.C. Esteban-Matías, L. Klinkner, and J. Payá. Experimental analysis of a paraffin-based cold storage tank. *International Journal of Refrigeration*, 36(6):1632–1640, 2013. doi: 10.1016/j.ijrefrig.2013.05.001.

[88] A. Castell, M. Belusko, F. Bruno, and L.F. Cabeza. Maximisation of heat transfer in a coil in tank PCM cold storage system. *Applied Energy*, 88(11):4120–4127, 2011. ISSN 03062619. doi: 10.1016/j.apenergy.2011.03.046. URL http://www.sciencedirect.com/science/article/pii/S0306261911002169.

[89] A. López-Navarro, J. Biosca-Taronger, J.M. Corberán, C. Peñalosa, A. Lázaro, P. Dolado, and J. Payá. Performance characterization of a PCM storage tank. *Applied Energy*, 119:151–162, 2014. ISSN 03062619. doi: 10.1016/j.apenergy.2013.12.041. URL http://www.sciencedirect.com/science/article/pii/S0306261913010404.

[90] G. Ziskind. 12 – Modelling of heat transfer in phase change materials (PCMs) for thermal energy storage systems. In *Advances in Thermal Energy Storage Systems*, pages 307–324. 2015. ISBN 9781782420880. doi: 10.1533/9781782420965.2.307.

[91] Abduljalil A. Al-abidi, Sohif Bin Mat, K. Sopian, M.Y. Sulaiman, and Abdulrahman Th. Mohammed. CFD applications for latent heat thermal energy storage: a review. *Renewable and Sustainable Energy Reviews*, 20:353–363, 2013. ISSN 13640321. doi: 10.1016/j.rser.2012.11.079.

[92] Yvan Dutil, Daniel R. Rousse, Nizar Ben Salah, Stéphane Lassue, and Laurent Zalewski. A review on phase-change materials: Mathematical modeling and simulations. *Renewable and Sustainable Energy Reviews*, 15(1):112–130, 2011. ISSN 13640321. doi: 10.1016/j.rser.2010.06.011.

[93] R. Al Shannaq and M.M. Farid. 10 – Microencapsulation of phase change materials (PCMs) for thermal energy storage systems. In *Advances in Thermal Energy Storage Systems*, pages 247–284. 2015. ISBN 9781782420880. doi: 10.1533/9781782420965.2.247.

[94] Hakeem Niyas, Sunku Prasad, and P. Muthukumar. Performance investigation of a lab–scale latent heat storage prototype – Numerical results. *Energy Conversion and Management*, 135:188–199, 2017. doi: 10.1016/j.enconman.2016.12.075.

[95] Andrew J. Parry, Philip C. Eames, and Francis B. Agyenim. Modeling of Thermal Energy Storage Shell-and-Tube Heat Exchanger. *Heat Transfer Engineering*, 35(1): 1–14, jan 2014. doi: 10.1080/01457632.2013.810057.

[96] Saleh Almsater, Alemu Alemu, Wasim Saman, and Frank Bruno. Development and experimental validation of a CFD model for PCM in a vertical triplex tube heat exchanger. *Applied Thermal Engineering*, 116:344–354, 2017. doi: 10.1016/j.applthermaleng.2017.01.104.

[97] Radouane Elbahjaoui and Hamid El Qarnia. Numerical Study of a Shell-and-Tube Latent Thermal Energy Storage Unit Heated by Laminar Pulsed Fluid Flow. *Heat Transfer Engineering*, 38(17):1466–1480, nov 2017. doi: 10.1080/01457632.2016.1255083.

[98] A. Sciacovelli, F. Gagliardi, and V. Verda. Maximization of performance of a PCM latent heat storage system with innovative fins. *Applied Energy*, 137:707–715, 2015. doi: 10.1016/j.apenergy.2014.07.015.

[99] Z.N. Meng and P. Zhang. Experimental and numerical investigation of a tube-in-tank latent thermal energy storage unit using composite PCM. *Applied Energy*, 190: 524–539, 2017. doi: 10.1016/j.apenergy.2016.12.163.

[100] Yosr Allouche, Szabolcs Varga, Chiheb Bouden, and Armando C. Oliveira. Validation of a CFD model for the simulation of heat transfer in a tubes-in-tank PCM storage unit. *Renewable Energy*, 89:371–379, 2016. doi: 10.1016/j.renene.2015.12.038.

[101] Christoph Zauner, Florian Hengstberger, Mark Etzel, Daniel Lager, Rene Hofmann, and Heimo Walter. Experimental characterization and simulation of a fin-tube latent heat storage using high density polyethylene as PCM. *Applied Energy*, 179:237–246, 2016. doi: 10.1016/j.apenergy.2016.06.138.

[102] Hannah Neumann, Valeria Palomba, Andrea Frazzica, Dominik Seiler, Ursula Wittstadt, Stefan Gschwander, and Giovanni Restuccia. A simplified approach for modelling latent heat storages: application and validation on two different fin-and-tubes heat exchangers. *Applied Thermal Engineering*, 2017. doi: 10.1016/j.applthermaleng.2017.06.142.

[103] Deborah A. Kaminski and Michael K. Jensen. *Introduction to thermal and fluids engineering*. Wiley & Sons, USA, 1st editio edition, 2011. ISBN 1118103483.

[104] Hans Dieter Baehr and Karl Stephan. *Wärme- und Stoffübertragung*. Springer Berlin Heidelberg, Berlin, Heidelberg, 2013. ISBN 978-3-642-36557-7. doi: 10.1007/978-3-642-36558-4. URL http://link.springer.com/10.1007/978-3-642-36558-4.

[105] T. X. Li, J. X. Xu, T. Yan, and R. Z. Wang. Development of sorption thermal battery for low-grade waste heat recovery and combined cold and heat energy storage. *Energy*, 107:347–359, 2016. doi: 10.1016/j.energy.2016.03.126.

[106] Rebecca Weber, Henner Kerskes, and Harald Drück. Development of a combined hot water and sorption store for solar thermal systems. *Energy Procedia*, 48:464–473, 2014. doi: 10.1016/j.egypro.2014.02.055. URL http://dx.doi.org/10.1016/j.egypro.2014.02.055.

[107] Andreas Hauer. Sorption theory for Thermal Energy Storage. In Halime Ö Paksoy, editor, *Thermal Energy Storage for Sustainable Energy Consumption*, pages 393–408. Springer Netherlands, Dordrecht. ISBN 978-1-4020-5290-3. doi: 10.1007/978-1-4020-5290-3_24.

[108] Y. Z. Lu, R. Z. Wang, M. Zhang, and S. Jiangzhou. Adsorption cold storage system with zeolite-water working pair used for locomotive air conditioning. *Energy Conversion and Management*, 44(10):1733–1743, 2003. doi: 10.1016/S0196-8904(02)00169-3.

[109] Yuri I. Aristov. Adsorptive transformation and storage of renewable heat: Review of current trends in adsorption dynamics. *Renewable Energy*, 110:105–114, 2017. doi: 10.1016/j.renene.2016.06.055.

[110] Valeria Palomba, Salvatore Vasta, and Angelo Freni. Experimental testing of AQSOA FAM Z02/water adsorption system for heat and cold storage. *Applied Thermal Engineering*, 124:967–974, 2017. doi: 10.1016/j.applthermaleng.2017.06.085.

[111] V. Palomba, B. Dawoud, A. Sapienza, S. Vasta, and A. Frazzica. On the impact of different management strategies on the performance of a two-bed activated carbon/ethanol refrigerator: An experimental study. *Energy Conversion and Management*, 142:322–333, 2017. doi: 10.1016/j.enconman.2017.03.055.

[112] Patrizia N. Melograno, Salvatore Vasta, Francois Boudehenn, and Jochen Döll. Quality Level Assessment of Sorption Chillers Installed in Solar Cooling Plants. *Energy Procedia*, 91:356–365, 2016. doi: 10.1016/j.egypro.2016.06.283.

[113] Yu.I. Aristov, A. Sapienza, D.S. Ovoshchnikov, A. Freni, and G. Restuccia. Reallocation of adsorption and desorption times for optimisation of cooling cycles. *International Journal of Refrigeration*, 35(3):525–531, 2012. ISSN 01407007. doi: 10.1016/j.ijrefrig.2010.07.019.

[114] Heike Schreiber, Franz Lanzerath, Christiane Reinert, Christoph Grüntgens, and André Bardow. Heat lost or stored: Experimental analysis of adsorption thermal energy storage. *Applied Thermal Engineering*, 106:981–991, aug 2016. doi: 10.1016/j.applthermaleng.2016.06.058.